

INVESTIGATION OF THE EFFECT OF HYDRATED LIME ON LOW
TEMPERATURE CRACKING OF ASPHALT CONCRETE

A THESIS SUBMITTED TO
THE GRADUATE SCHOOL OF NATURAL AND APPLIED SCIENCES
OF
MIDDLE EAST TECHNICAL UNIVERSITY

BY

BAŐAK VARLI BİNGÖL

IN PARTIAL FULFILLMENT OF THE REQUIREMENTS
FOR
THE DEGREE OF DOCTOR OF PHILOSOPHY
IN
CIVIL ENGINEERING

DECEMBER 2019

Approval of the thesis:

**INVESTIGATION OF THE EFFECT OF HYDRATED LIME ON LOW
TEMPERATURE CRACKING OF ASPHALT CONCRETE**

submitted by **BAŐAK VARLI BİNGÖL** in partial fulfillment of the requirements
for the degree of **Doctor of Philosophy in Civil Engineering, Middle East
Technical University** by.

Prof. Dr. Halil Kalıpçılar

Dean, Graduate School of **Natural and Applied Sciences**

Prof. Dr. Ahmet Türer

Head of the Department. **Civil Engineering**

Prof. Dr. Murat Güler

Supervisor. **Civil Engineering, METU**

Examining Committee Members:

Prof. Dr. İsmail Özgür Yaman

Civil Engineering, METU

Prof. Dr. Murat Güler

Civil Engineering, METU

Prof. Dr. Mustafa Şahmaran

Civil Engineering, Hacettepe University

Assist. Prof. Dr. Hande Işık Öztürk

Civil Engineering, METU

Assist. Prof. Dr. Elif Çiçek

Civil Engineering, Hacettepe University

Date: 26.12.2019

I hereby declare that all information in this document has been obtained and presented in accordance with academic rules and ethical conduct. I also declare that, as required by these rules and conduct, I have fully cited and referenced all material and results that are not original to this work.

Name. Last name : Varli Bingöl, Başak

Signature :

ABSTRACT

INVESTIGATION OF THE EFFECT OF HYDRATED LIME ON LOW TEMPERATURE CRACKING OF ASPHALT CONCRETE

Varlı Bingöl, Başak
Doctor of Philosophy, Civil Engineering
Supervisor : Prof. Dr. Murat Güler

December 2019, 234 pages

The main objective of this study is to investigate the effect of hydrated lime on low-temperature cracking resistance of hot mix asphalt (HMA) mixtures. To this end, a comprehensive laboratory experimental program is established to evaluate the influence of hydrated lime modification, aggregate type, aggregate gradation and asphalt binder aging on temperature-related failure of HMA specimens. These specimens prepared from materials obtained from Turkish General Directorate of Highways are fabricated following the Superpave® method of mix design. Thermal stress restrained specimen tests (TSRST), direct tension tests (DTT) and indirect tensile tests (IDT) are performed to investigate the influence of hydrated lime modification as well as other mix design variables on the low temperature cracking resistance of HMA. Also, dynamic mechanical analysis (DMA), dynamic shear rheometer (DSR), and rotational viscosity (RV) tests are conducted to investigate the influence of HL on changing the rheological properties of asphalt binder. In addition to all the aforementioned tests, scanning electron microscopy (SEM) is conducted to observe the interaction of hydrated lime particles and asphalt binder at submicron levels. To develop robust conclusions, a few statistical analyses methods are utilized

to identify the significant variables influencing the fracture strength and low temperature cracking of HMA; the resulting findings proved the significance of hydrated lime modification in increasing the fracture resistance of HMA when exposed to low temperatures.

Keywords: Low Temperature Cracking, Hydrated Lime, Tensile Strength, Fracture Strength, Fracture Temperature

ÖZ

SÖNMÜŞ KİREÇİN ASFALT BETONUNUN DÜŞÜK SICAKLIK KIRILMALARINA ETKİSİNİN İNCELENMESİ

Varlı Bingöl, Başak
Doktora, İnşaat Mühendisliği
Tez Yöneticisi: Prof. Dr. Murat Güler

Aralık 2019, 234 sayfa

Bu çalışmanın temel amacı, sönmüş kireçin sıcak karışım asfalt (HMA) karışımlarının düşük sıcaklıkta çatlama direnci üzerindeki etkisini araştırmaktır. Bu amaçla, sönmüş kireç modifikasyonunun, agrega tipinin, agrega derecesinin ve asfalt bağlayıcı yaşlanmanın HMA örneklerinin sıcaklığa bağlı deformasyon etkisini değerlendirmek için kapsamlı bir laboratuvar deneysel programı oluşturulmuştur. Karayolları Genel Müdürlüğünden elde edilen malzemelerden hazırlanan bu örnekler, Superpave® karışım dizaynı yöntemi ile üretilmiştir. Sönmüş kireç modifikasyonunun, diğer karışım tasarım değişkenlerinin, HMA'nın düşük sıcaklıkta çatlama direncine etkisinin araştırılması için ısıl gerilmeyi sınırlandırılmış örnek testi (TSRST), doğrudan gerginlik testi (DTT) ve dolaylı gerginlik testi (IDT) yapıldı. Ayrıca, HL'nin asfalt binderinin reolojik özelliklerini değiştirmedeki etkisini araştırmak için dinamik mekanik analiz (DMA), dinamik kesme reometresi (DSR) ve dönme viskozite (RV) testleri yapılmıştır. Yukarıda belirtilen tüm testlere ek olarak, sönmüş kireç parçacıklarının ve asfalt bağlayıcı maddenin etkileşimini mikron altı seviyelerde gözlemlemek için taramalı elektron mikroskopisi (SEM) gerçekleştirilir. Güçlü sonuçlar geliştirmek için, kırılma mukavemetini ve HMA'nın düşük sıcaklıkta çatlama direncini etkileyen önemli değişkenleri tanımlamak için birkaç

istatistiksel analiz yöntemi kullanıldı. Elde edilen bulgular, sönmüş kireç modifikasyonunun, düşük sıcaklıklara maruz kaldığında HMA'nın kırılma direncinin arttırılmasındaki önemini kanıtlamıştır.

Anahtar Kelimeler: Düşük Sıcaklık Kırılması, Sönmüş Kireç, Çekme Dayanımı, Kırılma Dayanımı, Kırılma Sıcaklığı

To Murat. Umut and Ada

ACKNOWLEDGMENTS

I owe my deepest gratitude to Professor Dr. Murat Güler for his guidance, advice, criticism and insight throughout the research.

Besides my advisor, I would like to thank the rest of my thesis committee: Prof. Dr. İsmail Özgür Yaman, Prof. Dr. Mustafa Şahmaran, Asst. Prof. Dr. Hande Işık Öztürk and Asst. Prof. Dr. Elif Çiçek for their help, valuable advices and insightful comments.

I thank my fellow lab mates in Transportation Laboratory: Yalçın Karakaya, Dr Ayhan Öner Yücel, Laleh Sorkhi for their helps and all the fun we have had together during my research. I also would like to thank my friend Murat Can Çömlekçi for being such a good friend.

I am thankful to Reza Shabani and Ömer Can Pamuk for their friendship and stimulating discussions they made for this study. In particular. Ahmet Sağlam, laboratory technician for providing me the able assistance all through the research period and helping hand in the gigantic laboratory task required for this research.

My special thanks goes to Dr. Ali Arabzadeh, Dr. Vesile Hatun Akansel, Dr. Eren Yağmur and Dr. Murat Şahin, who supported me during my Phd, for being more than a friend and for their countless help.

The last but not the least, I would like to thank my family: my parents, my husband (Murat), my brother (Umut), my daughter (Ada) and my grandmom for supporting me spiritually throughout the PhD program and my life in general. This research work would not be completed without their encouragement and belief in me. It was because of their sincere supports that I was able to sail through the difficulties I faced during this study.

TABLE OF CONTENTS

ABSTRACT.....	v
ÖZ.....	vii
ACKNOWLEDGMENTS	x
TABLE OF CONTENTS.....	xi
LIST OF TABLES	xv
LIST OF FIGURES	xvii
LIST OF ABBREVIATIONS.....	xxii
CHAPTERS	
1 INTRODUCTION	1
1.1 Background	1
1.2 Research Hypotheses.....	4
1.3 Scope	5
1.4 Outline of Research.....	6
2 LITERATURE REVIEW	7
2.1 Introduction	7
2.2 Low Temperature Cracking of Asphalt Mixture.....	7
2.3 Factors Affecting Thermal Fatigue Cracking.....	12
2.3.1 Material Factors	13
2.3.2 Environmental Factors	17
2.3.3 Asphalt Mixture Properties	21
2.4 Hydrated Lime.....	25

2.4.1	Production of Hydrated Lime	26
2.4.2	Effect of Hydrated Lime on Asphalt Mixtures Properties.....	27
2.4.3	Effect of Hydrated Lime on Low-Temperature Performance of Asphalt Concrete	32
2.4.4	Hydrated Lime Chemical Interactions.....	34
2.4.5	Addition Techniques of Hydrated Lime to Asphalt Mix.....	37
2.5	Tests Performed to Determine The Thermal Properties of Asphalt Concrete.....	39
2.5.1	Thermal Stress Restrained Specimen Test	39
2.5.2	The Indirect Tensile Strength Test	42
2.5.3	Direct Tension Test	43
2.6	Test Methods to Evaluate The Effect of Hydrated Lime on Asphalt Binder 45	
2.6.1	Dynamic Mechanical Analysis Technique	45
2.6.2	Dynamic Shear Rheometer.....	49
2.6.3	Rotational Viscosity Test	50
2.6.4	Scanning Electron Microscopy.....	52
3	METHODOLOGY	53
3.1	Introduction.....	53
3.2	Sample Preparation	54
3.2.1	Design of Experiments for Laboratory Testing.....	55
3.2.2	Materials Used in the Experimental Program	61
3.2.3	Superpave Mixture Design	64
3.2.4	Sample Preparation for Compaction	68
3.2.4.1	Process of Hydrated Lime Addition.....	68

3.2.5	Preparation of beam specimens	71
3.3	Sample Preparation for DTT and TSRST	73
3.3.1	Test Setup for Thermal Stress Restrained Specimen Test	76
3.3.1.1	Elements of TSRST Frame	77
3.3.1.2	Programming for Test Control.....	79
3.3.1.3	The system control.....	80
3.4	Thermal Stress Restrained Specimen Test	83
3.5	Sample Preparation for DTT Testing	85
3.6	Direct Tension Test (DTT).....	87
3.7	Sample preparation for IDT Testing	89
3.8	Indirect Tension Test (IDT)	93
3.9	Characterization Tests for Bitumen and Mastic	93
3.9.1	Scanning Electron Microscope (SEM) of Mastic Phase	93
3.9.1.1	Sample Preparation for SEM Analysis	95
3.9.2	DMA Analysis of Mastic Phase.....	96
3.9.2.1	Sample Preparation for DMA Analysis	98
3.9.3	Rotational Viscometer of Bitumen	99
3.9.4	Rheological Analysis of Bitumen Using Dynamic Shear Rheometer	100
4	RESULTS AND ANALYSIS OF TEST DATA	103
4.1	Introduction	103
4.2	ANOVA Analysis for Mixture Tests	103
4.2.1	Analysis for TSRST results.....	103
4.2.1.1	Analysis of Fracture Strength From TSRST Data.....	104

4.2.1.2	Analysis of TSRST Results Fracture Temperature	111
4.2.2	Analysis of ANOVA for Direct Tension Test Results	116
4.2.2.1	Analysis of Direct Tension Test Results at 0°C.....	117
4.2.2.2	Analysis of Direct Tension Test Results at -10°C	121
4.2.3	Analysis of ANOVA for Indirect Tension Test Results.....	127
4.2.3.1	Indirect Tension Test Results at 0°C.....	128
4.2.3.2	Indirect Tension Test Results at -10°C	133
4.3	Bitumen Testing.....	139
4.3.1	Dynamic Shear Rheometer	140
4.3.2	SEM Analysis of Mastic Phase	142
4.3.3	Dynamic Mechanical Analysis (DMA) on Mastic Phase.....	148
4.3.4	Rotational Viscosity of Mastic Phase.....	149
5	CONCLUSIONS AND RECOMMENDATIONS	151
5.1	Introduction.....	151
5.2	Conclusions.....	151
5.3	Recommendations For Future Work.....	155
	REFERENCES	157
	APPENDICES	
A.	Fracture Plots.....	171
B.	Dynamic Mechanical Analysis Results	219
C.	ANOVA Results	222
D.	Software Manuals	225
	CURRICULUM VITAE	233

LIST OF TABLES

TABLES

Table 2.1 Importance of hydrated lime according to usage areas.....	28
Table 2.2 The effect of adding HL on bitumen fracture toughness (After Little and Petersen. 2005).....	33
Table 2.3 Comparison of tensile elongation data (Petersen et al.,1987).....	34
Table 2.4 Components adsorbed and not adsorbed on HL (Petersen at al.,1987) ..	35
Table 2.5 Hydrated lime addition methods (National Lime Association., 2003) ...	37
Table 2.6 Literature survey for used temperature and strain rates in DTT (Karakaya. 2015)	44
Table 2.7 Viscosity of fillers (Lesueur. 2009)	51
Table 3.1 Test variables used in DTT and IDT	57
Table 3.2 Test variables used in TSRST.....	57
Table 3.3 Two-level full factorial design matrix for DTT and IDT	58
Table 3.4 Two-level full factorial design matrix for TSRST.....	60
Table 3.5 Aggregate properties used in the study (a) limestone. (b) basalt.....	61
Table 3.6 Asphalt binder properties	62
Table 3.7 Superpave compaction parameters for different traffic levels.	65
Table 3.8 Superpave HMA Design Requirements.....	65
Table 3.9 Parameters selected for mixing and compaction.	67
Table 3.10 Mixture properties.....	67
Table 3.11 HL Gradation Analysis (% passing)	69
Table 3.12 Chemical Properties of Hydrated Lime	70
Table 3.13 Increase in IDT for different contents of hydrated lime	71
Table 3.14 Summary of test variables for prepared specimens	73
Table 3.15 Specimen coding for TSRST	83
Table 3.16. Specimens tested for DTT	86
Table 3.17 Specimens tested for IDT.....	91

Table 4.1 Specimen names and replicate number	104
Table 4.2 Descriptive statistics of the fracture strength	105
Table 4.3 ANOVA analysis for fracture strength.....	105
Table 4.4 Fracture strength values for variables	106
Table 4.5 Descriptive statistics of fracture temperature	111
Table 4.6. ANOVA analysis for fracture temperature	112
Table 4.7 Fracture temperatures according to test variables	113
Table 4.8 Specimen names and replicate numbers used in DTT at 0°C	117
Table 4.9 Descriptive statistics of DTT performed at 0°C.....	117
Table 4.10 ANOVA analysis of DTT performed at 0°C.....	118
Table 4.11 DTT results at 0°C for each test variable	119
Table 4.12 Sample names and replicate numbers for DTT at -10°C.....	122
Table 4.13 Descriptive statistics of DTT performed at -10°C.....	122
Table 4.14 ANOVA analysis for -10°C DTT.....	123
Table 4.15 DTT results at -10°C for each test variable	124
Table 4.16 Sample names and replicate numbers for IDT performed at 0°C	128
Table 4.17 Descriptive statistics of IDT performed at 0°C	128
Table 4.18 ANOVA analysis of IDT performed at 0°C.....	129
Table 4.19 Values of IDT performed at 0°C according to test variables	130
Table 4.20 Sample names and replicate numbers for IDT	133
Table 4.21 Descriptive statistics of -10°C IDT	134
Table 4.22 ANOVA analysis of IDT performed at -10°C.....	134
Table 4.23 Values of IDT performed at -10°C according to test variables.....	135
Table C.1 Response for DTT 0°C.....	222
Table C.2 Response for DTT -10°C	222
Table C.3 Response for TSRST Fracture Stress	223
Table C.4 Response for TSRST Fracture Temperature.....	223
Table C.5 Response for IDT -10°C	224
Table C.6 Response for IDT 0°C	224

LIST OF FIGURES

FIGURES

Figure 2.1. Low temperature cracking (Behnia et al., 2017)	8
Figure 2.2. Asphalt concrete pavement thermal cracking schema (Jung D. et al., 1993)	9
Figure 2.3. Change of thermal stress gradients through pavement (Haas et al., 1987)	9
Figure 2.4. Example of large transverse crack (Molenaar, 2007).....	10
Figure 2.5. Pumping of fines (Arabzadeh. A., 2015).....	11
Figure 2.6. Temperature range of thermal fatigue cracking (Carpenter, 1983).....	12
Figure 2.7. Stiffness behavior of asphalt binder (Roberts et al., 1996)	13
Figure 2.8. Asphalt behavior according to temperature change (Breen & Stephens., 1967)	14
Figure 2.9. Ideal temperature range for good asphalt pavement performance (Bureau of Materials and Physical Research, 2005).....	15
Figure 2.10. Compacted asphalt mix specimen	16
Figure 2.11. Evaluation of aging (Xu.M. et al., 2017).....	20
Figure 2.12. Asphalt concrete structure (Pavement Interactive, 2019).....	21
Figure 2.13. Prediction of mix stiffness by Bonnaure et al., (1977) method.....	23
Figure 2.14. Hydrated lime effect on asphalt mixtures (EULA, 2011)	25
Figure 2.15. The Lime Cycle (Wikipedia, 2019).....	26
Figure 2.16. Stiffening effect of limestone filler and hydrated lime vs temperature (After Wortelboer et al. 1996).....	30
Figure 2.17. HL volume fraction versus stiffness ratio graph (After Little and Petersen. 2005).....	32
Figure 2.18. Fracture toughness (After Little and Petersen .2005).....	33
Figure 2.19. Illustration of strong hydrogen bonding (Petersen & Glaser. 2011) ..	36
Figure 2.20. TSRST device (Marasteanu et al., 2007).....	40

Figure 2.21. Thermally Induced Stress Curve from a Monotonic Cooling (after Jackson, 1992).....	41
Figure 2.22. Thermally Induced Stress Curve from a Cyclic Cooling (after Jackson, 1992).....	41
Figure 2.23. IDT Strength Test (Shodhganga, 2019).....	42
Figure 2.24. Fractured DTT specimen	43
Figure 2.25. Perkin Elmer Pyris Diamond DMA analyzer	46
Figure 2.26. Stress and strain as a function of time with dynamic (sinusoidal) loading (Ward and Hadley. 1993).	46
Figure 2.27. DSR testing geometry	50
Figure 2.28. Hydrated lime temperature dependence stiffening effect	52
Figure 3.1. The outline of the tasks performed in Methodology section.	54
Figure 3.2. Flow diagram for fractional factorial experimental design.....	56
Figure 3.3. Selected gradations for the study (a) limestone, (b) basalt	63
Figure 3.4. Superpave gyratory compactor used in this study	66
Figure 3.5. Hydrated lime used as mineral filler	69
Figure 3.6. Addition of lime to aggregate	71
Figure 3.7. Specimen dimensions after cutting with diamond saw machine from Superpave samples	72
Figure 3.8. Previous sticking process (after Arabzadeh., 2014).....	74
Figure 3.9. Centering of specimen and loading platens during gluing process.....	75
Figure 3.10. Details of apparatus used for specimen centering.....	75
Figure 3.11. Schematic for TSRST setup (after Marasteanu et al., 2007).	77
Figure 3.12. (a) TSRST main components (b) Environment chamber dimensions	78
Figure 3.13. Abaqus Analysis for TSRST specimen.....	79
Figure 3.14. Software and testing machine communication layout	80
Figure 3.15. TSRST software panel	81
Figure 3.16. TSRST fracture test results (a) a specimen fractured after test. (b) stress versus temperature data plotted for a specimen	84

Figure 3.17. DTT (a) Sample preparation. (b) sticking to platens and (c) testing process.....	85
Figure 3.18. DTT test results (a) a view of specimen during the test. (b) a specimen fractured after test	87
Figure 3.19. LVDT and RTD connections for DTT	88
Figure 3.20. Software used for DTT	88
Figure 3.21. Cutting sections of IDT specimens.....	89
Figure 3.22. (a) Environmental chamber and IDT testing machine. (b)Cracked IDT specimen	92
Figure 3.23. IDT testing machine	93
Figure 3.24. SEM Test setup (The Quanta FEG 400 User's Manual).....	94
Figure 3.25. SEM Sample holder.....	95
Figure 3.26. Prepared sample combination for SEM analysis.....	96
Figure 3.27. DMA testing machine.....	97
Figure 3.28. Typical DMA results	98
Figure 3.29. Prepared sample combination for DMA analysis.....	99
Figure 3.30. Sample combinations for viscosity analysis	100
Figure 3.31. Representation of DSR (Asphalt institute. Lexington 1994).....	101
Figure 3.32. Two components of complex modulus (Anton Paar, 2019).....	101
Figure 4.1. Fracture strength versus temperature for specimens fabricated using limestone aggregates	108
Figure 4.2. The influence of aggregate type on fracture strength.....	109
Figure 4.3. The influence of gradation on fracture strength	109
Figure 4.4. The influence of aging on fracture strength	110
Figure 4.5. The influence of HL on fracture strength	111
Figure 4.6. The influence of aggregate type on fracture temperature.....	114
Figure 4.7. The influence of gradation on fracture temperature	114
Figure 4.8. The influence of HL on fracture temperature.....	115
Figure 4.9. The influence of aging on fracture temperature	116
Figure 4.10. The influence of aggregate type on DTT at 0°C	119

Figure 4.11. The influence of gradation on DTT at 0°C	120
Figure 4.12. The influence of aging on DTT at 0°C	121
Figure 4.13. The influence of hydrated lime content on DTT at 0°C	121
Figure 4.14. The influence of aggregate type on DTT at -10°C.....	125
Figure 4.15. The influence of gradation on DTT at -10°C.....	125
Figure 4.16. The influence of aging on DTT at -10°C	126
Figure 4.17. The influence of HL content on DTT at -10°C.....	126
Figure 4.18. Comparison test results for DTT at 0°C and -10°C.....	127
Figure 4.19. The influence of aggregate type on IDT at 0°C	131
Figure 4.20. The influence of gradation on IDT at 0°C	131
Figure 4.21. The influence of aging on IDT at 0°C.....	132
Figure 4.22. The influence of HL content on IDT at 0°C	133
Figure 4.23. The influence of aggregate type on IDT at -10°C.....	136
Figure 4.24. The influence gradation on IDT at -10°C	136
Figure 4.25. The influence of aging on IDT at -10°C	137
Figure 4.26. The influence of HL content on IDT at -10°C.....	138
Figure 4.27. IDT results comparison	138
Figure 4.28. Bitumen performance tests.....	139
Figure 4.29. DSR master curve for extracted bitumen from mixtures	140
Figure 4.30. Mastic complex modulus at (a) 25°C, (b) 45°C, (c) 65°C	142
Figure 4.31. SEM test results of mastics prepared with unaged bitumen and (a) HL+ Limestone. (b) HL + Basalt	143
Figure 4.32. SEM test results of mastics prepared with aged bitumen and (a) HL+ Limestone. (b) HL + Basalt	144
Figure 4.33. SEM test results of mastics prepared with (a) Unaged bitumen and HL+ Limestone. (b) Aged bitumen and HL+ Limestone.....	145
Figure 4.34. SEM test results of mastics prepared with (a) Unaged bitumen and HL+ Basalt. (b) Aged bitumen and HL+ Basalt	145
Figure 4.35. Spectra of the element distribution of HL with (a)unaged-limestone. (b) unaged-basalt.....	146

Figure 4.36. Spectra of the element distribution of HL with (c)aged-basalt. (d) aged-limestone	147
Figure 4.37. Tg of various mastic compositions.....	148
Figure 4.38. Comparison the viscosities of EB.....	150
Figure A.1. Fracture plots of samples tested with TSRST.....	171
Figure A.2. Fracture plots of samples tested with DTT at -10°C.....	179
Figure A.3. Fracture plots of samples tested with DTT at 0°C.....	187
Figure A.4. Fracture plots of samples tested with IDT at -10°C	197
Figure A.5. Fracture plots of samples tested with IDT at 0°C.....	208
Figure B.1. DMA curves and Tg of unaged bitumen.....	219
Figure B.2. DMA curves and Tg of aged bitumen.....	219
Figure B.3. DMA curves and Tg of unaged bitumen mastic containing limestone	219
Figure B.4. DMA curves and Tg of aged bitumen mastic containing limestone..	220
Figure B.5. DMA curves and Tg of bitumen mastic containing basalt	220
Figure B.6. DMA curves and Tg of aged bitumen mastic containing basalt.....	220
Figure B.7. DMA curves and Tg of bitumen mastic containing basalt and hydrated lime	221
Figure B.8. DMA curves and Tg of aged bitumen mastic containing basalt and hydrated lime	221
Figure D.1. Software for TSRST	225
Figure D.2. Software for DTT.....	Error! Bookmark not defined. 228
Figure D.3. Software for IDT	231

LIST OF ABBREVIATIONS

ABBREVIATIONS

A: Aged Specimen

AASHTO: American Association of State Highway and Transportation

AC: Asphalt Cement

ANOVA: Analysis of Variance

ASTM: American Society of Testing and Materials

B: Basalt Aggregate

BC: Basalt Coarse Graded Mix

BF: Basalt Fine Graded Mix

BST: Bituminous Surface Treatments

C: Coarse Gradation

DMA: Dynamic Mechanical Analysis

DSR: Dynamic Shear Rheometer

DTT: Direct Tension Test

ESAL: Equivalent Single Axle Load

F: Fine Gradation

FHWA: Federal Highway Administration

H: Hydrated Lime Added Mixture

HL: Hydrated Lime

HMA: Hot Mix Asphalt

IDT: Indirect Tension Test

L: Limestone Aggregate

LC: Limestone Coarse Graded Mix

LF: Limestone Fine Graded Mix

LVDT: Linear Variable Displacement Transducers

NMAS: Nominal Maximum Aggregate Size

RV: Rotational Viscometer

SEM: Scanning Electron Microscope

Superpave: Superior PERforming Asphalt PAVements

Tg: Glass Transition Temperature

TGDH: Turkish General Directorate of Highways

TSRST: Thermal Stress Restrained Specimen Test

U: Unaged Specimen

Z: Neat Mixture

CHAPTER 1

INTRODUCTION

1.1 Background

Asphalt is defined as “Dark brown to black cementitious material in which the predominant constituents are bitumen that occur in petroleum process” by the American Society for Testing and Materials (ASTM). Also, American Association of State Highway Transportation Officials (AASHTO) described asphalt as “asphalt-based cement that is produced from petroleum residues either with or without the addition of non-particulate organic modifiers”. Being waterproof and adhesive, asphalt is one of the most useful materials used in civil engineering for various constructions. The largest usage area of asphalt is the construction of Hot Mix Asphalt (HMA) that is mainly used for the flexible pavements and Bituminous Surface Treatments (BST).

For asphalt pavement structures, asphalt behaves as viscoelastic material due to its temperature sensitivity. At high temperatures, asphalt behaves as plastic materials while it becomes nearly elastic at extremely low temperatures in cold climate regions and becomes quite brittle affecting its thermal and fatigue performance. Thermal cracking is one of the main types of distresses for asphalt concrete pavements. Thermal cracking in asphalt concrete pavements can occur by two different mechanisms, namely, low temperature cracking and thermal fatigue cracking. Low temperature cracking occurs when the air temperature, hence the pavement temperature, drops below the fracture temperature of asphalt concrete. This type of fracture is generally observed in areas of extremely cold regions such as northern states of United States, Alaska and Canada, etc. Thermal fatigue cracking, on the other hand, occurs generally at moderate temperatures with large daily temperature cycles resulting in fatigue failures in asphalt concrete.

The basic mechanism for low temperature cracking is the significant volumetric change in the form of shrinkage of surface course as a result of excessive drop in air temperature. Since asphalt concrete is a thermo-plastic material, it behaves differently with temperature changes; it shrinks when the temperature drops and expands when it rises. When the temperature drops, the surface course is restrained to freely shrink due to friction at bottom of the surface course, as a result, high tensile stresses occur and eventually cause fracture when the strength of the surface layer is exceeded. As the air temperature drops, pavement layers cool down and causes contraction of both aggregate and binder, initiating the development of micro-cracks at the surface of pavement. These micro-cracks are later followed by top-down breaking, which are called transverse cracks formed generally perpendicular to the direction of travel. Transverse cracks are developed typically with crack opening sizes of around 2.5-3.5 mm on the pavement surface. When these cracks are not sealed off with proper sealant materials, surface water can enter through the crack openings and infiltrate to the sub-layers of the pavement which can cause structural damages due to strength loss in the subgrade. Also, the freeze-thaw cycles in the subgrade during the spring season may cause significant volume changes, i.e., shrinkage and swelling, resulting in deterioration in the roadway profile. As a consequence, the pavement performance will decrease together with its useful service life if a timely repair is not performed to low temperature induced cracks in the surface layer. Delayed maintenance of the transverse cracks can also increase the cost of rehabilitation when the structural failures show up at intermediate and advanced level of distresses.

Studies have shown that low temperature cracking is affected by many factors: asphalt and aggregate source, binder grading, aggregate gradation and mix volumetric properties. The use of mineral fillers is also believed to have a significant influence on low temperature performance of asphalt concrete. In earlier studies, it has been proved that mineral fillers improve the performance of asphalt concrete mixtures when used as a bond-strengthening and crack arresting agent that are also suitable with physico-chemical properties of both asphalt binder and mineral

aggregate. These types of fillers generally control the plastic and viscoelastic characteristics of mixture by changing the viscosity of mixture.

Hydrated lime has been used for many years as a mineral filler or antistripping agent in hot mix asphalt (HMA) mixtures in all over the world. Previous studies showed that it can also improve the rutting and fatigue performance of asphalt concrete around 75% (Eula. 2011); however, the most important improvement is achieved by the increased resistance to moisture damage, which are mainly governed by the adhesion between asphalt binder and mineral aggregate. Besides, hydrated lime serves as a rejuvenating agent to reduce the amount of aging and increase the stiffness of asphalt mixture.

When hydrated lime is added to asphalt mixture, it first starts reaction with the mineral aggregate, as a result of this, improved bonding is achieved between aggregate and asphalt binder. When hydrated lime reacts with the bitumen, it attenuates the effect of polar molecules causing better bonding with aggregate and hence increasing resistance to binder stripping. In many of the research outcomes, it is reported that the use of hydrated lime in asphalt mixtures can improve mixture's resistance to moisture damage, chemical aging, rutting and fatigue distresses.

The performance of asphalt – hydrated lime mix depends also on the technique by which the hydrated lime is added to asphalt mixture. In the literature, there are several methods reported for the addition of hydrated lime: i) to inject hydrated lime directly into a drum mixer and mix with aggregate, ii) to mix it with aggregate in a pug mill, iii) to add hydrated lime to moist aggregate with marination, iv) to add slurry lime to dry aggregate with or without marination. Previous studies show that the most effective method for adding hydrated lime is to mix with moist aggregate to achieve the best structural performance from the mixture. Typical percent of hydrated lime is not recommended to be less than 1 percent and more than 2.5 percent by mass of the dry aggregate. It is also suggested that during mixing moisture content of aggregate be around 3 percent for coarse aggregate and 6 percent for fine aggregate higher than their surface saturated moisture contents to start reaction

between hydrated lime and aggregate. In previous studies, the effect of hydrated lime in asphalt mixtures were investigated mainly for fatigue and rutting performance of asphalt concrete. However, very limited studies are available to highlight the potential benefits of hydrated lime for the thermal performance of asphalt concrete. The main objective of this study thus relies on investigating thermal performance of asphalt concrete modified with hydrated lime by varying several mixture design variables, i.e., aggregate source, gradation, asphalt binder aging, and hydrated lime content. To carry out the study, several test methods are selected to determine the low temperature cracking resistance of asphalt concrete modified with hydrated lime. Statistical analyses are then utilized to identify the significant mix design variables for asphalt concrete to resist low temperature cracking.

1.2 Research Hypotheses

The research hypotheses for this thesis can be stated as follows:

1. Hydrated lime improves bonding between bitumen and aggregate in asphalt concrete, thereby increasing its resistance to low temperature cracking.
2. Hydrated lime reduces oxidative aging of bitumen, thus reducing potential for low temperature cracking in asphalt concrete.

As a result of this study, firstly, it is aimed to determine the mixture properties and suitable test methods to determine the low temperature performance of asphalt concrete. It is expected that the results of the study will help the practitioners understand the low temperature fracture mechanism of asphalt concrete, create design parameters that reduce the cracking potential and understand the effect of hydrated lime on low temperature fracture.

1.3 Scope

In the study program, different mix designs were produced by varying aggregate source and gradation in two combinations as without hydrated lime and with hydrated lime added mixtures. Besides, a portion of mixture samples were long term aged in the oven to study the effect of hydrated lime on low temperature cracking resistance for the aged samples. In the first phase of the study, two different types of aggregates, basalt and limestone, and two types of gradations, coarse and fine, were used to prepare asphalt mixture samples using the same bitumen type according to AASHTO M323, Standard Specification for Superpave Volumetric Mix Design, and AASHTO R35, Standard Practice for Superpave Volumetric Design for Asphalt Mixtures. Mix designs were done first without using lime content, named as untreated mixtures, after that 2% hydrated lime by weight of dry aggregate was added to each mixture by replacing the mineral filler contents. In the experimental program, a total of 64 asphalt concrete samples were prepared for Indirect Tension Test (IDT), Direct Tension Test (DTT) and Thermal Stress Restrained Specimen Testing (TSRST).

In the second phase, compacted Superpave samples were cut using a diamond saw to produce specimens for IDT, DTT and TSRST, and then tested for low temperature cracking resistance by using each of these test methods.

In the third phase, interaction of hydrated lime with bitumen was investigated on mastic samples produced by mixing bitumen with aggregate filler and hydrated lime. Rheological properties of the mastic samples were measured using Dynamic Shear Rheometer (DSR), Dynamic Mechanical Analysis (DMA), and Rotational Viscometer (RV) devices. Interaction of hydrated lime with bitumen was also investigated using Scanning Electron Microscope (SEM) was used to observe the distribution characteristics of hydrated lime particles in the bitumen matrix and also identify the existence of transition zone between particle and bitumen.

In the final phase of the study, statistical analyses of variance (ANOVA) were conducted on the test outcomes to identify the significant mix design variables for mixtures with/without lime content. Based on the research findings, conclusions and recommendations were also given regarding the lime content used, test methods and the expected improvement in the thermal properties of asphalt concrete.

1.4 Outline of Research

In Chapter 2, the low cracking mechanism of asphalt concrete is discussed with a comprehensive literature review. Factors affecting the type of cracks are explained in detail. In addition, chemical mechanism of hydrated lime as an additive for asphalt mixtures, has been extensively reviewed in terms of its interaction with aggregate and bitumen, and also its effect on low temperature cracking. Furthermore, the experimental setups used to determine the low temperature performance of asphalt concrete modified with hydrated lime have been extensively described.

In Chapter 3, experimental design, test variables selected for mix designs are discussed. Also, setup for TSRST and DTT testing procedures and specimen preparation are presented.

In Chapter 4, results of statistical analyses on test outcomes are discussed in detail. Also, statistical parameters to identify significant mix design factors are compared in order to determine the effect of hydrated lime on low temperature cracking.

In Chapter 5, results and discussions are given based on the results of analyses presented in the previous chapter.

In Chapter 6, summary of the research outcomes followed by a brief discussion of recommendations for future work are given.

CHAPTER 2

LITERATURE REVIEW

2.1 Introduction

In this chapter, the effect of Hydrated Lime (HL) on low temperature cracking in Hot Mix Asphalt (HMA) pavements are investigated in detail. Additionally, a thorough explanation is given regarding the asphalt concrete's low temperature cracking performance based on previous studies and the function of hydrated lime on asphalt mixture performance is described in the following sections.

2.2 Low Temperature Cracking of Asphalt Mixture

Pavement structural distresses is one of the main problems for the asphalt concrete during its service life. One of the major reasons for distresses is the low temperature cracking due to high temperature differentials during climatic changes. The appearance of low-temperature cracks is generally transverse to the direction of traffic as observed in Figure 2.1. The low temperature crack intervals differ for fresh and older pavement and are observed as 30 m (100 ft) and 3 m (10 ft), respectively.

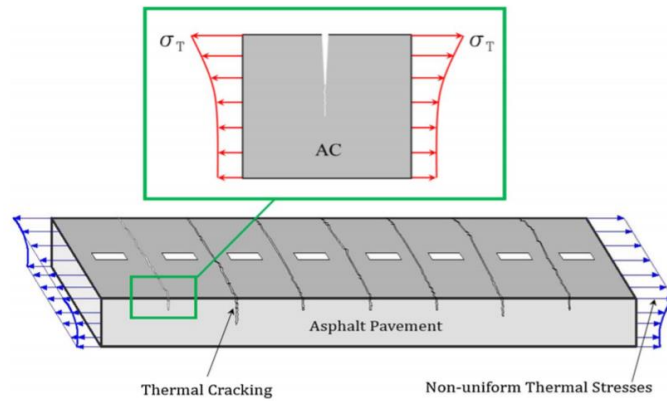


Figure 2.1. Low temperature cracking (Behnia et al., 2017)

Climatic factors cause expansion or contraction on asphalt concrete. Due to expansion of asphalt concrete, spalling problem occurs while contraction causes evaluation of transverse cracks. When the pavement's temperature cooled down, pavement contracts and appropriately tensile stress developed (Figure 2.1). Due to contraction, friction occurs between the base layer and the pavement. If tensile stress is equivalent to the asphalt concrete's strength, micro cracks occur at pavement surface. Repetition of temperature cycles causes crack propagation at full depth (Janoo, Bayer Jr, & Walsh, 1993). In Figure 2.2, thermal cracking phenomena is schematized.

According to the study conducted by Sugawara et al. (1982), it is indicated that micro-crack starts from the weak points of the pavement such as center or side lines, corners of ditches or center-side lines, and the edges of core sampling.

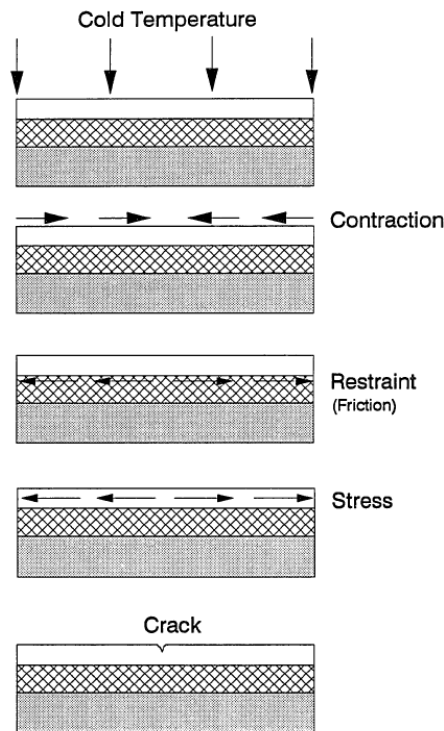


Figure 2.2. Asphalt concrete pavement thermal cracking schema (Jung D. et al., 1993)

As reported by Haas et al. (1987), at the surface layer of asphalt concrete, thermal stress develops to the highest value and continuously decreases with depth. This action occurs due to temperature gradient that remains between pavement foundation and air. At the top of the surface is more prone to thermal cracking. Figure 2.3 shows thermal stress gradients varying with depth.

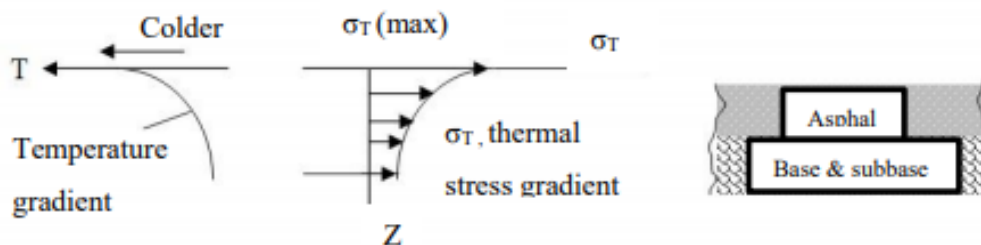


Figure 2.3. Change of thermal stress gradients through pavement (Haas et al., 1987)

As the asphalt pavement length is much larger than its width, low temperature cracks occur perpendicular to the traffic flow, as mentioned previously, and these cracks expand over time (Figure 2.4). After formation of cracks, pavement deterioration continues intensely and consequently, cracks expand. When the cracks are around 2.5-3.5 mm, water leaks into the pavement and that situation can cause serious damage and inability of the pavement over time. The fundamental reason of the pavement deterioration due to freeze-thaw cycle in spring is infiltration of water from the cracks. Therefore, cracks should be sealed by quite cost coatings with special sealants. However, the sealant, which is not applied on time, would cause rapid deterioration of the pavement and would further increase the cost of rehabilitation.



Figure 2.4. Example of large transverse crack (Molenaar, 2007)

Another important problem caused by the presence of water in a pavement structure is saturation of the base layer. The movement of traffic loads through pavement causes water pressure to increase. By the effect of the increased pressure, water

transferred from the cracks (Figure 2.5). While pouring out water from cracks, it pumps soil particles together. This results in material loss and reduced support of carrier system at the pavement. Consequently, additional cracks occur around transverse cracks under traffic loading. As a result, the pavement's service life is reduced and the driving comfort is severely affected.



Figure 2.5. Pumping of fines (Arabzadeh. A., 2015)

Thermal cracks occur as a result of high cooling rate or low temperatures caused by climatic factors and is one of the main problems causing pavement to deteriorate. Thermal cracking is a subject that has been extensively researched by Asphalt Research Community and still remains as one of the most complex deterioration types. When the temperature cycle is observed over the pavement, it becomes sensitive to thermal stress or stresses caused by traffic (Gerritsen & Jongeneel, 1988). It was determined that the main cause of the development of transverse cracks occurring in Western Texas is thermal fatigue cracking of asphalt concrete (Carpenter, S.H., Lytton, & Epps., 1974). Nevertheless, further researches have shown that other factors may also be effective (Carpenter, H. & Lytton, 1977, Anderson, O. & Epps, 1983).

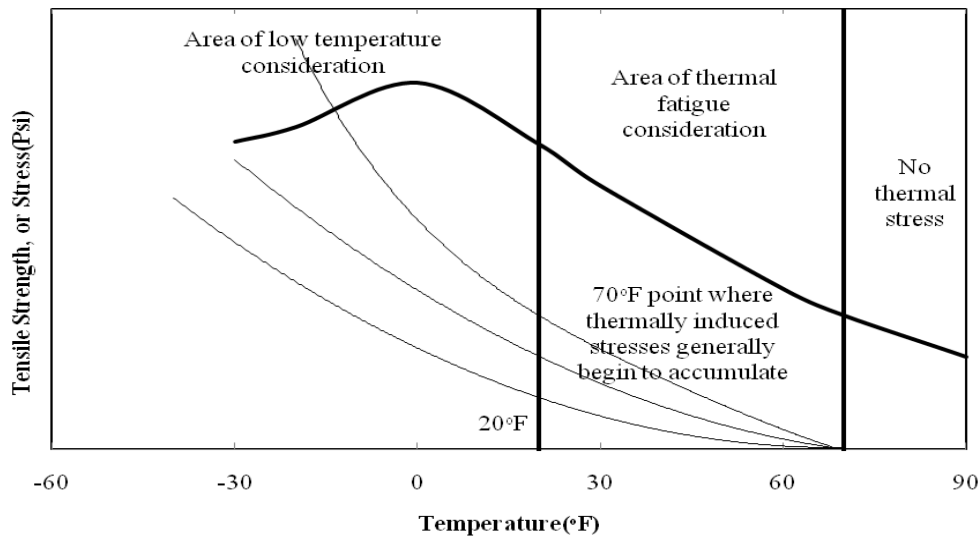


Figure 2.6. Temperature range of thermal fatigue cracking (Carpenter, 1983)

According to Carpenter (1983), thermal fatigue temperature usually occurs between -7°C (20°F) and 21°C (70°F), (Figure 2.6). At the temperatures above the specified range, thermal stresses disappear due to the relaxation of asphalt concrete. When the temperature falls below the specified range, low temperature cracks appear.

2.3 Factors Affecting Thermal Fatigue Cracking

Low temperature cracking in asphalt pavements are affected by several factors. These factors are classified by Haas et al. (1987) under three main elements as material, environmental and pavement structure geometry. When the factors that affect low temperature cracking were examined, the results showed significant interactions between climatic effect - pavement layer thickness and pavement aging – binder properties. In the following section, each factor is explained extensively and their effect on low temperature cracking are mentioned.

2.3.1 Material Factors

Asphalt concrete is a complex material that consists explicitly of aggregate and bitumen. Also, in recent years, the addition of modifiers to improve the properties of asphalt concrete and to increase its resistance to stresses has been a conventional method. Material-based improvements can be controlled differently from environmental and climatic conditions.

a) Asphalt Cement

Besides the significance of aggregate, asphalt cement is another important element in the mixture. The most important factor that determines the behavior of asphalt concrete at low temperatures is the temperature-stiffness relationship which can be observed in Figure 2.7. At low temperatures stiffness or consistency and temperature sensitivity are the most important elements.

Stiffness is defined as the hardness of the object. In other words, it is the resistance towards deformations in the response of applied force. In addition to this concept, flexibility is also worth mentioning. To clarify, the more flexible the object is, the less stiff behavior it may express.

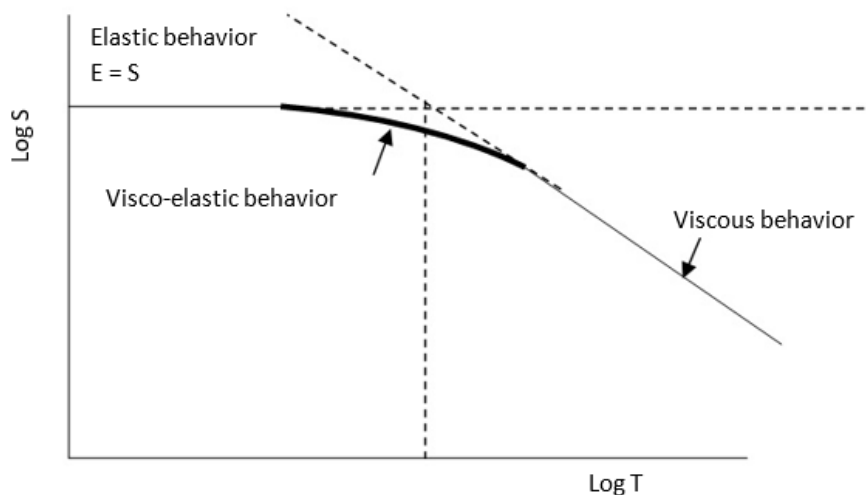


Figure 2.7. Stiffness behavior of asphalt binder (Roberts et al., 1996)

Stiffness is an important parameter in determining the behavior of pavement under traffic loads and it is obtained by dividing the stress induced in the material by strain which is a way to determine the thermal fatigue behavior of asphalt mixtures. The stiffness of asphalt mixtures is time independent in short loading times whereas it becomes viscous in long loading times. The stiffness of the binder is influenced by harmful factors that leads to the aging of the asphalt cement, such as temperature, moisture and applied stress. Figure 2.8 illustrates the relationship between time and asphalt stiffness. Additionally, it is observed that utilizing binders having low stiffness is more effective to minimize low temperature cracking at asphalt concrete (Roberts, Kandhal, Brown, & Lee, 1996).

Thermal properties of asphalt concrete are among the main characteristics that influence the thermal fatigue cracking performance of asphalt concrete. Asphalt concrete, which is a thermoplastic material, exhibits liquid, rubbery, and glassy behaviors with temperature change. Transition from visco-elastic state to elastic state and vice versa, is known as the glass transition temperature, T_g , which is demonstrated in Figure 2.8. In other words, it is the gradual transition in asphalt concrete from glassy state into rubbery or viscous state with the temperature increase. Glass transition temperature is always lower than melting temperature of the material. Glass transition occurs as a result of the change of volume becoming irregular due to the effect of temperature change. (Breen & Stephens, 1967).

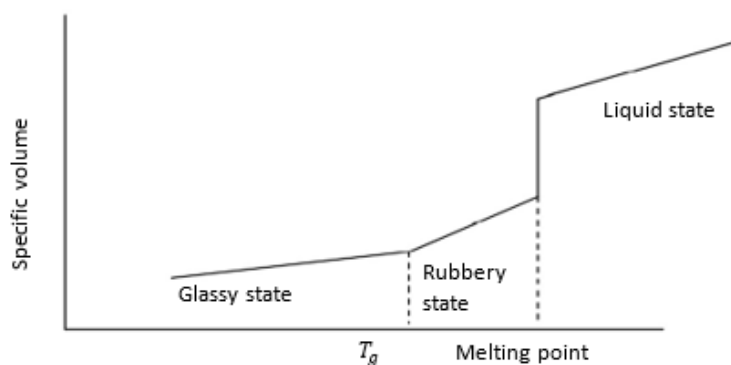


Figure 2.8. Asphalt behavior according to temperature change (Breen & Stephens., 1967)

Asphalt cement is considered as a visco-elastic material because it has both solid-like and liquid-like properties. These properties of asphalt cement are directly proportional to the temperature. Appropriately, asphalt acts as a liquid at high temperatures while performs like solid at low temperatures. Because of its liquid behavior asphalt cement tends to rut and solid behavior leads to cracking.

Using some modification techniques which are adding polymers, adhesives, acids, bases, and fillers increase the performance of asphalt concrete. These modifications are known to improve asphalt concrete's resistant to the rough climatic effects. As it is shown in Figure 2.9, binder III shows acceptable performance without any distress. A number of modifiers, such as polymer type, crumb rubber, are added to extend the binder's high performance range. After the usage of modifiers, binder II shows better performance compared to binder III and binder I shows better behavior than all.

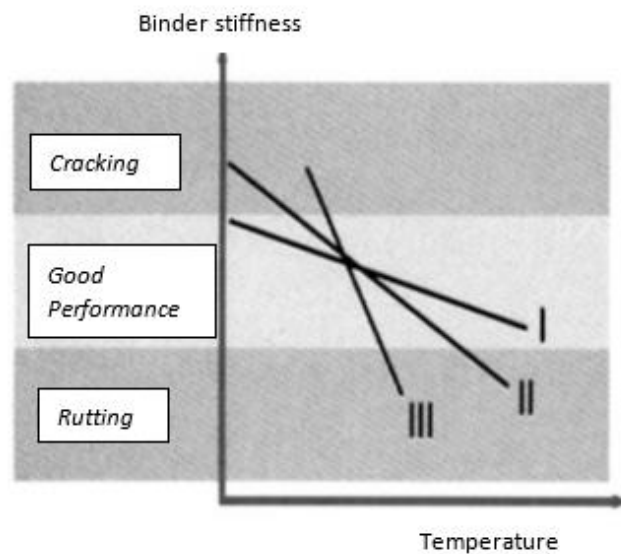


Figure 2.9. Ideal temperature range for good asphalt pavement performance (Bureau of Materials and Physical Research, 2005)

b) Aggregate Type and Gradation

Aggregates are materials composed of different gradation of crushed stone, gravel, sand and mineral materials. Selected aggregates are graded in specific proportions and mixed with asphalt binders to form the pavement. The most important function of aggregates in mixtures is that they act as a skeleton and create a load-supporting mechanism. It constitutes the most significant portion of the volume and weight of the asphalt mixture as a total of 90 to 95 percent of by weight and 75 to 85 percent by volume. (Figure 2.10).

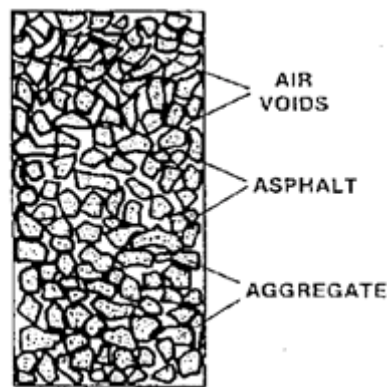


Figure 2.10. Compacted asphalt mix specimen

It was thought that aggregate had no effect on low temperature cracking; however, it was argued that binder directly affects the performance of mixture at low temperatures. However, another group of researchers rejected that argument by emphasizing that the effect of aggregate on low temperature cracking is as important as binder.

Maximum resistance to low temperature cracking can be achieved by the use of aggregates with high abrasion resistance, low freeze-thaw loss and low absorption. Since the bitumen between the particles with absorptive aggregates will be less than the non-absorptive ones, low temperature cracking resistance will be lower in this type of aggregates. Gradation of the mixture is thought to be decisive in increasing the resistance to cracking but has comparably a little effect on low temperature

cracking (Vinson et al.,1989). Just Epps et al. (1999) concluded that gap graded aggregate distribution increased low temperature cracking performance more than dense graded one in the mixture.

c) Asphalt Cement Content

A change in the optimum bitumen ratio does not influence the low temperature behavior of the asphalt mixture. Decrease of mixture stiffness and increase of coefficient of thermal contraction occurs as the asphalt content ratio increases. Thermal stress which occurs after the modification of asphalt content is too close to the previous one.

d) Air Void Content

Age hardening of asphalt mixtures is directly affected by air void and bitumen content changes (Gerritsen et al.,1988). Increase in air voids at asphalt mixtures indicates that the mixture becomes more suitable for age hardening, or this situation can be explained as increasing the bitumen content causes asphalt concrete to be less age hardened. In addition, the increase in binder content results decrease in initial stiffness (Gerritsen & Jongeneel, 1988). Finally, the degree of compaction in asphalt mixtures and resulting void ratio are not the parameters that significantly affect the performance of mixtures at low temperatures.

2.3.2 Environmental Factors

Low temperature cracking is common in regions that are exposed to cold weather because of climatic conditions, while thermal cracking is observed in regions with very high temperature difference between day and night. Environmental factors can be classified as:

a) Temperature

According to Al-Qadi et al. (2005) it is stated that one of the most important criteria of low temperature cracking is the environment temperature. In other words, when the temperature decreases, the pavement shrinks due to extreme binder aging, pavement volume changes and stiffness increase, resulting in the increase of cracking potential of the pavement. As the rate of temperature change in the pavement increases, the aging effect of the binder increases as well and that situation raises the probability of cracking at low temperatures (Kliewer, 1996).

Performance based grading system was created within the SHRP program to determine the behavior of binders under low temperature via a series of laboratory tests. For example, PG 64-32, which is one of the classifications determined within the program, states that the binder can tolerate 64°C depending on the seven days design temperature and that it can perform without cracking under low temperatures to a minimum of -32°C. Determining the pavement surface temperature standard conversion procedure is applied and pavement surface temperature is said to be 10-15°C hotter than the air temperature. SHRP program defines in-field air temperature in the design standards.

The optimum temperature ranges for determining the thermal fatigue effect on the pavement has been determined as between -7°C to 21°C. The predominant cracking mode at temperatures below -7°C is low temperature cracking, while at temperatures above 21°C no thermal cracking occurs (Carpenter, 1983).

It was studied by many researchers how effected low temperature cracking by temperature change. It is stated that when the pavement temperature falls below glass transition temperature, it was observed that the frequency of cracking increases (Vinson et al., 1996). Also, Shah (2004) concluded that PG grading system demonstrates higher performance against low temperature cracking compared to different rating systems. Besides, Nam and Bahia (2004) reported

that in order to define the low temperature behavior of asphalt concrete, it is necessary to specify the glass temperature of the mixture. According to the study by Minnesota Department of Highway (2007), it is proved that in general, obtained glass temperatures are so close to the fracture temperatures of tested mixtures.

b) Rate of Cooling

It is assumed that the cooling rate in asphalt concrete pavements is around 1.4 to 2.7°C per hour according to the analysis of pavement temperature (LTTP) in the United States (Alavi M.Z., 2014). One of the oldest works on cooling rate belongs to Fabb (1974) who tested specimens at different cooling rates between 5°C, -10°C and 27°C and founded that fracture temperature is not linked to the cooling rate. In 1982 this study was verified by testing with different cooling rates as 3°C, 6°C, 12°C, 18°C, 24°C and 30°C. That experiments showed that cooling rates which are faster than 5°C does not affect the cracking temperature (Alavi M.Z., 2014). The Strategic Highway Research Program (SHRP) conducted an extensive study on the effects of various factors on low temperature behavior of asphalt mixtures with Thermal Stress Restrained Test (TSRST). These factors were determined as binder type, aggregate type, mixture air voids, aging levels, cooling rates, and specimen size. Also, the effect on tensile strength on samples showed differences. Researchers noted in previous years that cooling rates more than 5°C have no effect on cracking temperature or cooling rate. Bahia et. al., (2012) also reported that increasing cooling rate increases cracking temperature and decreases the fracture stress.

a) Pavement Aging

Time varying environmental conditions cause the asphalt binder to harden as a result of chemical reactions (oxidation, solar radiation, induction of temperature

etc.) in bitumen and this phenomenon is called aging (Papagianakis and Masad, 2007, Figure 2.11). Aging of asphalt concrete causes structural hardening and therefore it becomes more susceptible to thermal cracking. According to Kliewer and Zeng (1996) when temperature increases at pavement surface, asphalt concrete becomes more aged. Aging of bitumen directly causes the aging of asphalt pavement. The aging of binder also affects the strain and stress failure appearing and the stiffness of the material. It is accepted that older pavements are more prone to thermal cracking than new pavements.

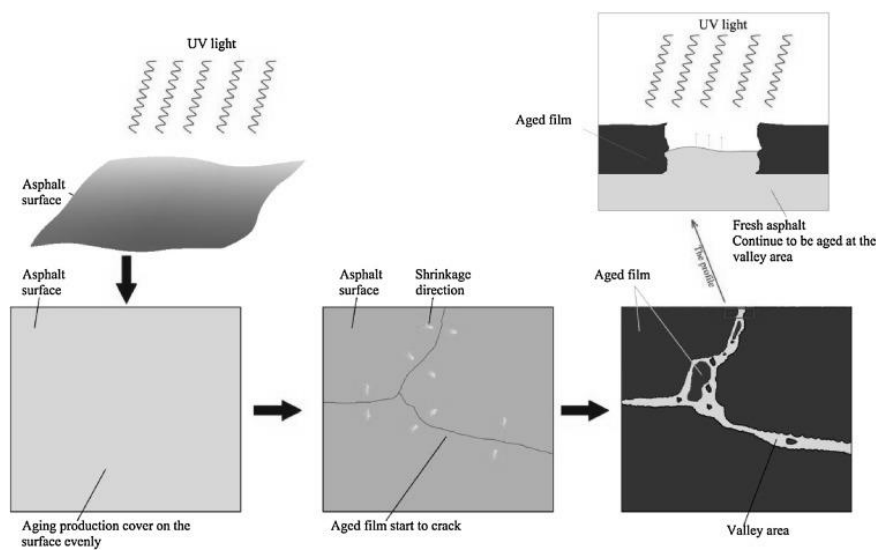


Figure 2.11. Evaluation of aging (Xu.M. et al., 2017)

Gerritsen et al., (1988) carried out thermal fatigue tests at two different temperatures to investigate the aging effect on asphalt concrete samples. Their results showed that aged samples at 10 degrees were broken under less cycle and more fragile at 0 degrees. According to Jung and Vinson (1994), low temperature cracking in pavement is related to the binder aging. Mouillet (2004) performed a series of tests on same binders with different polymer modifiers. Bitumen samples were aged by rolling thin film oven (RTFO) and pressure aging vessel (PAV) tests were implemented to simulate service conditions. According to the

test results, binder aging process increased the temperature required to reach stiffness criterion. Kliewer et al., (1996) aged asphalt concrete slab and cylindrical specimens at 50°C and 85°C for 100 days and they measured fracture temperature and fracture stress by TSRST. Consequently, they found out that SHRP long term aging process shows the aging effect on field conditions.

2.3.3 Asphalt Mixture Properties

With the characteristics of the components of the asphalt mixture, the properties of the mixture must be explained. Aggregates, bitumen and air voids form asphalt mixture with heterogeneous structure which is demonstrated in Figure 2.12. Each component affects the behavior and resistance of asphalt concrete against distress.

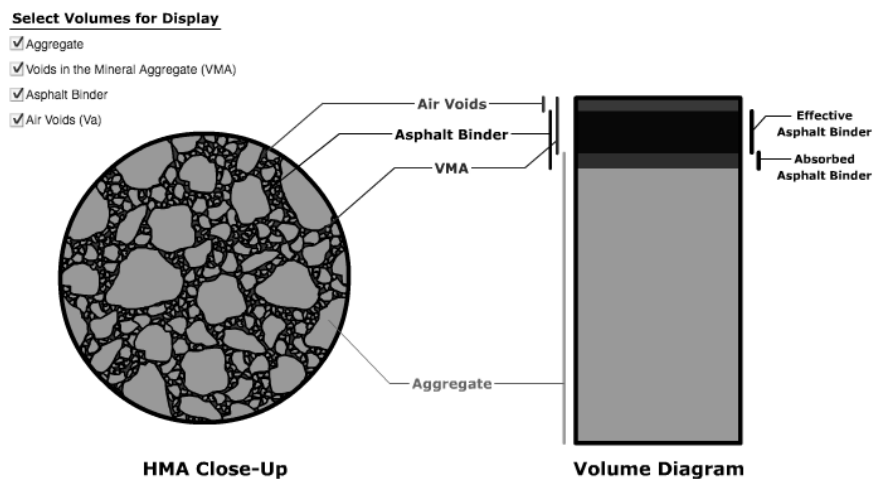


Figure 2.12. Asphalt concrete structure (Pavement Interactive, 2019)

a) Stiffness of asphalt mixture

The flexible pavements are subjected to different types of loading; especially traffic loading and climatic changes become very important factors in terms of asphalt concrete performance. Stiffness which is obtained by dividing the stress by strain, is the most important factor determining the resistance of mixtures against fatigue. Studies have shown that mixtures with high stiffness are more resistant to low temperature cracking than those with low stiffness and this indicates a strong link between stiffness and fracture of asphalt mixtures.

While determining the stiffness or relationship between strain-stress in viscoelastic materials, dynamic complex modulus method is used which consists of real and imaginary parts. The imaginary part represents the internal damping while the real part indicates the elastic stiffness (Huang, 2004).

To improve the low temperature performance of asphalt concrete, determination of mixture stiffness is of great importance. Although there are direct measurement methods for the determination of the mixture stiffness, the empirical method was developed by Bonnaure et al. (1977) to determine the stiffness of asphalt mixtures. The monograph indicated in the Figure 2.13 determines the mixture stiffness by extrapolation using the binder and air gaps in the mixture

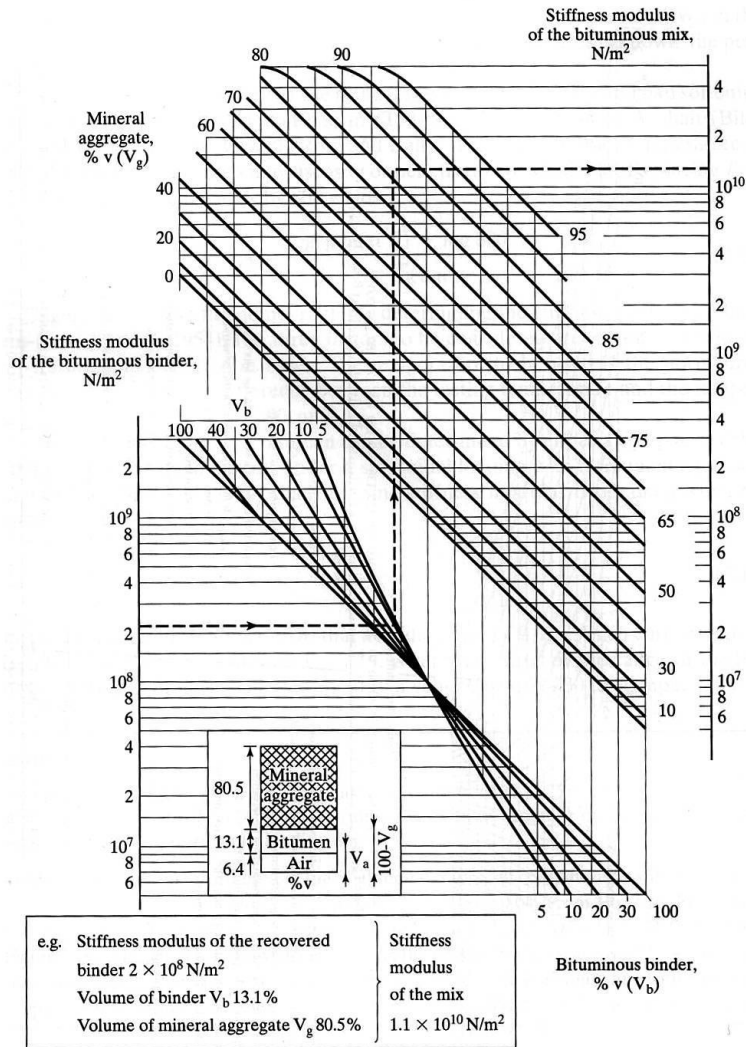


Figure 2.13. Prediction of mix stiffness by Bonnaure et al., (1977) method

b) Asphalt Mixture's Thermal Properties

Asphalt concrete has a volumetric expansion and contraction with increasing and decreasing temperature. To determine the performance of asphalt concrete under low temperatures, thermal coefficient of expansion/contraction and glass transition temperature should be determined. Since the stresses in pavements are build up due to the contraction, the coefficient of expansion/contraction, denoted by α , is called only the thermal coefficient of contraction which is defined by Equation (2.1) and (2.2).

$$\alpha = \frac{d\varepsilon^T(T)}{dT} \quad (2.1)$$

where ε^T = thermal strain and T =temperature

If the relationship is not linear. strain is obtained by;

$$\varepsilon^T = \int_{T_i}^T \alpha(T') dT' = \int_0^t \alpha [T(t')] \frac{dT(t')}{dt'} dt' \quad (2.2)$$

where T_i = initial temperature; T' = temperature integral variable;

t = time integral variable

According to Collieu & Powney (1973), material's thermal coefficient is dependent on temperature but for the asphalt mixtures reduction of coefficient determined before and after glass transition. Bahia et al. (1993) fit an equation to obtain change of volume versus temperature as shown in Equation 2.3.

$$v = C_v + \alpha_g(T - T_g) + R(\alpha_l - \alpha_g) \ln \left[1 + \exp \left(\frac{T - T_g}{R} \right) \right] \quad (2.3)$$

where v = specific volume at temperature T ; C_v = volume at a given temperature; T_g =glass transition temperature; R = constant that defines the temperature; α_l = thermal coefficient for $T > T_g$; and α_g = thermal coefficient for $T < T_g$

2.4 Hydrated Lime

The use of lime and lime products in buildings, roads or other structures has a very old history. The first known example of the usage of the lime in the construction is pyramids back in 4000BC. Over time, many improvements have been observed in the usage area of lime products. One of the essential products of lime is Hydrated lime (HL), which is the subject of this study.

In the past, the use of hydrated lime as a mineral filler in hot mix asphalt (HMA) was a common application. Furthermore, the use of hydrated lime improves many features and performance of HMA.

Hydrated lime use is less advanced in Europe than American. In spite of this, Sanef Motorway company built a 1740 km highway with hydrated lime treated bearing course and reported that the hydrated lime increases the durability of the asphalt mixture by 20-25% (EULA, 2011). The effect of hydrated lime on asphalt mixture is as shown in Figure 2.14.

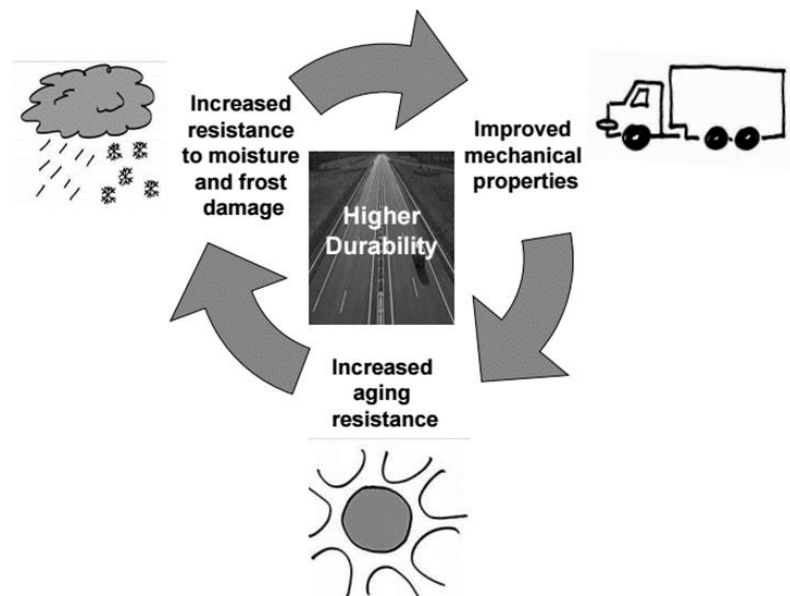


Figure 2.14. Hydrated lime effect on asphalt mixtures (EULA, 2011)

2.4.1 Production of Hydrated Lime

To understand the chemical composition of hydrated lime, it is important to know the production process of hydrated lime. The mechanism starts from crumbling of raw material, limestone and it continues with burning and adding water (Figure 2.15).

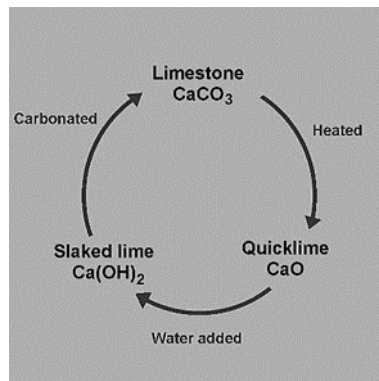


Figure 2.15. The Lime Cycle (Wikipedia, 2019)

Hydrated lime, which is a white powder material that has a particle density around 2.2 Mg/m^3 and apparent density ranging from 0.35 to 0.80 Mg/m^3 is basically a material obtained by burning limestone at high temperatures, removing carbon dioxide and then adding water. The first stage of the reaction is referred to as quicklime removed from carbon dioxide that is illustrated in Equation 2.4.



The equation shows that calcium carbonate (CaCO_3) is separated into two phases as solid (CaO) and gas (CO_2) as a result of heat treatment (around 900 degrees). Carbon dioxide produced as a result of the burning process is removed with the kilns. When water added to quicklime, a completely different material, hydrated lime, is obtained.

The hydration process starts with the addition of water at the boiling point to the quicklime and with this application it is believed that the water moves to the pores of the lime particles. As a result, the particles are broken and new surfaces are formed where the water can move. During the slaking process, the volume expands about 2.5-3 times because of the reaction of lime and water. It must be noted that calcium oxide is the only compound that can combine with water (Lazell, E.W., 1915). The chemical reaction is illustrated in Equation 2.5.



2.4.2 Effect of Hydrated Lime on Asphalt Mixtures Properties

Hydrated lime is a multifunctional additive and according to Lesueur (2010), its effects on asphalt mixture are categorized as follows:

- Moisture damage resistance
- Chemical ageing resistance
- Improving mechanical properties

Moisture damage is a type of distress which weakens the bond between bitumen and aggregate and causes aggregate loss (stripping) after a while. Another type of water induced damage is flushing which is loss of aggregate occurs from the bottom layer of pavement.

Table 2.1 Importance of hydrated lime according to usage areas.

Road agency / State of USA	Resist stripping	Improve aging resistance	Stiffen binder	Improve fracture toughnees	Alter properties of fines
Arizona	1	3	2	3	2
California	1	2	3	3	3
Colorado	1	3	3	3	1 (when appropriate)
Federal HighWay Administration (FHWA)	1	2	3	2	3
Georgia	1	3	3	3	3
Mississippi	1	1	2	—	3
Nevada	1	3	3	2	1
Oregon	1	2	3	3	3
South Carolina	1	2	2	2	2
Texas	1	3	2	3	2
Utah	1	2	2	2	2

Level of importance: 1- very important. 2- moderately important. 3- less important (Hicks. R. G. and Scholz.T. V.. 2003)

According to the research conducted in 2003, as shown in Table 2.1, preventing moisture damage has been identified as a first purpose for using hydrated lime. Hydrated lime reacts with both aggregate and bitumen separately and acts as an anti-stripping agent. It modifies the aggregate surface and strengthens the bond between the asphalt and aggregate. The polar molecules in the bitumen are neutralized by hydrated lime and are prevented from spreading to the bitumen and aggregate interface. Only non-acidic surfactants can be found in this interface and these molecules cannot be easily replaced with water. This allows increasing the moisture resistance of HMA (Huang et al., 2005).

It is believed that hydrated lime can reduce the chemical aging of bitumen. Aging can be defined as hardening of asphalt binder due to oxidative aging or evaporation of volatiles in bitumen. Aging may occur during the production of bitumen or throughout its service life. Aging levels should be considered when evaluating the mechanical properties of bitumen. There are generally 3 different levels of aging:

- 1) Unaged bitumen: obtained as neat form directly from the refinery and its viscosity is important for determining the workability

- 2) Short-term aged bitumen: aged during the production of the mixture, placement and compaction.
- 3) Long-term aged bitumen: highly aged at the end of pavement's service life.

According to the study conducted by Chachas et al. (1971), recovered bitumen obtained from the field aged mixtures prepared with hydrated lime was found to be softer than the reference samples. Also, it was found that aging of modified bitumen with hydrated lime has less sensitivity and the viscosity increases more slowly in comparison with untreated asphalt mixture (Petersen et al., 1987). The reason is the addition of hydrated lime decreases the carbonyl formation and increases the asphaltenes content. This situation reduces hardening susceptibility (Verhasselt & Puiatti, 2004).

The effect of HL as a filler on pavement over different temperatures has been explored by many researchers. Due to the behavior of physical filler, stiffening impact is quite high but when the temperature falls below 25°C, the effect begins to decrease (Wortelboer et al., 1996; Hopman et al., 1999; Khattak and Kyatham, 2008; Lesueur and Little, 1999; Pilat et al., 2000; and Lackner et al., 2005). Dealing with this, Lesueur et al. (2013) suggested that at high temperatures, voids in HL particles are filled with bitumen so it increases the volume fraction of particles, but when the temperature falls below, that bitumen filled particles becomes deformable.

Figure 2.16 shows the effect of hydrated lime and limestone filler comparison with the same bitumen type (70/100) at 10 radians. The results show that the stiffening effect of hydrated lime is apparent at high temperatures and decreases with the decreasing temperature.

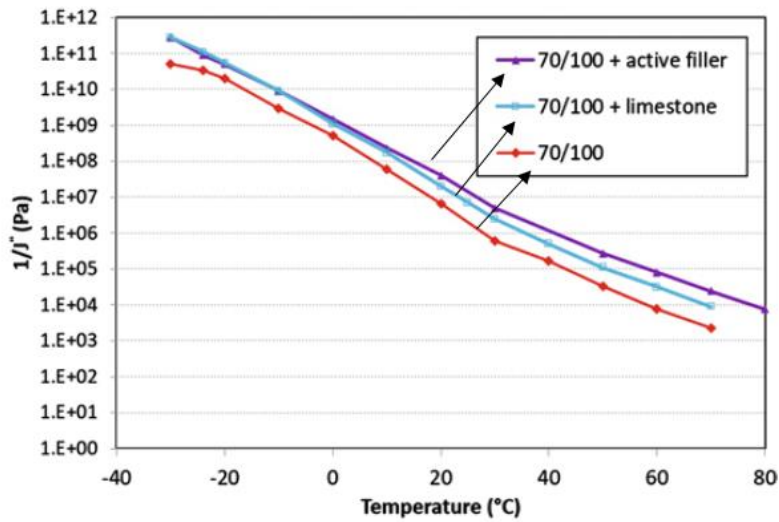


Figure 2.16. Stiffening effect of limestone filler and hydrated lime vs temperature (After Wortelboer et al., 1996)

The durability of a bond between aggregate and bitumen varies according to the type and size of aggregate, etc. The usage of siliceous aggregates makes this bond difficult to be durable. While cationic surfactants in bitumen can bond with silica atoms, anionic surfactants are replaced by water (Curtis et al., 1993).

According to Leseueur et al., (2013), HL has a solubility effect which is a sufficient solvent to precipitate calcium ions on the aggregate surface. Accordingly, when siliceous sands and gravels treated with HL, they gain moisture damage resistance. Accordingly, moist aggregate surfaces treated using HL (Blazek et al., 2000). By using HL as aggregate surface treatment, as a result of the interaction of the carbon dioxide in the atmosphere with HL, results in the precipitation of calcium carbonate. This results in higher surface area due to high roughness. It also forms a more secure bond with bitumen (Ramond and Lesueur, 2004).

According to Lesueur (2013), the modifying effect of HL on siliceous aggregate surface cannot be expected for limestone aggregate, but the usage of HL improves the bond between bitumen and aggregate surface (Huang et al., 2005; Mohammad et

al., 2008). It has been proven by many researchers that HL changes and stabilizes clay properties.

Lesueur and Little (1999) used the Marion-Pierce method in assessing the stiffening effect. and offered the following Equation 2.6.

$$\eta_0 = \eta_{0,m} \left(1 - \frac{\phi}{\phi_m}\right)^{-2} \quad (2.6)$$

where $\eta_{0,m}$: viscosity of unmodified asphalt; η_0 : filled asphalt's viscosity; ϕ_m : maximum packing factor; and ϕ : filler's volume fraction.

According to this study, in most minerals ϕ_m value is about 63%. The maximum packing factor, ϕ_m , is a parameter related to Rigden air voids defined as compacted filler's air void.

Lesueur and Little (1999) investigated the effects of adding 4% and 7.5% limestone filler and hydrated lime in two different bitumen samples (AAD and AAM) that have different chemical compositions at high temperatures ranging from 50 to 100 °C. In the first one, there are high asphaltene and polar chemical content; the other contains very low asphaltene and has less polarity. At the end of the study, the bitumen samples were substantially stiffened due to fillers at high temperatures. The fillers were substantially hardened at temperatures between 50 and 100 ° C; however, for the bitumen type AAD-1, when ϕ_m is only 20% for hydrated lime used as a filler, while the value of ϕ_m for limestone used as a filler is about 63%. The results of this study as given in Figure 2.17.

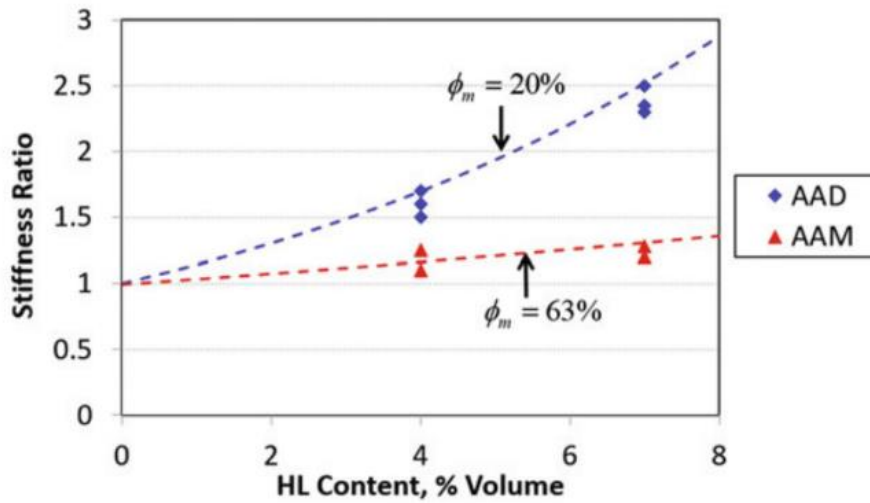


Figure 2.17. HL volume fraction versus stiffness ratio graph (After Little and Petersen. 2005)

To compare the stiffening effects of limestone and HL on bitumens of AAD and AAM, Kim et al., (2003) used the dynamic shear rheometer (DSR). They used the data to calculate the generalized Einstein coefficient and maximum volumetric packing factor. The result of this study, as given in Figure 2.17, show that stiffening effect of hydrated lime is higher than limestone.

2.4.3 Effect of Hydrated Lime on Low-Temperature Performance of Asphalt Concrete

Lesueur and Little (1999) prepared beam specimens with neat bitumen and HL added bitumen and loaded them monotonically with a speed of 1.2 mm/min up to -30°C until it failed. Fracture toughness data were recorded (Table 2.2) according to ASTM E 399. Fracture toughness were evaluated after TFO-PAV aging. They also compared the surface energy values for two types of bitumens. When the Table 2.2 is analyzed, it is seen that fracture toughness is improved with the use of HL and doubles this value when used at 20% of the bitumen weight.

Table 2.2 The effect of adding HL on bitumen fracture toughness (After Little and Petersen. 2005)

Bitumen	Unaged		Aged	
	0% HL	20% HL	0% HL	20% HL
AAD	38 ± 12	71 ± 23	40 ± 10	71 ± 6
AAM	34 ± 5	67 ± 4	37 ± 8	69 ± 19

Figure 2.18 shows the fracture toughness ratios in comparison with HL added and neat bitumen. The results show that the ratio of fracture toughness values is much higher in HL added samples. According to this study, it is thought that HL is more effective in distributing crack energy.

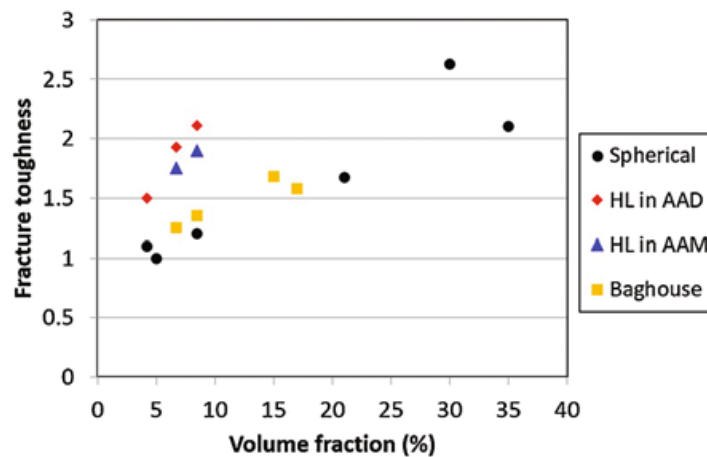


Figure 2.18. Fracture toughness (After Little and Petersen .2005)

Petersen et al. (1987) tested ribbon-shaped specimens for tensile elongation at brittle fracture region. The results showed that the HL-containing mixtures were more elongated than those that were untreated before the low temperature cracking (Table 2.3). The aged samples containing HL were, therefore, more flexible in the brittle temperature zone. The bitumen added to the HL result in higher performance

pavement. By further elongating under the ductile flow, the pavement will behave more resistant to fracture and transverse cracking at low temperatures.

Table 2.3 Comparison of tensile elongation data (Petersen et al.,1987)

Asphalt	Treatment	Temperature (°C)	Elongation ^a (%)	Tensile Stress ^b (kPa)	Elongation At Maximum Tensile Stress ^c	Stiffness Modulus (kPa)
Boscan	None	-5	10.6	560	10.2/710	2.24×10^4
		-10	4.8	830	4.1/850	3.68×10^4
	20% Limestone	-5	4.0	1,000	3.5/1,100	6.19×10^4
		-10	2.8	1,680	2.8/1,680	1.13×10^5
	20% High-calcium lime	-5	15+	680	15.0/680	2.06×10^4
		-10	11.7	1,170	9.8/1,240	4.37×10^4
West Texas-Maya blend	None	-5	5.5	650	4.5/850	3.24×10^4
		-10	4.4	1,340	4.4/1,340	4.89×10^4
	20% Limestone	-5	4.0	1,580	3.7/1,750	8.74×10^4
		-10	0.75	1,310	0.8/1,310	1.56×10^5
	20% High-calcium Lime	-5	13.0	920	9.8/1,170	4.06×10^5
		-10	8.3	2,170	8.3/2,170	6.12×10^4

2.4.4 Hydrated Lime Chemical Interactions

It is essential to understand the reaction mechanism formed by HL with bitumen. Reducing the interactions in the asphalt microstructures is one of the known features of hydrated lime, reducing the harmful effects of these structures. Unlike other mineral fillers, hydrated lime is chemically highly reactive. Due to low molecular weight, chemical reaction of HL has high relative concentration. The basic structure of HL provides the formation of insoluble calcium salts by reacting with carboxylic acids. As HL is not dissolved in bitumen, acidic components are separated from the asphalt base by adsorption on HL particles.

Petersen et al. (1987) carried out the analysis from the Boscan asphalt, which has irreversibly adsorbed components on the hydrated lime particles (Table 2.4). That

particles separated from bitumen by dissolving in toluene; then particles were filtered and washed. Results show that the adsorbed components contain approximately 5% bitumen and highly acidic elements. These components were removed by hydrated lime and the remaining 95% asphalt was not adsorbed by lime.

Table 2.4 Components adsorbed and not adsorbed on HL (Petersen et al., 1987)

Asphalt fraction	Percent of total asphalt	Concentration, mol/1,000 g	
		Carboxylic acids	2-Quinolone types
Adsorbed on high-calcium lime	5.6	0.83	0.15
Adsorbed on dolomitic lime	4.7	0.80	0.23
Not adsorbed on high-calcium lime	94.4	<0.005	<0.005
Not adsorbed on dolomitic lime	95.3	<0.005	<0.005

Then it is worth questioning how adsorption of carboxylic acid and 2-quinolone-containing components could change the physical properties of unabsorbed bitumen. The answer to this can be given based on the data in Figure 2.19, which was derived from a thermodynamic study by Peterson, (1971). Accordingly, Carboxylic acid and 2-quinolone interact with each other to generate hydrogen-bonded dimers.

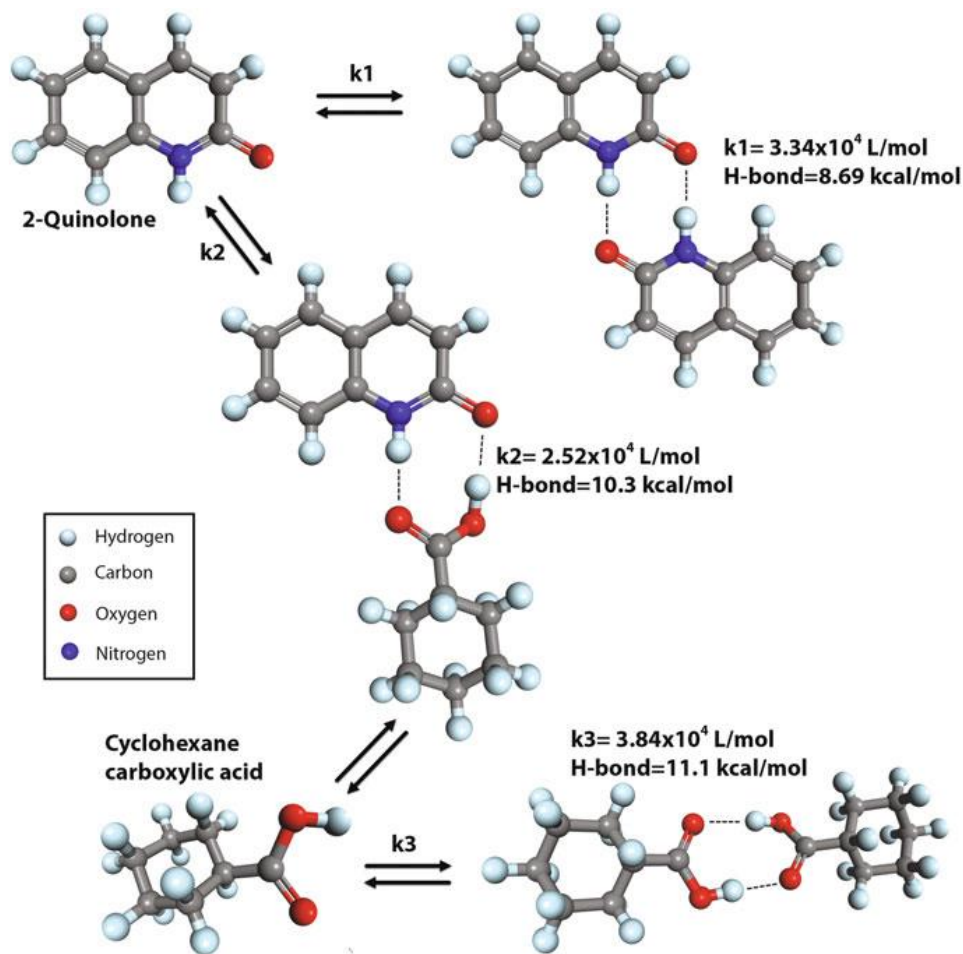


Figure 2.19. Illustration of strong hydrogen bonding (Petersen & Glaser. 2011)

Studies have shown that the effect of HL is dependent on the source of bitumen, and that the bitumen containing highly polar, high asphaltene responds more to the HL effect. Many studies have also shown that the most critical impact increases the δ value and improves the low temperature flow and aging characteristics.

2.4.5 Addition Techniques of Hydrated Lime to Asphalt Mix

The performance of asphalt – hydrated lime mix depends also on the mixing technique. There are several methods for the addition of hydrated lime to asphalt mixtures according to National Lime Association:

- Hydrated lime into drum mixer
- Hydrated lime added to aggregate in pug mill
- Dry hydrated lime added to moist aggregate with marination
- Slurry lime added to aggregate with or without marination

The methods of adding HL to the aggregate are summarized in Table 2.5 and preferred lime addition methods in different states of America are specified.

Table 2.5 Hydrated lime addition methods (National Lime Association., 2003)

State	Method of Adding Hydrated Lime to Asphalt				
	In Drum	Dry Hydrated Lime to Dry Aggregate	Dry Hydrated Lime to Wet Aggregate	Lime Slurry to Aggregate	Is Lime-Treated Aggregate Marinated?
Arizona			√*		No
California				√*	Required
Colorado			√*	√	Optional
Georgia	√	√**			No
Mississippi			√		No
Nevada			√		Required
Oregon			√*		Optional
South Carolina			√*		No
Texas	√		√*	√	No
Utah				√*	Optional

* Hydrated lime and wet aggregate mixed in pug mill

** Hydrated lime added this way for both batch and drum plants

Method of injection into drum was used in early 1980s of Georgia by injecting hydrated lime at the downstream of the point. The aim of adding hydrated lime close

to the asphalt is to reduce the carried exhaust gases into the baghouse. Also, HL was thought to interact with bitumen rather than aggregate. To prevent the production of exhaust gases, they improved methods, either increasing the length of the drum or using double drums, which are static and rotating at the drying and heating phase.

Adding hydrated lime to aggregate in a pugmill is another technique. The silo is refilled by pneumatically. Hydrated lime delivered from the silo to the weigh pot and transferred to the pugmill. Before the mixing process, aggregates should have at least 3% of water content. Mixing occurs in pugmill and from there, hydrated lime – aggregate mixture sends to the drum mixer.

Another technique is adding dry hydrated lime to moist aggregate, followed by marinating the treated aggregate. Required hydrated lime must be at the range of 1-2.5 % of the mass of the dry aggregate. It is recommended that moisture content has to be 3 percent for coarse aggregate and 6 percent for fine aggregate during the mixing step. With moisture on the aggregate surface, lime is dispersed and ionized on the aggregate surface.

Mixing lime slurry with aggregate have also been used. After the mixing process, the mixture is transferred directly to the hot mix asphalt facility. The use of lime slurries adds more water than ordinary usage and it may increase the water content at aggregate. Usage of lime slurries needs specialized equipment.

Marination is very common in California, Nevada, and Utah. While the aggregate is stockpiled during marination, the moisture content of the mixture will decrease; as a result, the resistance to moisture damage will be improved in the lime-aggregate mixture. If the marination period is kept too long, the lime content, however, can be reduced by washing out of the aggregate, which must be monitored carefully in field to prevent this problem.

2.5 Tests Performed to Determine The Thermal Properties of Asphalt Concrete

For the last decade, different tests have been used to determine the measurement of asphalt concrete's low temperature performance. These tests include, for example, Indirect Tensile Test (IDT), Direct Tension Test (DTT) and Thermal Stress Restrained Specimen Test (TSRST). According to Vinson et al. (1989), the following factors influence the selection of a testing method:

- The importance of simulating field conditions
- Appropriateness of test results for the mechanistic models
- Methods used for aging test specimens
- Ease of performing test procedure
- Equipment and operational cost of testing equipment

2.5.1 Thermal Stress Restrained Specimen Test

Vinson et al. (1989) found that TSRST provides the most reliable method for evaluating the low temperature cracking resistance of asphalt concrete. Application of this testing machine dates back to 1960s when researchers fabricated TSRST for characterizing the response of asphalt when exposed to low temperatures (Monismith, et al., 1965; Fabb, 1974; Carpenter, 1983; Arand, 1987; Sugawara, et al., 1984; Janoo, 1989 and 1993).

One of the basic (or the most fundamental) features of TSRST is maintaining specimen length when the specimen is subjected to temperature changes. Maintaining the specimen length when the temperature drops, results in the generation of thermally induced tensile stresses. The test equipment is designed to test the sample with minimum user input, collect data and report the results. Test system is composed of a step motor applying load, a rigid frame, load and temperature control systems, a data acquisition system, sample alignment stand, and

software that is shown on Figure 2.20. Of course, all the interactions including controlling the TSRST and acquiring the data are coordinated using a computer system.

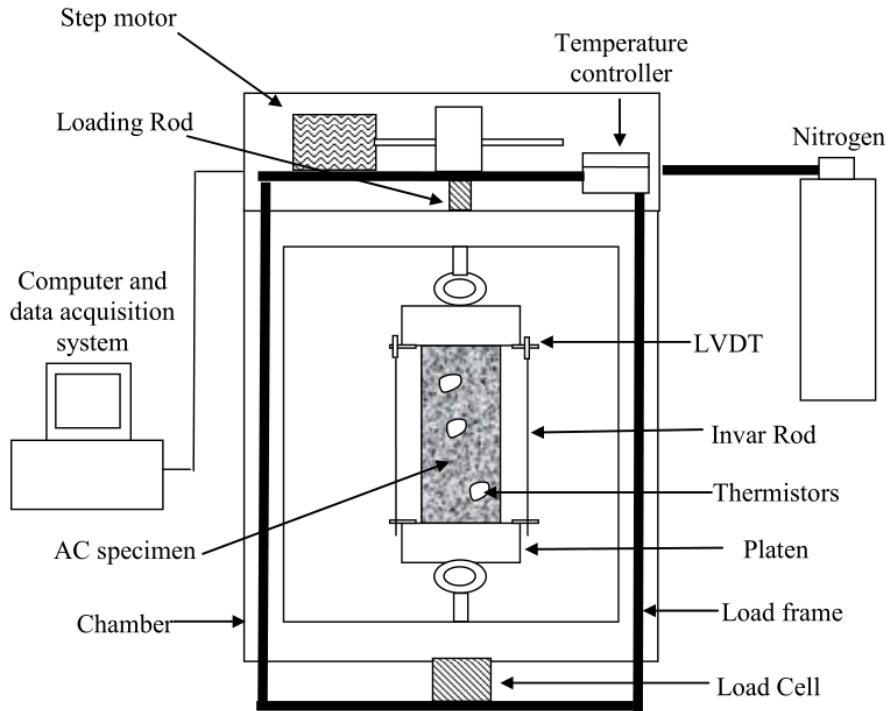


Figure 2.20. TSRST device (Marasteanu et al., 2007)

Test starts with placing the sample into cooling chamber and subjecting it to a cooling rate of $10^{\circ}\text{C}/\text{hour}$ using liquid nitrogen that is sprayed into the environmental chamber of TSRST. The sample contracts as it cools down, but there is a closed loop electronic system that implements an external tensile load on the sample to avoid the sample length from changing (Jung and Vinson, 1994). TSRST is also equipped with two Linear Variable Differential Transformers (LVDTs) to measure the thermal strain of specimen.

The air is circulated by the fans that are embedded into the environmental chamber. A resistive temperature detector (RTD) is used to control the temperature inside the chamber. The temperature controller calculates the amount of nitrogen that should

be supplied/sprayed to reach the target temperature. TSRST can apply both monotonic and cyclic loads. The outputs of the TSRST are fracture strength and temperature. Typical results for both monotonic and cyclic loadings are presented in Figures 2.21 and 2.22.

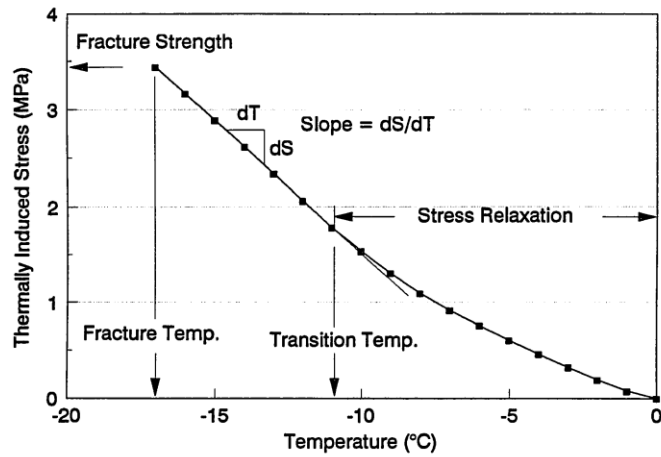


Figure 2.21. Thermally Induced Stress Curve from a Monotonic Cooling (after Jackson, 1992)

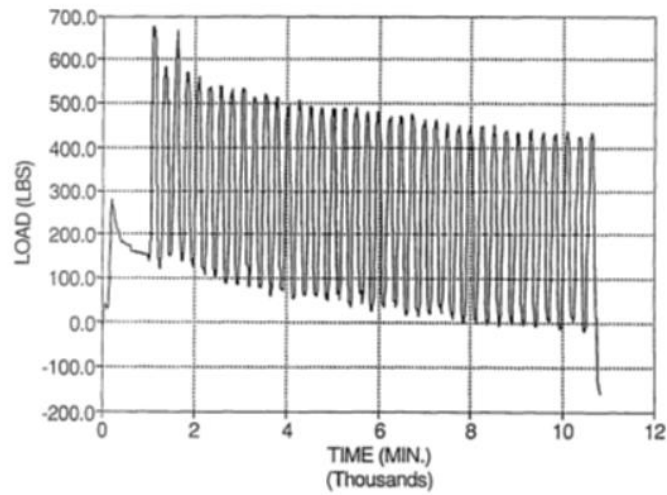


Figure 2.22. Thermally Induced Stress Curve from a Cyclic Cooling (after Jackson, 1992)

2.5.2 The Indirect Tensile Strength Test

The Indirect Tensile Test (IDT) is used to determine the rutting and thermal cracking potential of asphalt mixtures at appropriate loading rates. In this test, the disc-shaped samples are subjected to a constant load along the vertical loading axis. An indirect tension occurs in the direction of the sample diameter (see Figure 2.23).

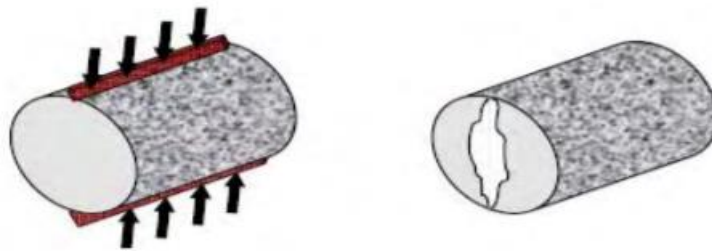


Figure 2.23. IDT Strength Test (Shodhganga, 2019)

Roque and Buttlar (1992) stated that IDT was able to simulate the stresses caused by traffic-related dynamic loads on the pavement surface and therefore provide a suitable evaluation technique for the determination of the asphalt mixture strength. Creep compliance is calculated from horizontal and vertical deformation data (Roque and Buttlar, 1992). The cracking temperature is the temperature at which thermal stresses generated equal to tensile strength; therefore, asphalt concrete specimens should be tested at different temperatures. Such way of low characterization allows the determination of the low temperature performance of the mixtures under thermal loading (s). However, IDT creep and strength tests require complex analyses to determine the fracture temperature and equivalent thermal stresses of the mixtures. Epps, (1998) and Marasteanu et al. (2007) found that the fracture temperatures obtained from TSRST were higher than those estimated using IDT. Epps (1998) attributed the reason for such discrepancy to the selected failure assumptions (tensile strength and temperature that tensile strength determined) rather than properly simulating the conditions occurring in the field.

Compressive load results in the formation of indirect tensile stress in sample. The tensile stress that results in the fracture of specimen is calculated using the following Equation 2.7.

$$S_t = \frac{2000 P}{\pi t D} \quad (2.7)$$

where S_t =IDT strength, kPa; P = Load that specimen fractured, N; t = Specimen height, mm; and D = Specimen diameter, mm

2.5.3 Direct Tension Test

Direct tension test (DTT), developed by Haas (1973), is a method used to determine the tensile properties of asphalt mixtures at low temperatures. The test is performed under constant tensile stress applied on a rectangular specimen until it is fractured (Figure 2.24).



Figure 2.24. Fractured DTT specimen

Although French (1979) and others have reported that DTT can be successfully performed, there are still some difficulties in achieving repeatability. Preparation of the sample takes a long time and requires a skilled technician, although the test itself is simple and short.

Needless to say, height to diameter ratio and maximum aggregate size are all important factors for DTT results. The sample preparation techniques (gluing, alignment, etc.) are of great importance to ensure the broken plane is sufficiently far away from the ends and, of course, perpendicular to the sample axis.

Among controlling parameters of DTT, the rate of extension and test temperature are very important factors for the reliability of test results. According to Roberts et al. (1996), the appropriate temperature range to measure the tensile stress of a mixture should be between -46°C and 0° . Deformation rate is one of the key parameters that should be selected carefully, because inadequate strain rate allows the mixture to relax excessively. Haas (1973) suggested a range between 2.4 to 12 cm/s. A detailed literature survey is provided in Table 2.6.

Table 2.6 Literature survey for used temperature and strain rates in DTT (Karakaya, 2015)

Researchers	Temperature range ($^{\circ}\text{C}$)	Strain rate
Jackson, 1992	-17.8 and -34.4	8.5e-6 cm/s
Jung & Vinson, 1996	-30 to +5	1.0 mm/min
Huang et al., 2003	-12 and 0	N.A.
Gonzalez et al., 2006	+8.3 and +20	1 to 0.0057 mm/min
Mun & Lee, 2010	-10 and +5	0,001 ϵ/s
Wang et al., 2011	-35 to -10	N.A.
Lee et al., 2011	5	2.1e-5 to 5.5e-5 ϵ/s
Xie et al., 2011	15 and 25	0.1 to 18 mm/min
Lee et al., 2012	5	N.A.
Forough et al., 2013	-7 to +21	1.27 mm/min
Underwood & Kim, 2013	10	0.6902 ϵ/s
Yoo & Al-Qadi, 2013	25	0.02 mm/s
Hamzah et al., 2013	15	25.4 mm/min
Zeng et al., 2014	5	5 mm/min
Yoo & Kim, 2014	20	0.02 mm/s

2.6 Test Methods to Evaluate The Effect of Hydrated Lime on Asphalt Binder

Hydrated lime is a mineral filler with particles sizes smaller than about 74 μm . The unique properties of hydrated lime influence the rheological properties of bitumen (Rodriquez et al., 1995; Lesueur et al., 1995; Lesueur and Little, 1999; Anderson et al., 1996; Craus et al., 1978; Petersen et al., 1987a, b, c, d; Johannson, 1998; Johannson et al., 1996; Bahia et al., 1992). It is reported that binder properties significantly affect the low temperature performance of asphalt mixture (Isacsson and Zeng, 1998). The effect of hydrated lime on bitumen can be determined using the following testing and analyses methods:

- Dynamic Shear Rheometer (DSR)
- Dynamic Mechanical Analysis (DMA)
- Rotational Viscosity Test (RV)
- Scanning Electron Microscope (SEM) Analysis

2.6.1 Dynamic Mechanical Analysis Technique

Dynamic Mechanical Analysis (DMA) is a popular and efficient technique that is used for measuring transitions in materials (Figure 2.25). DMA characterizes the mechanical responses of materials. With DMA, the viscous and elastic components of bitumen are determined. The dynamic response of a visco-elastic material is separated into two parts, the elastic part (E') and the viscous damping component (E''). If the tested sample is fully elastic, the stress and strain phase difference (time lag) become zero degrees (Figure 2.26).



Figure 2.25. Perkin Elmer Pyris Diamond DMA analyzer

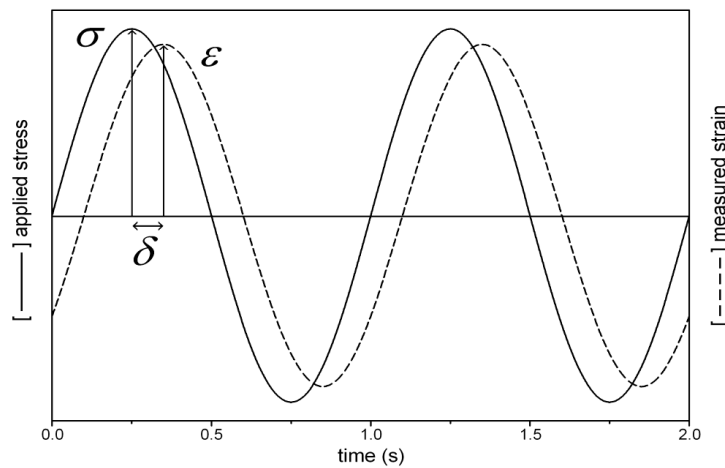


Figure 2.26. Stress and strain as a function of time with dynamic (sinusoidal) loading (Ward and Hadley. 1993).

When a material is completely viscous, the phase difference becomes 90° . But most of the materials show viscoelastic properties and act as an elastic solid or viscous liquid. These types of materials show the phase difference between extremes and such phase difference is used to determine:

- Storage and loss modulus
- Loss factor

- Complex and dynamic viscosity
- Transition temperatures
- Creep and stress relaxation (William and Perkins, 1999).

DMA analyzer is used for calculating the viscoelastic properties with the help of transient or dynamic oscillatory movements. Performing creep relaxation test, the stress is applied to the sample and this stress is kept constant while the time-dependent deformation is measured. After a short time, the stress is removed and the amount of recovery is measured. When performing stress relaxation test, a constant deformation is applied to the sample and the stress required to maintain this deformation is calculated. Then, the sample is released in the unstressed state and the recovery is determined with respect to time. Most DMA measurements are performed using single frequency or constant deformation (strain) with shifting temperature (Sepe, 1992).

With ideal viscoelastic materials, a time-dependent stress is applied within a time window of t and at variable angular frequencies. Equation 2.9 provides more information on dependence of such stress on the other variables.

$$\sigma(t) = \sigma_0 \sin \omega t \quad (2.9)$$

where $\sigma(t)$: applied stress; ω : angular frequency; σ_0 : amplitude; and t : time
the stress vector is known as the sum of two components such as Equation 2.10 and 2.11.

$$\sigma' = \sigma_0 \cos \delta \quad (2.10)$$

where σ' : in phase with deformation; σ_0 : amplitude; δ : phase angle;

$$\sigma'' = \sigma_0 \sin \delta \quad (2.11)$$

where σ'' : out of phase with deformation; σ_0 : amplitude; and δ : phase angle

The real modulus or storage modulus G' , refers to the measurement of rigidity and resistance to deformation of sample. It is expressed by the Equation 2.13.

$$G' = G^* \cos \delta \quad (2.13)$$

where G^* : complex modulus; and δ : phase angle

The imaginary or loss modulus G'' refers to the loss of mechanical energy through dissipation. It is expressed by Equation 2.14.

$$G'' = G^* \sin \delta \quad (2.14)$$

The complex modulus, shown in figure 2.26, can be calculated as shown in Equation 2.15.

$$G^* = \sqrt{(G')^2 + (G'')^2} \quad (2.15)$$

Glass transition temperature (T_g) is an essential property of amorphous materials. Below this temperature, the energy required for large amplitude molecules to move is quite low. Approaching the thermodynamic equilibrium is rather slow without this movement. Such slow fashion of reaching thermodynamic equilibrium causes the material to age physically. The glass transition, considered an Ehrenfest second-order transition, manifests itself by showing variations in the thermodynamic related properties such as specific volume, thermal coefficient of expansion/contraction and specific heat capacity (Turner et al., 1997).

There are various analysis techniques for determining the glass transition temperature. These are thermal (Wunderlich, 1981), physical (Kovacs, 1964), mechanical (McCrum et al., 1967) and electrical (Hutchinson et al., 1992) techniques. The glass transition temperature is the temperature at which a cooled viscous amorphous material is subjected to a hard, glassy condition or vice versa.

This temperature, in the context of rheological experiments, can be defined as follows (Rieger, 2001):

- 1- The temperature at which G' reaches a constant value
- 2- The temperature at which $\tan\delta$ reaches the maximum value
- 3- The temperature at which G'' reaches its maximum value
- 4- The temperature at which G' reaches the maximum variation with frequency

It should be noted that T_g depends on the time or frequency at which measurements are performed. Although definition number 2 is widely used to find glass transition temperature, according to some researchers, using definition number 3 will be more practical for this purpose (Boyer, 1977).

2.6.2 Dynamic Shear Rheometer

DSR is used for executing DMA in bitumen samples (Anderson et al., 1994). In the DMA, sinusoidal strain is applied to the sample and the resulting stress is acquired as function of frequency. This type of test is called strain controlled that is quite common. DSR can also determine the viscoelastic properties of bitumen - through sinusoidal loading mode; in this way, the resulting stiffness and viscosity responses are obtained at different temperatures, stress-strain levels and test frequencies.

DMA requires preparing samples sandwiched between DSR parallel discs as shown in the Figure 2.27. After preparing and placing the samples between the plates, sinusoidal strain is applied. The resulting stress is calculated based on the torque transmitted in response to the strain applied.

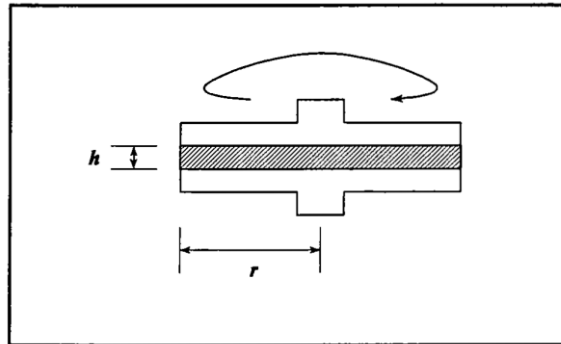


Figure 2.27. DSR testing geometry

The strain applied during DMA should be kept as small as possible to keep the test in a linear viscoelastic zone. This value should be maintained below 0.5 percent at low temperatures, but may increase at high temperatures (Goodrich, 1988).

Different disc sizes can be used for testing the rheological properties of bitumen. The higher the stiffness of the bitumen, the smaller the size (i.e., diameter) of the disc used for such testing purpose. If test temperature decreases, again due to increase in the stiffness of bitumen, smaller diameter discs must be used to accurately determine the dynamic characteristics and prevent (Goodrich, 1988) applying excess torque on DSR spindle.

2.6.3 Rotational Viscosity Test

Viscosity is generally defined as the resistance of fluid to the flow. In the context of viscosity, materials show two different behaviors: Newtonian and Non-Newtonian. The former behavior is indicative of a material whose viscosity does not depend on shear rate variations. The latter behavior is indicative of a material with variable shear stresses and shear strain ratios.

According to the study conducted by Kim et al. (2003 and 2004), viscosity of bitumen slightly increased with the addition of hydrated lime. To see the stiffening effect of hydrated lime in the mastic prepared with 5% mineral filler and 5% bitumen, 1% and 2% of mineral fillers were replaced with hydrated lime. The test results were evaluated using the softening point test. The results showed that samples

prepared with hydrated lime had a softening point of approximately 2.5° to 8°C higher than those containing no hydrated lime (European Committee for Standardization, 2009). In Table 2.7, stiffening effects of different mineral fillers were compared and it was observed that hydrated lime’s stiffening effect is twice higher than those of other filler materials (Lesueur, 2009).

Table 2.7 Viscosity of fillers (Lesueur, 2009)

Filler type	[η]
Limestone	3.8
Limestone	2.6 - 3.9 (25 °C) 3.0 - 3.7 (70 °C)
Limestone	2.5 (65 °C) 2.4 (135 °C)
Dolomitic limestone	4.9 (25 °C) 4.4 (70 °C)
Hydrated lime	3.2 - 10
Lime	7
Sandstone	2.8 (25 °C) 4.0 (70 °C)
Siliccous filler	2.4 (65 °C) 2.4 (135 °C)
Granite	2.7 - 4.2 (25 °C) 3.5 - 4.1 (70 °C)
Fly ash	10.2 (25 °C) 14.1 (70 °C)
Slate dust	4.2
Ball clay	3.2
Kaolin	6.7
Carbon black	2.6 (65 °C) 3.9 (135 °C)
Asbestos	16.5
Polyester fibers	26 - 34
Mineral fibers	26

It is widely accepted that temperature change has a great influence on viscosity. Studies show that viscosity decreases with increasing temperature (Masson et al., 2002). Stiffening effect of hydrated lime on low temperatures is similar to other mineral fillers (Lakner et al., 2005). In Figure 2.28, temperature-dependent stiffening effect of hydrated lime was compared with that of limestone filler. Two different mastics were prepared by mixing 70/100 bitumen with 50% limestone and a mixture of hydrated lime and limestone fillers containing 40% hydrated lime. The inverse of the imaginary compliance ($1 / J''$) versus temperature data, obtained at 10 rad / s, are

visualized in Figure 2.28. At higher temperatures, high stiffening occurs while it is normal at low temperature region (Wortelboer et al., 1996).

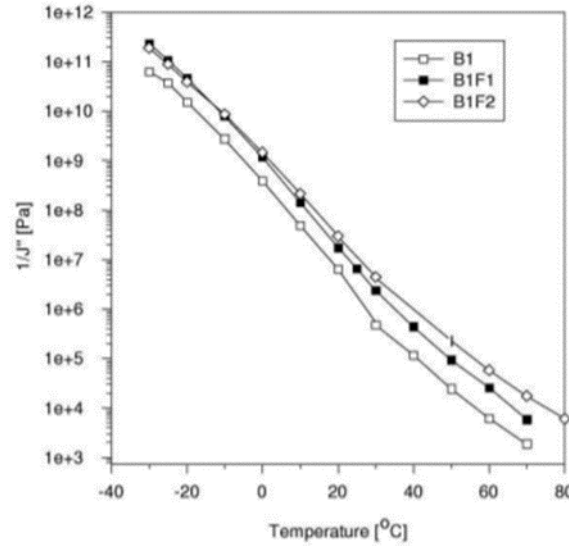


Figure 2.28. Hydrated lime temperature dependence stiffening effect

2.6.4 Scanning Electron Microscopy

Scanning Electron Microscope (SEM) is a machine used to determine the sample surface, morphology and composition. The electron beams – emitted from the electron gun of SEM - interact with the specimen and then produce signals from which surface topography and composition are detected and determined, respectively. According to previous studies, irregular structure of fillers can be observed by microscopic analysis (Ishai and Tons, 1977).

Antunes et al. (2015) conducted a series of studies, to define the physical properties of - and interaction between - bitumen, hydrated lime and other fillers. The results obtained from these studies proved the surface texture irregularity and cloudy shape of hydrated lime particles. Rizkiyantoro (2010) compared SEM images obtained from hydrated lime and ordinary Portland cement and concluded that small particle sizes and irregular shapes of hydrated lime particles are important reasons for the superior behavior of hydrated lime in terms of filling voids in the mastic and the resulting enhanced aggregate interlock.

CHAPTER 3

METHODOLOGY

3.1 Introduction

This section covers details on materials selection and sample proportioning for mix design. Besides, compaction of asphalt mixture samples and calculation of volumetric properties are discussed according to Superpave mix design methodology. Results of bitumen and mixture characterization tests according to relevant standards are presented. Procedure for producing test specimens from Superpave compacted samples are discussed. And finally, preparation of test setups for Indirect Tensile Test (IDT), Direct Tension Test (DTT) and Thermal Stress Restrained Test (TSRST) and testing procedures to measure low temperature cracking resistance of asphalt concrete specimens are illustrated in detail. All the laboratory investigations were performed in the transportation laboratory of the Middle East Technical University (METU). Mix designs and characterization of asphalt and bitumen are performed in accordance with ASTM and AASHTO standards as well as Turkish General Directorate of Highways (TGDH) specifications. Figure 3.1 visualizes the steps taken for accomplishing this study.

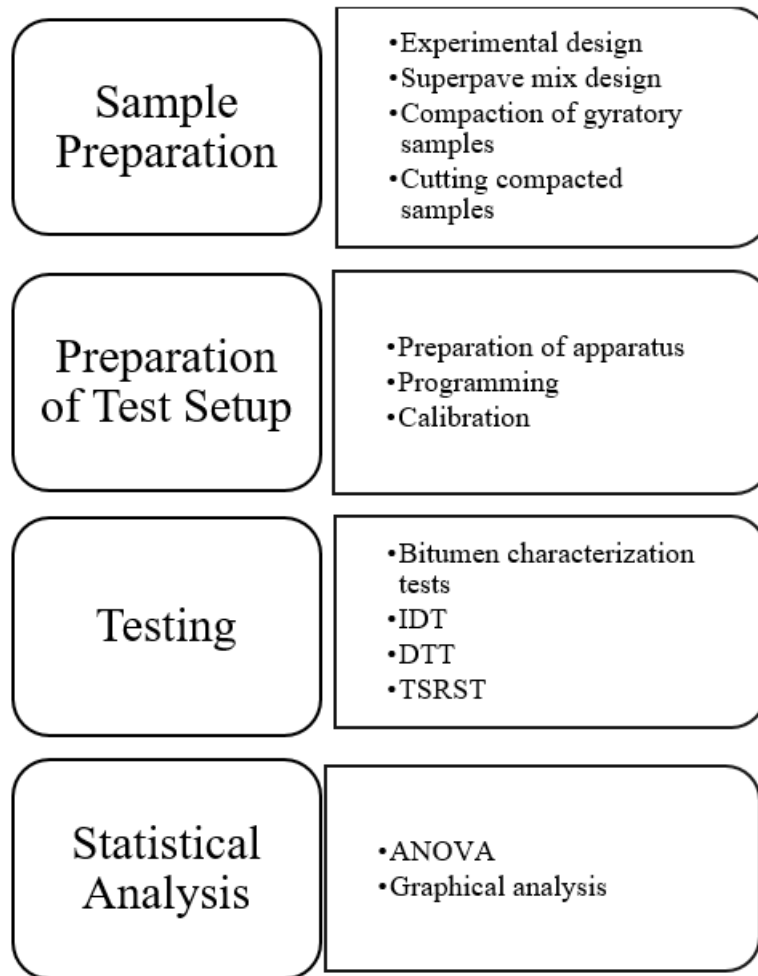


Figure 3.1. The outline of the tasks performed in Methodology section.

3.2 Sample Preparation

The sample preparation stage starts with the determination of the mix design variables which are aggregate type and gradation, hydrated lime content and whether the specimens are aged or not. After determining the mix design variables, the preparation of the samples to be tested took place in the following steps, respectively:

- Sieving
- Mixing
- Compacting mixture samples with gyratory compactor
- Producing beam specimens from compacted samples

- Calculating volumetric properties of the beam specimens

The mix design for test specimens used in the study were determined in a way that the effect of hydrated lime on low temperature cracking resistance for different aggregate types and gradations can be clearly demonstrated. Low temperature performance was also examined for long term oven aged specimens which were subjected to 85°C for 120 hours to simulate five to ten years of aging in the field according to AASHTO R30 procedures.

3.2.1 Design of Experiments for Laboratory Testing

For more than a decade, low temperature performance of asphalt concrete has attracted the attention of many researchers. The use of hydrated lime to improve low temperature resistance of asphalt concrete has not been thoroughly elaborated in the existing literature. To understand how lime content interacts with asphalt mixture from the perspective low temperature resistance, it necessary to investigate the effects of mix design parameters, i.e., aggregate type and gradation, optimum asphalt content, and aging of asphalt bitumen on low temperature cracking of HMA. For this purpose, an experimental program containing these variables was prepared and the number of test samples was determined. The flowchart in Figure 3.2 illustrates the experimental design used in the study. As indicated in Figure 3.2 two different types of aggregates, basalt and limestone, were used, and the aggregate fractions were adjusted to obtain two different gradations as course and fine. Each gradation was mixed with 50/70 bitumen and one group of these mixtures was modified with hydrated lime and the other group was prepared as neat, i.e., without hydrated lime. Afterwards, half of the test samples modified with hydrated lime and neat samples were aged for 5 days under 80 degrees in the oven according to AASHTO R30 specification. Each sample was also tested at two different temperatures (0°C and -10°C) in direct tension test and indirect tension test. Also, specimens were tested for the evaluation of low temperature cracking resistance using thermal stress restrained specimen test.

Optimum asphalt contents were calculated separately for each mix design combinations produced by changing aggregate type and gradation. Also, all mixture samples were compacted to a design air void content of 4%. In the experimental factorial design, the following variables were taken into consideration:

- Two types of aggregates (basalt and limestone).
- Two types of gradations (coarse and fine).
- Tested temperature (0 °C and -10°C).
- Aging (aged and not aged).
- Hydrated lime content (2% and 0%).

2⁵ two-level factorial design was selected for IDT and DTT (Table 3.1) whereas 2⁴ design was used for TSRST because of the fact that temperature is not a variable for TSRST, in which the test is started from initial temperature of 5 °C and dropped at a rate of -10 °C per hour. Hence, the design of experiment includes the main effects of aggregate type, gradation type, hydrated lime content and aging as depicted in Figure 3.2.

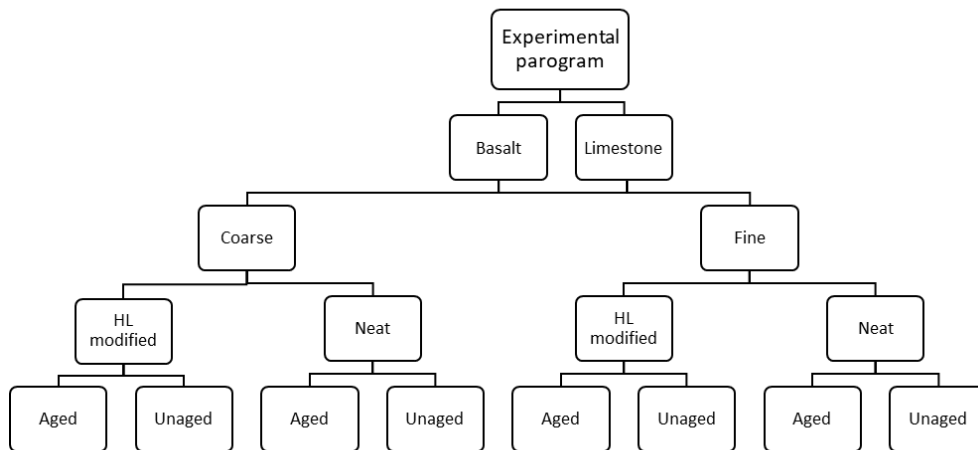


Figure 3.2. Flow diagram for fractional factorial experimental design.

In the scope of the study, a total of sixty-four (64) samples were produced to test at target temperatures 0°C and -10°C in IDT and DTT. In addition to this, sixteen (16) samples were prepared for the TSRST testing program. The test mixtures were compacted using a Superpave gyratory compactor, after which each sample was cut into specified dimensions to produce at least two replicates per testing combination. The design variables and the naming codes used for the DTT and IDT specimens are presented in Table 3.1, and for the TSRST specimens in Table 3.2. Later, by these data presented in Table 3.1 and Table 3.2, the specimens to be tested for IDT, DTT (Table 3.3) and TSRST (Table 3.4) defined by experimental design.

Table 3.1 Test variables used in DTT and IDT

Specimen no:	Name of variable	Variable code	Level	Symbols
1	Aggregate Type	X1	2 (+1,-1)	L.B
2	Gradation	X2	2 (+1,-1)	F.C
3	Aging	X3	2 (+1,-1)	H.Z
4	Lime Content	X4	2 (+1,-1)	A.U
5	Test Temperature	X5	2 (+1,-1)	0.10

Table 3.2 Test variables used in TSRST

Specimen no:	Name of variable	Variable code	Level	Symbols
1	Aggregate Type	X1	2 (+1,-1)	L.B
2	Gradation	X2	2 (+1,-1)	F.C
3	Aging	X3	2 (+1,-1)	H.Z
4	Lime Content	X4	2 (+1,-1)	A.U

Table 3.3 Two-level full factorial design matrix for DTT and IDT

No:	X1	X2	X3	X4	X5	Sample coding
1	-1	-1	-1	-1	-1	BCUZ10
2	-1	-1	-1	-1	1	BCUZ0
3	-1	-1	-1	1	-1	BCUH10
4	-1	-1	-1	1	1	BCUH0
5	-1	-1	1	-1	-1	BCAZ10
6	-1	-1	1	-1	1	BCAZ0
7	-1	-1	1	1	-1	BCAH10
8	-1	-1	1	1	1	BCAH0
9	-1	1	-1	-1	-1	BFUZ10
10	-1	1	-1	-1	1	BFUZ0
11	-1	1	-1	1	-1	BFUH10
12	-1	1	-1	1	1	BFUH0
13	-1	1	1	-1	-1	BFAZ10
14	-1	1	1	-1	1	BFAZ0
15	-1	1	1	1	-1	BFAH10
16	-1	1	1	1	1	BFAH0
17	1	-1	-1	-1	-1	LCUZ10
18	1	-1	-1	-1	1	LCUZ0
19	1	-1	-1	1	-1	LCUH10

Table 3.3 Two-level full factorial design matrix for DTT and IDT cont.

No:	X1	X2	X3	X4	X5	Sample coding
20	1	-1	-1	1	1	LCUH0
21	1	-1	1	-1	-1	LCAZ10
22	1	-1	1	-1	1	LCAZ0
23	1	-1	1	1	-1	LCAH10
24	1	-1	1	1	1	LCAH0
25	1	1	-1	-1	-1	LFUZ10
26	1	1	-1	-1	1	LFUZ0
27	1	1	-1	1	-1	LFUH10
28	1	1	-1	1	1	LFUH0
29	1	1	1	-1	-1	LFAZ10
30	1	1	1	-1	1	LFAZ0
31	1	1	1	1	-1	LFAH10
32	1	1	1	1	1	LFAH0

Table 3.4 Two-level full factorial design matrix for TSRST

No:	X1	X2	X3	X4	Sample coding
1	-1	-1	-1	-1	BCUZ
2	-1	-1	-1	1	BCUH
3	-1	-1	1	-1	BCAZ
4	-1	-1	1	1	BCAH
5	-1	1	-1	-1	BFUZ
6	-1	1	-1	1	BFUH
7	-1	1	1	-1	BFAZ
8	-1	1	1	1	BFAH
9	1	-1	-1	-1	LCUZ
10	1	-1	-1	1	LCUH
11	1	-1	1	-1	LCAZ
12	1	-1	1	1	LCAH
13	1	1	-1	-1	LFUZ
14	1	1	-1	1	LFUH
15	1	1	1	-1	LFAZ
16	1	1	1	1	LFAH

3.2.2 Materials Used in the Experimental Program

In this study, two different types of aggregates, basalt and limestone, were used which were obtained from the quarries in Ankara and Konya. The bitumen used was selected in accordance with Turkish General Directorate of Highways (TGDH) standards.

Before the design process, aggregate and bitumen properties to be used in the mixture should be determined. Since coarse and fine designs are made separately for dolomite and basalt, specific gravity, water absorption and percent loss using Los Angeles (LA) test values were determined for each aggregate gradation. The properties of the materials used are shown in the Table 3.5.

Table 3.5 Aggregate properties used in the study (a) limestone. (b) basalt

Measured Properties	Aggregates		Standard
	Limestone Fine	Limestone Coarse	
Specific Gravity	2.754	2.778	ASTM C127
Average Absorption (%)	0.685	0.614	ASTM C128
LA Abrasion Value (%)	18%	18%	ASTM C131

(a)

Measured Properties	Aggregates		Standard
	Basalt Fine	Basalt Coarse	
Specific Gravity	2.499	2.530	ASTM C127
Average Absorption (%)	1.978	2.177	ASTM C128
LA Abrasion Value (%)	14%	14%	ASTM C131

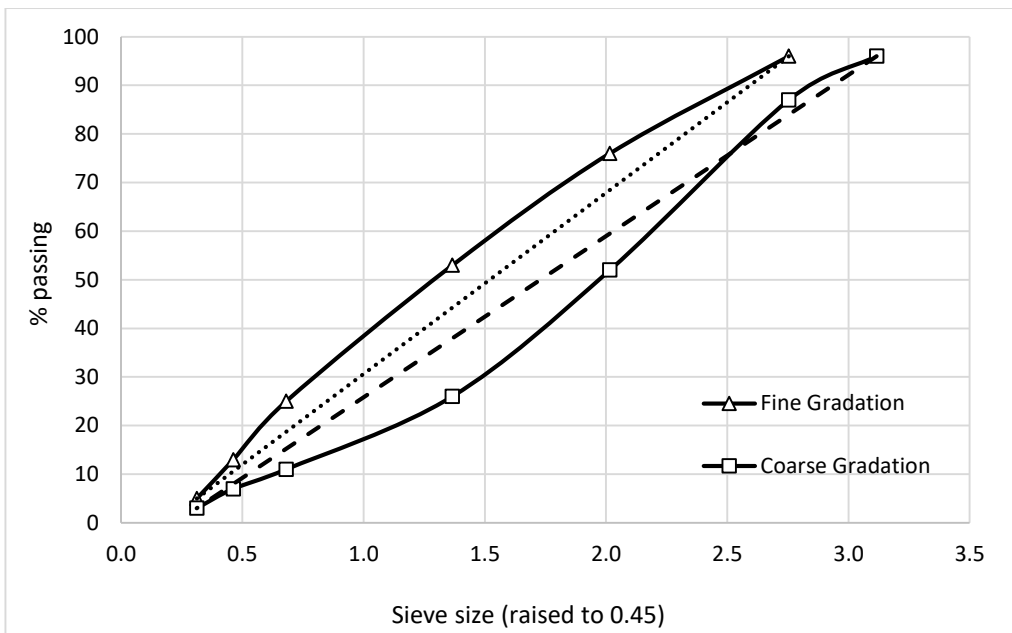
(b)

One type of binder that is 50/70 was used to fabricate the asphalt mixtures. Softening point, ductility, penetration, flash and fire point and specific gravity values of the bitumen were determined according to the relevant specifications (Table 3.6).

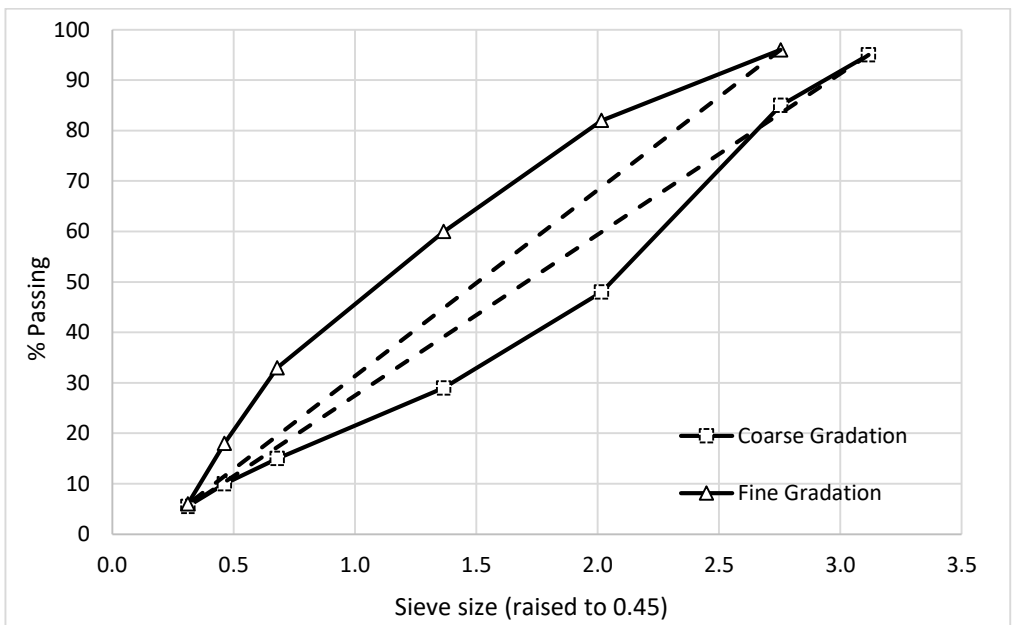
Table 3.6 Asphalt binder properties

ASPHALT BINDER PROPERTIES		SPECIFICATION
Penetration	55	ASTM D5
Ductility	>100	ASTM D113
Flash & Fire	304°C & 345 °C	ASTM D92
Viscosity @ 135°C	158	ASTM D4402
Softening Point	51.2°C	ASTM D36
Specific Gravity	1.02	ASTM D70

Mixture designs were done first without using lime content, named as untreated mixtures, after that 2% hydrated lime by weight of dry aggregate was added to each mixture by replacing the mineral filler contents. Gradation charts for both coarse and fine gradations are shown in Figure 3.3 for limestone and basalt aggregates, respectively. It can be seen that fine and coarse gradations are quite close for both aggregate types.



(a)



(b)

Figure 3.3. Selected gradations for the study (a) limestone, (b) basalt

3.2.3 Superpave Mixture Design

The Superpave mix design was performed according to AASHTO M323, Standard Specification for Superpave Volumetric Mix Design, and AASHTO R35, Standard Practice for Superpave Volumetric Design for Asphalt Mixtures, specifications. The samples were prepared with a diameter of 150 mm, height of 115 mm and approximately 5000 g aggregate for each sample. To determine the optimum bitumen ratio, five different bitumen ratios, each replicated three times, were tried. The aggregate properties to be used in the pavement structure that is designed according to this method, must meet the relevant specifications. The sample is compacted by applying 600 kPa pressure with an internal angle of 1.25 degrees from the top. This method aims to reach the compression obtained by using the rolling wheel compactor in the field.

Within the Superpave mix design, there are three density criteria classified as N_{in} , N_{des} and N_{max} , which represent different density levels for field compactions. For instance, N_{in} is the compaction level corresponding to field density when it is first laid on the field. N_{des} value specifies the number of gyrations required to achieve a 4% void ratio or 96% of the theoretical maximum specific gravity. This value is also used to determine the optimum bitumen content when 4% void ratio is achieved. N_{max} indicates the tendency for rutting to occur during the service life of the pavement.

According to the specifications AASHTO M323 and AASHTO R35 in the Superpave method, the number of gyrations to be applied for different traffic levels and the mixture volumetric properties are shown in Table 3.7 and Table 3.8.

Table 3.7 Superpave compaction parameters for different traffic levels.

ESALS (Millions)	Compaction Parameters		
	N _{in}	N _{des}	N _{max}
<0.3	6	50	75
0.3 to <3	7	75	115
3 to <30	8	100	160
≥30	9	125	205

Table 3.8 Superpave HMA Design Requirements

Design ESALs (millions)	Required Relative Density, % G _{mm}			VMA, Percent Minimum					VFA Range, Percent	Dust to Binder Ratio Range
	N _{in}	N _{des}	N _{max}	Nominal Maximum Aggregate Size, mm						
				37.5	25	19	12.5	9.5		
< 0.3	≤ 91.5	96	≤ 98.0	11	12	13	14	15	70–80	0.6–1.2
0.3 to < 3	≤ 90.5								65–78	
3 to < 10	≤ 89.0								65–75	
10 to < 30										
≥ 30										

After compacting the samples, the optimum bitumen contents were calculated by selecting 4% void ratio together with the specification limits given in these tables. Four optimum bitumen contents were determined for basalt and limestone aggregates, as course and fine gradations. Totally, 64 cylindrical samples were fabricated for IDT and DTT and 16 for TSRST. A picture of the design samples is shown in Figure 3.4.



Figure 3.4. Superpave gyratory compactor used in this study

Compaction process starts with mixing aggregates with bitumen at the selected mixing temperature. Then, the samples are placed in oven for 3 hours at the mixing temperature to achieve short term aging. Finally, they are compacted using a gyratory compactor for 10^6 ESAL traffic at the selected compaction temperature. Table 3.9 lists the elements of mix design used in the study.

Table 3.9 Parameters selected for mixing and compaction.

Design Parameters	Selected Parameters
Ndes	100
Cumulative traffic assumed	3-10 million
Mixing temperature	151°C
Compacting temperature	141°C
Air void content	4%

To determine the optimum bitumen content for 4% air void, the sample's bulk specific gravity (AASHTO T166) and theoretical maximum density (AASHTO T209) values were measured and given in Table 3.10. After determining the optimum bitumen contents, voids filled with asphalt (VFA) and voids in mineral aggregates (VMA) were calculated. A total of 64 mixes for IDT and DTT and 16 mixes for TSRST were prepared.

Table 3.10 Mixture properties

Mixture Combinations	Opt. Asphalt Content (%)	VMA	VFA	Max. Theoretical Specific Gravity	Bulk SG
Limestone Course	5.80	16.13	74.87	2.566	2.462
Limestone Fine	5.50	15.41	74.02	2.573	2.470
Basalt Course	5.30	14.47	71.47	2.374	2.276
Basalt Fine	5.50	15.74	74.33	2.376	2.280

3.2.4 Sample Preparation for Compaction

Before starting the IDT, DTT and TSRST tests, the cylindrical samples prepared with gyratory compactor were cut into beam specimens of 50x65x140 mm dimensions. During the mix design process, the optimum bitumen ratios were determined for both coarse and fine gradations respectively, as 5.80% and 5.50% for limestone and 5.3% and 5.5% for basalt aggregates, then according to full factorial experimental design 2% HL added by replacement method to specified specimens. Cylinder samples were produced using 7500 g aggregate to achieve a sample height of at least 165 mm height at $N_{des} = 100$ gyrations for 3-10 million ESAL.

To understand the effect of HL content on the test mixtures, two sample combinations: one with 2% HL by weight of dry aggregate and one without HL were prepared. In order to keep the total mineral filler content constant in the mixture, HL was replaced with the mineral filler of the original aggregate. During HL addition, the aggregate surface was moistened to ensure a homogeneous distribution of HL. Aggregates were then conditioned at 170°C in an oven for at least 6 hours for marination. The 50/70 binder was heated in oven at 160°C for two hours and the bitumen temperature was maintained about five degrees above the mixing temperature to compensate the heat loss during the mixing process. After the aggregate and binder were mixed at the mixing temperature, they were subjected to two hours of short-term aging in oven at the compaction temperature. At the end of this period. the mixtures were compacted using a Superpave gyratory compactor at the compaction temperature.

3.2.4.1 Process of Hydrated Lime Addition

To exchange HL (Figure 3.5) with aggregate filler section, HL sieve analysis was performed and the maximum particle size was observed as # 40 mesh. The sieve analysis data for HL are given in Table 3.11.

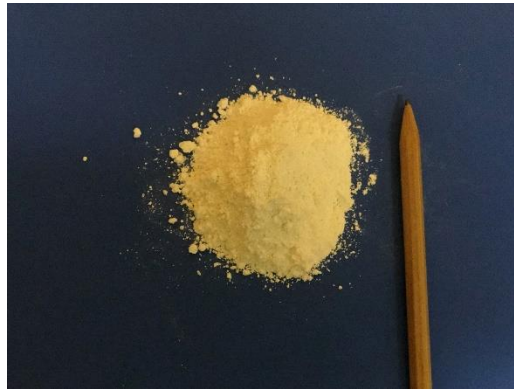


Figure 3.5. Hydrated lime used as mineral filler

Table 3.11 HL Gradation Analysis (% passing)

HL Gradation	
no 10	100
no 40	99.5
no 80	95.5
no 200	81

Table 3.12 represents the chemical properties of hydrated lime obtained from X-ray fluorescence (XRF). The composition shows that, hydrated lime contains approximately 98 % CaO. Also, it includes pozzolanic materials (SiO_2 , Al_2O_3 , Fe_2O_3) very few around 0.3%.

Table 3.12 Chemical Properties of Hydrated Lime

Chemical Composition (%)	Hydrated Lime
CaO	97.9
MgO	1.02
SO ₃	0.642
SiO ₂	0.162
Al ₂ O ₃	0.071
Fe ₂ O ₃	0.069
Na ₂ O	0.048
Cl	0.038
P ₂ O ₅	0.015
K ₂ O	0.015

Preliminary study was conducted to understand the effect of lime content on mixture strength at low temperature condition using IDT results. For this purpose, HL was obtained from Turkish Lime Industry Association and used as additive to prepare several dummy samples. Two lime contents, 2% and 3%, were selected to observe the influence of lime content on the IDT strength of the dummy mixtures. The results of this preliminary study is given in Table 3.13. It can be seen that, 2% lime produced higher IDT strength than does 3% lime content. Based on these results, it was, therefore, decided that Type I hydrated lime at 2% be used in the test mixtures.

Table 3.13 Increase in IDT for different contents of hydrated lime

	% Increase in IDT	Strength
Additive Type	2%	3%
Hydrated Lime	23.0	11.8

The selected hydrated lime content, 2% by dry weight of the aggregate, was used in the mixtures by replacing with the mineral portion of the original aggregate. Before the addition process, the mineral filler part of the aggregate was removed according to the HL sieve analysis results and then hydrated lime was added to the text mixtures. In this method, dry lime was added to the surface moistened aggregate, which is accepted as one of the most preferred method in the literature. It is important that while applying this method, the moisture level must be around 2-3% higher than the moisture level for saturated surface dry aggregate of test mixtures (Figure 3.6).

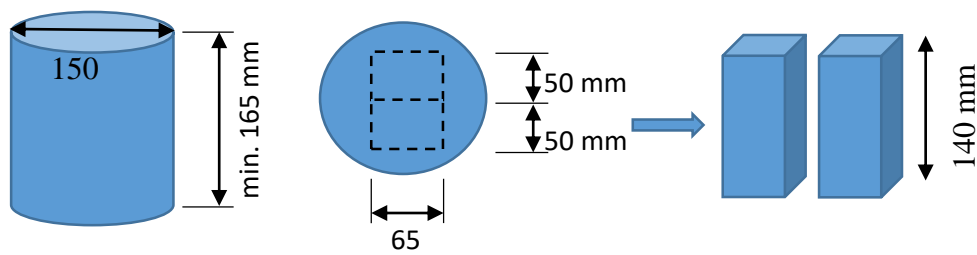


Figure 3.6. Addition of lime to aggregate

3.2.5 Preparation of beam specimens

The cylinder samples formed after compaction were cut into 50 * 65 * 140 mm sections using a diamond saw machine (Figure 3.7 (a)). According to Vinson et al.

(1989), it is concluded that this aspect ratio does not affect the results statistically if it is kept constant. Based on this research finding, the cross section of the specimens was determined to be 50 * 65 mm and the aspect ratio remained between 4 and 6 for each test specimen. To obtain smooth plane and prevent overheating of the specimens, the sewing machine was constantly cooled with water and the beams were allowed to dry prior to experiments (Figure 3.7 (b)). Finally, test variables for prepared samples are summarized in Table 3.14.



(a)



(b)

Figure 3.7. Specimen dimensions after cutting with diamond saw machine from Superpave samples

Table 3.14 Summary of test variables for prepared specimens

Test Variables	Explanations
Aggregate Type	Basalt (B). Limestone (L)
Gradation	Coarse (C). Fine (F)
Lime Treatment	Hydrated Lime (H). Neat (Z)
Aging	Aged (A). Unaged (U)
Test Temperature	0 °C; -10 °C (IDT & DTT)
Size of Test Specimens	100 mm dia. x 40 mm (IDT) 50 mm x 65 mm x 140mm
Number of Compacted Samples	80

3.3 Sample Preparation for DTT and TSRST

To perform the DTT and TSRST, the test specimens must be mounted on the loading platens. This step is very important for the precision of test outcomes; the specimens must be so centered between the loading platens that the eccentricity is minimized during loading to prevent the generation moment forces. The centering process is carried out by attaching O-ring to the center of both ends of the specimens and then fixing it to the platens mounted on the wall as seen in Figure 3.8. In this method, the platens having protrusions at their centers ensured the centricity of the specimens with the platens.

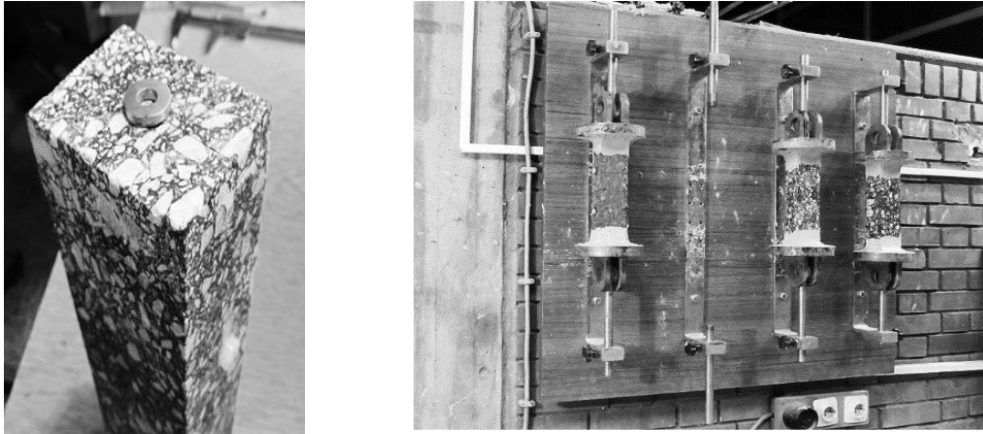


Figure 3.8. Previous sticking process (after Arabzadeh., 2014)

The accuracy and reliability of the test results are based on the strength of the epoxy used and the centricity of the specimens and the loading plates when these components are glued together. If one does not glue the specimens and the plates in a careful fashion, unwanted moments will occur on the sample resulting in premature failure at the corner regions. In other words, these moments lead to unexplained stiffness reductions during the experiment as well as obtaining erroneous results during the analyses.

Sikadur®-31 epoxy was used during the bonding of the specimens as in the previous studies by Qadir, A., (2010). Manufacturers indicate that within 24 hours the tensile strength obtained reaches on concrete surface around 40-60 MPa, and on steel surface around 14-16 MPa. Before starting the gluing process, the platens should be cleaned with acetone to remove the contaminations and then ensure full adhesion of epoxy to the specimen surface. In this study, a new apparatus was developed for better centering of the specimens to the loading platens. First, the specimen was placed on the lower loading platen. which is fixed on the preparation tray. Then, the upper platen - with epoxy applied on it - is placed on the other side of specimen. Loading platens are centered on both sides of the specimen with two comparators mounted across each other and then tightened by bolts to remain at centered position (Figure 3.9 (a) and Figure 3.10). Fully centered specimen on the platens reduces the momentum effect that may occur during the experiment, ensuring a uniform distribution of the tensile load and a normal fracture of the specimen. As it is shown

in Figure 3.9 (b), after the specimen is bonded to the platens with epoxy, the holding apparatus is mounted between the platens to keep the specimen at room temperature for 24 hours while curing the epoxy resin.

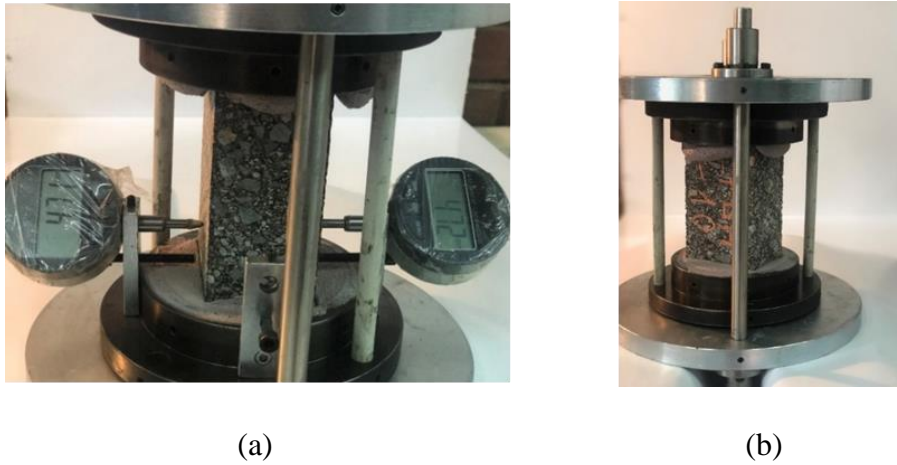


Figure 3.9. Centering of specimen and loading platens during gluing process

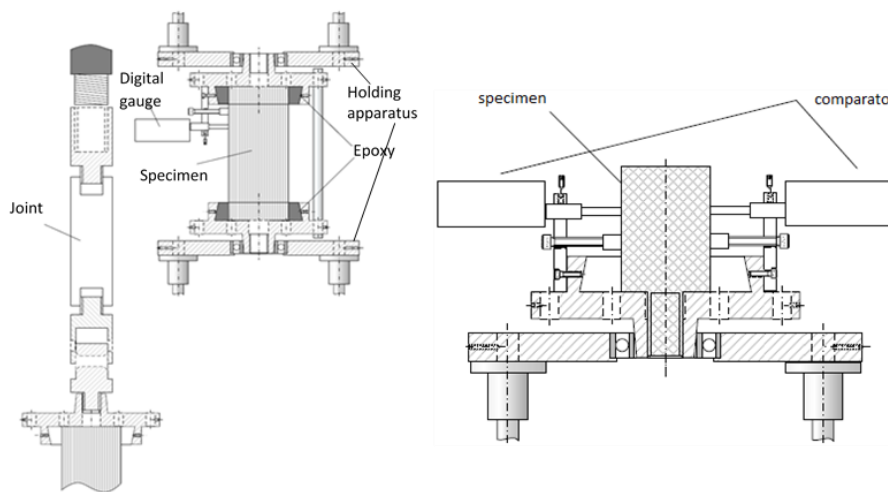


Figure 3.10. Details of apparatus used for specimen centering

3.3.1 Test Setup for Thermal Stress Restrained Specimen Test

TSRST is considered one of the most effective testing methods used for determining the low temperature performance of asphalt concrete in a phenomenological approach closely simulating what happens in the field. TSRST evaluates the low temperature cracking resistance of a restrained beam or cylindrical hot mix asphalt (HMA) specimen exposed temperature reduction. The sample is placed in the TSRST environmental chamber capable of decreasing temperature at a rate of 10 degrees Celsius per hour. As the temperature decreases, the sample contracts, but the control unit that applies an external tensile load to the sample prevents the sample from shortening. Linear Variable Differential Transformers (LVDT's) mounted on two sides of the specimen measure the temperature related deformations, and such data enable the control unit to pull the specimen back to compensate for the decrease in length of the specimen (Figure 3.11). The test ends upon fracture of the specimen indicating the mixture strength is exceeded by further temperature reduction.

TSRST, although a promising method for evaluating low temperature cracking resistance, requires significant amount of time for specimen preparation before starting the tests. Compacted slab specimens should be cut into beams, dried and then epoxied to the loading platens requiring 24 hours for epoxy to be cured till it is hard enough to start testing. During the gluing stage, the specimens must be correctly centered to the platens; otherwise they may create eccentric loading which results in moment forces and eventually premature failure of specimen.

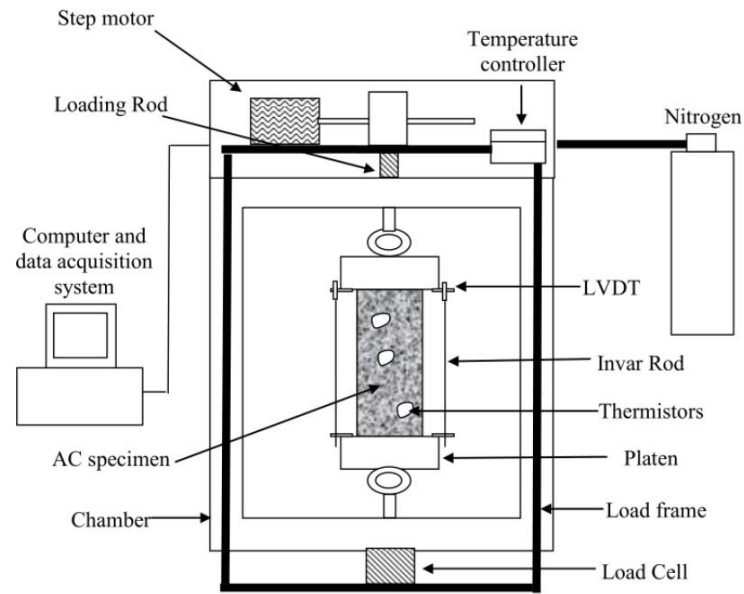


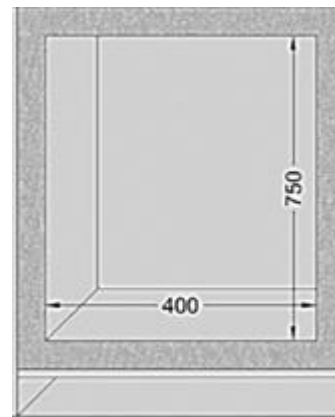
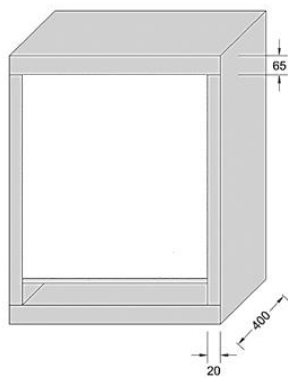
Figure 3.11. Schematic for TSRST setup (after Marasteanu et al., 2007).

3.3.1.1 Elements of TSRST Frame

The TSRST device is designed to test the thermal properties of asphalt concrete specimens. The outer layer of the test frame is made of steel sheets and the inner layer is made of XPS foam material for temperature insulation. Refrigerating chamber, servo motor and compressor unit are three main sections of the TSRST frame. In addition, a computer is used for controlling testing variables, i.e., rate of temperature reduction, conditioning time, load control, deformation measurements, etc., and data acquisition system (Figure 3.12).



(a)



(b)

Figure 3.12. (a) TSRST main components (b) Environment chamber dimensions

The structural design of the TSRST machine is realized by welding the two 65 mm thick steel plates from the top and bottom to the other two 20 mm thick steel plates. 170 mm thick foam material is used for curbing the heat transfer from the chamber to surrounding environment. According to Qadir (2010), maximum vertical deflection in the chamber reaches 90 microns if the maximum load applied to the asphalt concrete sample reaches 30 kN, which is the maximum loading capacity. Since this deformation is considered to be minimal, it is accepted that the test results will not be affected by deformation of the frame. Besides, the effect of deflection on the frame is compensated by the controlled loading through an installed servo motor. The TSRST device is controlled by a personal computer that operates according to

changes in electrical signals from LVDTs placed on two sides of the specimen. The LVDTs are mounted on the top platen where the sample is adhered, while the elongation bars are attached to the bottom platen. As a result of the decrease in specimen length detected by LVDTs, the servo motor pulls the specimen back to its initial length, thereby inducing tensile stress to specimen until fracture.

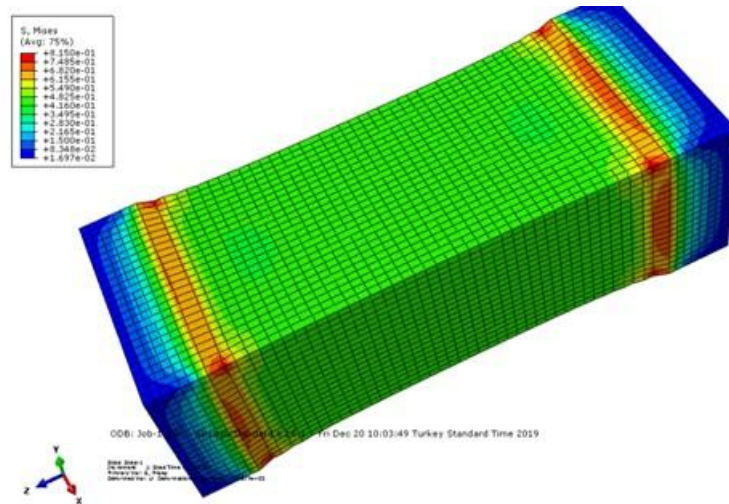


Figure 3.13. Abaqus Analysis for TSRST specimen

Figure 3.13 shows the 3D model of typical TSRST specimen that is developed by ABAQUS software. It should be noted that dimensions throughout modelling used same as real specimen has and specified boundary conditions the same as the sample. Analysis shows that stress distribution is maximum at the points where specimen is epoxied to the loading plates.

3.3.1.2 Programming for Test Control

LabVIEW® software with user interface is used to control the experiment and collect data. The software is in graphical programming language and allows the application of the experiment to be done quickly and accurately. Transducer signal conditioners,

a data acquisition card, and a personal computer are connected to the data acquisition system. This system processes and maintains the electrical signals from the load cell, two LVDTs and RTDs for analyses. The process is presented in the Figure 3.14.

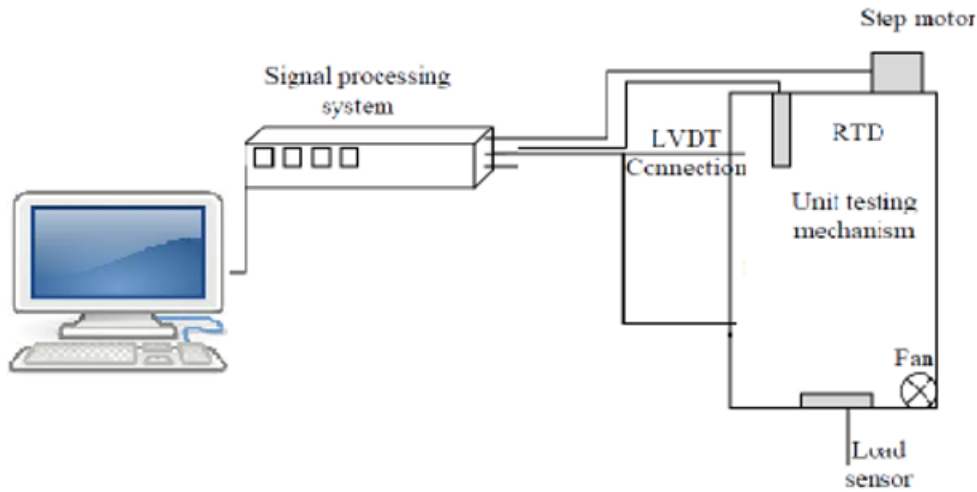


Figure 3.14. Software and testing machine communication layout

Tailored for this study, the machine operates in 2 different modes which are the measurement of fracture strength and both fracture strength and temperature. Program must be run in different modes, so that two different measurements can be performed. The conditioning mode is the same for the two different measurement types that lasts for 3 hours to reach thermal equilibrium at the set temperature (Arabzadeh & Guler. 2019). Determination of fracture strength and temperature is controlled by LVDT readings, which is called the displacement-profile mode.

3.3.1.3 The system control

System control components are motor, cooler, fans and power switch for turning on and off the power. To start any testing procedure, the system control modes must be all switched on to activate the control units. Power mode must be turned on to supply power to the cooler, servo motor and all other sensors within the system. The

nitrogen mode is only used for glass transition temperature measurements to support the cooling system. Fans are used to facilitate internal air circulation within the environmental chamber to achieve uniform temperature distribution. Cooler is the main part of the environmental chamber necessary to reduce the temperature at a controlled rate defined in the control software.

a) The motor control

In displacement mode, it is important that the motor control system regularly adjusts the sample length - tending to shrink due to temperature decrease - to accurately measure fracture temperature and fracture strength. Before starting the test, the sample must be placed correctly in the machine and fully secured between the joints. At this stage, the motor is manually controlled, the upper joint is moved up and down so that the appropriate position for the sample can be determined. Then, the load on the specimen should be zeroed by the zero load cell button (Figure 3.15).

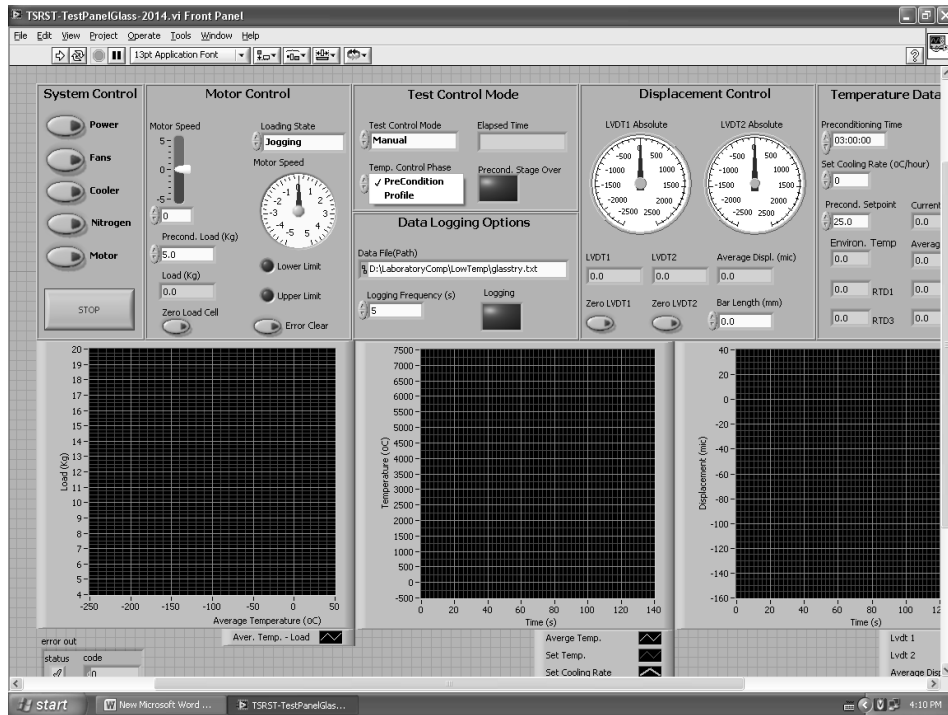


Figure 3.15. TSRST software panel

b) Test control mode

In control mode, the user is allowed to select the appropriate loading mode for the test. According to the programming method specifically tailored for this study, there are three options for loading mode: jogging, conditioning, and direct tension. In jogging mode, the motor is controlled manually so that the specimen can be placed properly between the joints. In the case of the conditioning mode, the preconditioning time takes at least three hours to reach the target temperature. Once the target temperature is reached, the experiment is started. The program does not allow the experiment to be started before the three-hour period. In the program, there is a section for writing the name of the file directory where the test data are to be saved, and after the corresponding name is assigned, the data are exported to the directory per second, i.e., the logging interval is one second.

c) The displacement control

Displacement parameters are arranged in this section. Firstly, two LVDT's must be fixed to aluminum brackets and they should be zeroed. Then, the test is started and the compressor cools down the environmental chamber to 5 degrees Celsius, the initial test temperature. In the meantime, negative readings are taken from LVDTs due to shrinkage of the sample, while positive readings are obtained from the shrinkage of the extension rods. The shrinkage of the extension rods is removed from the LVDT readings to eliminate the test setup related errors.

d) The temperature control

In this section of the software, data on preconditioning duration and target temperature must be specified. The specimens are conditioned at two different temperatures: 0 and -10 degrees Celsius, for three hours. In this mode, when the temperature of the specimen is lower than the specified temperature, the cooler and fans will operate until the specimen reaches the target temperature. When the

specimen temperature is lower than set temperature, the program sends false signal to the fans and the cooler to stop their operation.

3.4 Thermal Stress Restrained Specimen Test

Within the generated experimental matrix, the specimens listed in Table 3.15 were tested for fracture strength and fracture temperature using two replicate specimens for each combination of test variables.

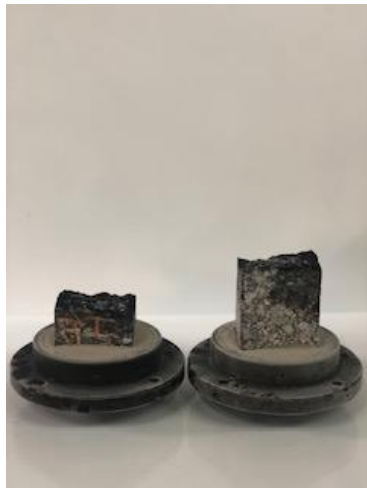
Table 3.15 Specimen coding for TSRST

No	Aggregate type	Gradation	Aging	Lime content
1	B	C	U	Z
2	B	C	U	H
3	B	C	A	Z
4	B	C	A	H
5	B	F	U	Z
6	B	F	U	H
7	B	F	A	Z
8	B	F	A	H
9	L	C	U	Z
10	L	C	U	H
11	L	C	A	Z
12	L	C	A	H
13	L	F	U	Z
14	L	F	U	H
15	L	F	A	Z
16	L	F	A	H

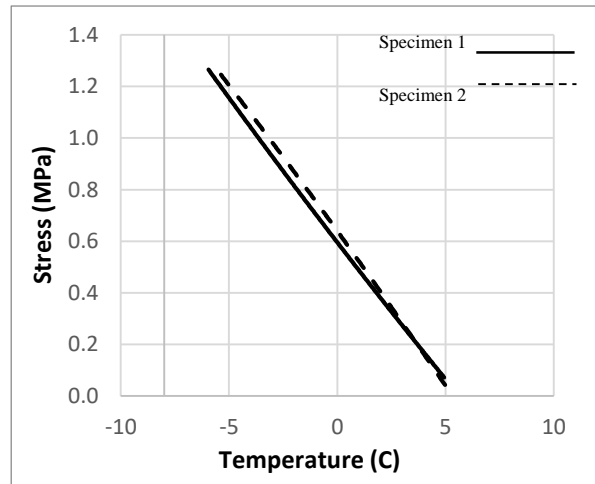
Symbols used: B-Basalt; L-Limestone; C-Coarse; F-Fine; U-Unaged; A-Aged; Z-No Modification; H-Lime Modified

The beam samples fixed to the loading plates are mounted on the TSRST with pins. LVDTs and RTDs are then placed on the specimens. Then, the machine is switched to fracture mode and the necessary entries for the correct operation of the program must be entered. The sample is firstly conditioned for 3 hours at 5°C to reach thermal equilibrium (Arabzadeh A., 2015). After that, - using the LabView ® interface

specifically designed for this study- the machine is switched to fracture mode and the sample temperature is reduced at a rate of 10°C /hour. As the temperature decreases, the stress in the sample increases. The test continues until the sample breaks (Figure 3.16). The data during the experiment is logged every 5 sec.



(a)



(b)

Figure 3.16. TSRST fracture test results (a) a specimen fractured after test. (b) stress versus temperature data plotted for a specimen

During the experiment, the program records the load applied to the specimen measured using a load cell, the target temperature and the current temperature of the specimen measured with RTDs and the displacements using LVDT sensors until the experiment is over. At the end of test, the temperature and the load at which the specimen breaks are calculated and graphically presented as the fracture temperature and fracture strength, respectively, of the test specimen.

3.5 Sample Preparation for DTT Testing

Specimens for DTT were prepared based on a two-level fractional factorial design ($2^{5-1} = 16$) producing a total of 16 test combinations with two replicates. The selected test variables are aggregate type, gradation, aging condition, lime content and test temperature. According to the current literature, it is appropriate to perform the experiment at 0°C and -10°C in order to determine the low temperature performance of asphalt concrete. The test variable combinations are listed in the Table 3.16.

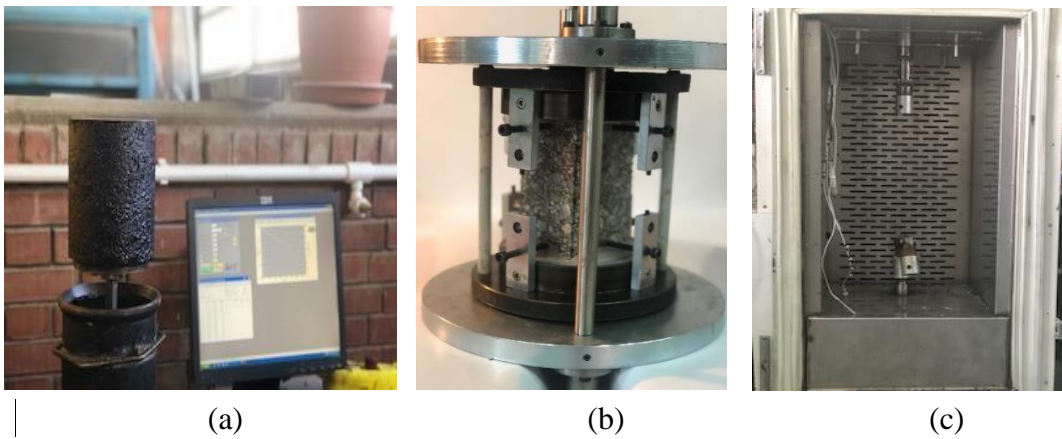


Figure 3.17. DTT (a) Sample preparation. (b) sticking to platens and (c) testing process

Table 3.16. Specimens tested for DTT

No	Aggregate type	Gradation	Aging	Lime content	Test temperature
1	B	C	U	Z	-10
2	B	C	U	Z	0
3	B	C	U	H	-10
4	B	C	U	H	0
5	B	C	A	Z	-10
6	B	C	A	Z	0
7	B	C	A	H	-10
8	B	C	A	H	0
9	B	F	U	Z	-10
10	B	F	U	Z	0
11	B	F	U	H	-10
12	B	F	U	H	0
13	B	F	A	Z	-10
14	B	F	A	Z	0
15	B	F	A	H	-10
16	B	F	A	H	0
17	L	C	U	Z	-10
18	L	C	U	Z	0
19	L	C	U	H	-10
20	L	C	U	H	0
21	L	C	A	Z	-10
22	L	C	A	Z	0
23	L	C	A	H	-10
24	L	C	A	H	0
25	L	F	U	Z	-10
26	L	F	U	Z	0
27	L	F	U	H	-10
28	L	F	U	H	0
29	L	F	A	Z	-10
30	L	F	A	Z	0
31	L	F	A	H	-10
32	L	F	A	H	0

Symbols used: B-Basalt; L-Limestone; C-Coarse; F-Fine; U-Unaged; A-Aged; Z-No Modification; H-Lime Modified

Specimen preparation stage is the same as it mentioned in section 3.3 (Figure 3.17). When the specimen is placed in the test device, loading platens are fixed with pins from the top and bottom. The LVDTs are attached to the top platens on each side of the specimen tighten by screws. Next, using a tape RTD sensor is attached on front

surface of the specimen (Figure 3.18 (a)). After preconditioning for 3 hours at the target temperature (0°C or -10 °C), the specimen is pulled at a rate of 100 micro-strain per minute until it fractures (Figure 3.18 (b)). The test data are recorded and analyzed for the maximum load reached during tensioning to calculate the tensile strength of the specimen.

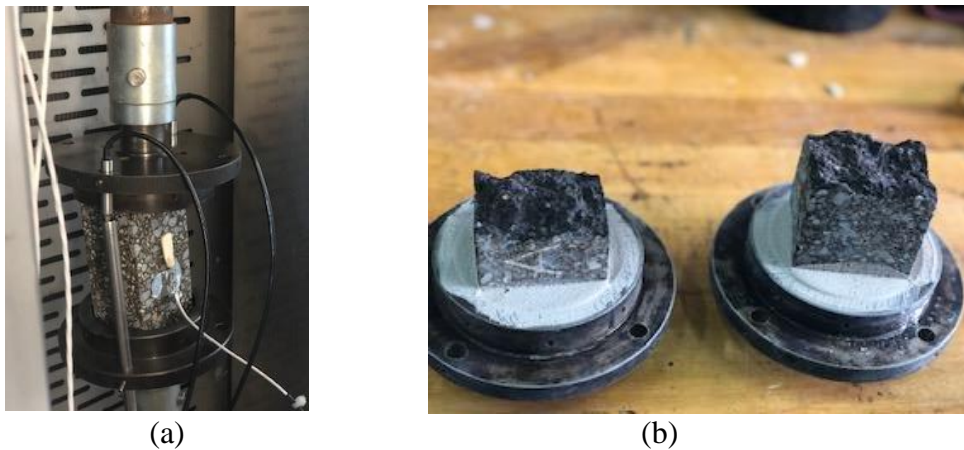


Figure 3.18. DTT test results (a) a view of specimen during the test. (b) a specimen fractured after test

3.6 Direct Tension Test (DTT)

In order to determine thermal cracking resistance of asphalt mixtures, different laboratory investigations have been performed with TSRST machine. However, lab-specific standards increase the diversity among the studies. In this study, Direct Tension Test (DTT) is performed using the TSRST device. Since the tests are performed at 0°C and -10°C, the capacity of TSRST's compressor is suitable for testing at these temperatures obviating the need to use liquid nitrogen.

As mentioned earlier, each sample is glued to the loading platens by centering and the epoxy is allowed for curing in 24 hours. Then, LVDT and RTD sensors are mounted on the upper platen and the specimen surface, respectively, before starting the tests in the TSRST device (Figure 3.19). The change in the length of the specimen

is detected by the LVDTs, and the temperature readings of specimen is detected by RTD's attached to both sides of the specimen. The $100 \mu\text{s} / \text{min}$ strain rate is applied by the servo motor until the fracture of the test specimen.

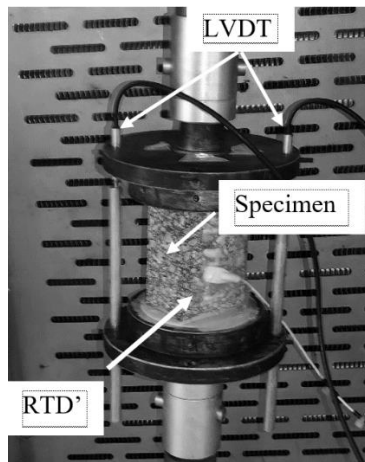


Figure 3.19. LVDT and RTD connections for DTT

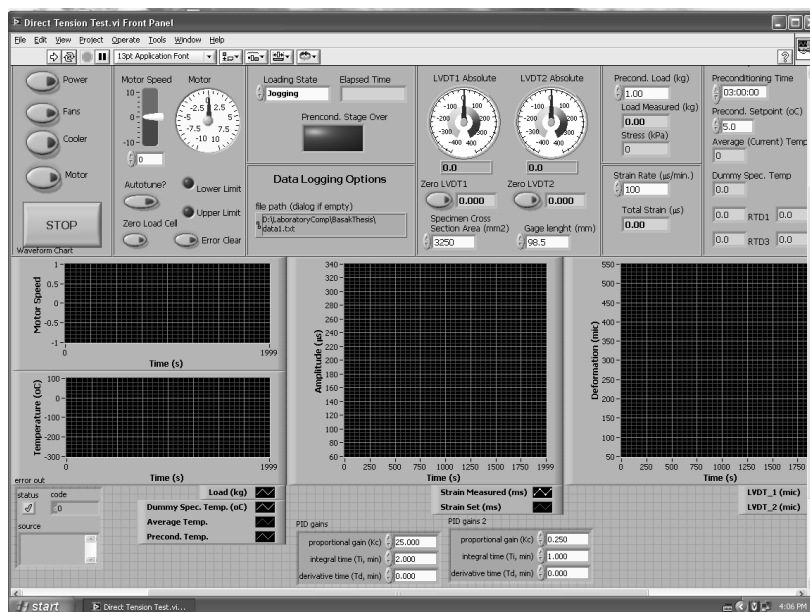


Figure 3.20. Software used for DTT

The use of all buttons in the system control and motor control sections is as described in section 3.3.1.3 for TSRST (Figure 3.20). In the test control mode, the specimen is pre-conditioned for 3 hours at the test temperature (either 0°C or -10°C) and then the direct tension mode is started to apply loading.

3.7 Sample preparation for IDT Testing

All the test specimens for IDT were prepared following the same procedures explained for the fabrication of TSRST and DTT specimens. The compacted samples were cut using a diamond saw machine to obtain two specimens per mix design from the center of samples. The specimen thickness was selected as 40 mm, so that the peak loading would not exceed the load cell capacity of the testing frame (Figure 3.21). Hydrated lime was added to the aggregate blends that were brought to moisture levels around 3% higher than their surface saturated dry densities.

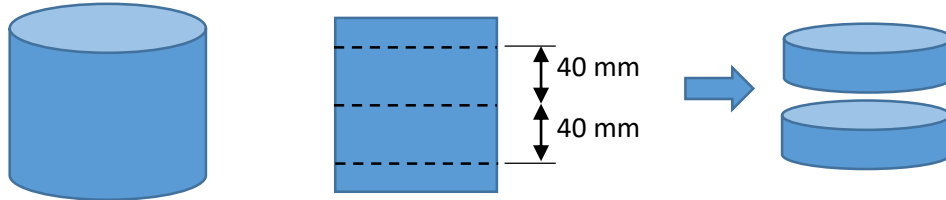


Figure 3.21. Cutting sections of IDT specimens

Each specimen was tested for the IDT strength according to AASHTO T322 and NCHRP 530 guidelines. Test temperatures were suggested as 0°C, -10°C and -20°C; experiments to determine the IDT strength of the specimens under low temperature were performed at 0°C and -10°C, which is the nominal temperature as suggested by Anderson, R. M., (1998) and R. B. McGennis, (1998). The specimens were conditioned in an environment chamber (Figure 3.22 (a)) at the target temperature for at least 6 hours to make sure that a complete temperature equilibrium was

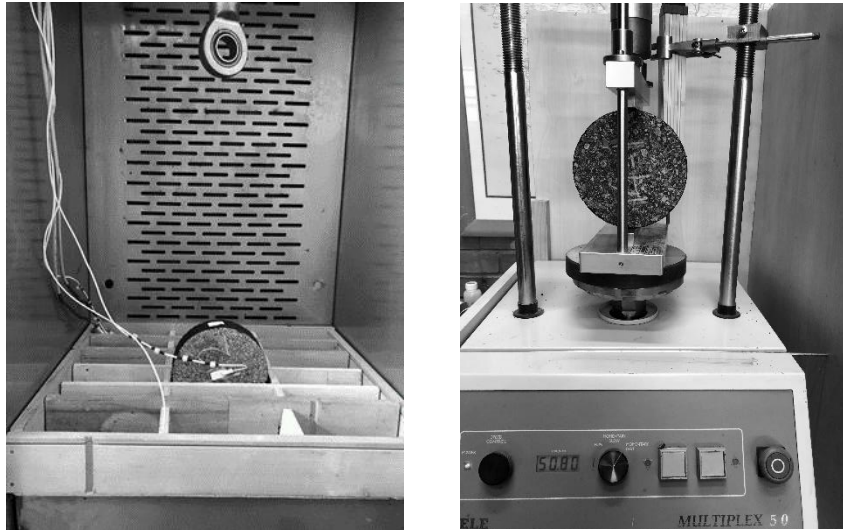
achieved before testing. Since the specimen aging was one of the factors in the experimental program, the compacted gyratory samples were long term oven aged at 85° C for 120 hours according to the AASTHO R30 guidelines. After reaching temperature equilibrium, the specimens were placed into the steel loading strips (Figure 3.22 (b)) and loading was applied at 12.5 mm/min deformation rate till they fractured (Figure 3.22(c)) according to the AASHTO T322 procedures. This loading speed was chosen due to the fact that time-dependent deformations during loading may affect the measured strength of the specimen. At the end of each test, the maximum force and the corresponding deformation were recorded to calculate the IDT strength of the specimens.

Table 3.17 Specimens tested for IDT

No	Aggregate type	Gradation	Aging	Lime content	Test temperature
1	B	C	U	Z	-10
2	B	C	U	Z	0
3	B	C	U	H	-10
4	B	C	U	H	0
5	B	C	A	Z	-10
6	B	C	A	Z	0
7	B	C	A	H	-10
8	B	C	A	H	0
9	B	F	U	Z	-10
10	B	F	U	Z	0
11	B	F	U	H	-10
12	B	F	U	H	0
13	B	F	A	Z	-10
14	B	F	A	Z	0
15	B	F	A	H	-10
16	B	F	A	H	0
17	L	C	U	Z	-10
18	L	C	U	Z	0
19	L	C	U	H	-10
20	L	C	U	H	0
21	L	C	A	Z	-10
22	L	C	A	Z	0
23	L	C	A	H	-10
24	L	C	A	H	0
25	L	F	U	Z	-10
26	L	F	U	Z	0
27	L	F	U	H	-10
28	L	F	U	H	0
29	L	F	A	Z	-10
30	L	F	A	Z	0
31	L	F	A	H	-10
32	L	F	A	H	0

Symbols used: B-Basalt; L-Limestone; C-Coarse; F-Fine; U-Unaged; A-Aged; Z-No Modification; H-Lime Modified

According to the experimental design, a total of 16 test combinations were produced with two replicates for each tested specimen. The design of experiment was generated by a two level fractional factorial design ($2^{5-1} = 16$) - ignoring the effect of three level interactions between the mix design parameters (Table 3.17).



(a)



(b)

Figure 3.22. (a) Environmental chamber and IDT testing machine. (b) Cracked IDT specimen

3.8 Indirect Tension Test (IDT)

In the scope of the experiment, ELE Multiplex 50 coupled with data acquisition system was used. To reach the maximum load on the samples, a 5-ton capacity load cell was used and deformation as well as load values were recorded (Figure 3.23). The loading speed is selected as 12.5 mm / minute using the program written in LabVIEW® language. The samples were pre-conditioned at test temperatures, which are 0°C and -10°C, for at least 6 hours before testing according to AASTHO T322 guidelines.

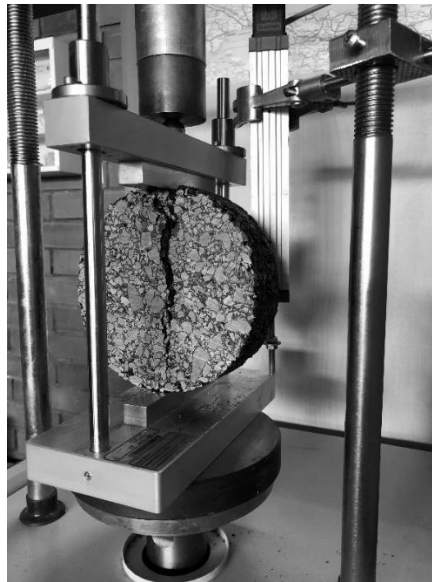


Figure 3.23. IDT testing machine

3.9 Characterization Tests for Bitumen and Mastic

3.9.1 Scanning Electron Microscope (SEM) of Mastic Phase

Scanning electron microscope is a scanning system with focused electron beam to produce images of a sample surface. The method is effectively used for conveniently scanning of conductive and non-conductive materials. To investigate the interaction

of hydrated lime with bitumen, FEI Quanta 400 FEG scanning electron was used at Metu Central Laboratory (Figure 3.24). Since the prepared bitumen samples were not conductive in nature they were coated with carbon/gold film before mounting on the sample holder (Figure 3.25).

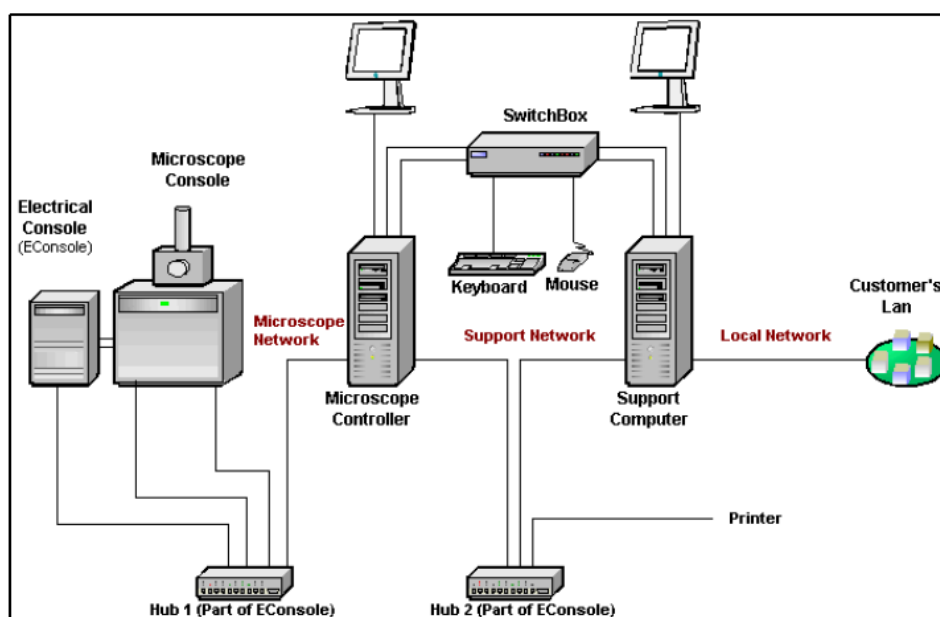


Figure 3.24. SEM Test setup (The Quanta FEG 400 User's Manual)

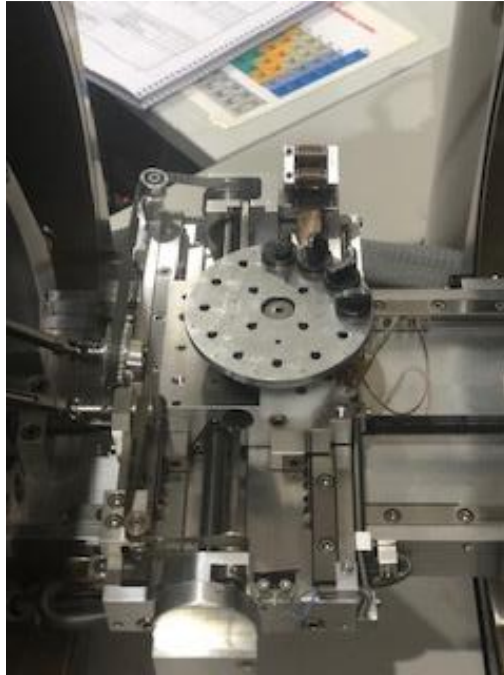


Figure 3.25. SEM Sample holder

3.9.1.1 Sample Preparation for SEM Analysis

Bitumen with penetration grade of 50/70 was mixed with the combinations of basalt-HL and limestone-HL filler parts (Figure 3.26). Different mixtures were prepared by addition of aggregate filler in proportion to the percentages determined in the HMA design stage. An average of 5.25% asphalt binder was used in HMA by weight for the mix designs. While preparing the mixture, basalt and limestone fillers were added exactly in proportion to the amount of fillers in mixtures and HL was added about 28% of the bitumen weight.

Asphalt binder, basalt-limestone fillers and hydrated lime were heated in the 150-160°C range. The fillers and hydrated lime were then added to the bitumen, mixed thoroughly with a lab mixer to prevent agglomeration and achieve homogeneous dispersion. The resulting mixtures were poured into prepared silicone molds and allowed to cool. The same operations were performed for aged bitumen as well.

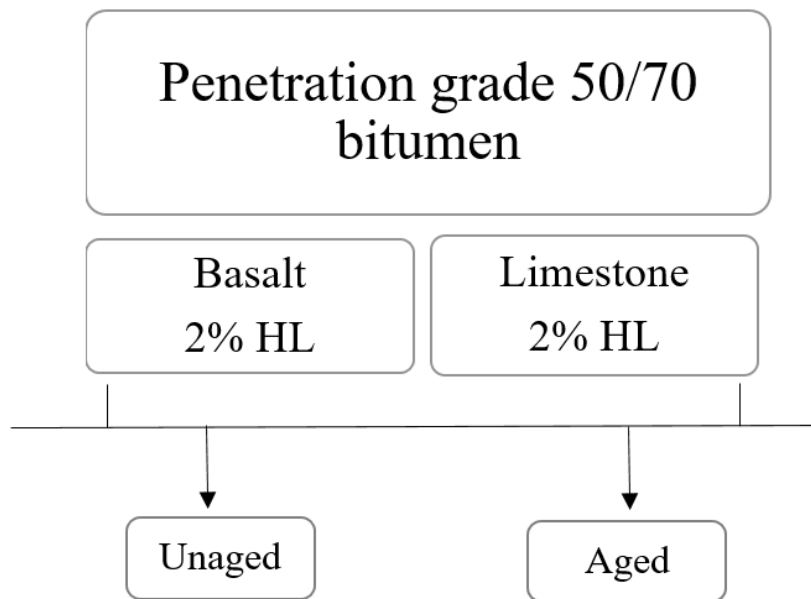


Figure 3.26. Prepared sample combination for SEM analysis

3.9.2 DMA Analysis of Mastic Phase

DMA tests were performed at METU Central Lab using Perkin Elmer Pyris Diamond DMA machine, which has an analysis temperature range between $-150 + 600^{\circ}\text{C}$, a frequency range between $0.01 - 100 \text{ Hz}$, and a heating/cooling rate of $0.01^{\circ}\text{C} - 20^{\circ}\text{C} / \text{min}$. The device is capable of applying a maximum load of 18 N (Figure 3.27).



Figure 3.27. DMA testing machine

Glass transition temperature of bitumen was determined based on DMA results at a constant frequency of 10 Hz and temperature range between -60 to 20°C. The analysis mode was selected as strain controlled and the specimens were prepared with the dimensions of (38 mm x 9 mm x 3 mm). From the test results, relationships between storage modulus, loss modulus and phase angle are obtained, from which glass transition temperature can be determined according to:

- Peak value of loss modulus
- Intersection of two tangents drawn via storage modulus
- Peak point of phase angle (Figure 3.28)

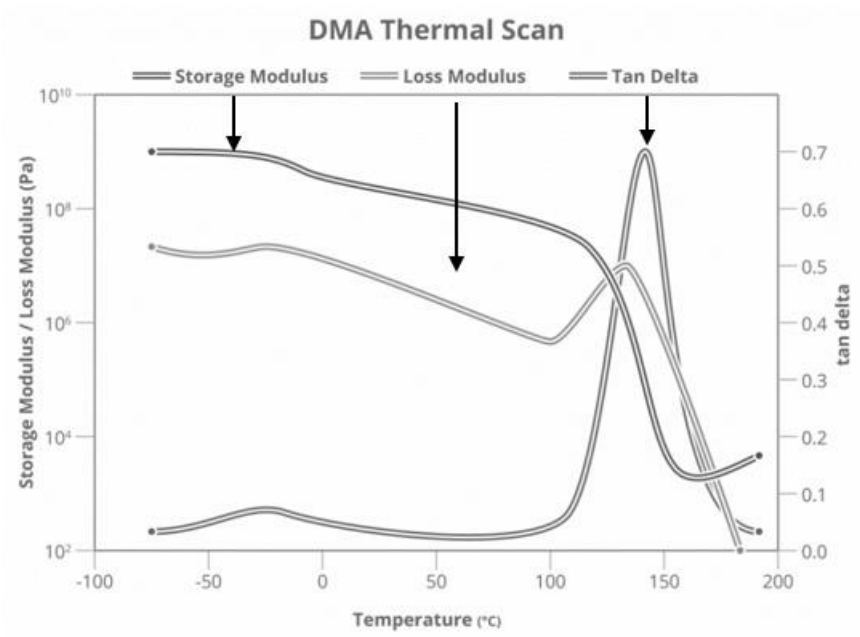


Figure 3.28. Typical DMA results

3.9.2.1 Sample Preparation for DMA Analysis

Bitumen with penetration grade of 50/70 was mixed with the combinations of basalt, basalt-HL, limestone, limestone-HL filler parts (Figure 3.29) for both aged and unaged bitumen. Different mixtures were prepared by addition of aggregates (filler) in proportion to the percentages determined in the HMA design stage. An average of 5.25% asphalt binder was used in HMA (by weight) for designs. While preparing the mixture, basalt and limestone fillers were added exactly in proportion to the amount of fillers in mixtures and HL was added about 28% of the bitumen weight. Asphalt binder, basalt-limestone fillers and hydrated lime were heated in the 150-160°C range. The fillers and hydrated lime were then added to the bitumen, mixed regularly to prevent agglomeration and achieve homogeneous dispersion. The resulting mixtures were poured into prepared silicone molds producing sample dimension of

38 mm x 9 mm x 3 mm) and allowed to cool. The same operations were also performed for the aged bitumen- mastic phase.

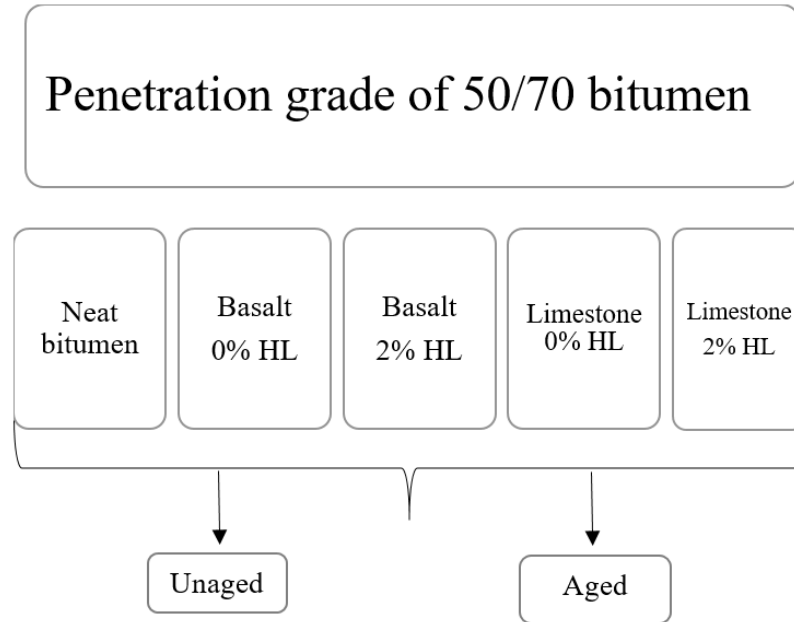


Figure 3.29. Prepared sample combination for DMA analysis

3.9.3 Rotational Viscometer of Bitumen

The rotational viscometer was used to test the viscosity of extracted bitumen from unaged samples prepared with/without HL and aggregates of basalt and limestone (Figure 3.30). Viscosity values were obtained using Brookfield Rotational Viscometer (RV) in order to determine the effect of hydrated lime on viscosity for un-aged bitumen samples. The test was implemented at a constant speed of 20 rpm within a temperature range between 120 °C to 180 °C. Bitumen samples were recovered from HMA samples without loss of filler according to the TS EN 12697-1 standard with the asphalt analyzer and the bitumen-ethylene mixture obtained from the test recycled according to the TS EN 12697-3 test standard. According to the standard, firstly compacted mixture should be warmed until it becomes workable. Then, specimen should be transferred into the wire basket placed on the filter paper.

Glass cylinder with a separator (trichloroethylene) is placed under the wire basket. There is a heater on the glass cylinder and condenser in which continuous cold water passes. As the temperature of the heater increases, the dissolvent will boil, and start to drip onto the sample by hitting cold water through the evaporator. As a result, the bitumen in the mixture will decompose from the aggregate.

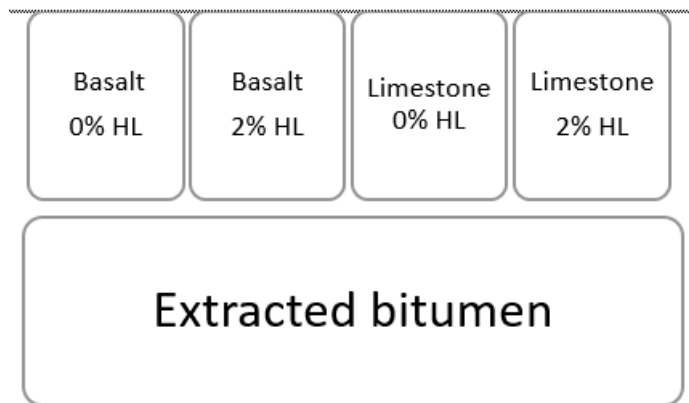


Figure 3.30. Sample combinations for viscosity analysis

3.9.4 Rheological Analysis of Bitumen Using Dynamic Shear Rheometer

Bitumen is a viscoelastic material that has a dominant elastic behavior (i.e., more solid) at lower temperatures and a dominant viscous (i.e., more liquid) behavior at higher temperatures. Dynamic shear rheometer (DSR) can be used to calculate both viscous and elastic properties of bitumen. During the test, the asphalt sample is sandwiched between two circular plates, and the upper plate (or spindle) oscillates while the bottom plate is fixed (Figure 3.31). In this section of the study, the influence of hydrated lime modification on bitumen was investigated using extracted unaged bitumen samples.

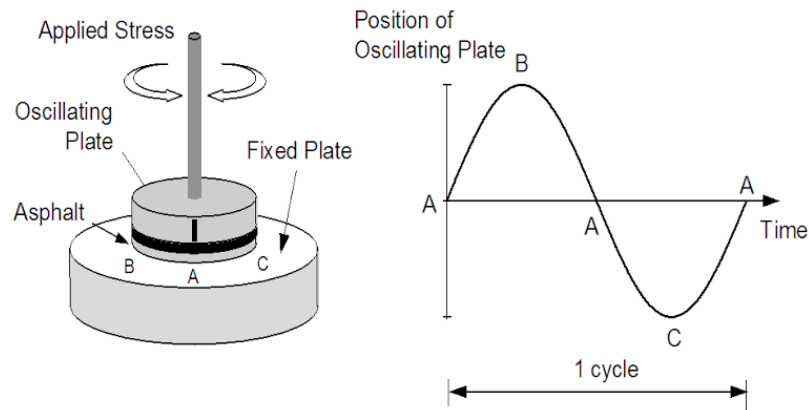


Figure 3.31. Representation of DSR (Asphalt institute. Lexington 1994)

It is worth noting that, DSR is mainly used to determine the complex shear modulus (G^*) that has two components: storage and loss. Simply put, G^* is used for defining fatigue rutting behaviors of asphalt binder. This value is an important parameter to determining the strength of asphalt. Storage modulus (G') and loss (viscous) modulus (G'') are the two components of this parameter (Figure 3.32). Analyses were performed for extracted bitumen obtained from un-aged basalt/basalt-HL, limestone/limestone-HL mixtures using 25 mm diameter plates with a gap of 1 mm at both temperature and frequency sweep tests. Complex modulus (G^*) and phase angle (δ) values were obtained from the test results.

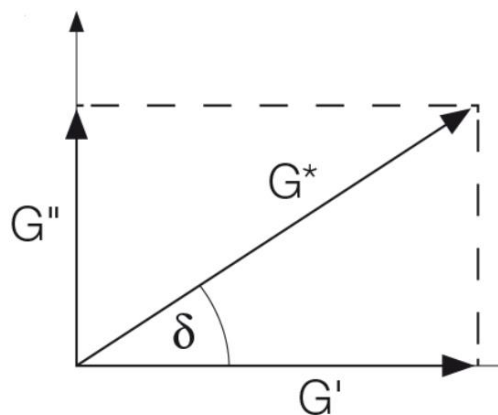


Figure 3.32. Two components of complex modulus (Anton Paar, 2019)

CHAPTER 4

RESULTS AND ANALYSIS OF TEST DATA

4.1 Introduction

This section covers the evaluation of results of statistical analyses on test data performed within the scope of the study. The effects of experimental variables on Thermal Stress Restrained Test (TSRST), Indirect Tensile Test (IDT), Direct Tension Test (DTT) results were analyzed based on statistical analysis of variance (ANOVA) for mixtures with/without hydrated lime.

4.2 ANOVA Analysis for Mixture Tests

TSRST, DTT and IDT tests were performed on mixture specimens and the results were evaluated in different categories. TSRST data were analyzed on the basis of fracture strength and fracture temperature while DTT and IDT data were evaluated solely based on fracture strength. for which the analysis results are presented individually.

4.2.1 Analysis for TSRST results

A total of 32 TSRST beam specimens were tested. These specimens vary according to the type of aggregate (basalt and limestone, symbolized by B and L), gradation (coarse and fine, symbolized by C and F), hydrated lime content (containing 2% hydrated and 0% lime, symbolized by H and Z) or whether the specimens were aged or unaged (symbolized by A and U). For instance, specimen given by LCUH code indicates that limestone is used with coarse gradation, also the specimen prepared with hydrated lime at unaged form. ANOVA analyses were performed by defining

dependent and independent variables. The experimental design variables were classified as independent variables, and the results as dependent variables. In other words, fracture strength and temperature are dependent variables while the test outcomes as dependent variables. Based on the ANOVA analyses, the effects of input (independent) variables on output (dependent) variables will be explained in detail. It can be seen from Table 4.1 that 2 replications were used per mixture combination.

Table 4.1 Specimen names and replicate number

Specimen Code	No. of Replicates	Specimen Code	No. of Replicates
BCUZ	2	LCUZ	2
BCUH	2	LCUH	2
BCAZ	2	LCAZ	2
BCAH	2	LCAH	2
BFUZ	2	LFUZ	2
BFUH	2	LFUH	2
BFAZ	2	LFAZ	2
BFAH	2	LFAH	2

4.2.1.1 Analysis of Fracture Strength From TSRST Data

As mentioned in detail in the previous chapter, the fracture strength of the specimens was measured using the TSRST setup through controlled reduction of temperature. The test results show that the maximum strength obtained is 2.620 MPa while the minimum strength is 1.190 MPa with an average strength value of 1.842 MPa (see Table 4.2). As can be seen from the table, the standard deviation of the measured strengths is 0.413 MPa.

Table 4.2 Descriptive statistics of the fracture strength

Statistical Parameter	Value (MPa)
Mean	1.842
Standard Deviation	0.413
Maximum Strength	2.620
Minimum Strength	1.190

In addition to the analyses presented above, variables affecting the fracture strength were also determined by ANOVA. In Table 4.3, the effect of each variable used in the experimental program on fracture strength is also given at 95% of confidence level.

Table 4.3 ANOVA analysis for fracture strength

Source	Probability
Aggregate Type	0.044
Gradation	0.007
Hydrated Lime Content	0.368
Aging	0.479

One-way ANOVA analysis was performed to determine the effect of each variable used on the TSRST results. The analysis indicates that the design variables: aggregate type and gradation are influential on fracture strength at a confidence level of 5% (i.e., $p < 0.05$). When evaluating the ANOVA results, p values close to zero must be considered as dominant factors for the dependent variable, i.e., test outcomes. Therefore, for the TSRST data analyzed, statistical analyses show that hydrated lime and aging are not significant parameters for the fracture strength of the specimens.

Table 4.4 shows the average fracture strength obtained from each design parameter. Accordingly, the average fracture strength of mixtures prepared with basalt aggregate is nearly 88% of those fabricated using limestone. The fact that limestone results in higher fracture strength compared with basalt is in agreement with the findings of Qadir (2010) and Arabzadeh (2015), investigating the influence of aggregate type on asphalt concrete thermal cracking. Also, the study conducted by Drüschner et al. (2004) has shown that the low absorption capacity of basalt can cause low fracture strength in TSRST.

Table 4.4 Fracture strength values for variables

Design Parameters	Levels	Symbol	Average	Standard Deviation	Median
			MPa	MPa	MPa
Aggregate Type	Limestone	L	1.963	0.384	1.865
	Basalt	B	1.722	0.417	1.655
Gradation	Coarse	C	2.010	0.275	2.085
	Fine	F	1.674	0.466	1.510
Hydrated Lime Content	Neat (zero)	Z	1.790	0.371	1.715
	2% included	H	1.894	0.457	1.865
Aging	Aged	A	1.883	0.478	1.855
	Unaged	U	1.801	0.347	1.715

The results in Table 4.3 indicates that aggregate type and gradation are influential design parameters for asphalt mixture thermal cracking with a p value of less than 0.05. In this study, two different gradations, course and fine, were used for both basalt and limestone aggregates. However, according to Vinson et al., (1989),

gradation was not found to be significant variable for low temperature cracking performance of asphalt concrete. (From the Table 4.4, the average fracture strength measured is 2.010 MPa for the coarse gradation and 1.674 MPa for the fine gradation. indicating that the coarse graded specimens outperformed better than the fine graded specimens). The disagreement between the outcomes of this study and Vinson et al. (1989) may result from the difference in aggregate source, mineralogical structure, and asphalt-aggregate adhesion properties. Another important factor might be the degree of aggregate interlock in asphalt mixtures where stone-stone contact is more predominant in coarse graded aggregate structure, as the aggregate size is increased, which provides higher resistance to contraction and deformation under low temperature conditions (Tan et al., 2008).

In this study, to investigate the effect of hydrated lime, first the filler portion of mixture aggregate was replaced with an equal amount of hydrated lime, secondly aggregate was thoroughly mixed with dry hydrated lime and finally mixed with bitumen at optimum content to prepare asphalt mixture samples. The mixture samples were then compacted to produce test specimens for TSRST testing program. However, the results of ANOVA for this testing program show that the addition of hydrated lime has no positive effect on fracture strength of asphalt concrete specimens. Similarly, the aging of the asphalt mixtures has also no effect on fracture strength as shown in Table 4.3. In Table 4.4, the aged specimens have an average fracture strength of 1.883 MPa, whereas the strength of unaged specimens is observed to have 1.801 MPa. The aged specimens seem to have slightly higher fracture strength. but the results are very close to each other.

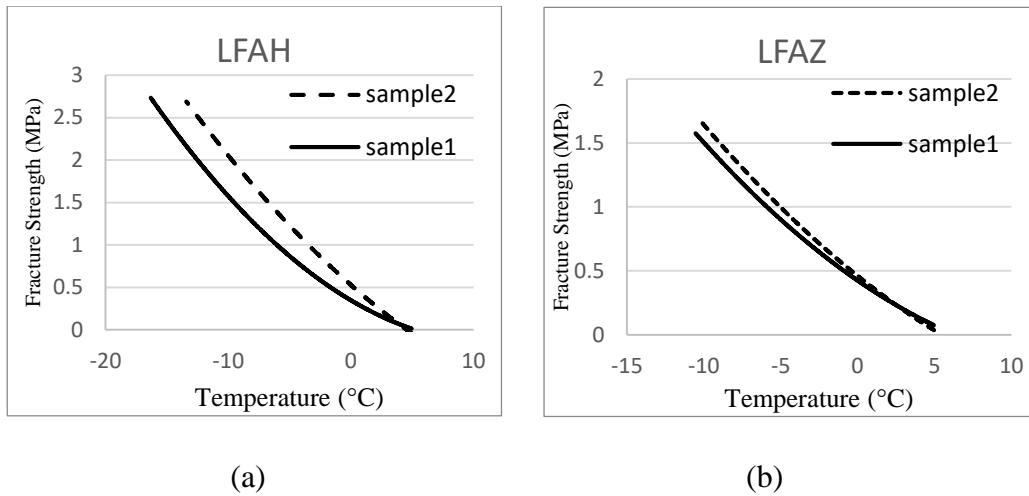


Figure 4.1. Fracture strength versus temperature for specimens fabricated using limestone aggregates

In Figure 4.1(a), 2% hydrated lime was added to one of the fine graded aged specimens that is prepared with limestone aggregate while the other was prepared as neat (Figure 4.1(b)), and tested to determine its low temperature fracture performance. It should be emphasized that properties of the prepared specimens are the same except that they contain hydrated lime. For the reliability of the experiments, 2 replicates were prepared from each specimen to check for the consistency of the results. For the given specimen combinations, the graphs also show that the hydrated lime added blends show higher fracture strength.

Two different aggregate types, basalt and limestone, were used during the preparation of the mixtures. Figure 4.2 shows the effect of aggregate type on fracture strength of the mixtures. It can be observed that the fracture strength of the specimens with limestone are higher than those prepared with basalt aggregate. Based on these outcomes, aggregate type can be considered as a significant factor for fracture strength of asphalt concrete according to the ANOVA analysis. The results presented in the figure are given for 16 specimen combinations and the results for 32 specimens can be found in the appendix section.

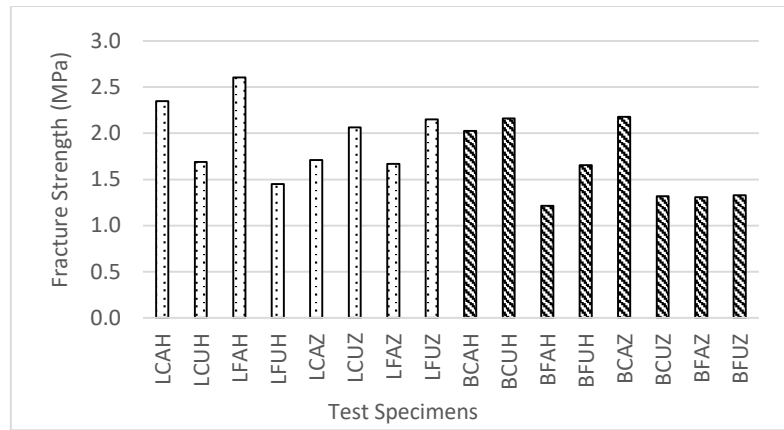


Figure 4.2. The influence of aggregate type on fracture strength

In the prepared asphalt mixtures, basalt and limestone aggregates were used with the nominal maximum aggregate size (NMAS) of 12.5 mm and 9.5 mm - for each aggregate type coarse and fine graded mixtures were prepared, respectively. Different combinations were formed for each gradation, whether including hydrated lime or not and aged or un-aged. Figure 4.3 shows the variation of fracture strength with gradation. The fracture strength of the mixtures prepared with the NMAS of 12.5 mm is significantly higher than those prepared with 9.5 mm. The graphical results for 32 specimens can be found in the appendix section.

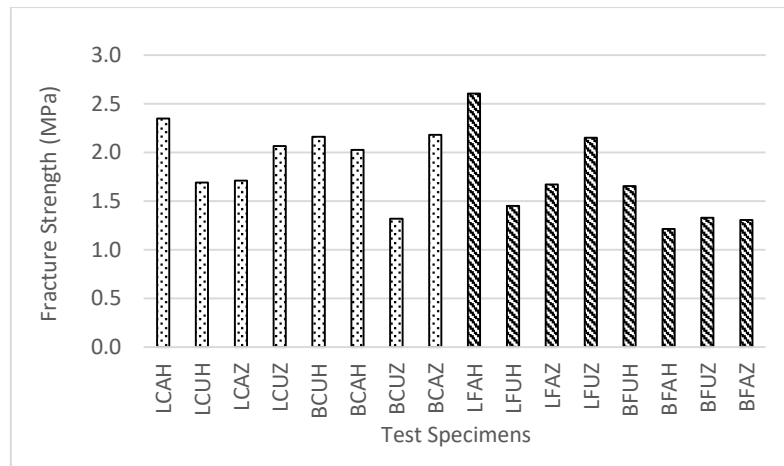


Figure 4.3. The influence of gradation on fracture strength

As indicated in the previous chapter, samples compacted with the gyratory compactor were subjected to long term aging at 85 ° C for five days in accordance with AASHTO R30 procedure. Then, the samples were cut to obtain replicate specimens with dimensions of 50*65*140 mm to be tested. From Figure 4.4, the results seem quite close for aged and un-aged specimens, but the fracture stress of the aged samples are higher than those of unaged ones. This can be explained by the fact that the use of HL may reduce the aging effect of bituminous mixtures. Lesueur et al. (2013) studied the effect of hydrated lime on aging behavior for both aggregate and bitumen as a combination of physical and chemical mechanisms. According to this study, chemical interactions between the hydrated lime and the acidic components in asphalt bitumen increase the aging resistance and hence adhesion in the mixture. Graphical results for 32 test specimens can be found in the appendix section.

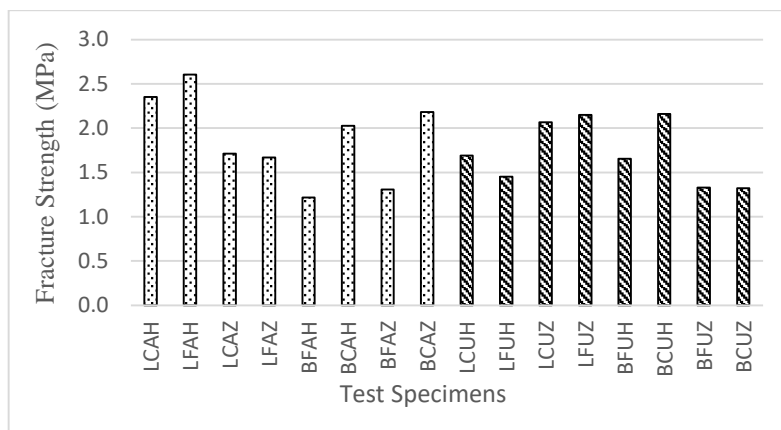


Figure 4.4. The influence of aging on fracture strength

The effect of hydrated lime on fracture resistance was evaluated graphically all together for all the specimens prepared. The first group of mixtures prepared without using hydrated lime - that are referred to as neat -, and the rest were prepared with hydrated lime. As it is evident from the Figure 4.5, the addition of hydrated lime to aggregate has a negligible influence on fracture strength as compared to those (neat) without hydrated lime.

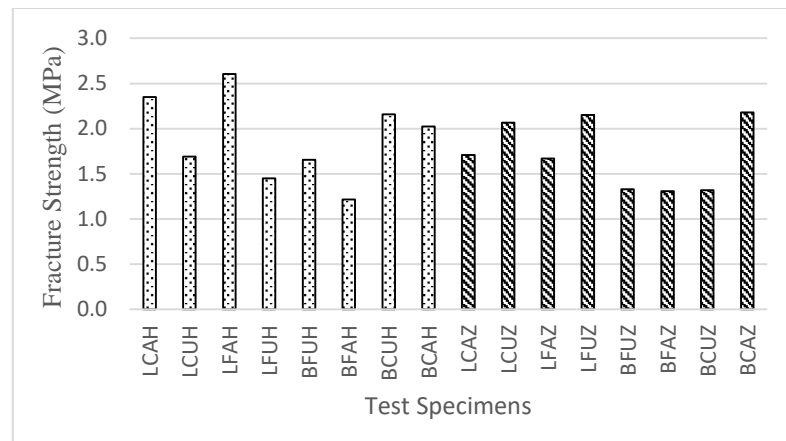


Figure 4.5. The influence of HL on fracture strength

4.2.1.2 Analysis of TSRST Results Fracture Temperature

In the scope of the study, the low temperature performance of the specimens was also evaluated based on fracture temperatures measured from TSRST testing program. The test results show that the average fracture temperature of the tested specimens is -12.140°C with a standard deviation of 3.262 (Table 4.5). However, the maximum fracture temperature for the test specimens was found -5.414°C and the minimum as -16.857°C .

Table 4.5 Descriptive statistics of fracture temperature

Statistical Parameter	Value
Mean	-12.140
Standard Deviation	3.262
Maximum Temperature	-5.414
Minimum Temperature	-16.857

In addition to the analyses given above, variables affecting fracture temperature were also determined by ANOVA. In Table 4.6 shows the effect of each variable used in TSRST testing program. One-way ANOVA analysis was performed to determine the effect of each variable on the TSRST results at 95% confidence level. The results of analyses show that fracture temperature is highly dependent on aggregate type,

gradation and hydrated lime content with probability of less than 0.05. As indicated before, probability values close to zero at the selected confidence level of 5% should be considered a significant factor.

Table 4.6. ANOVA analysis for fracture temperature

Source	Probability
Aggregate Type	0.000
Gradation	0.000
Hydrated Lime Content	0.001
Aging	0.098

Table 4.7 tabulates the influence of different variables – e.g., aggregate type, gradation, hydrated lime modification and aging - on fracture temperature. The mean value of fracture temperature for the specimens prepared with limestone is -14.025°C while it is -10.256°C for specimens with basalt aggregate.

According to the results of ANOVA analysis, the variation in gradations is the dominant variable for fracture temperature with a p-value of nearly 0. As can be seen from Table 4.7, the average fracture temperature is -13,682°C for coarse graded specimens while it is -10,599°C for fine graded ones. It should be emphasized that the specimens with lower fracture temperatures are preferred as they indicate higher resistance to low temperature condition in the field. ANOVA analysis also shows that the addition of hydrated lime seems to have significant influence on fracture temperature with a probability of nearly zero. Specimens prepared with 2% hydrated lime fractured at lower temperatures.

The results of the analysis show that the aging asphalt mixtures in the laboratory conditions has no effect on the fracture temperature. As shown in Table 4.7, the aged specimens show an average fracture temperature of -11,720°C whereas the unaged specimens have an average fracture temperature of -12,561°C.

Table 4.7 Fracture temperatures according to test variables

Design Parameters	Levels	Symbol	Average	Standard Deviation	Median
			°C	°C	°C
Aggregate Type	Limestone	L	-14.025	1.949	-13.984
	Basalt	B	-10.256	3.162	-9.981
Gradation	Coarse	C	-13.682	1.730	-13.673
	Fine	F	-10.599	3.649	-9.915
Hydrated Lime Content	Neat (zero)	Z	-11.254	3.348	-13.027
	2% included	H	-13.027	2.914	-13.342
Aging	Aged	A	-11.720	3.313	-13.286
	Unaged	U	-12.561	3.166	-13.537

Figure 4.6 presents the graphical test results in order to determine the effect of aggregate type on fracture temperatures. When the fracture temperatures are compared based on aggregate type, it can be seen that the specimens prepared using limestone were fractured at lower temperatures than those prepared using basalt. The data in Table 4.7 show that the average fracture temperature for specimens with limestone aggregate is around -14.025°C , which is around 27% lower than for those with basalt aggregate having an average fracture temperature of -10.256°C . This implies that in field conditions, in terms of aggregate type, mixtures with limestone will provide higher resistance to low temperature conditions than do basalt mixtures.

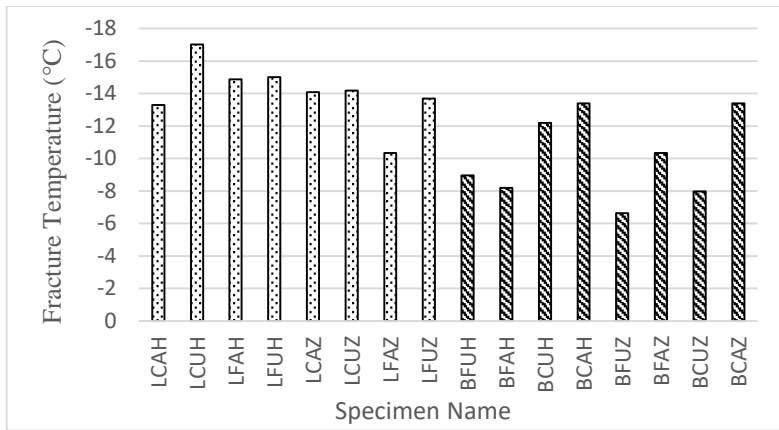


Figure 4.6. The influence of aggregate type on fracture temperature

Figure 4.7 presents the graphical test results in order to determine the effect of gradation on fracture temperatures. When the fracture temperatures of the specimens were compared, it was observed that the specimens prepared with coarse gradation were fractured at lower temperatures than those prepared using fine gradation. According to the test results, the fracture temperature of the specimens prepared with fine gradation increased around 23% compared to those prepared with coarse gradation (from -13.682°C to -10.599°C).

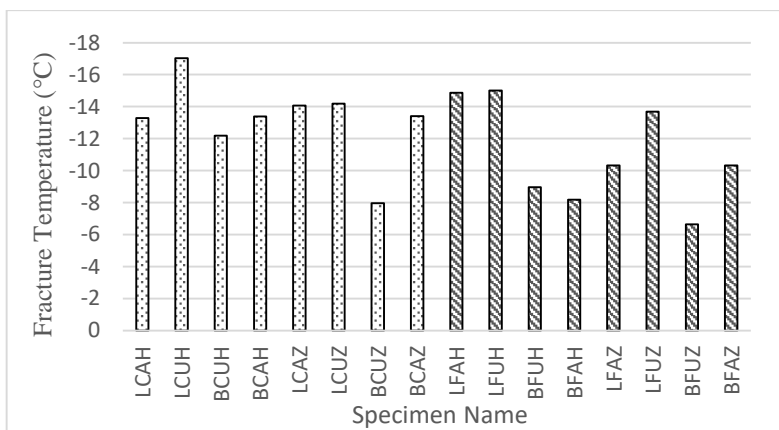


Figure 4.7. The influence of gradation on fracture temperature

Figure 4.8 presents the graphical test results on the effect of hydrated lime on the test mixtures in terms of fracture temperatures. It can be observed that the specimens prepared with 2% hydrated lime were fractured at lower temperatures than those prepared without hydrated lime content. According to the test results, the fracture temperature of the specimens prepared as neat condition increased around 14% (-11.254°C) compared to those prepared with 2% hydrated lime (-13.027°C). This proves that even at minor level hydrated lime improves low temperature performance of asphalt concrete.

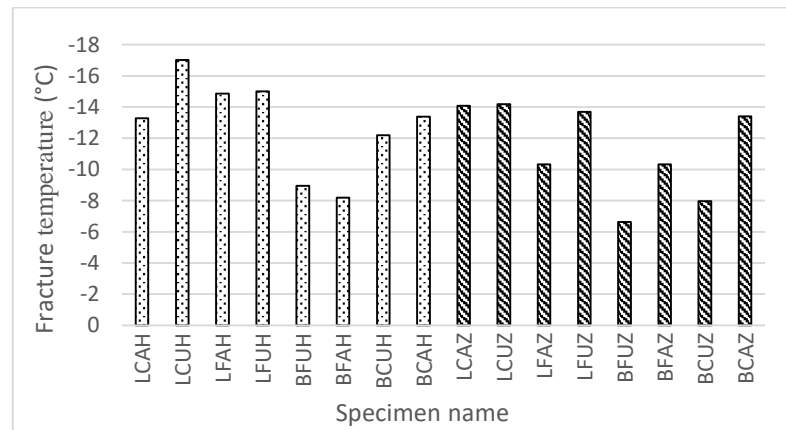


Figure 4.8. The influence of HL on fracture temperature

Figure 4.9 represents the graphical test results to indicate the effect of aging on fracture temperatures. It can be observed that aging does not seem to be a controlling factor on fracture temperatures; while average fracture temperature for the unaged specimens was found -12.561°C, it was measured -11.720°C for unaged ones with statistically negligible difference between them.

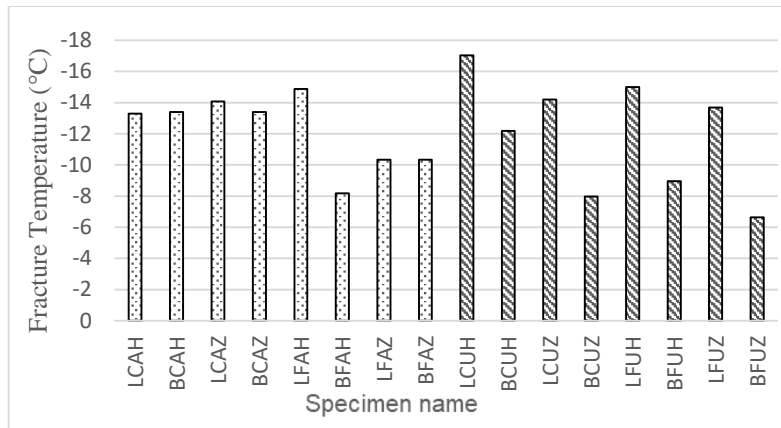


Figure 4.9. The influence of aging on fracture temperature

4.2.2 Analysis of ANOVA for Direct Tension Test Results

A total of 64 Direct Tension Test (DTT) specimens (32 for at 0°C and 32 for at -10°C) were tested. The test specimens were varied according to the type of aggregate (Basalt and Limestone, symbolized by B and L), gradation (Coarse and Fine, respectively, symbolized by C and F), hydrated lime content (including 2% hydrated lime and neat, respectively, denoted by H and Z) or whether they were aged or unaged, respectively, symbolized by A and U. For instance, a specimen with a code of BCAZ10 indicates that basalt is used with coarse gradation, and specimen is prepared using without hydrated lime, subjected to aging. Also, specimen code indicates that the test performed at a temperature of -10°C. ANOVA analyses were performed by first defining the dependent and the independent variables. The experimental design variables are treated as independent variables, and the results are considered as dependent variables. In other words, fracture strength and temperature are dependent variables.

4.2.2.1 Analysis of Direct Tension Test Results at 0°C

As explained in detail in the previous chapter, the fracture stresses generated by mechanically applying tension load using the TSRST setup were measured at a constant temperature of 0°C. The test specimen names and replicate numbers used in DTT can be seen from Table 4.8.

Table 4.8 Specimen names and replicate numbers used in DTT at 0°C

Specimen Code	No. of Replicates	Specimen Code	No. of Replicates
BCUZ0	2	LCUZ0	2
BCUH0	2	LCUH0	2
BCAZ0	2	LCAZ0	2
BCAH0	2	LCAH0	2
BFUZ0	2	LFUZ0	2
BFUH0	2	LFUH0	2
BFAZ0	2	LFAZ0	2
BFAH0	2	LFAH0	2

Results show that the average strength of all the specimens is 1.585 MPa with a standard deviation of 0,315 (Table 4.9). The maximum strength measured is 2.148 MPa and the minimum strength found is 1.038 MPa.

Table 4.9 Descriptive statistics of DTT performed at 0°C

Statistical Parameter	Value
Mean	1.585
Standard Deviation	0.315
Maximum Strength	2.148
Minimum Strength	1.038

In addition to the analyses given above, variables affecting fracture strength were also determined by ANOVA. In Table 4.10, the effect of each variable used in the experiment on fracture strength is shown. When ANOVA results are evaluated, it is seen that aggregate type and gradation are significant variables for the fracture strength of asphalt concrete specimens. This can be validated by observing the p-values being smaller 5% ($p < 0.05$) probability at 95% confidence level. According to results, the calculated probabilities are 0.000 for aggregate type, 0.007 for gradation, 0.091 for hydrated lime content and 0.233 for aging.

Table 4.10 ANOVA analysis of DTT performed at 0°C

Source	Probability
Aggregate Type	0.000
Gradation	0.007
Hydrated Lime Content	0.091
Aging	0.233

In Table 4.11, the effect of test variables on fracture strength is presented in detail. For each variable, mean fracture values, standard deviation and median can be seen. These values confirm the findings obtained from the ANOVA and provide further details.

Table 4.11 DTT results at 0°C for each test variable

Design Parameters	Levels	Symbol	Average	Standard Deviation	Median
			MPa	MPa	MPa
Aggregate Type	Limestone	L	1.38	0.28	1.38
	Basalt	B	1.80	0.19	1.86
Gradation	Coarse	C	1.47	0.30	1.46
	Fine	F	1.70	0.29	1.75
Hydrated Lime Content	Neat (zero)	Z	1.55	0.30	1.48
	2% included	H	1.63	0.33	1.65
Aging	Aged	A	1.65	0.34	1.70
	Unaged	U	1.52	0.28	1.46

Figure 4.10 shows the responses to the aggregate types used during the preparation of the specimens. It can be observed that the specimens prepared using basalt have higher fracture strength. The ANOVA analyses also confirms this finding. Indicating that the average fracture strength is increased by 30% by using basalt aggregate.

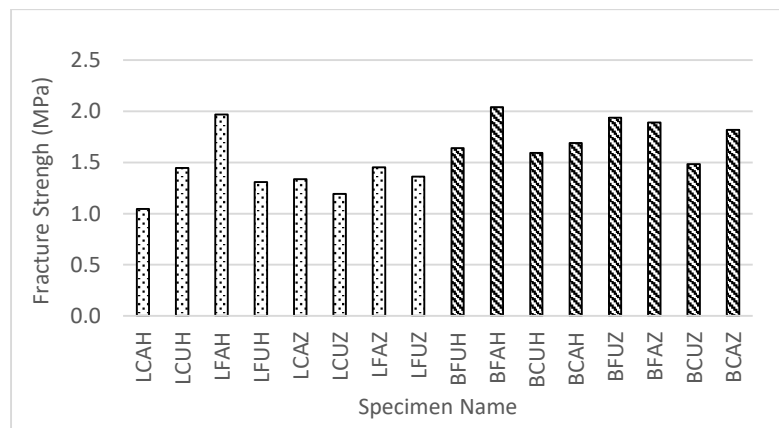


Figure 4.10. The influence of aggregate type on DTT at 0°C

Figure 4.11 shows the fracture strengths for two sets of specimens prepared with different gradations. As can be inferred from the figure, changes in aggregate gradation directly affect the fracture strength of the test specimens. In other words, specimens prepared with coarse gradation fractured under lower stresses than those prepared with fine gradation. The increase of fine fraction in mixture aggregate causes better aggregate interlock and hence higher fracture strength. On the other hand, it is known that fracture strength of asphalt concrete is affected predominantly by bitumen phase rather than aggregate (Tan et al., 2008). Therefore, the small difference between the strength of the coarse and fine graded mixtures may be because of the effect of film thickness between aggregate particles rather than characteristics of aggregate gradation.

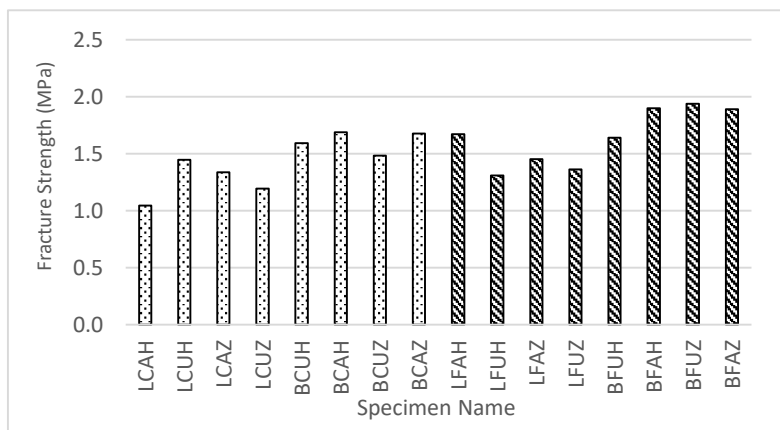


Figure 4.11. The influence of gradation on DTT at 0°C

Figure 4.12 shows that the samples subjected to aging fractured at higher stress. As mentioned earlier in the previous chapters, 16 samples – each replicated twice - were studied. The results obtained from each specimen can be seen in the appendix section. ANOVA results are consistent with the laboratory test results and indicate that the aged samples have higher fracture stress values than do the unaged ones. For example, the aged sample for the BCAH specimen broke at 1.780 MPa while the unaged version of the same combination broke at 1.340 MPa.

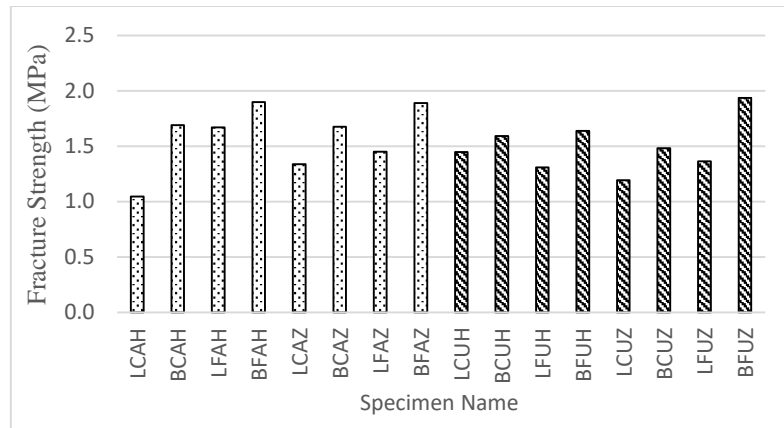


Figure 4.12. The influence of aging on DTT at 0°C

The tested specimens are grouped according to their hydrated lime content. Although the results are close to each other, the specimens prepared as neat have higher fracture values (Figure 4.13).

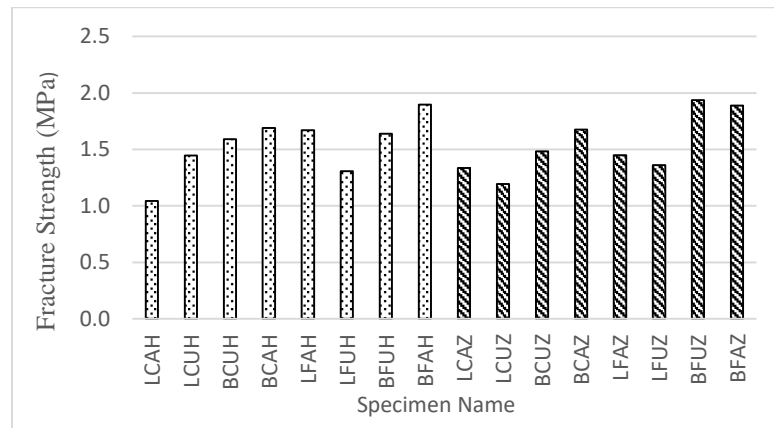


Figure 4.13. The influence of hydrated lime content on DTT at 0°C

4.2.2.2 Analysis of Direct Tension Test Results at -10°C

As explained previously, the fracture strengths were also measured using the TSRST setup at -10°C. It can be seen from Table 4.12 that the same specimen combinations were repeated for this testing program by using 2 replicates per specimen.

Table 4.12 Sample names and replicate numbers for DTT at -10°C

Specimen Code	No. of Replicates	Specimen Code	No. of Replicates
BCUZ10	2	LCUZ10	2
BCUH10	2	LCUH10	2
BCAZ10	2	LCAZ10	2
BCAH10	2	LCAH10	2
BFUZ10	2	LFUZ10	2
BFUH10	2	LFUH10	2
BFAZ10	2	LFAZ10	2
BFAH10	2	LFAH10	2

The test results show that the average strength value of the specimens is 2.414 MPa with a standard deviation of 0.573 (Table 4.13). However, the maximum strength was measured as 3.431 MPa and the minimum strength as 1.356 MPa.

Table 4.13 Descriptive statistics of DTT performed at -10°C

Statistical Parameter	Value
Mean	2.414
Standard Deviation	0.573
Maximum Strength	3.431
Minimum Strength	1.356

In addition to the analyses given above, one-way ANOVA analysis was performed to determine the effect of each variable used on DTT at -10°C. In Table 4.14, the statistical significance levels for each variable can be observed. The analysis shows that the all design variables: aggregate type, gradation, hydrated lime content and specimen aging are significant for fractured strength measured on DTT at -10°C at 95% confidence level (i.e., $p < 0.05$). It can be seen from the table that p value is

nearly zero for aggregate type and hydrated lime content while it also remains quite small for the other variables.

Table 4.14 ANOVA analysis for -10°C DTT

Source	Probability
Aggregate Type	0.000
Gradation	0.002
Hydrated Lime Content	0.000
Aging	0.022

In Table 4.15, the effect of test variables on fracture strength is presented in detail. For each variable, mean fracture values, standard deviation and median can be seen. The values confirm the findings obtained from the ANOVA analysis and provide details.

Table 4.15 DTT results at -10°C for each test variable

Design Parameters	Levels	Symbol	Average	Standard Deviation	Median
			MPa	MPa	MPa
Aggregate Type	Limestone	L	2.099	0.526	2.106
	Basalt	B	2.729	0.437	2.790
Gradation	Coarse	C	2.264	0.597	2.278
	Fine	F	2.564	0.502	2.737
Hydrated Lime Content	Neat (zero)	Z	2.132	0.544	2.156
	2% included	H	2.697	0.461	2.733
Aging	Aged	A	2.521	0.622	2.617
	Unaged	U	2.307	0.518	2.253

Figure 4.14 shows fracture stress results for both aggregate types of the prepared mixtures. These results were classified according to the use of limestone or basalt in the mixture samples. The graph clearly shows that the specimens prepared with basalt have higher fracture stress. This conclusion, also confirmed by ANOVA analysis, agrees with the one that was drawn for the other experiments performed within the scope of the thesis. The average fracture stress observed for limestone was measured 2.099 MPa, and with an increase of 30% 2.729 MPa for basalt.

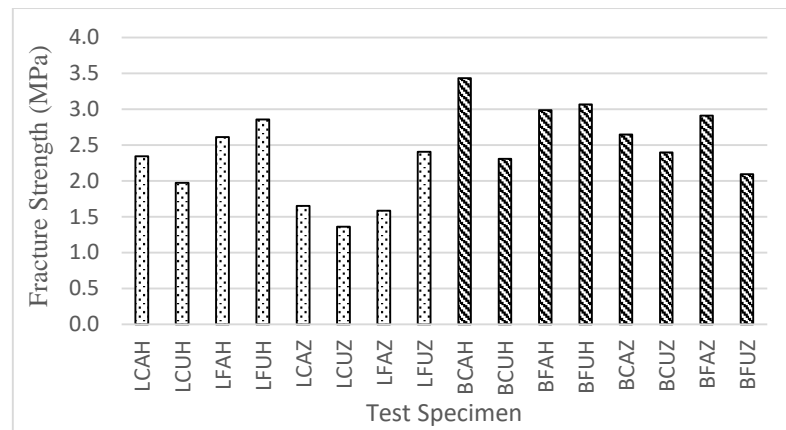


Figure 4.14. The influence of aggregate type on DTT at -10°C

The fracture stresses for the various samples that are separated into two groups for gradation are shown in Figure 4.15. It can be observed from the figure that the specimens fabricated using fine aggregate have higher fracture stress. However, it should be recalled from the previous ANOVA analysis that the impact of aggregate gradation remains low in terms of fracture stress.

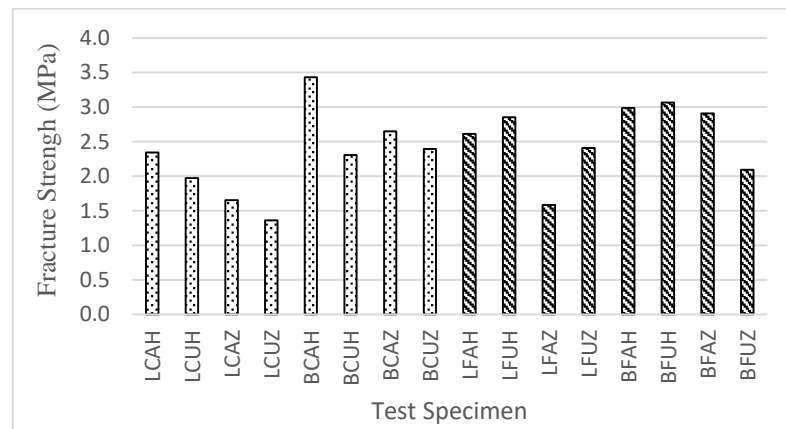


Figure 4.15. The influence of gradation on DTT at -10°C

The comparison of fracture stresses for aging effect for each mixture is shown in Figure 4.16. Mixtures were classified into 2 groups and the first group was subjected to long-term aging. The control group was prepared without aging and both groups

were tensioned at -10°C degree up to fracture. The test results show that the aged specimens have relatively higher fracture strength values. As the results of ANOVA show, aging has a p value of 0.022 indicating a significant test variable for the fracture strength of the specimens.

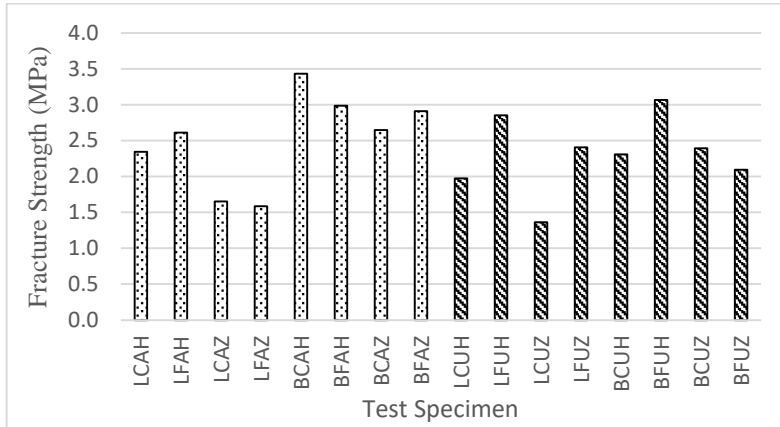


Figure 4.16. The influence of aging on DTT at -10°C

Figure 4.17 shows the effect of hydrated lime on DTT results obtained at -10°C degrees. It is seen that the specimens obtained using hydrated lime have higher fracture strength than those without hydrated lime. Statistical analysis of ANOVA confirms the effect of hydrated lime on fracture strength at -10°C degrees.

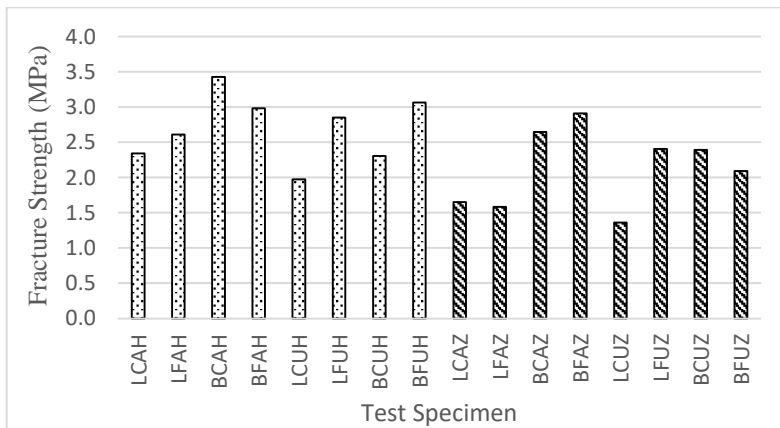


Figure 4.17. The influence of HL content on DTT at -10°C

Figure 4.18 displays the results of DTT at 0 °C and -10 °C. It is apparent that the fracture stresses at -10°C are higher than those at 0°C. At lower temperatures, the asphalt mixture would not experience relaxation as much as it can in higher temperatures and hence yield higher fracture strength. Also, the effect of hydrated lime on low temperature cracking resistance can be easily seen from the figure by noting increased strengths as compared to specimens without hydrated lime content.

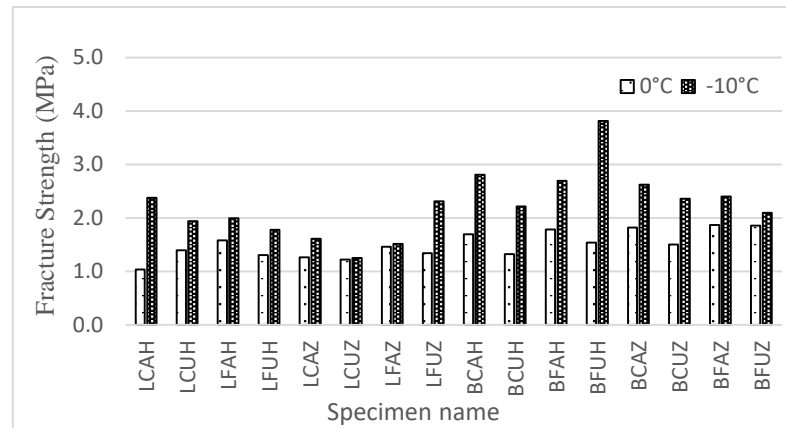


Figure 4.18. Comparison test results for DTT at 0°C and -10°C

4.2.3 Analysis of ANOVA for Indirect Tension Test Results

A total of 64 IDT specimens (32 for 0°C and 32 for -10 °C) were used in IDT testing program. These specimens vary according to the type of aggregate (Basalt and Limestone, symbolized by B and L), gradation (Coarse and Fine, symbolized by C and F), hydrated lime content (Including 2% hydrated lime and neat, symbolized by H and Z) or whether the samples were aged (Aged or unaged, symbolized by A and U). For instance, a specimen given by LCAH0 code indicates that Limestone is used with coarse gradation, sample prepared using with 2% hydrated lime at aged form and tested at 0°C. ANOVA analyses were performed by defining dependent and independent variables. The experimental design variables were illustrated as independent variables, and the results were evaluated as dependent variables. In other words, fracture strength and temperature are dependent variables.

4.2.3.1 Indirect Tension Test Results at 0°C

As explained in the previous chapter, the strength results from the 0°C temperature was determined by the IDT testing device. It can be seen from Table 4.16 that 2 replicates were made for each specimen combination.

Table 4.16 Sample names and replicate numbers for IDT performed at 0°C

Specimen Code	No. of Replicates	Specimen Code	No. of Replicates
BCUZ0	2	LCUZ0	2
BCUH0	2	LCUH0	2
BCAZ0	2	LCAZ0	2
BCAH0	2	LCAH0	2
BFUZ0	2	LFUZ0	2
BFUH0	2	LFUH0	2
BFAZ0	2	LFAZ0	2
BFAH0	2	LFAH0	2

Results show that the average strength value of the tested specimens is 3.447 MPa with a standard deviation of 0.639 (see Table 4.17). However, the maximum strength for the test specimens is 4.860 MPa and the minimum strength was found to be 2.574 MPa.

Table 4.17 Descriptive statistics of IDT performed at 0°C

Statistical Parameter	Value
Mean	3.447
Standard Deviation	0.639
Maximum Strength	4.860
Minimum Strength	2.574

In addition to the analyses given above, variables affecting IDT results performed at 0°C were also determined by ANOVA. In the Table 4.18, the effect of each variable used in the experiment on IDT is analyzed. One-way ANOVA analysis was performed to determine the effect of each variable used on the IDT results performed at 0°C. Confidence level of 95% was used for statistical analyses. The analyses show that IDT strength is directly dependent on aggregate type and gradation with probability of nearly zero. Values close to zero within the confidence interval of 5% were considered to be the dominant factor.

Table 4.18 ANOVA analysis of IDT performed at 0°C

Source	Probability
Aggregate Type	0.003
Gradation	0.001
Hydrated Lime Content	0.067
Aging	0.280

In the Table 4.19, the effect of test variables on fracture strength is presented in detail. For each variable, mean fracture values, standard deviation and median can be seen. The values confirm the findings obtained from the ANOVA analysis and provide details.

Table 4.19 Values of IDT performed at 0°C according to test variables

Design Parameters	Levels	Symbol	Average	Standard Deviation	Median
			MPa	MPa	MPa
Aggregate Type	Limestone	L	3.176	0.484	3.211
	Basalt	B	3.718	0.673	3.734
Gradation	Coarse	C	3.075	0.417	2.966
	Fine	F	3.819	0.613	3.781
Hydrated Lime Content	Neat (zero)	Z	3.298	0.730	3.048
	2% included	H	3.596	0.540	3.490
Aging	Aged	A	3.377	0.649	3.268
	Unaged	U	3.517	0.643	3.386

The mixture aggregate type has strong influence on IDT results. As can be seen from Figure 4.19, while the average strength was 3.176 MPa for the mixtures that prepared with limestone, it was measured 3.718 MPa for the mixtures that prepared with basalt. Similarly, the minimum strength for the mixtures that prepared with limestone was measured as 2.706 MPa while it was 2.966 MPa for the mixtures that prepared with basalt. The overall increase in the strength values when changing the aggregate type from limestone to basalt is around 17% (from 3.176 to 3.718 MPa).

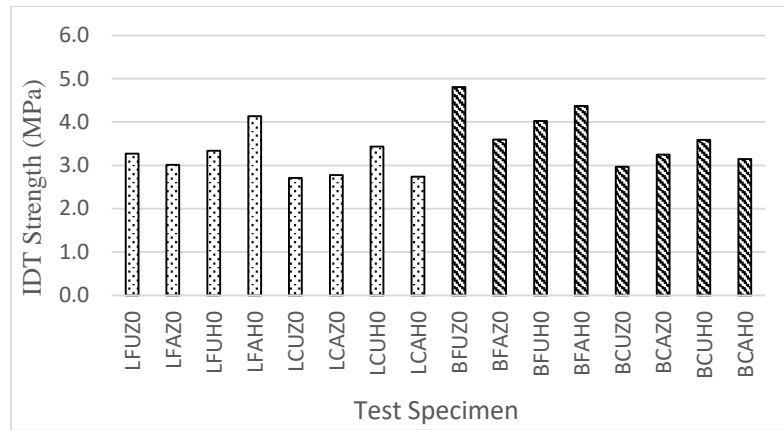


Figure 4.19. The influence of aggregate type on IDT at 0°C

According to the ANOVA analysis, mixture gradation is another important factor that affects the IDT of mixtures. It is obvious from Figure 4.20 that specimens with fine gradation have higher IDT strength than specimens prepared with coarse gradation. Even though the average strength for coarse graded mixtures was measured as 3.075 MPa, it was measured as 3.819 MPa for the fine graded ones. Similarly, the minimum strength for the coarse graded mixtures was measured as 2.706 MPa while it was 3.014 MPa for the fine graded mixtures. The overall increase in the strength values when changing the aggregate gradation from coarse to fine is around 24% (from 3.075 to 3.819 MPa).

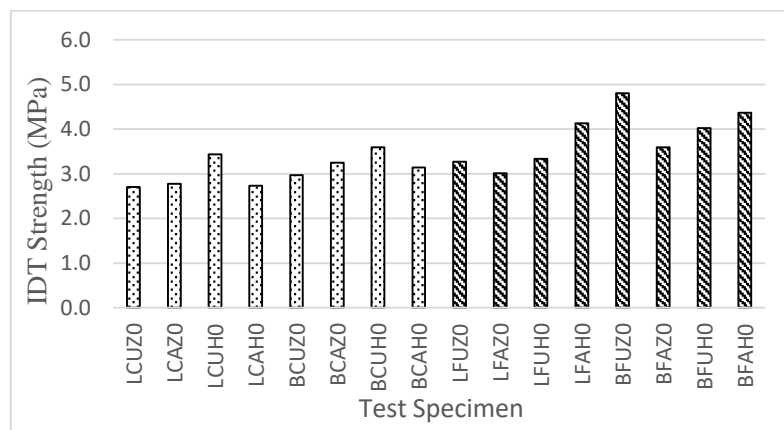


Figure 4.20. The influence of gradation on IDT at 0°C

The comparison between IDT strength and aging for each mixture is shown in Figure 4.21. Mixtures were divided into 2 groups as the first group was subjected to long-term aging and the other was tested as the unaged as control group. As the results of ANOVA indicate, aging of the specimens is not a significant variable on IDT strength. While the average strength was 3,377 MPa for the aged mixtures, it was measured 3.517 MPa for the unaged ones. Similarly, the minimum strength for the mixtures that were subjected to long term aging was measured as 2.735 MPa while it was 2.706 MPa for the unaged specimens. It should be noted that unaged specimens have higher IDT strength values, although statistically aging of specimens is not an effective factor.

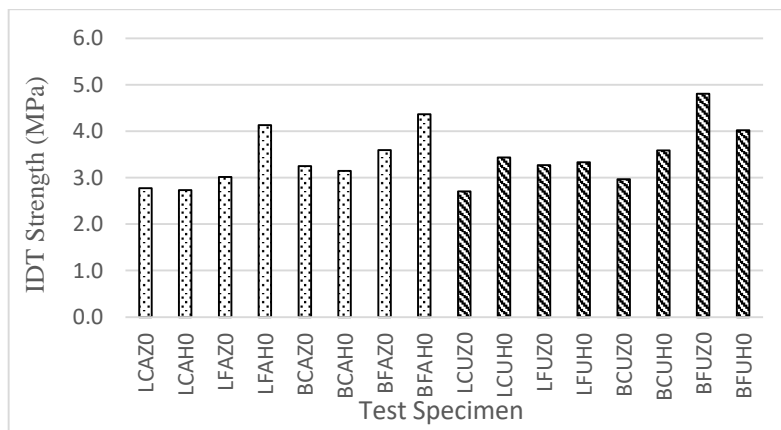


Figure 4.21. The influence of aging on IDT at 0°C

Figure 4.22 shows the responses for the addition of hydrated lime to the test specimens. In terms of the effect of lime content, it can be seen that the addition of lime to the test mixtures does not have a strong effect on IDT strength with a probability higher than 5%. However, to better understand the effect of lime content on the strength, graphical analyses of ANOVA results is needed. In Figure20, the results of IDT tests were plotted for no-lime and 2% lime content. According to the figure the addition of lime to the mixtures increased the IDT values up to around 9% (from 3.298 MPa to 3.596 MPa) in terms of the mean strength values.

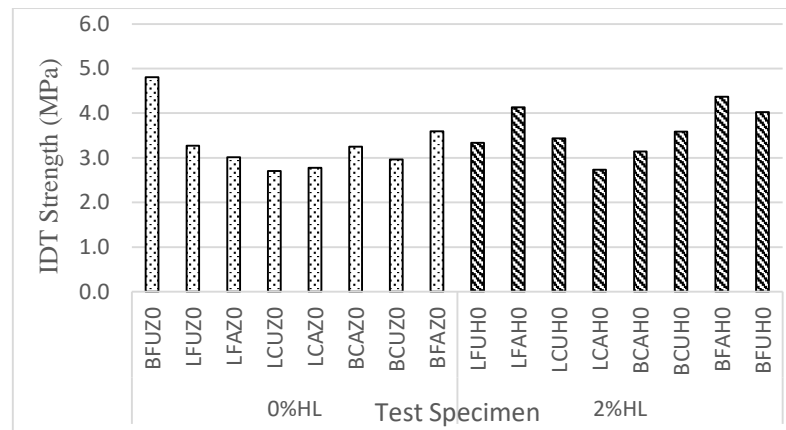


Figure 4.22. The influence of HL content on IDT at 0°C

4.2.3.2 Indirect Tension Test Results at -10°C

As explained in detail in the previous chapter, the strength results from the tests performed at -10°C was determined by the IDT testing device. It can be seen from Table 4.20 that 2 replications were made for each specimen combination.

Table 4.20 Sample names and replicate numbers for IDT

Specimen Code	No. of Replicates	Specimen Code	No. of Replicates
BCUZ10	2	LCUZ10	2
BCUH10	2	LCUH10	2
BCAZ10	2	LCAZ10	2
BCAH10	2	LCAH10	2
BFUZ10	2	LFUZ10	2
BFUH10	2	LFUH10	2
BFAZ10	2	LFAZ10	2
BFAH10	2	LFAH10	2

Results show that the average strength value of tested specimens is 4.332 MPa with a standard deviation of 0.746 (Table 4.21). However, the maximum strength for the test specimens is 5.685 MPa and the minimum strength found as 3.058 MPa.

Table 4.21 Descriptive statistics of -10°C IDT

Statistical Parameter	Value
Mean	4.332
Standard Deviation	0.746
Maximum Strength	5.685
Minimum Strength	3.058

In addition to the analyses given above, variables affecting the fracture strength were also determined by ANOVA. In Table 4.22, the effect of each variable used in the experiment on fracture strength is analyzed. When ANOVA results are evaluated, it is seen that aggregate type, gradation and hydrated lime content are important variables. This is confirmed by the p-values being smaller than 5% at confidence level of 95% (i.e., $p < 0.05$). According to this, the calculated probabilities are found for aggregate type and gradation 0.000, for hydrated lime content 0.009.

Table 4.22 ANOVA analysis of IDT performed at -10°C

Source	Probability
Aggregate Type	0.000
Gradation	0.000
Hydrated Lime Content	0.009
Aging	0.151

In Table 4.23, the effect of test variables on fracture strength is presented in detail. For each variable, mean fracture values, standard deviation and median can be seen. The values confirm the findings obtained from the ANOVA analysis and provide details.

Table 4.23 Values of IDT performed at -10°C according to test variables

Design Parameters	Levels	Symbol	Average	Standard Deviation	Median
			MPa	MPa	MPa
Aggregate Type	Limestone	L	3.828	0.584	3.822
	Basalt	B	4.835	0.515	4.953
Gradation	Coarse	C	4.057	0.713	3.908
	Fine	F	4.606	0.691	4.695
Hydrated Lime Content	Neat (zero)	Z	4.080	0.595	3.906
	2% included	H	4.583	0.812	4.953
Aging	Aged	A	4.390	0.782	3.914
	Unaged	U	4.273	0.727	4.436

The mixture aggregate type has a strong influence on IDT results. As can be seen from Figure 4.23, while the average strength was 3.828 MPa for the mixtures that prepared with limestone, it was measured 4.835 MPa for the mixtures that prepared with basalt. Similarly, the minimum strength for the mixtures that prepared with limestone, was measured as 1.918 MPa while it was 4.022 MPa for the mixtures that prepared with basalt. The overall increase in the strength values when changing the aggregate type from limestone to basalt is around 26% (from 3.828 to 4.835 MPa).

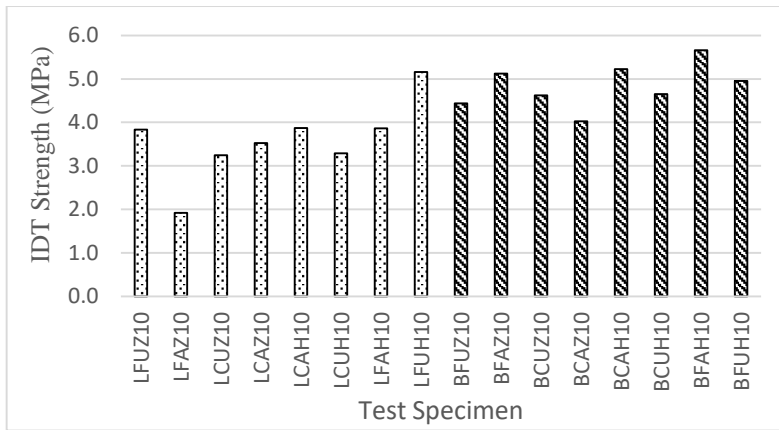


Figure 4.23. The influence of aggregate type on IDT at -10°C

According to the ANOVA analysis, mixture gradation is not a significant main factor that effects the IDT of mixtures. It is obvious from Figure 4.24 that, samples with fine gradation have higher IDT strength than samples prepared with coarse gradation. Even though the average strength for coarse graded mixtures was measured as 4.057 MPa, it was measured as 4.606 MPa for the fine graded ones. The overall increase in the strength values when changing the aggregate type from limestone to basalt is around 14% (from 4.057 to 4.606 MPa).

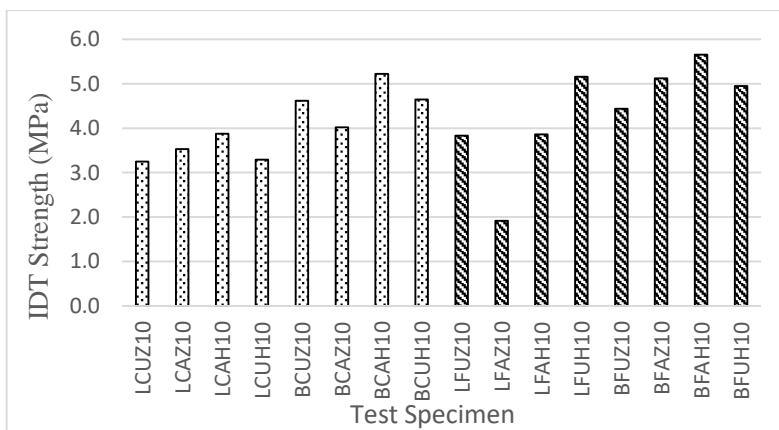


Figure 4.24. The influence gradation on IDT at -10°C

The comparison between IDT strength and aging for each mixture is shown in Figure 4.25. Mixtures were divided into 2 groups as the first group was exposed to long-term aging the other was accepted as the un-aged group. As the results of ANOVA indicate, aging of the specimens is not a significant variable on IDT strength. While the average strength was 4.390 MPa for the aged mixtures, it was measured 4.273 MPa for the unaged ones. It should be noted that aged specimens have higher IDT strength values, although statistically aging of specimens is not an effective factor.

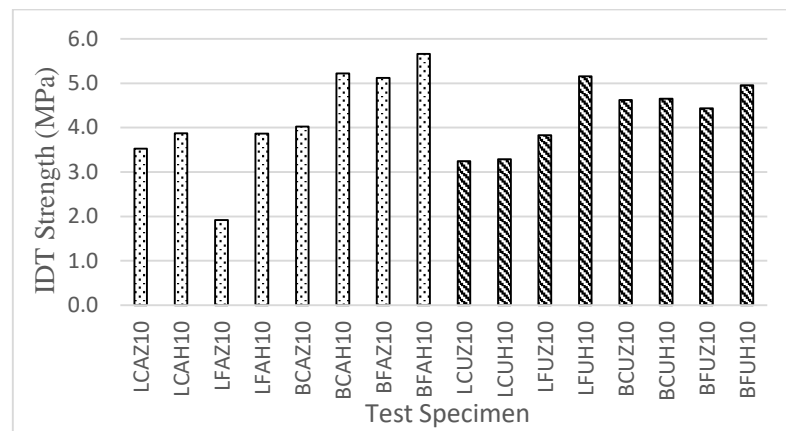


Figure 4.25. The influence of aging on IDT at -10°C

Figure 4.26 shows the responses for the addition of hydrated lime to the specimens. In terms of the effect of lime content, the addition of lime to the test mixtures strongly influences the IDT values with a probability of smaller than 5%. In Figure 5, the results of IDT tests were plotted for no-lime and 2% lime content. A careful observation of IDT values indicates that addition of lime to the test mixtures increased the IDT values for about 12% (from 4.080 to 4.583 MPa) in terms of the mean strength values. When no lime is used, the maximum IDT strength was found to be 5.119 MPa whereas it was 5.658 MPa for 2% lime content. There is also noticeable increase in the minimum strength values. While the minimum strength is 1.918 MPa for no-lime mixtures, it was found to be 3.291 MPa for 2% lime content.

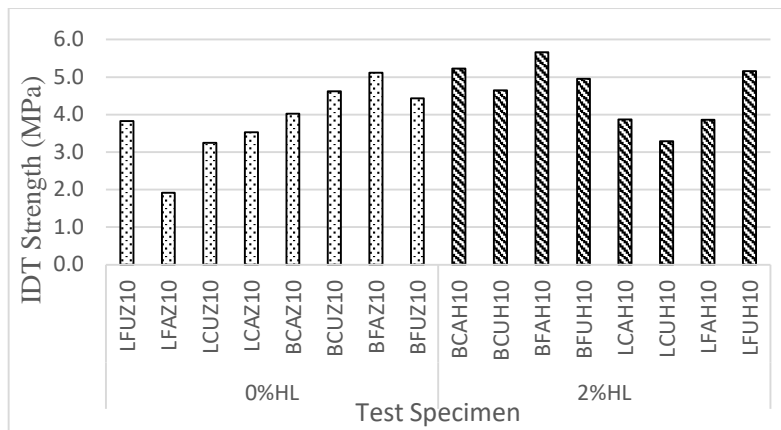


Figure 4.26. The influence of HL content on IDT at -10°C

Figure 4.27 presents the comparison of IDT results for all combinations at test temperatures of 0°C (zero) and -10°C (low). The results show that the addition of HL increases the tensile strength of the mixtures at both temperatures. At low temperature, maximum tensile strength of specimens prepared at 0% HL is 4.909 MPa while it is 5.658 MPa for specimens that contains 2% hydrated lime. Hydrated lime increases the tensile strength of specimen around 15%. However, at zero temperatures, no improvement was observed by using hydrated lime.

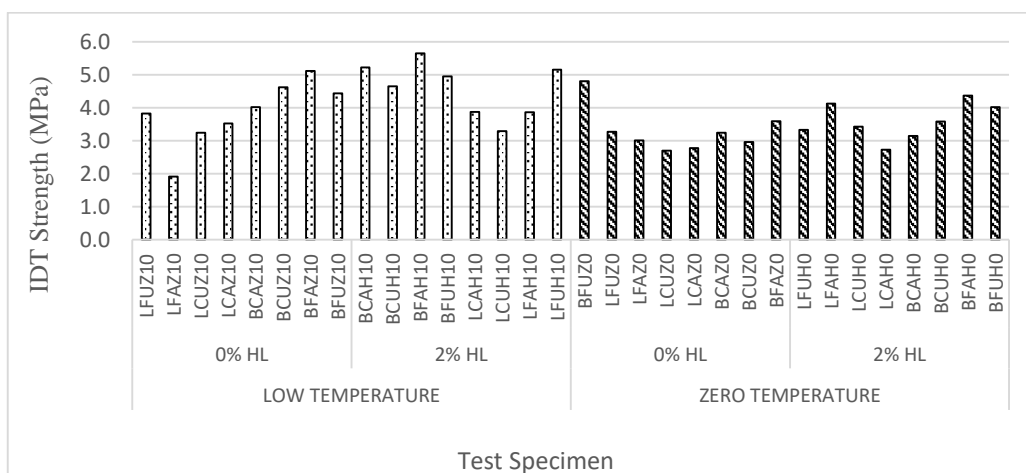


Figure 4.27. IDT results comparison

4.3 Bitumen Testing

In the study, tests were performed with 50/70 penetration graded bitumen. Several combinations were prepared using basalt and limestone filler parts with or without adding hydrated lime. During the preparation stage of the mastics, bitumen, aggregates and HL were heated in the oven at around 150 to 160°C. Then, according to the type of mixture either only basalt, limestone fillers or basalt + HL and limestone + HL were mixed with bitumen. The filler and hydrated lime were added to the bitumen part and mixed regularly until a homogeneous mixture was obtained. Test samples were then prepared to test low temperature performance by using HL in normal and laboratory aged bitumen. The experimental approach determined for the study is schematically as follows in Figure 4.28:

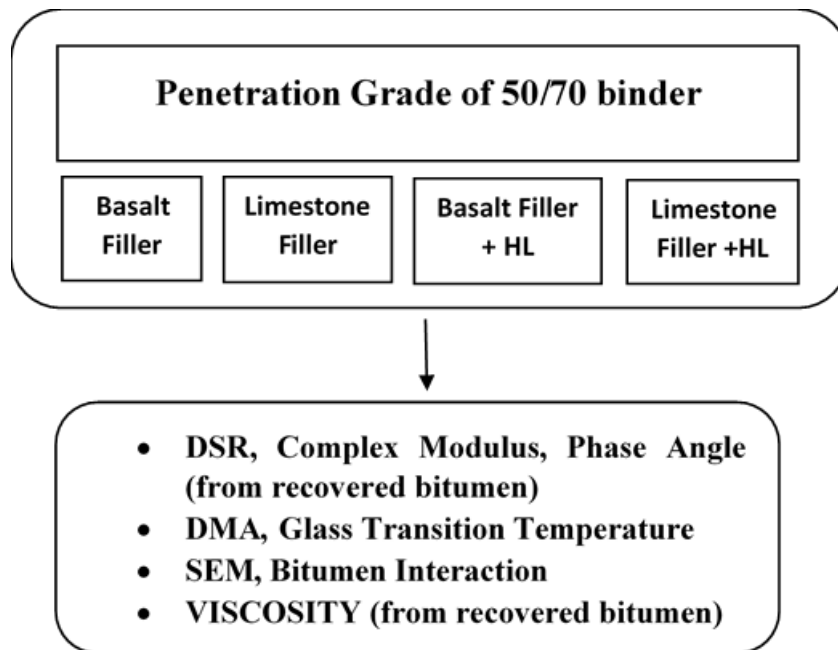


Figure 4.28. Bitumen performance tests

4.3.1 Dynamic Shear Rheometer

Asphalt bitumen is a viscoelastic material that has an elastic behavior (i.e., more solid) at lower temperatures and a viscous (i.e., more liquid) behavior at higher temperatures. Dynamic Shear Rheometer (DSR) can be used to calculate both viscous and elastic properties of bitumen. During the test, the asphalt sample is sandwiched between two circular plates, and the upper plate (or spindle) oscillates while the bottom plate is fixed. This study investigates the influence of hydrated lime modification on changing the elasticity of bitumen.

It is worth noting that DSR is mainly used to determine the complex shear modulus (G^*) that has two components: storage and loss modulus. Simply put, G^* is used for defining the fatigue and rutting behavior of asphalt binder. This value is an important parameter to determining the rheological behavior of asphalt bitumen. Elastic (storage) modulus (G') and loss (viscous) modulus (G'') are the two components of this parameter. In this study, DSR was performed using 25 mm diameter plates with a gap of 1 mm.

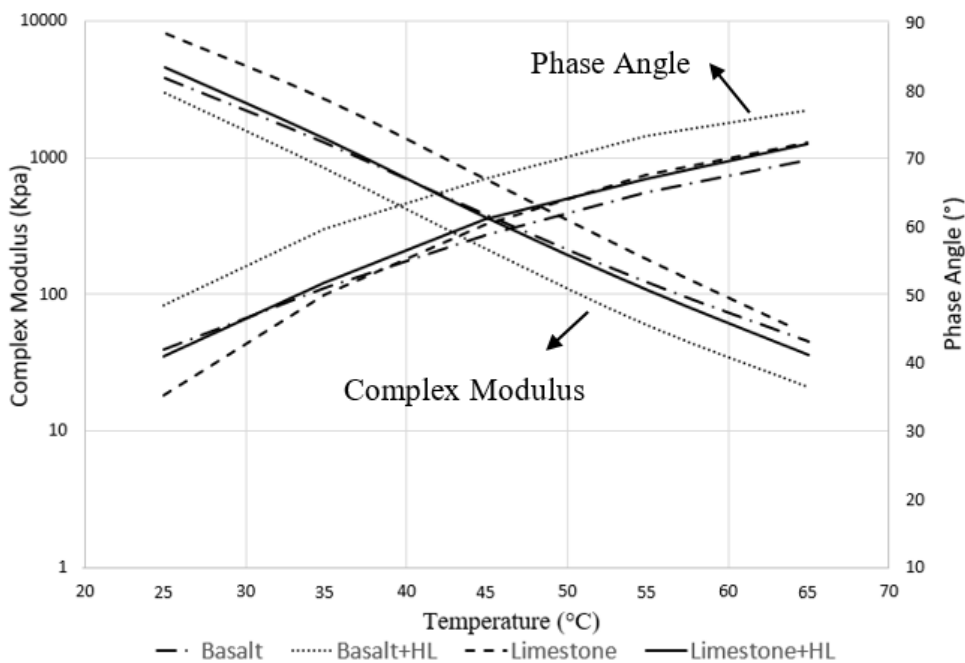
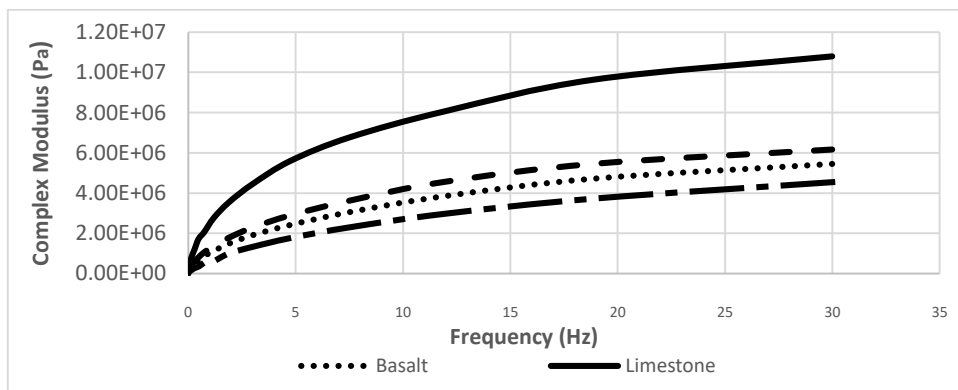
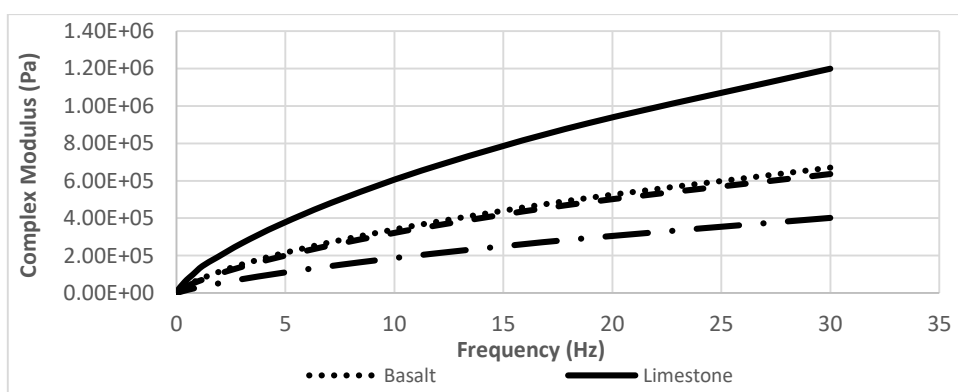


Figure 4.29. DSR master curve for extracted bitumen from mixtures

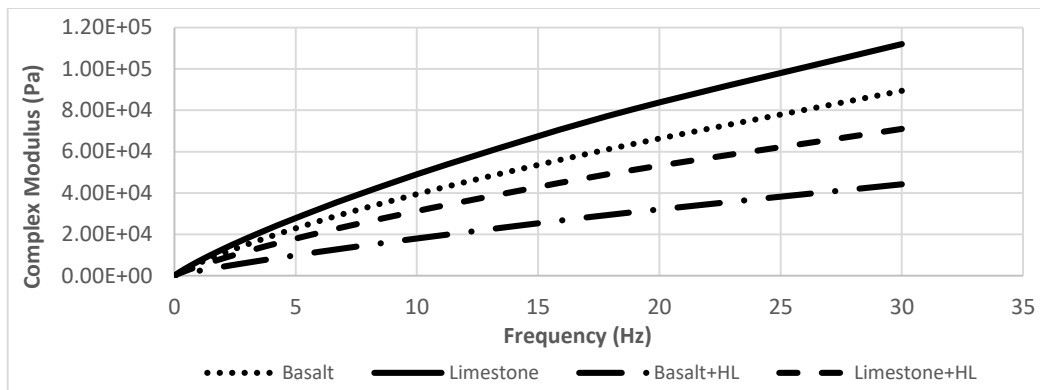
It is clearly seen from Figure 4.29 that the complex modulus of the extracted bitumen (called EB) from the mixture prepared with limestone is greater than others and the phase angle for the same EB is the smallest. This indicates that EB from limestone mixtures are more elastic (or stiffer). Also, the complex modulus at 0 °C and -10 °C of EB obtained by adding basalt + HL and limestone + HL are observed to be lower than the complex modulus of EB from basalt and limestone mixtures. The lowest complex modulus was observed by adding basalt fillers and HL simultaneously to the mixture. In this case, the phase angle also is the highest in comparison to other combinations. This shows that the addition of basalt fillers and HL at the same time into the bitumen improves rheological properties of bitumen to have a mixture more resistant to low temperature cracking.



(a)



(b)



(c)

Figure 4.30. Mastic complex modulus at (a) 25°C, (b) 45°C, (c) 65°C

Figure 4.30 shows that EB from limestone aggregate is stiffer than the others for each temperature and frequency. This shows that samples prepared with limestone may perform better in rutting at high temperature, conversely low temperature fracture potential may increase. At 25°C temperature, bitumen that was extracted from basalt + HL combination has the lowest complex modulus when compared with other extracted samples. That indicates that basalt+ HL combination has more elasticity at lower temperatures.

4.3.2 SEM Analysis of Mastic Phase

To understand the interaction of bitumen with hydrated lime. Scanning Electron Microscope (SEM) analysis was performed with the Quanta FEG Scanning Electron Microscope as previously mentioned. The main objective is to observe the agglomeration of hydrated lime in normal and aged bitumen. While performing the procedure, high spectrum of X-ray is emitted to view the designated areas.

The quality of the image obtained from the scanned samples is directly related to the chemical composition of the sample. In the obtained images, hydrated lime phase

appears as bright and cloudy shape, while bitumen phase appears as darker color. The gray parts obtained represent the interaction between these two materials. Examples of images appear in the form.

Unaged and aged bitumen mastics were prepared using both limestone + HL and basalt + HL combinations. Then, they are coated with gold atoms and placed in the vacuum medium in SEM before starting the experiment. Figures 4.31 - 4.34 show the collective internal structure of the mixtures between 500x and 20000x magnification levels.

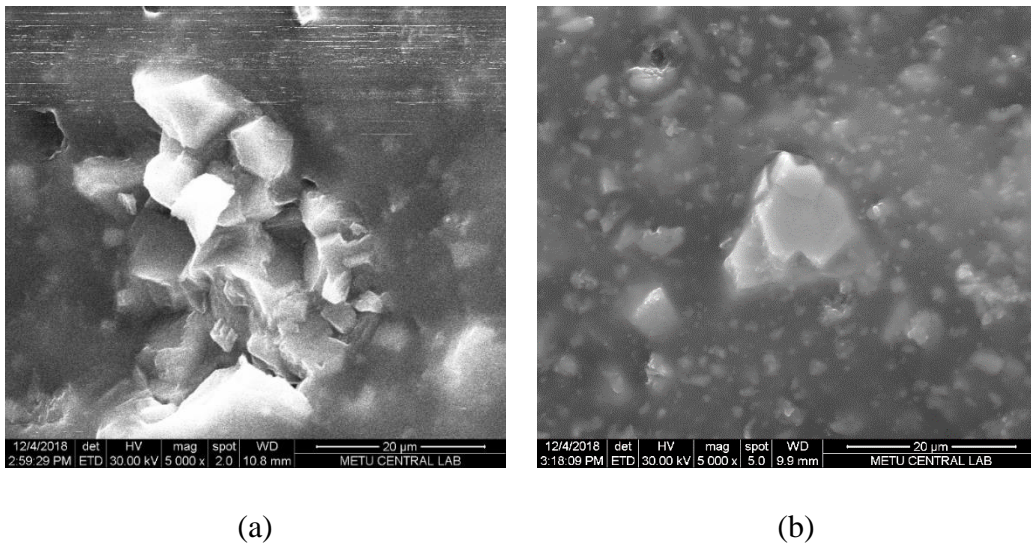


Figure 4.31. SEM test results of mastics prepared with unaged bitumen and (a) HL+ Limestone. (b) HL + Basalt

For mastics prepared with both basalt + HL and limestone + HL, hydrated lime has large specific surface area on aggregate fillers (Figure 4.31). SEM results show that hydrated lime has very small size and irregular cloud shape. This will ensure that gaps in asphalt mixtures can be filled. Decreasing the gaps will result in an increase in density and thus an increase in deformation resistance (Rizkiyantoro, P., 2010). However, regional agglomerated areas should not be ignored. A new asphalt binder modified with hydrated lime is obtained. This hydrated lime dispersion in the binder

can result in modulus improvement. For the basalt and hydrated lime combination with unaged bitumen, it is clearly seen that hydrated lime has more homogeneous distribution. As it can be seen in the Figure 4.31 (b), hydrated lime particles are distributed homogeneously in the matrix. However, for the mastics prepared with limestone and hydrated lime combination, agglomeration areas present (Figure 4.31 (a)).

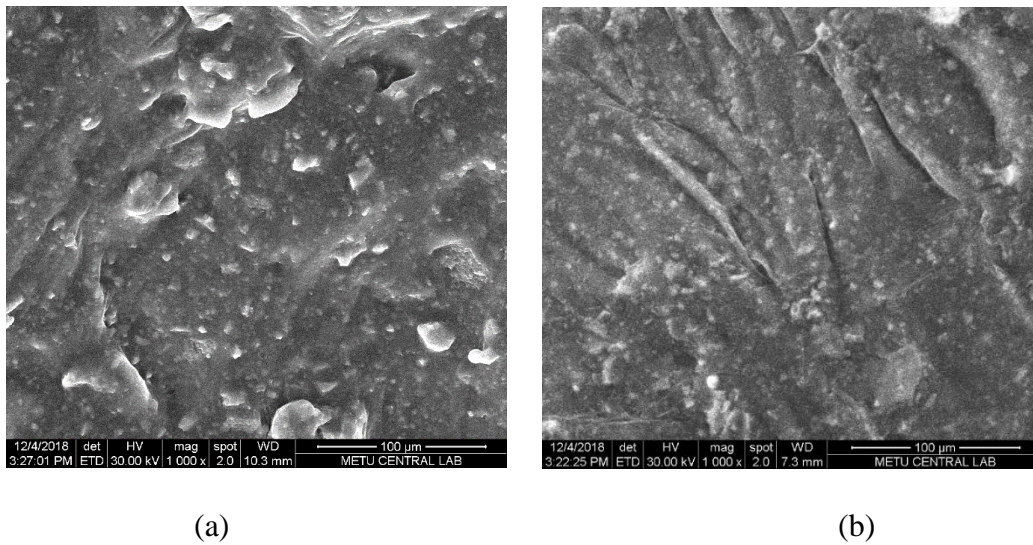
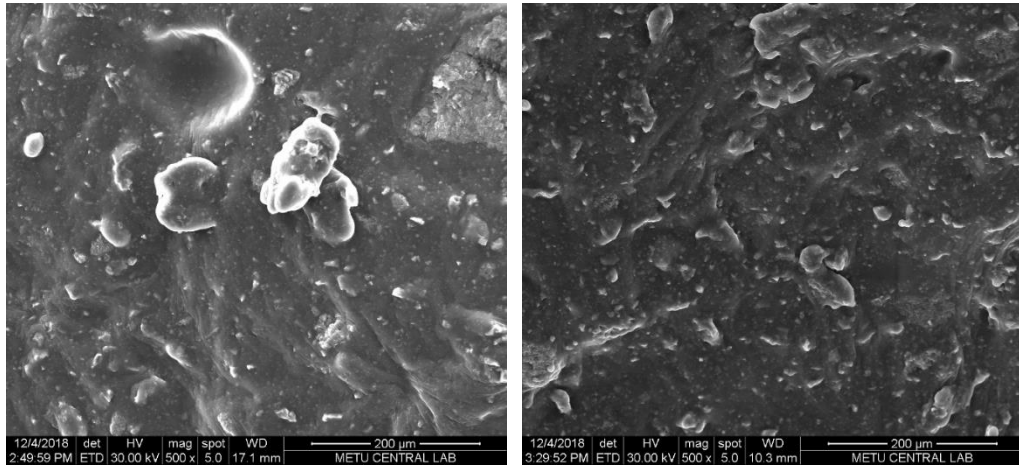


Figure 4.32. SEM test results of mastics prepared with aged bitumen and (a) HL+ Limestone. (b) HL + Basalt

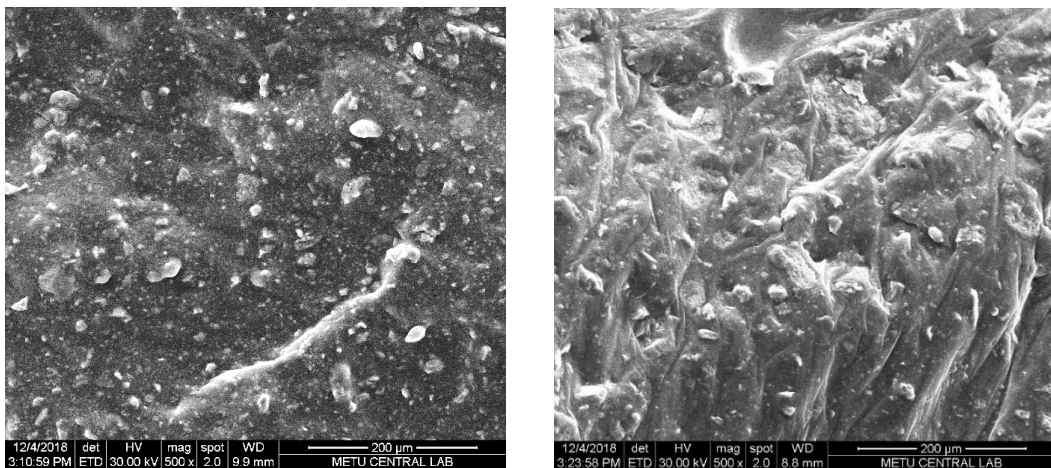
Figure 4.32 shows SEM analysis for mastics prepared with aged bitumen. Combination of basalt + HL, creates smooth wavy surface and hydrated lime distributed homogeneously compared with limestone + HL combination.



(a)

(b)

Figure 4.33. SEM test results of mastics prepared with (a) Unaged bitumen and HL+ Limestone. (b) Aged bitumen and HL+ Limestone



(a)

(b)

Figure 4.34. SEM test results of mastics prepared with (a) Unaged bitumen and HL+ Basalt. (b) Aged bitumen and HL+ Basalt

Figure 4.33 and Figure 4.34 illustrate the comparison of mastics with limestone + hydrated lime and basalt + hydrated lime that were prepared both aged and unaged bitumens. Results show that hydrated lime distribution is more homogenous with

aged bitumen compared with unaged one. Also, in the basalt and hydrated lime combination case, aged bitumen shows wavy surface.

The elemental compositions in the mixture is shown as spectra (Figures 4.35-4.36). The x-axis represents the number of x-rays and the y-axis represents the energy in KeV. The element concentration at the areas is presented graphically. These points are matched with the peaks in the periodic table and the current element definition is made.

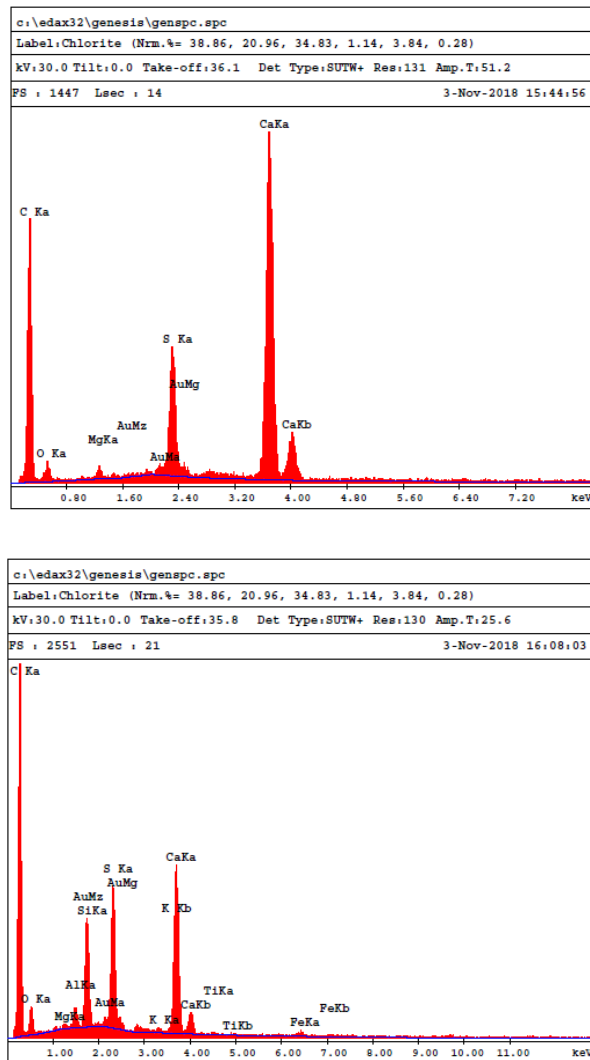


Figure 4.35. Spectra of the element distribution of HL with (a) unaged-limestone. (b) unaged-basalt

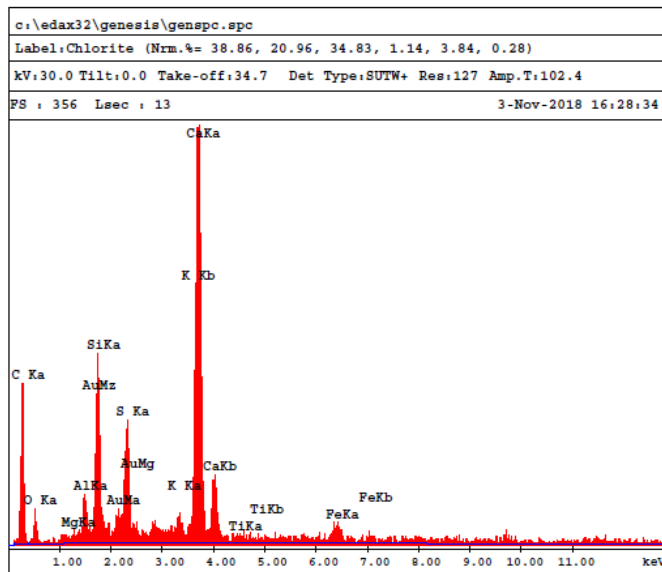
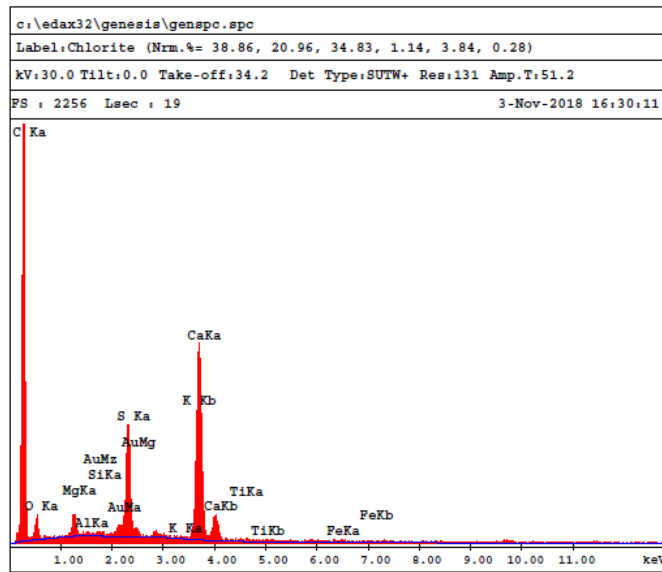


Figure 4.36. Spectra of the element distribution of HL with (c) aged-basalt. (d) aged-limestone

4.3.3 Dynamic Mechanical Analysis (DMA) on Mastic Phase

Figure 4.37 provides data on glass transition temperature obtained from dynamic mechanical analysis. It should be noted that tests were carried out using neat bitumen and bitumen-filler mastics prepared with basalt, limestone and combination of basalt + HL. Limestone, + HL together. Each combination was carried out for unaged and aged bitumen respectively. Results for all tested mastics can be seen from Appendix section.

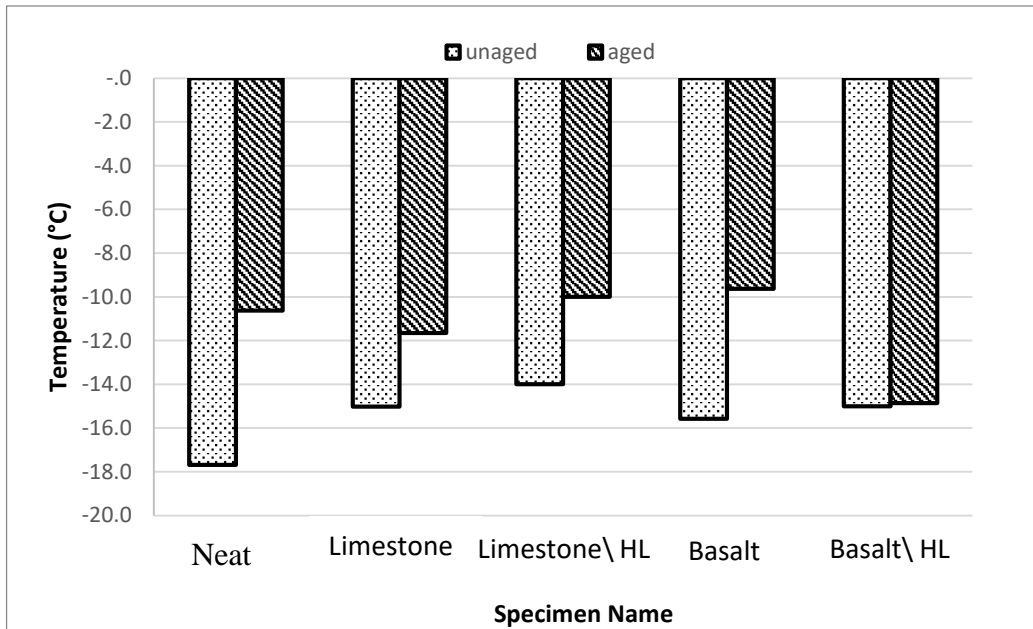


Figure 4.37. Tg of various mastic compositions

Dynamic Mechanical Analysis (DMA) is a very effective method for determining the glass transition temperature. Glass transition temperature is related with the viscoelastic behavior of binder. Lower glass transition temperature is associated with softer binder and less temperature dependency. It also suggests better low temperature cracking resistance. Unaged neat bitumen has a glass transition temperature of around -18°C. With the addition of filler to the bitumen, it is clearly

seen that T_g increases. According to the graph, the most sensitive combination is the addition of limestone and hydrated lime fillers together for unaged samples. As it is known from the literature, aging increases glass transition temperature and for the test specimens, T_g is increased up to -10°C for neat bitumen. While addition of limestone filler increases the T_g, around 2.5°C the combination of limestone and hydrated lime filler increase around 3.6°C. Surprisingly addition of basalt filler and hydrated lime combination makes glass transition temperatures for aged and un-aged samples around the same.

4.3.4 Rotational Viscosity of Mastic Phase

Viscosity values were obtained with Brookfield Rotational Viscometer (RV) to determine the effect of hydrated lime on viscosity for un-aged bitumen samples. The test was implemented at a constant speed of 20 rpm, within a temperature range of 118.40°C to 178.20°C and recorded as (Pa-s).

Solid particles added to the bitumen are known to increase the viscosity of the liquid (Coussot, 2005; Lesueur, 2009). In other words, the higher the volume of solid particles present in the bitumen, promotes the higher viscosity. This value increases faster as the interlocking of solid particles. According to Schiffner (2003), during the bitumen extraction nearly 40% of HL can't be recovered while it is less than 10% for limestone. This may indicate that hydrated lime has a stronger interaction with basalt.

Figure 4.38 shows the change in viscosity of bitumen obtained by extraction from four different mixtures (limestone, limestone+HL, basalt, basalt+HL). It is clearly seen that the addition of limestone and limestone + HL composition increases viscosity (in other words stiffness) at the temperature range selected for this study (Figure 4.38). For all temperatures at which the test is performed, the addition of basalt and basalt + HL combination makes almost no change when it is compared with neat bitumen viscosity results.

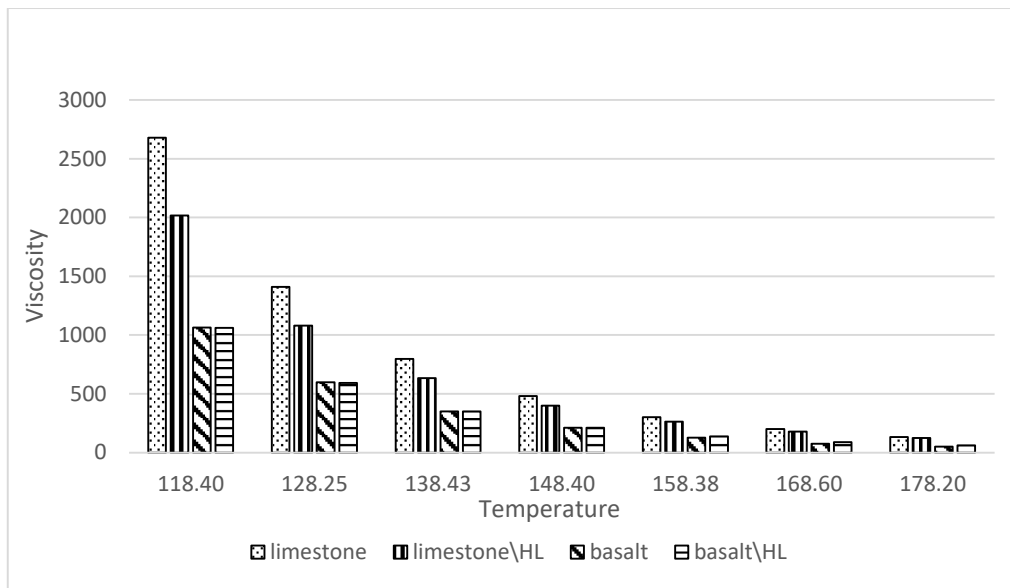


Figure 4.38. Comparison the viscosities of EB

CHAPTER 5

CONCLUSIONS AND RECOMMENDATIONS

5.1 Introduction

This chapter summarizes the results of this study and recommends the development of new methodologies that are hoped to provide a milestone for future studies. Although the statistical analysis results are universal, the summarized findings of the study may vary depending on the local variables such as experimental program, materials used, test procedures and conditions.

5.2 Conclusions

In the experimental program, the effect of hydrated lime on low temperature cracking of asphalt mixtures was tested. The two-fold experimental program of this study investigates the influence of hydrated lime (HL) on low temperature cracking performance of hot mix asphalt (HMA) and rheological properties of bitumen. To determine the effect of HL on low temperature cracking performance of asphalt mixtures, tests were performed on either prismatic beams or circular specimens, which were fabricated from Superpave gyratory samples. Two prismatic beams were obtained from each gyratory specimen, and each combination was tested with two replications for the tests performed with Thermal Stress Restrained Specimen (TSRST) set up. TSRST was performed on 32 beam samples with the dependent variables of fracture strength and temperature. A total of 64 beam samples were performed for Direct Tension Test (DTT) at two different temperature level and fracture strength was accepted as a dependent variable. A new set of 64 circular specimens were tested for Indirect Tensile Test (IDT) to investigate the effect of HL on low temperature performance at two different temperature levels. Fracture

strength is a dependent variable for IDT and DTT. For all mixture tests, aggregate type, gradation, HL content, and aging were accepted as independent variables. The results were tested using ANOVA analysis and the significance of presence of hydrated lime and other design parameters were determined. In addition, to determine the effect of hydrated lime on bitumen; mastics (containing hydrated lime and basalt / limestone fillers) were fabricated to perform Dynamic Mechanical Analysis (DMA) and Scanning Electron Microscope (SEM) analyses. Also, the bitumen obtained extracted from the mixtures were tested with Rotational Viscometer (RV) and Dynamic Shear Rheometer (DSR) and the results were interpreted. The findings of the research are as follows:

- 1) According to TSRST results, aggregate type significantly influenced the low temperature cracking resistance of asphalt mixtures. The mixtures prepared with limestone aggregate showed higher fracture resistance than those fabricated with basalt aggregate. Such behavior can be attributed to the surface texture and the shape of the aggregates which can affect the bitumen-aggregate interface.
- 2) Gradation was found to be a significant factor in determining low temperature performance. Specimens prepared with coarse gradation have higher fracture strength than those prepared by fine gradation with respect to TSRST results.
- 3) Aging was not found to be effective in low temperature cracking resistance according to TSRST. Results were quite comparable for aged and unaged specimens but the fracture stresses of aged samples were higher than those of unaged. This can be explained by the fact that the use of hydrated lime reduces the aging effect of bituminous mixtures.
- 4) According to ANOVA analyses, addition of hydrated lime to the mixtures was not found to be a significant factor ($p < 0.05$) for fracture resistance with respect to TSRST. However, when the results compared for samples whether they include hydrated lime or not, it is observed that specimens

modified by hydrated lime have higher low temperature fracture resistance.

- 5) When fracture temperatures of specimens are analyzed, it is seen that aggregate type is an influential factor for low temperature performance of asphalt concrete. It was observed that the specimens prepared using limestone were fractured at lower temperatures compared with those prepared using basalt. According to TSRST, it was observed that the specimens prepared with limestone were fractured at lower temperatures. When the results were analyzed in detail, specimens made with basalt, fractured approximately 27% higher temperatures.
- 6) Considering fracture temperatures of the specimens, it was observed that the specimens prepared with coarse gradation were fractured at lower temperatures than those prepared using fine gradation. According to the test results, the fracture temperature for fine gradation specimens increased up to about 23% compared to those prepared with coarse gradation.
- 7) Specimens prepared with 2% hydrated lime were fractured at lower temperatures than those containing no hydrated lime. According to the test results, the fracture temperature of the specimens prepared without hydrated lime increased up to around 14% compared to those prepared with 2% hydrated lime.
- 8) Based on the DTT results, which was performed at 0°C and -10°C, aggregate type is a significant variable for fracture resistance. Mixtures prepared with basalt aggregate, showed higher fracture resistance than those prepared with limestone aggregate. This can be explained by the fact that asphalt mixture relaxes during a test with such nature because bitumen behavior is highly dependent upon loading rate. It can be understood that hydrated lime has higher interaction with basalt aggregate.

- 9) Referring to DTT at both temperatures, specimens prepared with fine gradation has higher fracture strength than those prepared by coarse gradation. The overall increase in the strength values when changing the aggregate gradation from coarse to fine is around 24%.
- 10) Effect the aging of specimens was found to be insignificant based on DTT results at 0°C and -10°C.
- 11) Based on DTT results, addition of hydrated lime is a significant variable that increases the fracture strength of the mixtures at the temperature of -10°C. Fracture strength increased around 15% with addition of hydrated lime to the mixtures. However, at temperature of 0°C, hydrated lime was found to be insignificant variable.
- 12) IDT results at both at 0°C and -10°C showed that aggregate type is a significant variable for fracture strength. Basalt aggregate outperforms to limestone at both temperatures.
- 13) Gradation was found to be a significant factor in determining low temperature performance according to IDT results. Specimens prepared with fine gradation have higher fracture strength than those prepared by coarse gradation.
- 14) Effect the aging of specimens was found to be insignificant based on IDT at test temperatures of 0°C and -10°C.
- 15) According to ANOVA analysis, addition of hydrated lime to the mixtures was a significant factor ($p < 0.05$) for fracture resistance with respect to IDT at -10°C.
- 16) Based on DSR results, extracted bitumen from limestone mixtures have better fracture resistance at high temperature; conversely at low temperatures fracture potential of the mixtures may increase. For the minimum testing temperature (25°C), bitumen that was extracted from basalt + HL combination has the lowest complex modulus and the highest phase angle, which indicates more elasticity at lower temperatures.

- 17) Referring to Rotational Viscosity Analysis performed using extracted bitumen, addition of limestone and limestone + HL composition increases the viscosity at the temperature range selected for this study. For all temperatures at which the tests were conducted, addition of basalt and basalt + HL combination makes almost no change when it is compared with neat bitumen viscosity results.
- 18) According to the DMA results, most sensitive combination is the addition of limestone and hydrated lime fillers together to unaged bitumen. While addition of limestone filler increases the T_g , around 2.5°C the combination of limestone and hydrated lime filler increase around 3.6°C . Also, it was observed that addition of basalt filler and hydrated lime combination decreased glass transition temperatures for aged and unaged samples around the same level.
- 19) For both basalt and limestone specimens, HL has large specific surface area on aggregate fillers according to SEM analysis. For the basalt and hydrated lime combination with unaged bitumen, hydrated lime has more homogeneous distribution while there are agglomeration areas of limestone and hydrated lime combinations. Combination of basalt + HL yields smooth wavy surface and hydrated lime distributed homogeneously compared with limestone + HL combination.

5.3 Recommendations For Future Work

The following recommendation can be made for future studies to improve the effect of hydrated lime on the fracture performance of asphalt concrete at low temperatures:

- 1) To determine the effect of hydrated lime on low temperature cracking of asphalt concrete, different mixing technique for hydrated lime should be considered in the experimental studies and to improve the reliability of test results more replicate samples must be produced to eliminate the variability in both bitumen and mixture characterization tests.

REFERENCES

- AASHTO M 323-07. (2010). Superpave Volumetric Mix Design. In *Standard Specifications for Transportation Materials and Methods of Sampling and Testing (Part 1A Specifications)*, Thirtieth Edition. AASHTO, Washington D.C.
- AASHTO R 35-09. (2010). Superpave Volumetric Design for Hot Mix Asphalt (HMA). In *Standard Specifications for Transportation Materials and Methods of Sampling and Testing (Part 1A Specifications)*, Thirtieth Edition. AASHTO, Washington D.C.
- Alavi, M. Z., & Hajj, E. Y. (2014). Effect of cooling rate on the thermo-volumetric, thermo-viscoelastic, and fracture properties of asphalt mixtures. *Asphalt Pavements*, 1, 405-416.
- Al-Qadi, I. L., Hassan, M. M., & Elseifi, M. A. (2005). Field and theoretical evaluation of thermal fatigue cracking in flexible pavements. *Transportation research record*, 1919(1), 87-95.
- Anderson, D. A. (1996, April). Influence of fines on performance of asphalt concrete mixtures. In *Proceedings of the fourth annual aggregates symposium, Atlanta, GA*.
- Anderson, D. A., Christensen, D. W., Bahia, H. U., Dongre, R., Sharma, M. G., Antle, C. E., & Button, J. (1994). Binder characterization and evaluation, volume 3: Physical characterization. *Strategic Highway Research Program, National Research Council*, Report No. SHRP-A-369.
- Anderson, K. O., & Epps, J. A. (1983). *Asphalt concrete factors related to pavement cracking in west Texas* (No. FHWA-RD-TX-83-287-3 Intrm Rpt.). Texas Transportation Institute, Texas A & M University System.

- Antunes, V., Freire, A. C., Quaresma, L., & Micaelo, R. (2015). Influence of the geometrical and physical properties of filler in the filler-bitumen interaction. *Construction and Building Materials*, 76, 322-329.
- Arabzadeh, A. (2015). The influence of different mixture design variables on thermal fatigue cracking of asphalt concrete pavements (Master dissertation). Middle East Technical University, 19.
- Arabzadeh, A., & Guler, M. (2019). Thermal fatigue behavior of asphalt concrete: A laboratory-based investigation approach. *International Journal of Fatigue*, 121, 229-236.
- Arand, W. (1987). Influence of Bitumen Hardness on the Fatigue Behavior of Asphalt Pavements of Different Thickness Due to Bearing Capacity Of Subbase, Traffic Loading And Temperature. Sixth International Conference, Structural Design of Asphalt Pavements, Volume I, Proceedings, University of Michigan, July 13-17, 1987, Ann Arbor, Michigan. *Publication of: Michigan University, Ann Arbor.*
- ASTM C127. (2004). Standard Test Method for Density, Relative Density (Specific Gravity), and Absorption of Coarse Aggregate. In *Annual Book of ASTM Standards*.
- ASTM C131 - 12. (2012). Standard Test Method for Resistance to Degradation of Large -Size Coarse Aggregate by Abrasion and Impact in the Los Angeles Machine. *ASTM International*. <https://doi.org/10.1520/C0131>
- ASTM C136. (2011). Standard Test Method for Sieve Analysis of Fine and Coarse Aggregates. *Annual Book of ASTM Standards*, 1-5.
- ASTM D113-17. (2007). Standard Test Method for Ductility of Asphalt Materials 1. *American Society for Testing Materials*. <https://doi.org/10.1520/D0113-17.aware>
- ASTM D2041. (2015). Standard Test Method for Theoretical Maximum Specific Gravity and Density of Asphalt Mixtures. *American Society for Testing*

Materials, i(January), 8–9. <https://doi.org/10.1520/D2041>

ASTM D2726. (2014). Standard Test Method for Bulk Specific Gravity and Density of Non-Absorptive Compacted Bituminous Mixtures. *Www.Astm.Org*. <https://doi.org/10.1520/D1188-07E01.2>

ASTM D4402-15. (2015). Standard Test Method for Viscosity Determination of Asphalt at Elevated Temperatures Using a Rotational Viscometer. In *American Society of Testing and Materials (ASTM)*. <https://doi.org/10.1520/D4402>

ASTM D5. (2006). ASTM D5. Standard Test Method for Penetration of Bituminous Materials. *The American Society of the International Association for Testing and Materials.*, i, 5–8. <https://doi.org/10.1520/D0113-07.2>.

ASTM D6090 - 17. (2004). Standard Test Method for Softening Point Resins (Mettler Cup and Ball Method) 1. *American Society for Testing and Materials*, 99, 1–3. <https://doi.org/10.1520/D6090-99R08.2>

ASTM D70. (2014). Standard Test Method for Density of Semi-Solid Bituminous Materials (Pycnometer). *Annual Book of ASTM Standards*, 04, 1–4. <https://doi.org/10.1520/D0070-09E01.2>

ASTM D92. (2007). Standard Test Method for Flash and Fire Points by Cleveland Open Cup Tester. *Annual Book of ASTM Standards*. <https://doi.org/10.1520/D0092-12B>.

ASTM-C128. (1997). Standard Test Method for Specific Gravity and Absorption of Fine Aggregate. *Annual Book of ASTM Standards*.

Bahia, H. U., & Anderson, D. A. (1993). Glass transition behavior and physical hardening of asphalt binders (with discussion). *Journal of the Association of Asphalt Paving Technologists*, 62.

- Bahia, H. U., Anderson, D. A., & Christensen, D. W. (1992). The bending beam rheometer; a simple device for measuring low-temperature rheology of asphalt binders (with discussion). *Journal of the Association of Asphalt Paving Technologists*, 61.
- Bahia, H., Tabatabaee, H., & Velasquez, R. (2012). Asphalt thermal cracking analyser (ATCA). In *7th RILEM international conference on cracking in pavements* (pp. 147-156). Springer, Dordrecht.
- Behnia, B., Buttlar, W. G., & Reis, H. (2017). Nondestructive Low-Temperature Cracking Characterization of Asphalt Materials. *Journal of Materials in Civil Engineering*, 29(5), 04016294. doi:10.1061/(asce)mt.1943-5533.0001826
- Blažek, J., Šebor, G., Maxa, D., Ajib, M., & Paniagua, H. (2000). Effect of hydrated lime addition on properties of asphalt.
- Bonnaure, F., Gest, G., Gravois, A., & Uge, P. (1977). *A new method of predicting the stiffness of asphalt paving mixtures* (No. Monograph).
- Boyer RF. (1977). Transitions and relaxations. In: Mark HF, Bikales NM, (Ed.). *Encyclopedia of Polymer Science and Technology: Plastics, Resins, Rubbers, Fibers*. New York, NY; Wiley Interscience; pp. 745-839.
- Breen, J. J., & Stephens, J. E. (1967). The Glass Transition and Mechanical Properties of Asphalt. *Annual Conference of Canadian Technical Asphalt Association*.
- Bureau of Materials and Physical Research*. (2005). Retrieved from Illinois Department of Transportation: <http://www.dot.il.gov/materials/research/pdf/ptad4.pdf>
- C. V. Chachas, W. J. Liddle, D. E. Peterson and M. L. Wiley, Use of hydrated lime in bituminous mixtures to decrease hardening of the asphalt cement, *Report PB 213 170, Salt Lake City (Utah, USA): Utah State Highway Department, 1971*

- Carpenter, S. H. (1983). Thermal Cracking in Asphalt Pavements: An Examination of Models and Input Parameters. *United States Army Corps of Engineers Cold Regions Research and Engineering Laboratory*.
- Carpenter, S. H., & Lytton, R. L. (1977). *Thermal Pavement Cracking in West Texas* (No. FHWA-TX-77-18-4F Final Rpt.). Texas Transportation Institute, Texas A & M University.
- Carpenter, S. H., Lytton, R. L., & Epps, J. A. (1974). *Environmental Factors Relevant to Pavement Cracking in West Texas* (No. TTI-2-8-73-18-1 Intrm Rpt.). Texas Transportation Institute, Texas A & M University.
- Chachas, C. V., Liddle, W. J., Peterson, D. E., & Wiley, M. L. (1971). Use of hydrated lime in bituminous mixtures to decrease hardening of the asphalt cement. *Report PB, 213*, 170.
- Collieu, A. M., & Powney, D. J. (1973). *The mechanical and thermal properties of materials*. Edward Arnold (Publishers) Ltd., London, United Kingdom.
- Craus, J., Ishai, I., & Sides, A. (1978). Some physico-chemical aspects of the effect and the role of the filler in bituminous paving mixtures. *In Association of Asphalt Paving Technologists Proc* (Vol. 47).
- Curtis, C. W., Ensley, K., & Epps, J. (1993). *Fundamental properties of asphalt-aggregate interactions including adhesion and absorption* (No. SHRP-A-341). Washington, DC: National Research Council.
- D. Lesueur, "The colloidal structure of bitumen: Consequences on the rheology and on the mechanisms of bitumen modification", *Advances Colloid Interface Science* 145, pp.42-82, 2009
- D. N. Little and J. A. Epps, *The Benefits of Hydrated Lime in Hot Mix Asphalt*, Arlington (Virginia, USA): National Lime Association, 2001. Retrieved from <http://www.lime.org/ABenefit.pdf>

- Eisenmann, J., & Hilmer, A. (1987). Influence of wheel load and inflation pressure on the rutting effect at asphalt-pavements: experiments and theoretical investigations. In *International Conference on the Structural Design*.
- Epps, A. L. (1998). A comparison of measured and predicted low temperature cracking conditions. *Journal of the Association of Asphalt Paving Technologists*, 67.
- Epps, A. L. (1999). An approach to examine thermal fatigue in asphalt concrete. *Journal of the association of asphalt paving technologists*, 68, 319-348.
- EuLA (European Lime Association). (2011). "Hydrated lime: A proven additive for durable asphalt pavements—Critical literature review." European Lime Association, Asphalt Task Force, EU.
- European Committee for Standardization, (2009) EN 933-9: Tests for geometrical properties of aggregates. Part 9: Assessment of fines. Methylene Blue Test, Brussels (Belgium): European Committee for Standardization.
- Fabb, T. R. J. (1974). The influence of mix composition, binder properties and cooling rate on asphalt cracking at low temperatures. In *Association of Asphalt Paving Technologists Proc* (Vol. 43).
- Gerritsen, A. H., & Jongeneel, D. J. (1988). Fatigue properties of asphalt mixes under conditions of very low loading frequencies. In *Association of Asphalt Paving Technologists Technical Sessions, 1988, Williamsburg, Virginia, USA* (Vol. 57).
- Goodrich, J. L. (1988). Asphalt and polymer modified Asphalt properties related to the performance of Asphalt concrete mixes (with discussion). In *Association of Asphalt Paving Technologists Proc* (Vol. 57).
- Grebovicz, J., & Wunderlich, B. (1981). The glass transition of p-alkyl-p'-alkoxy-azoxybenzene mesophases. *Molecular Crystals and Liquid Crystals*, 76(3-4), 287-296.

- Haas, R. C. G. (1973). *A Method For Designing Asphalt Pavements To Minimize Low Temperature Shrinkage Cracking*. *The Asphalt Institute* (pp. 1-91). Research Report 73-1 (RR-73-1).
- Haas, R., Meyer, F., Assaf, G., & Lee, H. (1987). A Comprehensive Study of Cold Climate Airport Pavement Cracking (with Discussion). *In Association of Asphalt Paving Technologists Proc* (Vol. 56).
- Heukelom, W., & Wijga, P. W. O. (1971). Viscosity of dispersions as governed by concentration and rate of shear. *Journal of the Association of Asphalt Paving Technologists*, 40, 418-437.
- Hicks, R. G., & Scholz, T. V. (2003). Life Cycle Costs for Lime in Hot Mix Asphalt, 3 vol. *Arlington (Virginia, USA): National Lime Association*.
- Hiltunen, D. R., & Roque, R. (1994). A mechanics-based prediction model for thermal cracking of asphaltic concrete pavements (with discussion). *Journal of the Association of Asphalt Paving Technologists*, 63.
- Hopman, P., Vanelstraete, A., Verhasselt, A., & Walter, D. (1999). Effects of hydrated lime on the behaviour of mastics and on their construction ageing. *In Proceedings of the Durable and Safe Road Pavements, v International Conference, Held Kielce, Poland, 11-12 May 1999. Volume 1*.
- Huang, S. C., Robertson, R. E., Branthaver, J. F., & Claine Petersen, J. (2005). Impact of lime modification of asphalt and freeze–thaw cycling on the asphalt–aggregate interaction and moisture resistance to moisture damage. *Journal of materials in civil engineering*, 17(6), 711-718.
- Huang, Y. H. (2004). *Pavement Analysis and Design* Pearson Education. *Upper Saddle River, NJ, USA*.
- Isacsson, U., & Zeng, H. (1998). Low-temperature cracking of polymer-modified asphalt. *Materials and Structures*, 31(1), 58-63.

- Ishai, I. and Tons, E., "A Concept and a Test Method for a Unified Characterization of the Geometric Irregularity of Aggregate Particles", *American Society and Materials Journal of Testing and Evaluation*, Vol.5, January 1977, pp.3-15.
- Jackson, N. M. (1992). Analysis of thermal fatigue distress of asphalt concrete pavements.
- Jackson, N. M., & Vinson, T. S. (1996). Analysis of thermal fatigue distress of asphalt concrete pavements. *Transportation research record*, 1545(1), 43-49.
- Janoo, V., Bayer Jr, J., & Walsh, M. (1993). *Thermal stress measurements in asphalt concrete* (No. Crrel-93-10). Cold Regions Research and Engineering Lab Hanover Nh.
- Johansson, L. S., & Isacsson, U. (1998). Effect of filler on low temperature physical hardening of bitumen. *Construction and Building Materials*, 12(8), 463-470.
- Johansson, L. S., Branthaver, J. F., & Robertson, R. E. (1996). The influence of metal-containing compounds on enhancement and inhibition of asphalt oxidation. *Fuel Science and Technology International*, 14(8), 1143-1159.
- Jung, D., & Vinson, T. S. (1993). Thermal stress restrained specimen test to evaluate low-temperature cracking of asphalt-aggregate mixtures. *Transportation research record*, 12-12
- Kanerva, H. (1992). Effects of asphalt properties on low temperature cracking of asphalt mixtures. In *International Conference on Asphalt Pavements, 7th, 1992, Nottingham, United Kingdom* (Vol. 2).
- Karakaya, Y. (2015). Low temperature performance of asphalt concrete under direct tension loading (Middle East Technical University).
- Khattak, M. J., & Kyatham, V. (2008). Viscoelastic behavior of hydrated lime-modified asphalt matrix and hot-mix asphalt under moisture damage conditions. *Transportation Research Record*, 2057(1), 64-74.

- Kim, Y.-R., Little, D. N., & Song, I. (2003). Mechanistic evaluation of mineral fillers on fatigue resistance and fundamental material characteristics. In *Proceedings of the 82nd Transportation Research Board Meeting*, Transportation Research Board, Washington, D.C.
- Kliwer, J. E., Zeng, H., & Vinson, T. S. (1996). Aging and low-temperature cracking of asphalt concrete mixture. *Journal of Cold Regions Engineering*, 10(3), 134-148.
- Kovacs, A. J. (1964). Transition vitreuse dans les polymères amorphes. Etude phénoménologique. In *Fortschritte der hochpolymeren-forschung* (pp. 394-507). Springer, Berlin, Heidelberg.
- Lackner, R., Spiegl, M., Blab, R., & Eberhardsteiner, J. (2005). Is low-temperature creep of asphalt mastic independent of filler shape and mineralogy arguments from multiscale analysis. *Journal of Materials in Civil Engineering*, 17(5), 485-491.
- Lazell, E. W. (1915). *Hydrated lime: history, manufacture and uses in plaster, mortar, concrete; a manual for the architect, engineer, contractor and builder*. Jackson-Remlinger Printing Co.
- Lesueur, D. (2009). The colloidal structure of bitumen: Consequences on the rheology and on the mechanisms of bitumen modification. *Advances in colloid and interface science*, 145(1-2), 42-82.
- Lesueur, D. (2010). *Hydrated lime: A proven additive for durable asphalt pavements – Critical literature review*. Brussels: European Lime Association (EuLA). Retrieved from <http://www.eula.eu>
- Lesueur, D., & Little, D. N. (1999). Effect of hydrated lime on rheology, fracture, and aging of bitumen. *Transportation Research Record*, 1661(1), 93-105.
- Lesueur, D., Gerard, J. F., Claudy, P., Letoffe, J. M., Planche, J. P., & Martin, D. (1996). A structure-related model to describe asphalt linear viscoelasticity. *Journal of Rheology*, 40(5), 813-836.

- Lesueur, D., Petit, J., & Ritter, H. J. (2013). The mechanisms of hydrated lime modification of asphalt mixtures: a state-of-the-art review. *Road materials and pavement design*, 14(1), 1-16.
- Little, D. N., & Petersen, J. C. (2005). Unique effects of hydrated lime filler on the performance-related properties of asphalt cements: Physical and chemical interactions revisited. *Journal of Materials in Civil Engineering*, 17(2), 207-218.
- Marasteanu, M., Zofka, A., Tuross, M., Li, X., Velasquez, R., Li, X., & Ojo, J. (2007). Investigation of low temperature cracking in asphalt pavements national pooled fund study 776.
- Masson, J. F., Collins, P., Margeson, J., & Polomark, G. (2002). Analysis of bituminous crack sealants by physicochemical methods: Relationship to field performance. *Transportation Research Record*, 1795(1), 33-39.
- McCrum, N. G., Read, B. E., & Williams, G. (1967). Anelastic and dielectric effects in polymeric solids.
- Mohammad, L. N., Saadeh, S., Kabir, M., Othman, A., & Cooper, S. (2008). Mechanistic properties of hot-mix asphalt mixtures containing hydrated lime. *Transportation Research Record*, 2051(1), 49-63.
- Molenaar, A. A. A. (2007). Lecture notes CT4860 Structural Pavement Design, Design of Flexible Pavements. *Delft University of Technology, Delft, Netherlands*.
- Monismith, C. L., Secor, G. A., & Secor, K. E. (1965). Temperature induced stresses and deformations in asphalt concrete. In *Association of Asphalt Paving Technologists Proceedings* (Vol. 34).
- Mouillet, V., Molinengo, J. C., Durrieu, F., & Planche, J. P. (2004). Effect of ageing on the low temperatures cracking properties of bituminous binders: new insights from bending beam rheometer measurements. In *Fifth International*

- RILEM Conference on Reflective Cracking in Pavements* (pp. 351-358). RILEM Publications SARL.
- Nam, K., & Bahia, H. U. (2004). Effect of binder and mixture variables on glass transition behavior of asphalt mixtures (with discussion). *Journal of the Association of Asphalt Paving Technologists*, 73.
- National Lime Association. (2003). How to Add Hydrated Lime to Asphalt—An Overview of Current Methods. *Arlington (Virginia, USA): National Lime Association*.
- Papagiannakis, A. T., & Masad, E. A. (2017). *Pavement design and materials*. John Wiley & Sons.
- Pavement Interactive (2019). HMA Weight-Volume Terms and Relationships. Retrieved from <https://www.pavementinteractive.org/reference-desk/design/mix-design/marshall-mix-design/>
- Perkins, W. G. (1999). Polymer toughness and impact resistance. *Polymer Engineering & Science*, 39(12), 2445-2460.
- Petersen, J. C. (1971). A thermodynamic study by infrared spectroscopy of the association of 2-quinolone, some carboxylic acids, and the corresponding 2-quinolone-acid dimer. *Journal of Physical Chemistry*, 75, 1129–1135.
- Petersen, J. C., & Glaser, R. (2011). Asphalt oxidation mechanisms and the role of oxidation products on age hardening revisited. *Road Materials and Pavement Design*, 12(4), 795-819.
- Petersen, J. C., Plancher, H., & Harnsberger, P. M. (1987). Lime treatment of asphalt to reduce age hardening and improve flow properties. In *Association of Asphalt Paving Technologists Proceedings Technical Sessions, 1987, Reno, Nevada, USA* (Vol. 56).
- Pilat, J., Radziszewski, P., & Kalabiska, M. (2000). The analysis of visco-elastic properties of mineral-asphalt mixes with lime and rubber powder. In *Proceedings of the Papers Submitted For Review At 2nd Eurasphalt And*

Eurobitume Congress, Held 20-22 September 2000, Barcelona, Spain. Book 1-Session 1.

- Plancher, H., Green, E. L., & Petersen, J. C. (1976). Reduction of oxidative hardening of asphalts by treatment with hydrated lime—a mechanistic study. In *Proceedings of the Association Asphalt Paving Technologists* (Vol. 45, pp. 1–24). Lino Lakes, MN: Association Asphalt Paving Technologists (AAPT).
- products on age hardening revisited. *Road Materials Pavement Design*, 12.
- Puzinauskas, V. P. (1983). *Filler in asphalt mixtures. The Asphalt Institute, College Park* (No. 69-2). Md. Research Report.
- Ramond, G., & Lesueur, D. (2004). Adhesion liant granulat. *Materiaux routiers bitumineux*, 1, 177-203.
- Rieger, J. (2001). The glass transition temperature Tg of polymers—comparison of the values from differential thermal analysis (DTA, DSC) and dynamic mechanical measurements (torsion pendulum). *Polymer testing*, 20(2), 199-204.
- Rizkiyantoro, p. R. (2010). Comparative analysis of hydrated lime (hl) and ordinary portland cement (opc) as filler in asphalt concrete pavement (doctoral dissertation, universiti teknologi petronas).
- Roberts, F., Kandhal, P. S., Brown, E. R., & Lee, D. Y. (1996). *Hot Mix Asphalt Materials, Mixture Design and construction*. Lanham, Maryland: Research and Education Foundation.
- Rodríguez, M. G., Morrison, G. R., vanLoon, J. R., & Hesp, S. A. (1996). Low-Temperature Failure in Particulate-Filled Asphalt Binders and Asphalt Concrete Mixes (with discussion). *Journal of the Association of Asphalt Paving Technologists*, 65.
- Roque, R., & Buttlar, W. G. (1992). Development of a measurement and analysis system to accurately determine asphalt concrete properties using the indirect tensile mode. In *Asphalt Paving Technology: Association of Asphalt Paving*

- Technologists-Proceedings of the Technical Sessions* (Vol. 61, pp. 304-332).
Association of Asphalt Paving Technologist.
- Roussel, N., & Coussot, P. (2005). "Fifty-cent rheometer" for yield stress measurements: from slump to spreading flow. *Journal of rheology*, 49(3), 705-718.
- Shah, A. (2004). Influence of Binders & Mixture Properties on the Performance of Asphalt Concrete Pavements. *Phd Dissertetion*, Perdue University, pp.1-216
- Shodhganga (2019). IDT Strength Test Retrieved from https://shodhganga.inflibnet.ac.in/bitstream/10603/6226/10/10_chapter%205.pdf
- Sugawara, T., Kubo, H., & Moriyosi, A. (1982). Paving in Cold Area Mini-Workshop Canada. *Japan STP*.
- Turner, T. F., & Branthaver, J. F. (1997). DSC studies of asphalts and asphalt components. *Asphalt science and technology*, 59-101.
- Turner, T. F., & Branthaver, J. F. (1997). DSC studies of asphalts and asphalt components. *Asphalt science and technology*, 59-101.
- Verhasselt, A., & Puiatti, D. (2004). Effect of hydrated lime on ageing behaviour of bituminous mastics. In *Proceedings of the 3rd Eurasphalt and Eurobitume Congress Held Vienna, May 2004* (Vol. 1).
- Vinson, T. S., Janoo, V. C. & Haas, R. C. G. (1996). Temperature and Thermal Fatigue Cracking", *Summary Report for A-003A* of the Strategic Highway Research Program (SHRP), Washington, D.C.-USA.
- Vinson, T. S., Janoo, V. C., & Haas, R. G. (1989). Low Temperature and Thermal Fatigue Cracking. *Summary Report for A-003A of the strategic Highway Research Program (SHRP)*.
- Vinson, T. S., Jung, D. H., & Rooney, J. (1993). Pavement Performance and Low Temperature Cracking Resistance of Subarctic and Arctic Airfields.

Ward, I. M., & Hadley, D. W. (1993). *An introduction to the mechanical properties of solid polymers*.

Wikipedia (2019). The Lime Cycle. Retrieved from https://en.wikipedia.org/wiki/File:The_lime_cycle.jpg

Wortelboer, J. P., Hoppen, H. J., Ramond, G., & Pastor, M. (1996). Rheological properties of bitumen/filler mixtures. In *Eurasphalt & Eurobitume Congress, Strasbourg, 7-10 May 1996. Volume 2. Paper e&e. 4.079*.

Xu, M., Yi, J., Pei, Z., Feng, D., Huang, Y., & Yang, Y. (2017). Generation and evolution mechanisms of pavement asphalt aging based on variations in surface structure and micromechanical characteristics with AFM. *Materials Today Communications*, *12*, 106-118.

APPENDICES

A. Fracture Plots

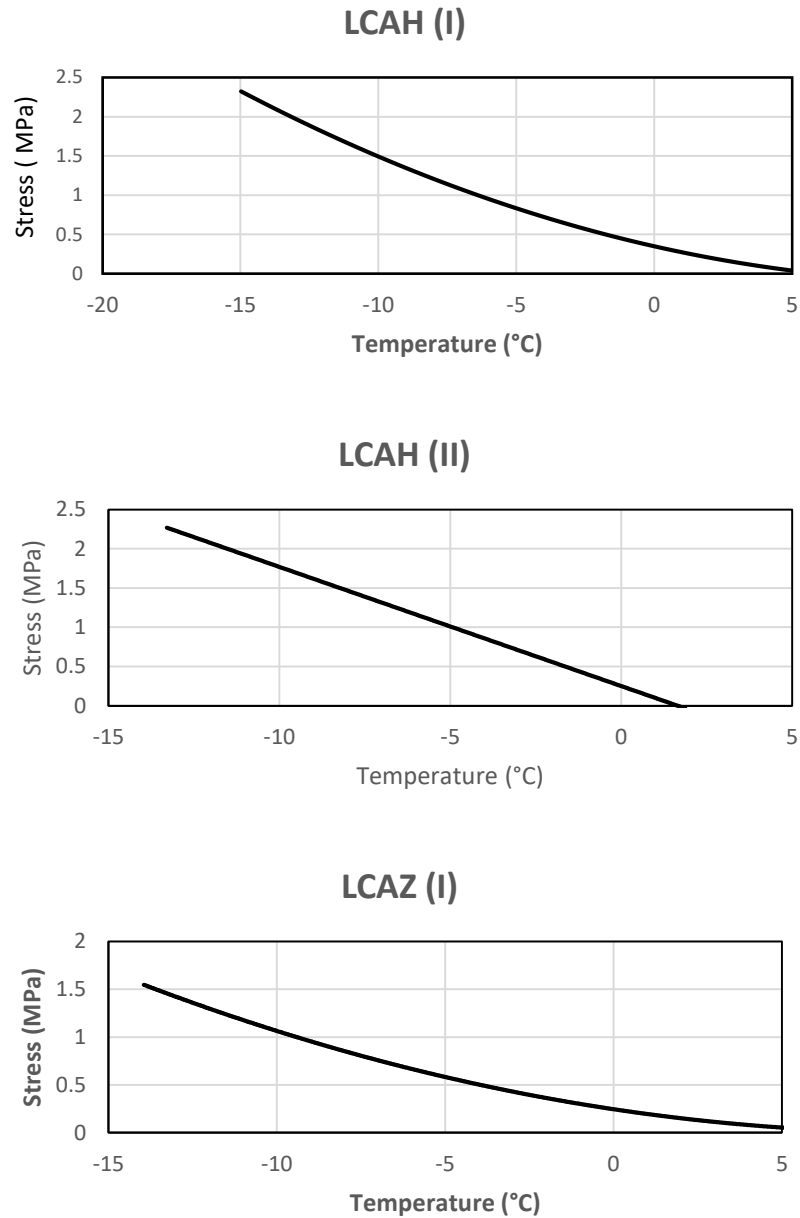


Figure A.1. Fracture plots of samples tested with TSRST

Symbols used: Aggregate: L=limestone. B=basalt; Gradation: C=Coarse. F=Fine; Aging: A=aged. U=unaged; Hydrated lime content: H=2% hydrated lime. Z=0% hydrated lime

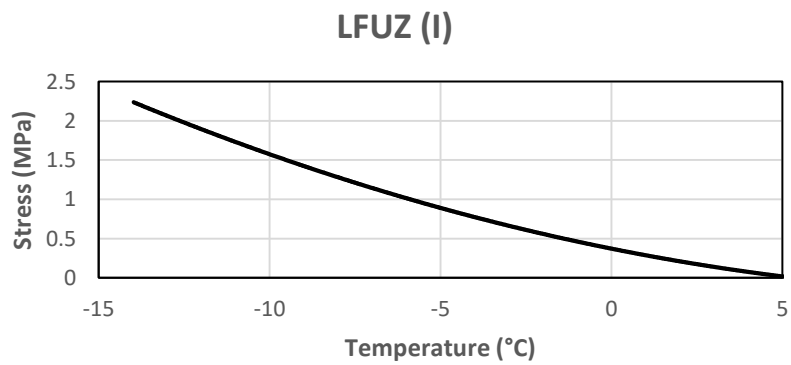
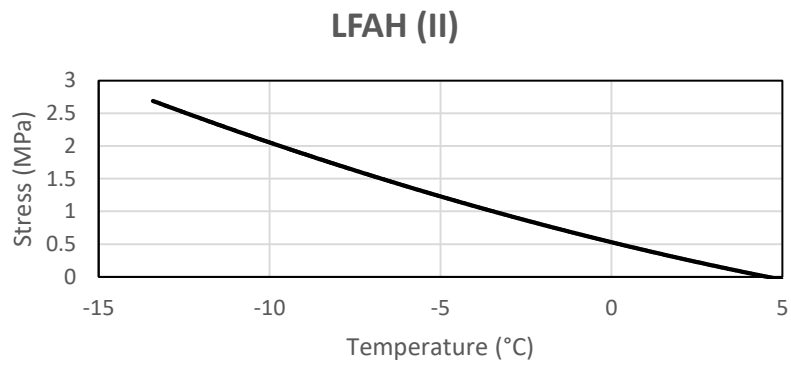
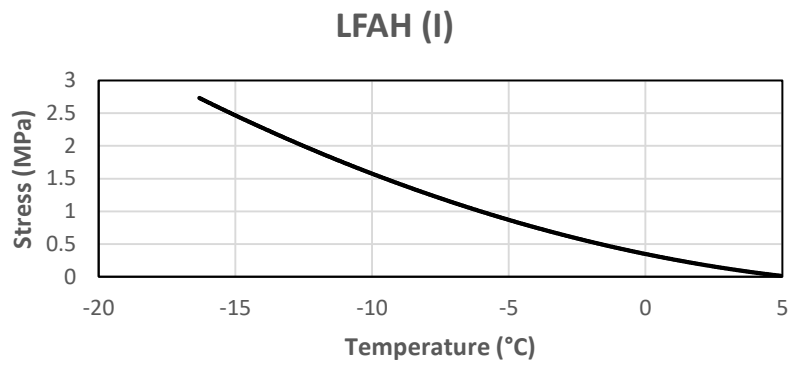


Figure A.1 (Continued)

Symbols used: Aggregate: L=limestone. B=basalt; Gradation: C=Coarse. F=Fine; Aging: A=aged. U=unaged; Hydrated lime content: H=2% hydrated lime. Z=0% hydrated lime

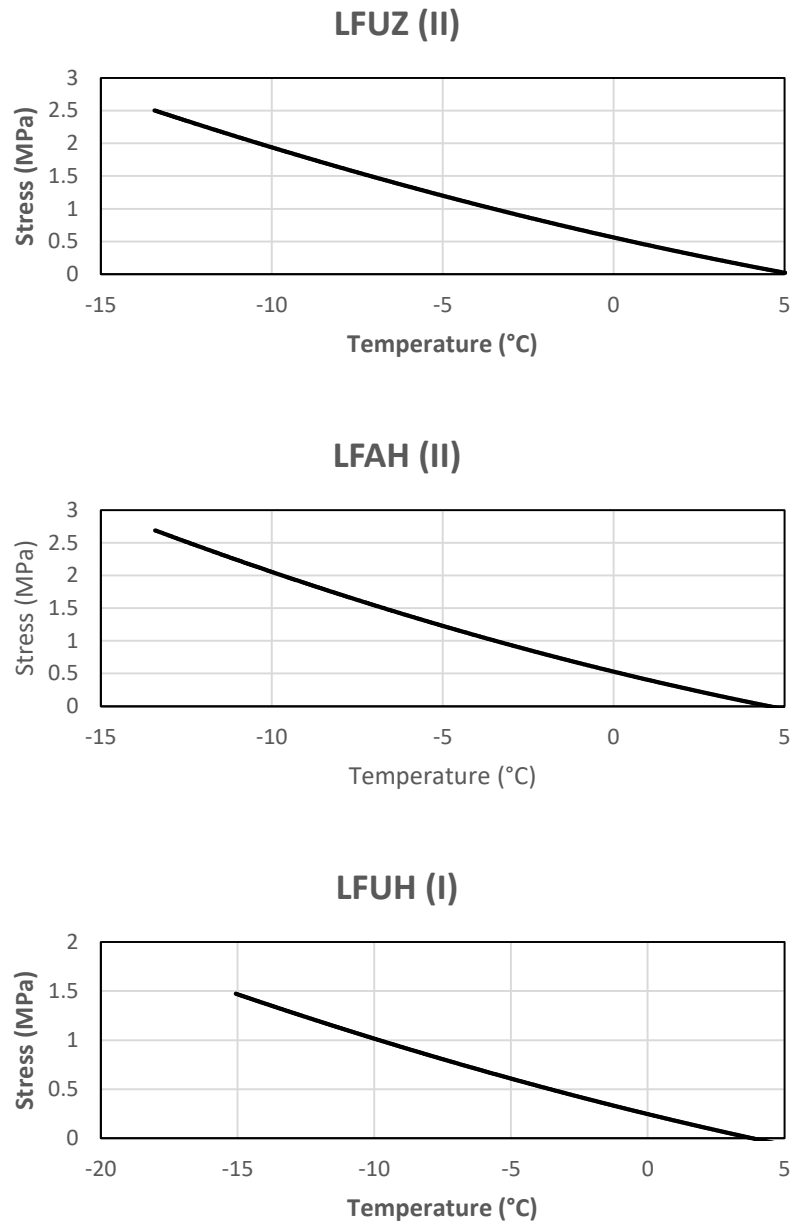


Figure A.1 (Continued)

Symbols used: Aggregate: L=limestone. B=basalt; Gradation: C=Coarse. F=Fine; Aging: A=aged. U=unaged; Hydrated lime content: H=2% hydrated lime. Z=0% hydrated lime

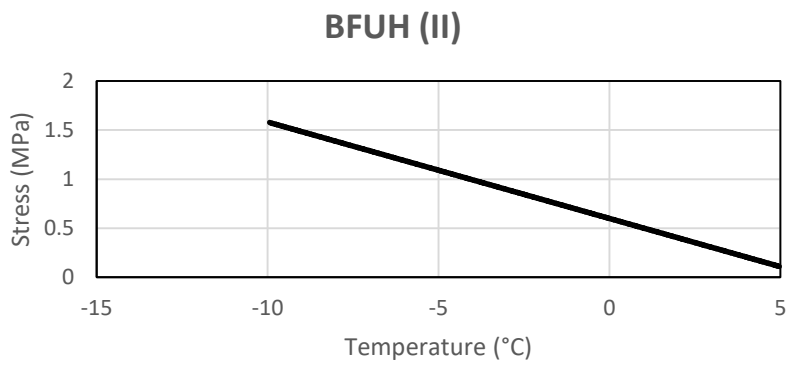
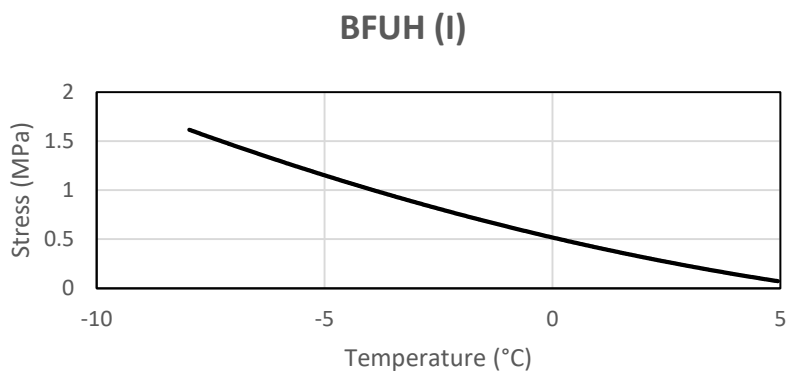
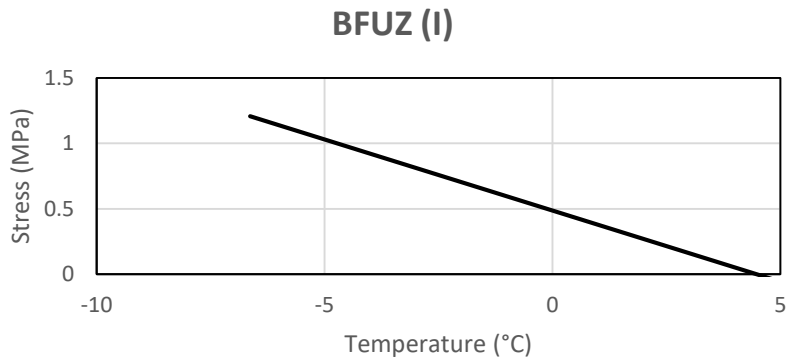


Figure A.1 (Continued)

Symbols used: Aggregate: L=limestone. B=basalt; Gradation: C=Coarse. F=Fine; Aging: A=aged. U=unaged; Hydrated lime content: H=2% hydrated lime. Z=0% hydrated lime

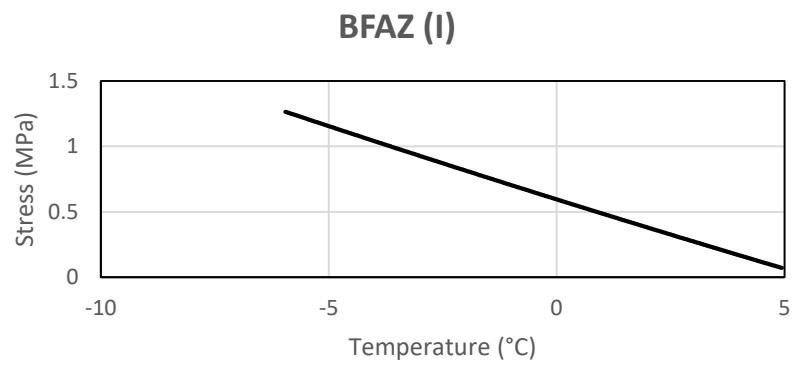
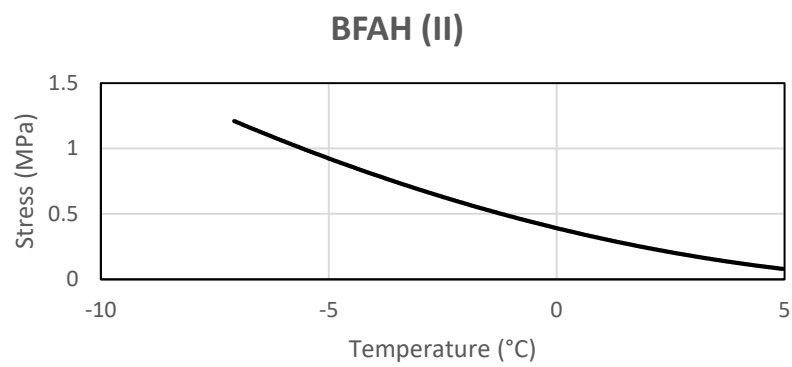
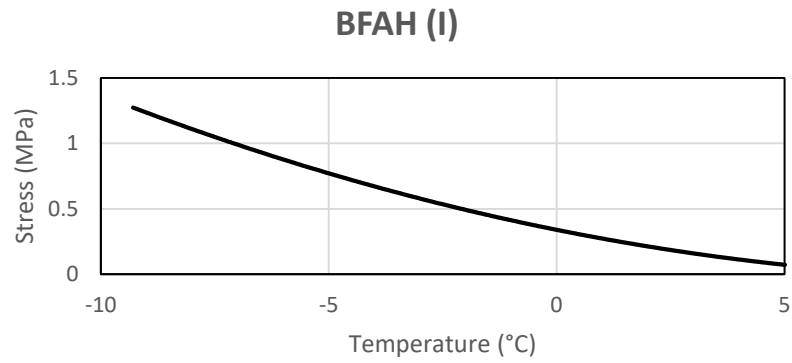


Figure A.1 (Continued)

Symbols used: Aggregate: L=limestone. B=basalt; Gradation: C=Coarse. F=Fine; Aging: A=aged. U=unaged; Hydrated lime content: H=2% hydrated lime. Z=0% hydrated lime

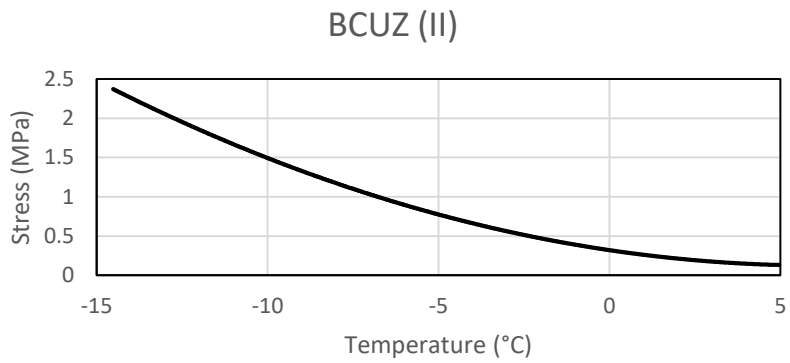
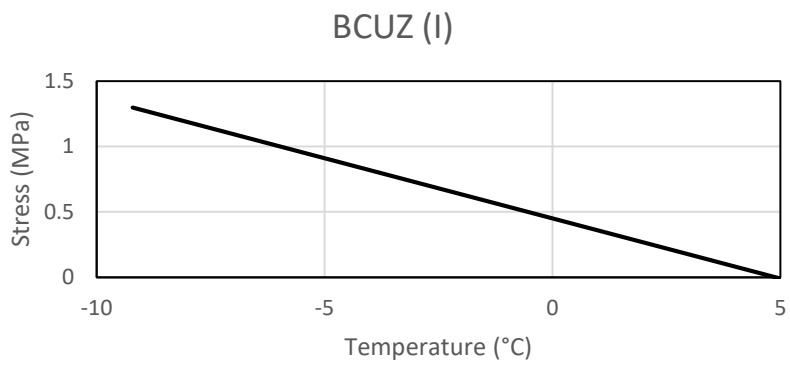
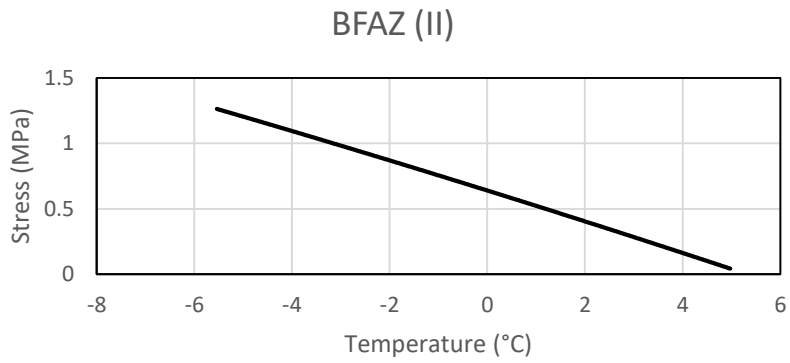


Figure A.1 (Continued)

Symbols used: Aggregate: L=limestone. B=basalt; Gradation: C=Coarse. F=Fine; Aging: A=aged. U=unaged; Hydrated lime content: H=2% hydrated lime. Z=0% hydrated lime

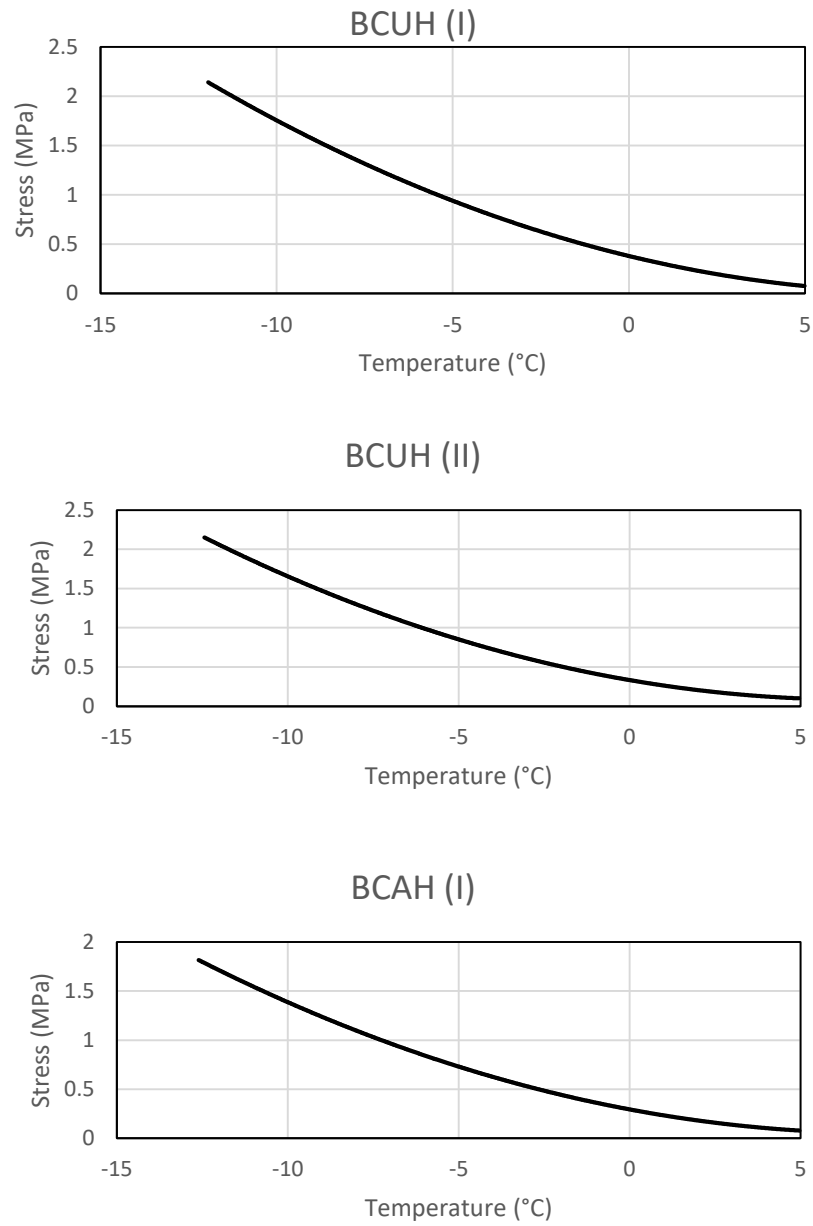


Figure A.1 (Continued)

Symbols used: Aggregate: L=limestone. B=basalt; Gradation: C=Coarse. F=Fine; Aging: A=aged. U=unaged; Hydrated lime content: H=2% hydrated lime. Z=0% hydrated lime

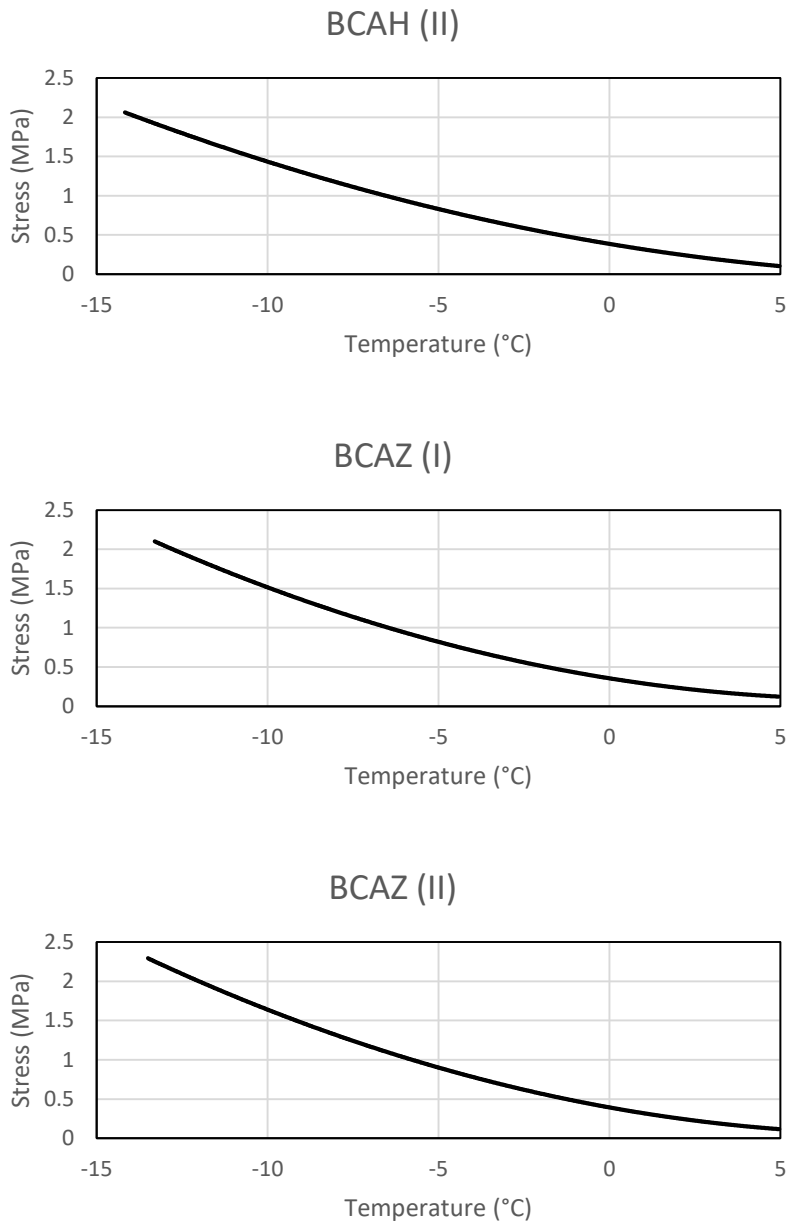


Figure A.1 (Continued)

Symbols used: Aggregate: L=limestone. B=basalt; Gradation: C=Coarse. F=Fine; Aging: A=aged. U=unaged; Hydrated lime content: H=2% hydrated lime. Z=0% hydrated lime

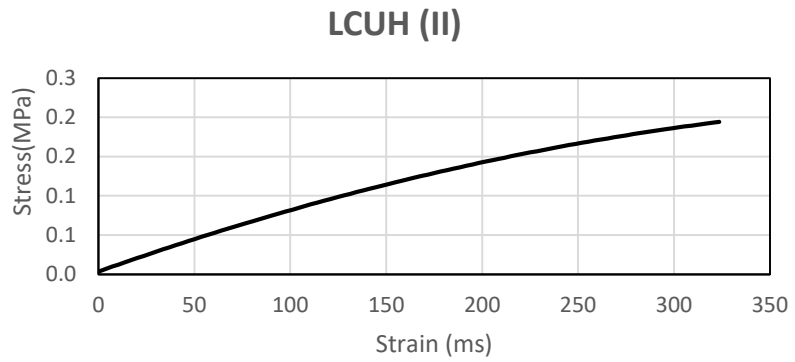
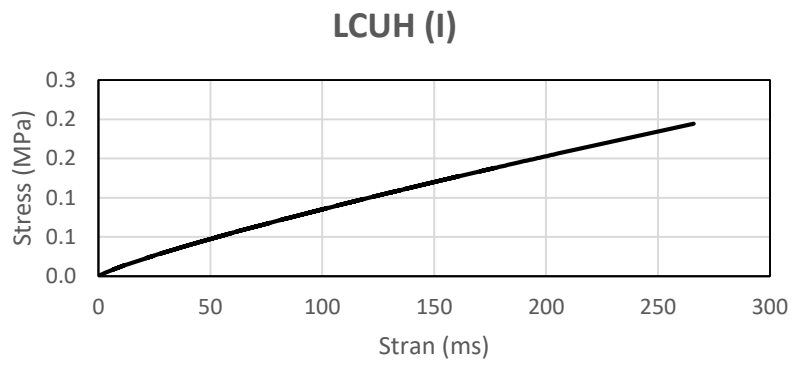
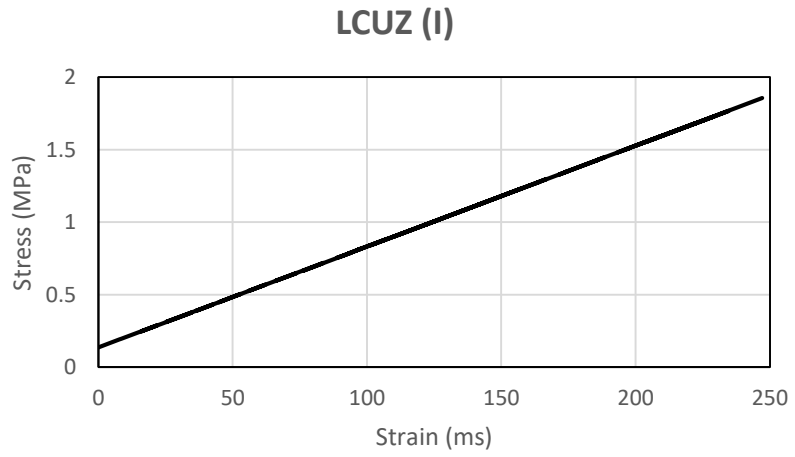


Figure A.2. Fracture plots of samples tested with DTT at -10°C

Symbols used: Aggregate: L=limestone. B=basalt; Gradation: C=Coarse. F=Fine; Aging: A=aged. U=unaged; Hydrated lime content: H=2% hydrated lime. Z=0% hydrated lime

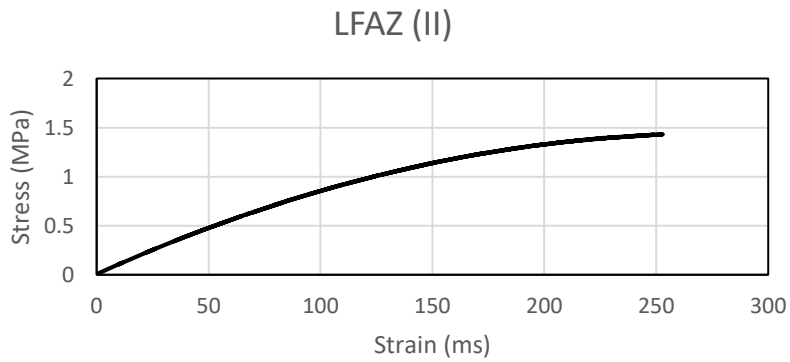
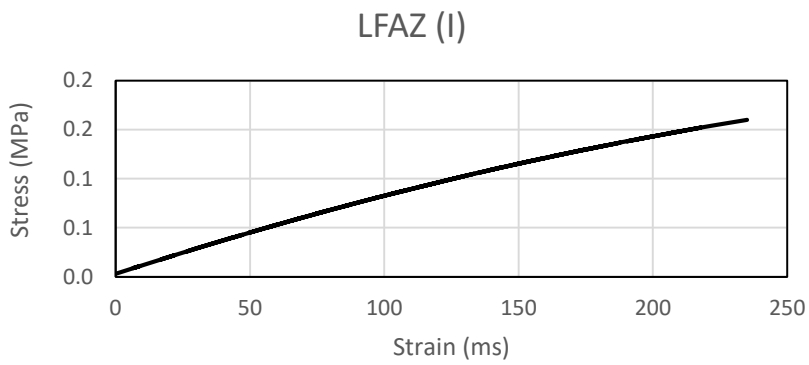
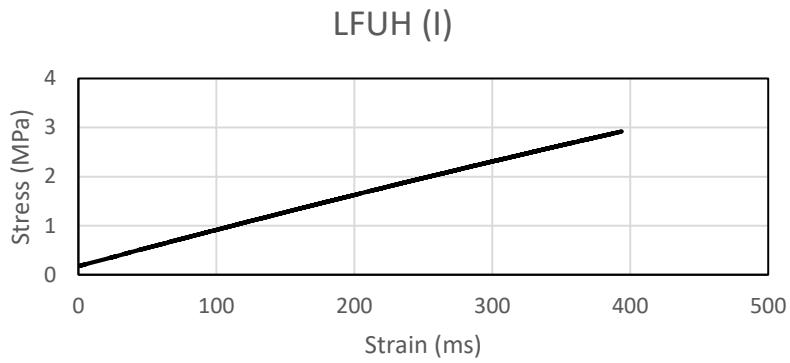


Figure A.2. (Continued)

Symbols used: Aggregate: L=limestone. B=basalt; Gradation: C=Coarse. F=Fine; Aging: A=aged. U=unaged; Hydrated lime content: H=2% hydrated lime. Z=0% hydrated lime

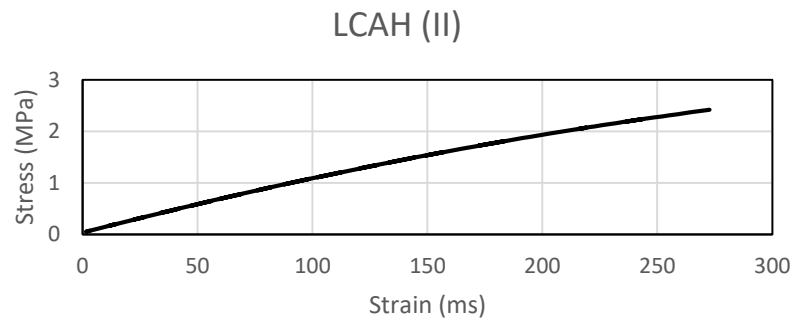
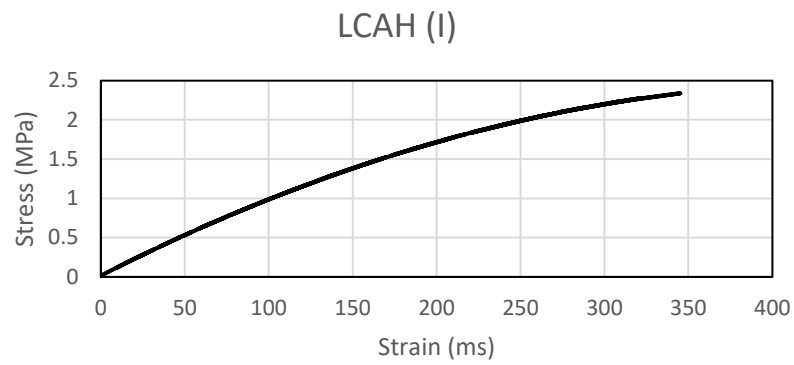
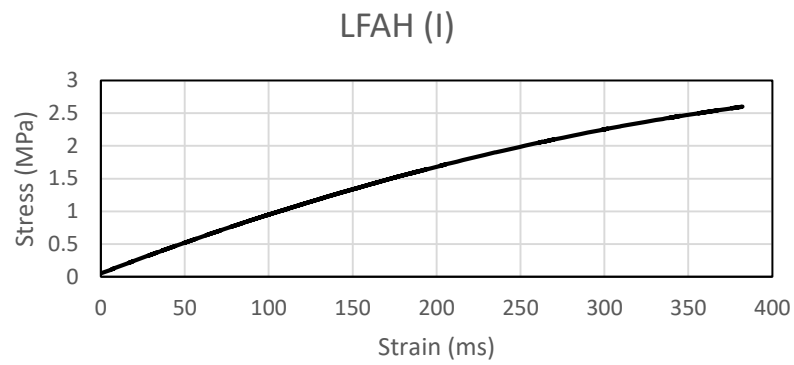


Figure A.2. (Continued)

Symbols used: Aggregate: L=limestone. B=basalt; Gradation: C=Coarse. F=Fine; Aging: A=aged. U=unaged; Hydrated lime content: H=2% hydrated lime. Z=0% hydrated lime

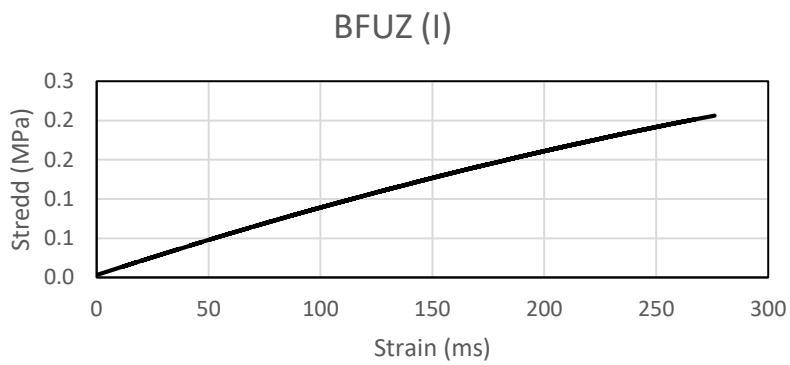
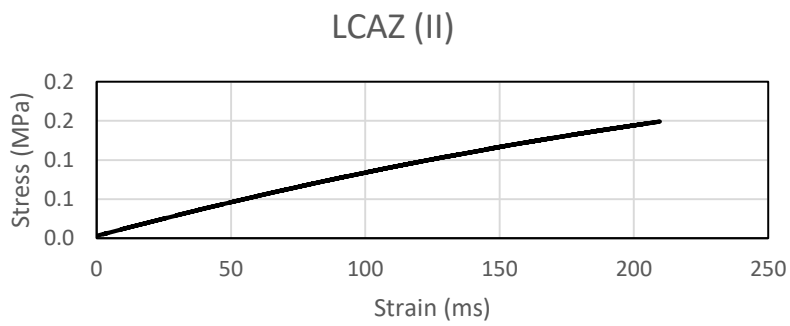
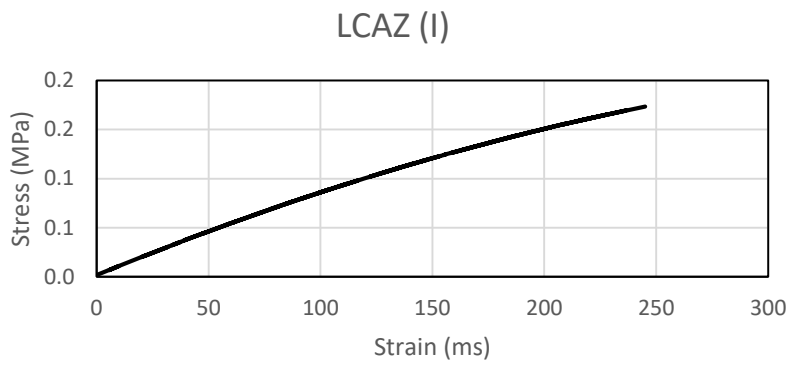


Figure A.2. (Continued)

Symbols used: Aggregate: L=limestone. B=basalt; Gradation: C=Coarse. F=Fine; Aging: A=aged. U=unaged; Hydrated lime content: H=2% hydrated lime. Z=0% hydrated lime

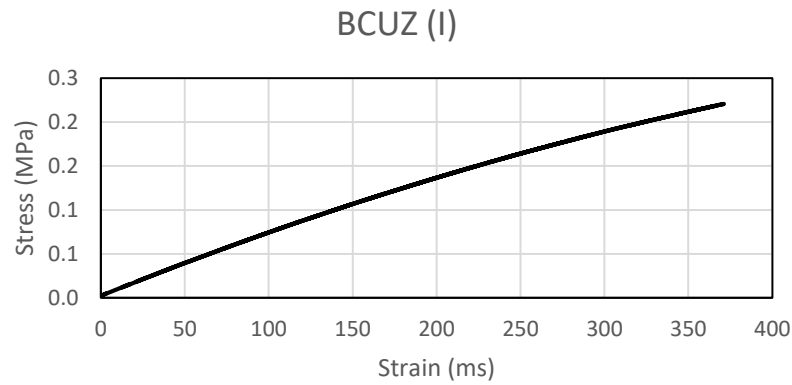
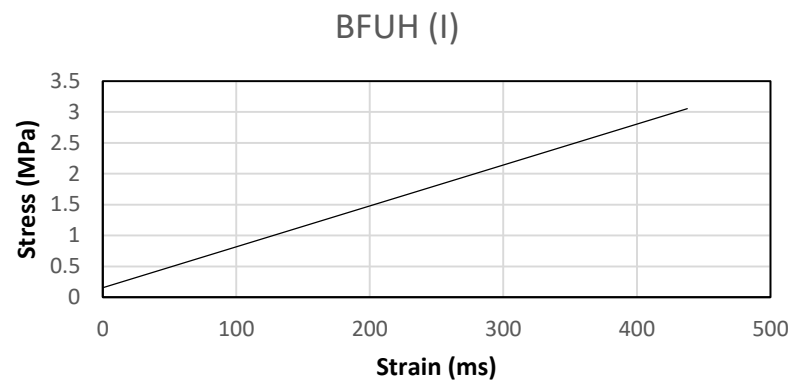
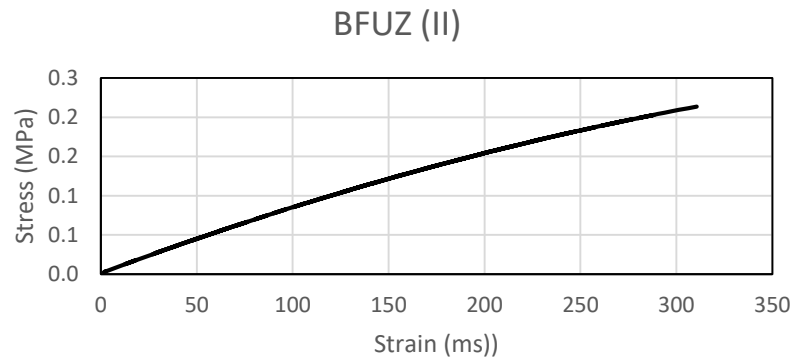


Figure A.2. (Continued)

Symbols used: Aggregate: L=limestone. B=basalt; Gradation: C=Coarse. F=Fine; Aging: A=aged. U=unaged; Hydrated lime content: H=2% hydrated lime. Z=0% hydrated lime

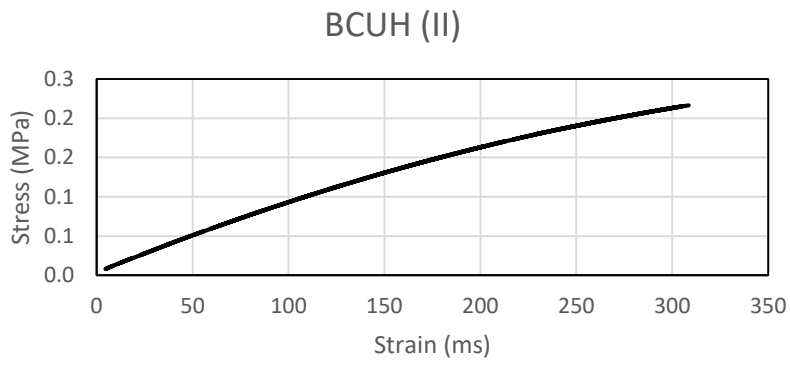
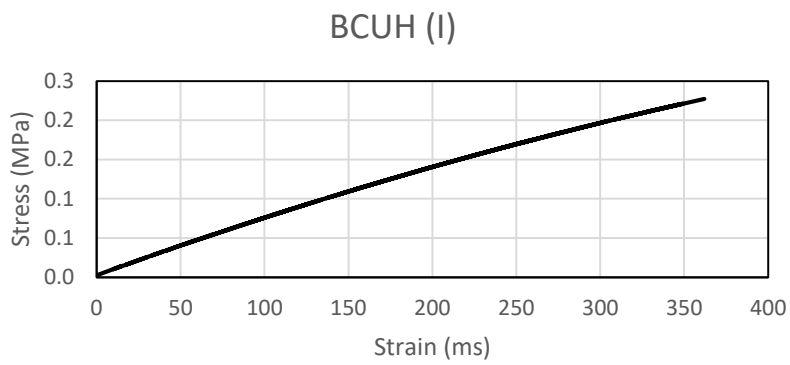
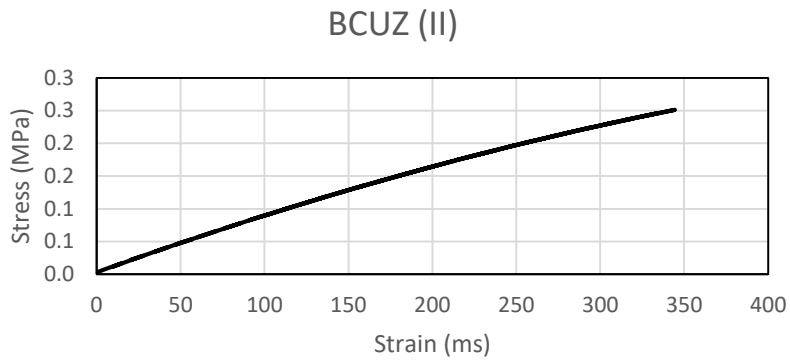


Figure A.2. (Continued)

Symbols used: Aggregate: L=limestone. B=basalt; Gradation: C=Coarse. F=Fine; Aging: A=aged. U=unaged; Hydrated lime content: H=2% hydrated lime. Z=0% hydrated lime

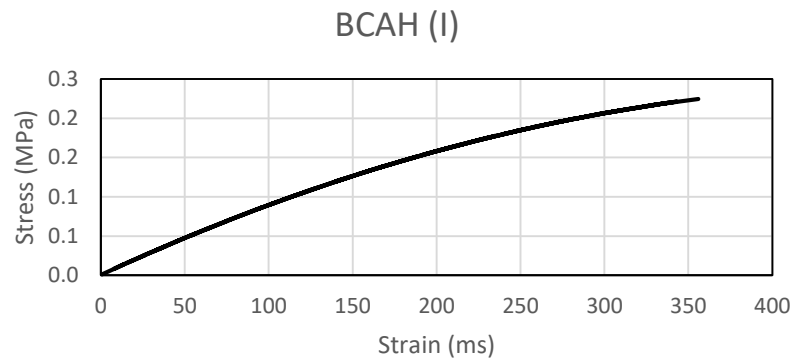
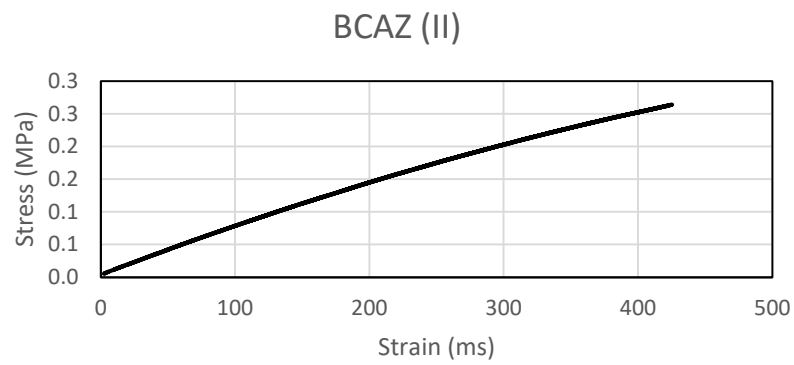
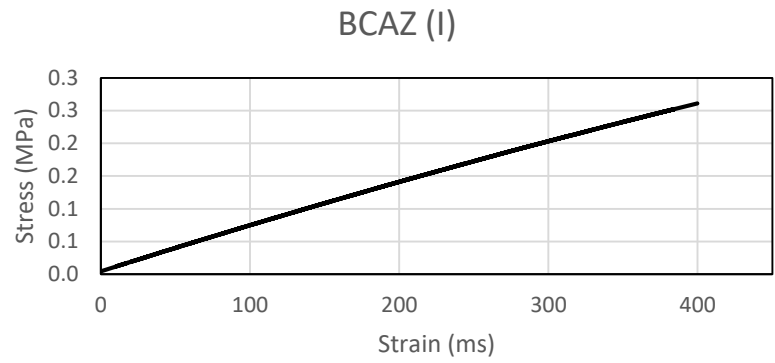


Figure A.2. (Continued)

Symbols used: Aggregate: L=limestone. B=basalt; Gradation: C=Coarse. F=Fine; Aging: A=aged. U=unaged; Hydrated lime content: H=2% hydrated lime. Z=0% hydrated lime

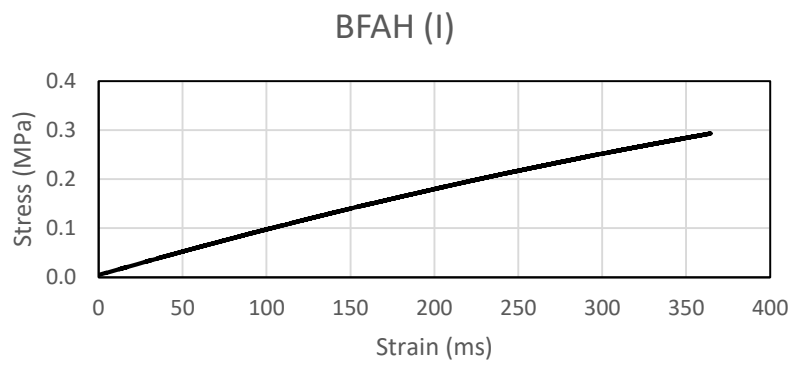
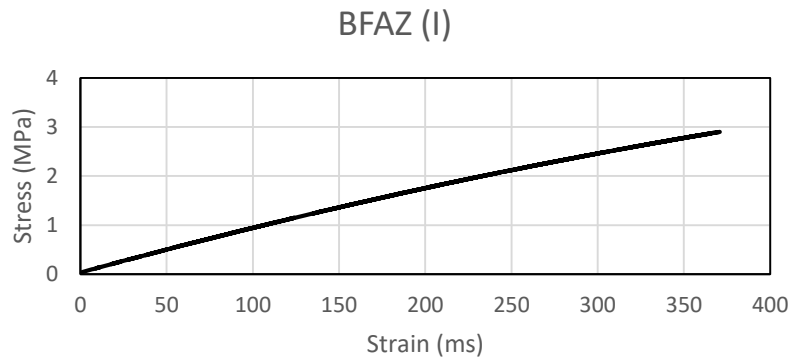


Figure A.2. (Continued)

Symbols used: Aggregate: L=limestone. B=basalt; Gradation: C=Coarse. F=Fine; Aging: A=aged. U=unaged; Hydrated lime content: H=2% hydrated lime. Z=0% hydrated lime

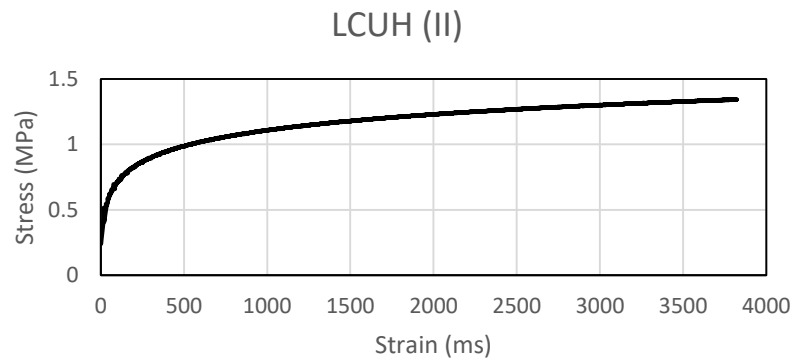
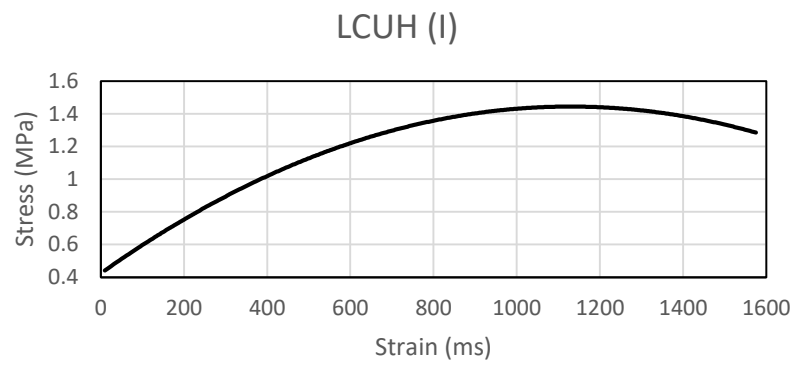
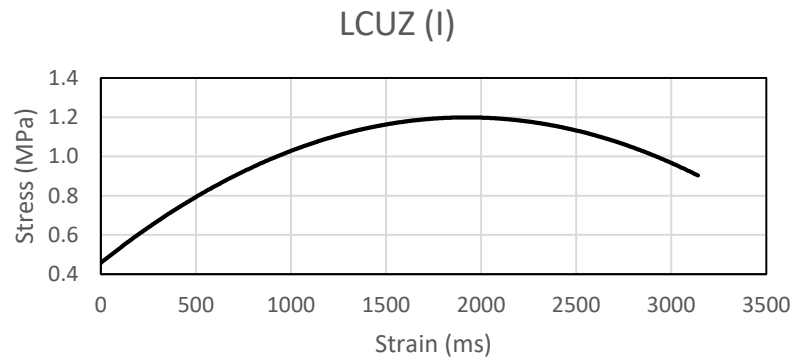


Figure A.3. Fracture plots of samples tested with DTT at 0°C

Symbols used: Aggregate: L=limestone. B=basalt; Gradation: C=Coarse. F=Fine; Aging: A=aged. U=unaged; Hydrated lime content: H=2% hydrated lime. Z=0% hydrated lime

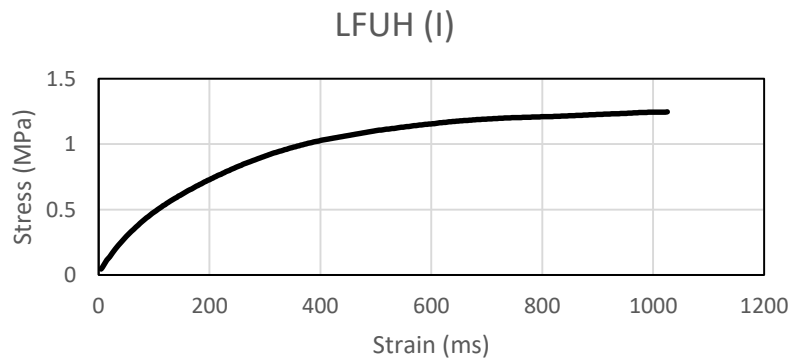
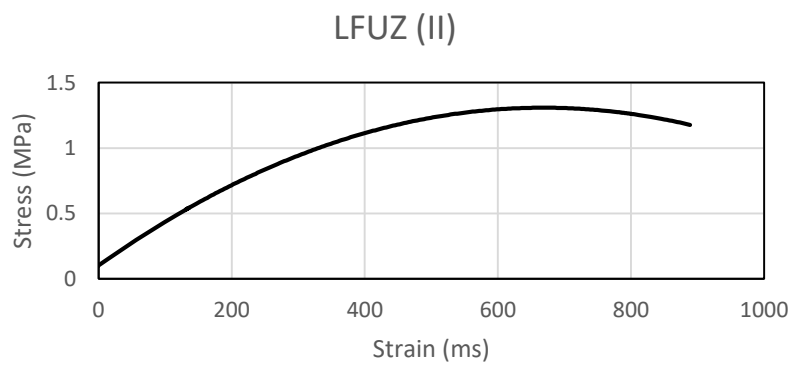
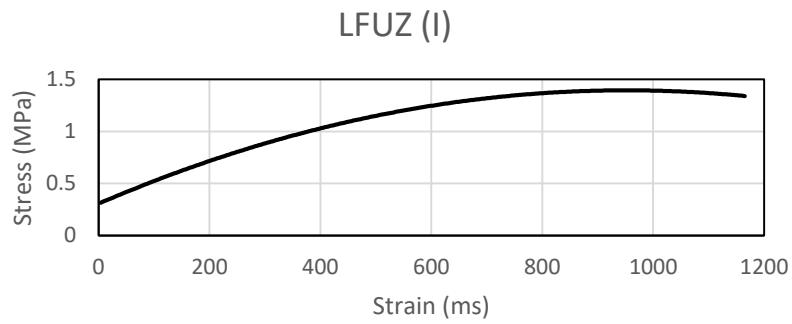


Figure A3 (continued)

Symbols used: Aggregate: L=limestone. B=basalt; Gradation: C=Coarse. F=Fine; Aging: A=aged. U=unaged; Hydrated lime content: H=2% hydrated lime. Z=0% hydrated lime

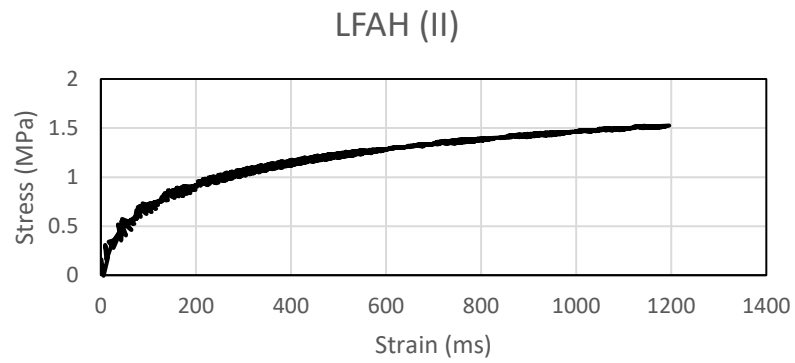
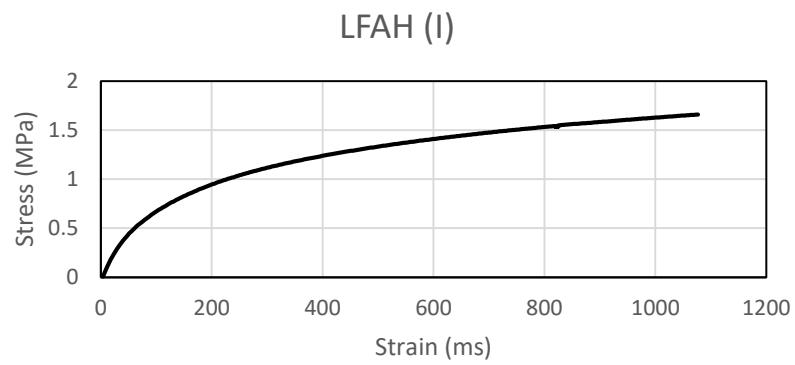
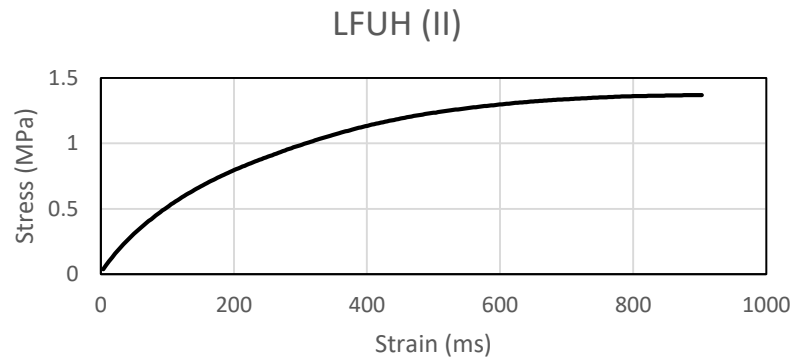


Figure A3 (continued)

Symbols used: Aggregate: L=limestone. B=basalt; Gradation: C=Coarse. F=Fine;
 Aging: A=aged. U=unaged; Hydrated lime content: H=2% hydrated lime. Z=0%
 hydrated lime

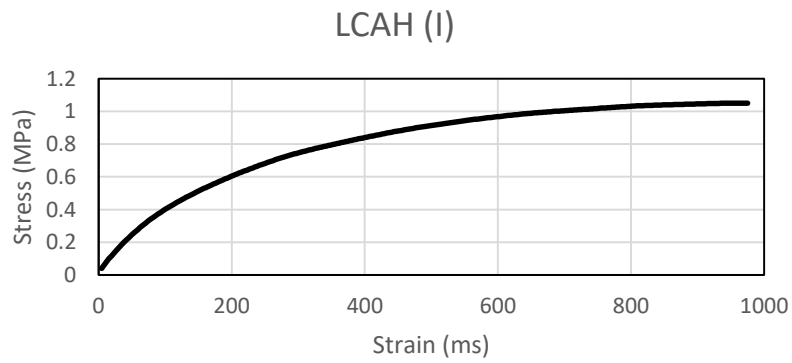
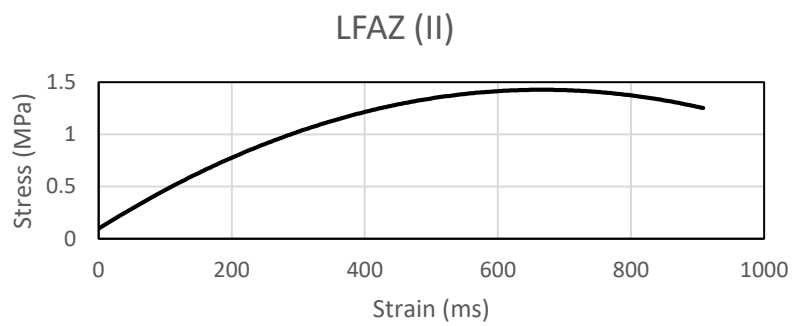
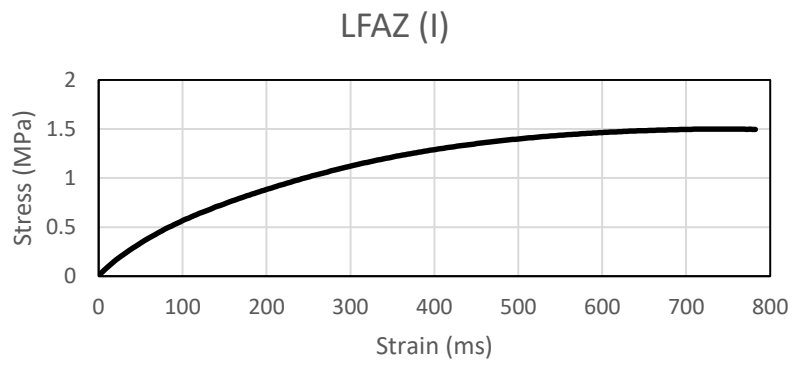


Figure A3 (continued)

Symbols used: Aggregate: L=limestone. B=basalt; Gradation: C=Coarse. F=Fine; Aging: A=aged. U=unaged; Hydrated lime content: H=2% hydrated lime. Z=0% hydrated lime

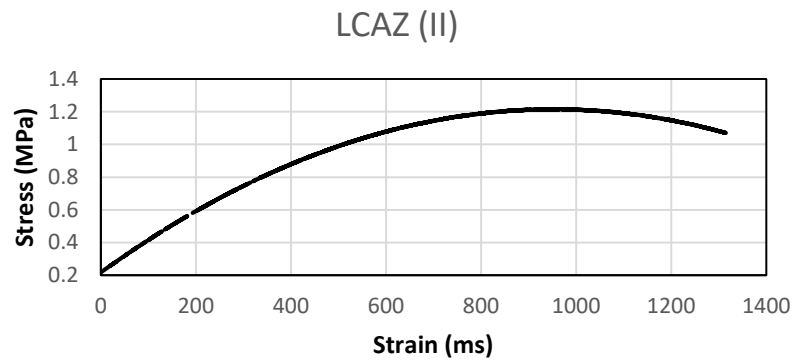
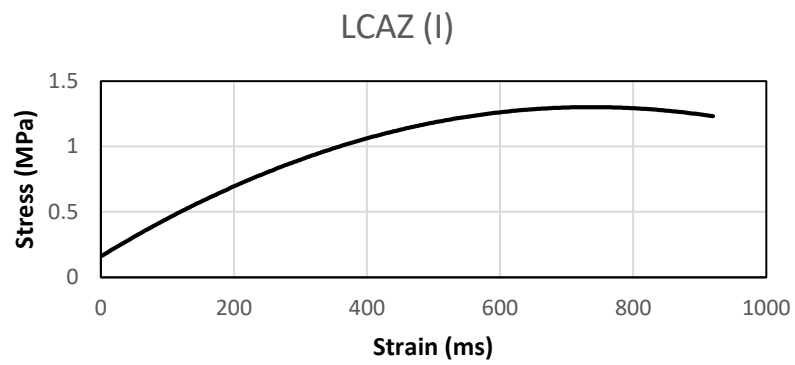
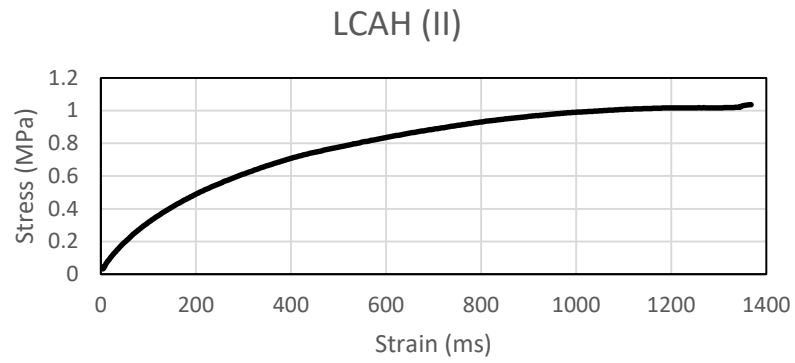


Figure A3 (continued)

Symbols used: Aggregate: L=limestone. B=basalt; Gradation: C=Coarse. F=Fine; Aging: A=aged. U=unaged; Hydrated lime content: H=2% hydrated lime. Z=0% hydrated lime

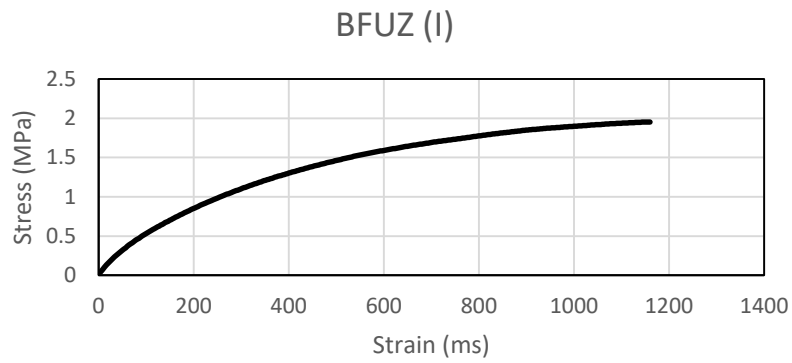
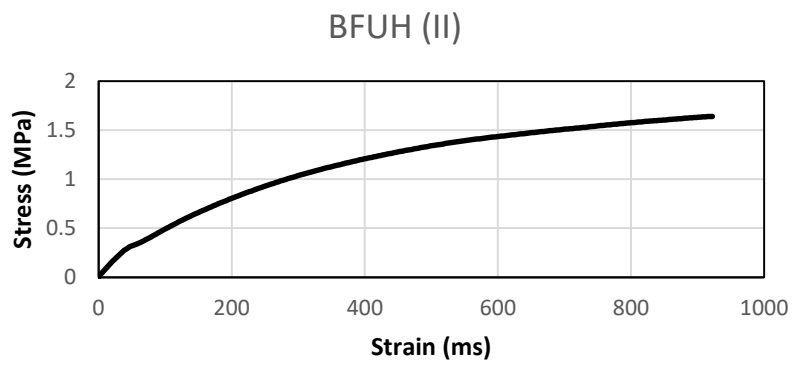
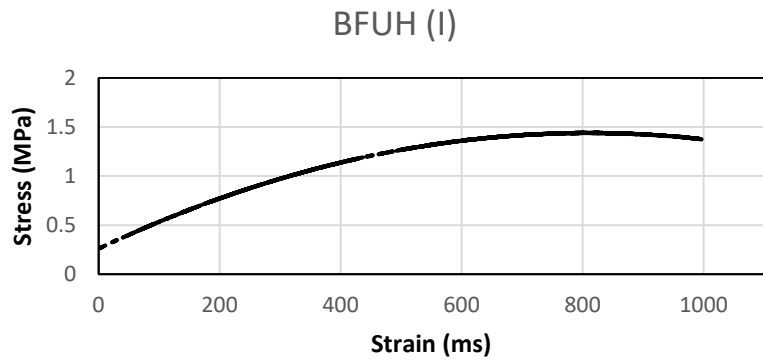


Figure A3 (continued)

Symbols used: Aggregate: L=limestone. B=basalt; Gradation: C=Coarse. F=Fine; Aging: A=aged. U=unaged; Hydrated lime content: H=2% hydrated lime. Z=0% hydrated lime

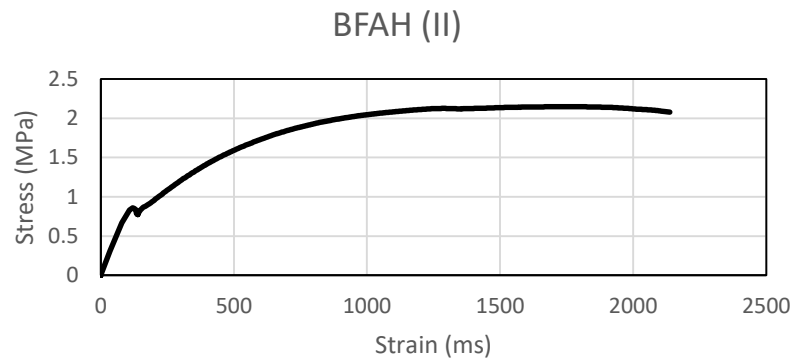
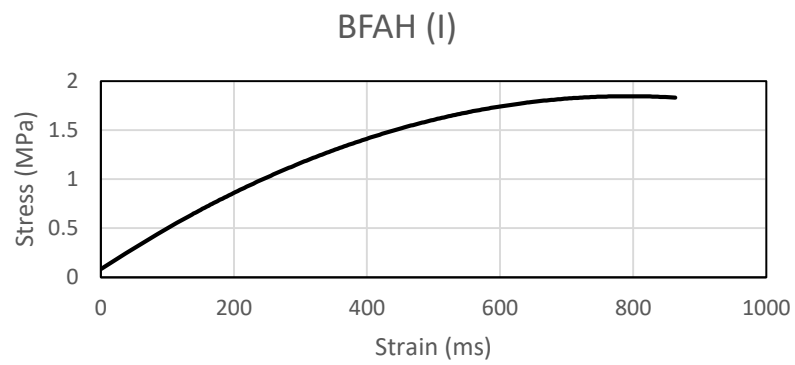
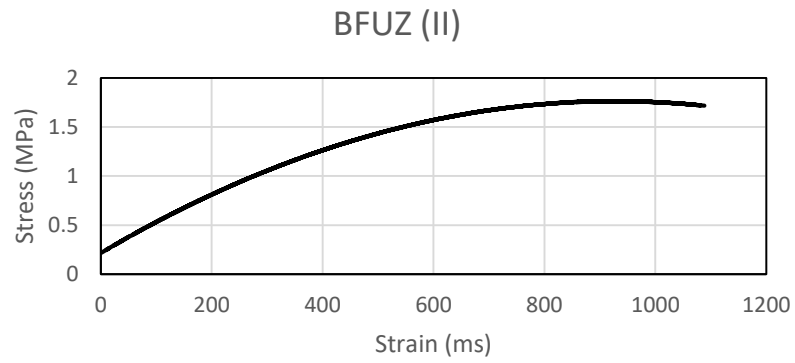


Figure A3 (continued)

Symbols used: Aggregate: L=limestone. B=basalt; Gradation: C=Coarse. F=Fine; Aging: A=aged. U=unaged; Hydrated lime content: H=2% hydrated lime. Z=0% hydrated lime

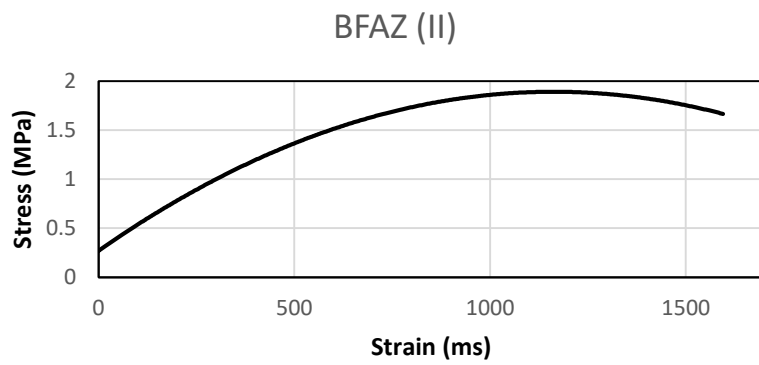
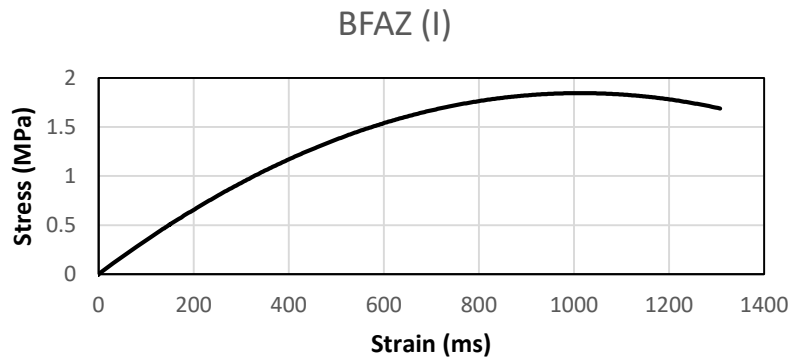


Figure A3 (continued)

Symbols used: Aggregate: L=limestone. B=basalt; Gradation: C=Coarse. F=Fine; Aging: A=aged. U=unaged; Hydrated lime content: H=2% hydrated lime. Z=0% hydrated lime

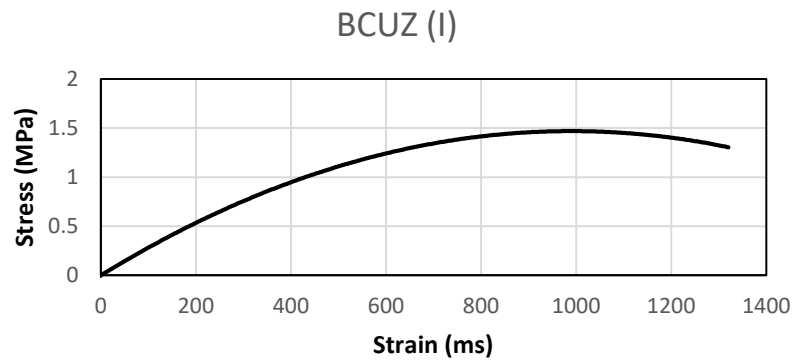
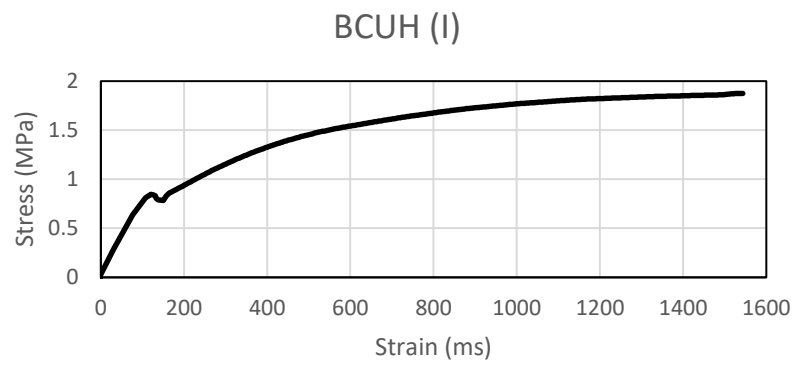
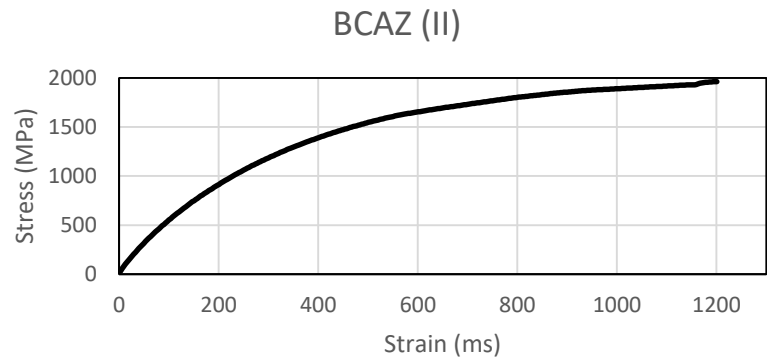


Figure A3 (continued)

Symbols used: Aggregate: L=limestone. B=basalt; Gradation: C=Coarse. F=Fine; Aging: A=aged. U=unaged; Hydrated lime content: H=2% hydrated lime. Z=0% hydrated lime

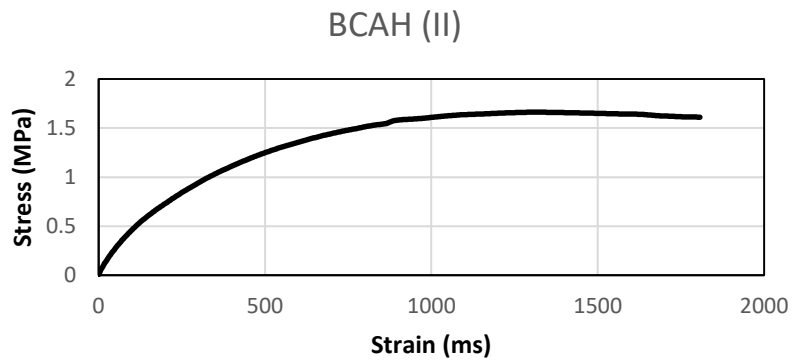
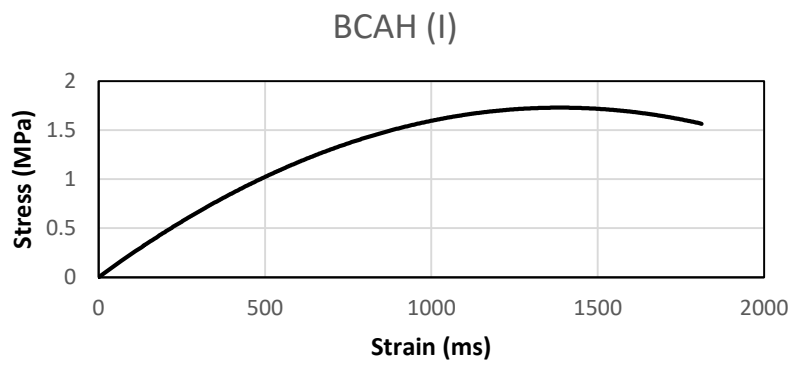
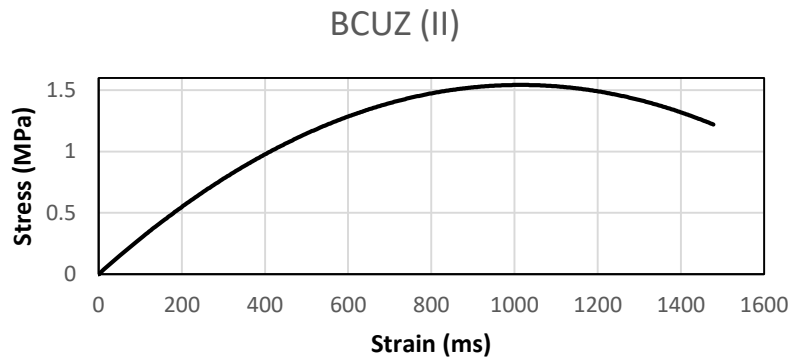


Figure A3 (continued)

Symbols used: Aggregate: L=limestone. B=basalt; Gradation: C=Coarse. F=Fine; Aging: A=aged. U=unaged; Hydrated lime content: H=2% hydrated lime. Z=0% hydrated lime

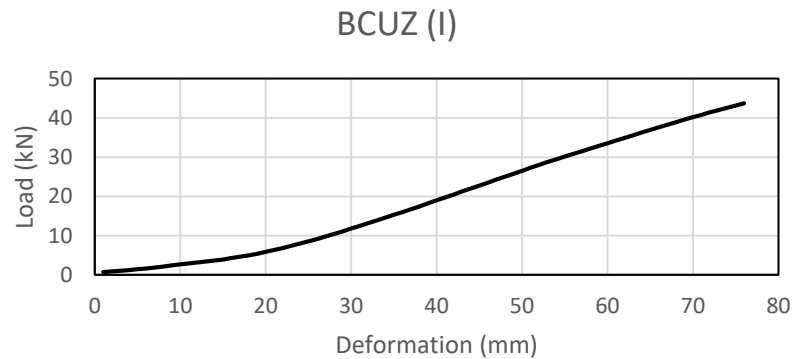
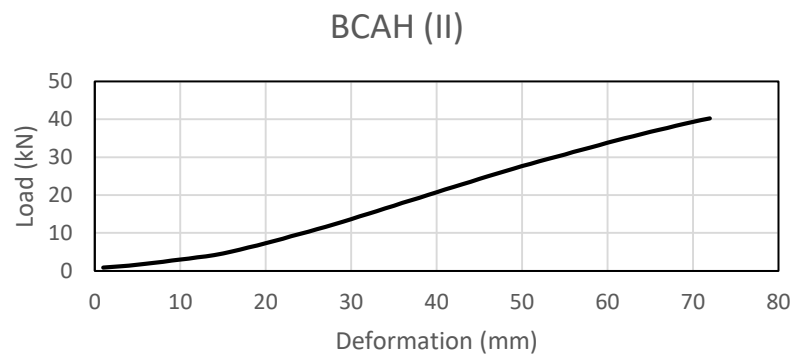
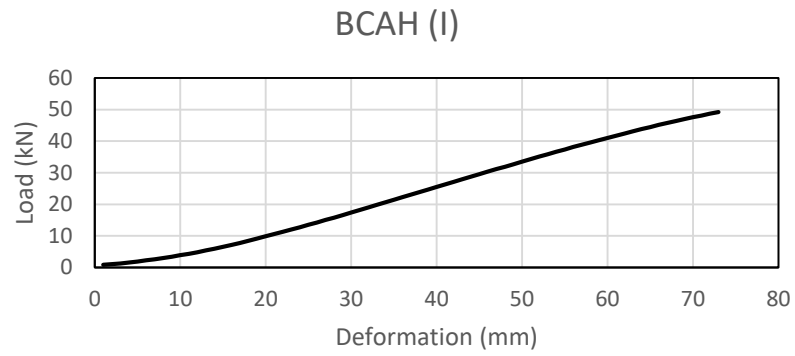
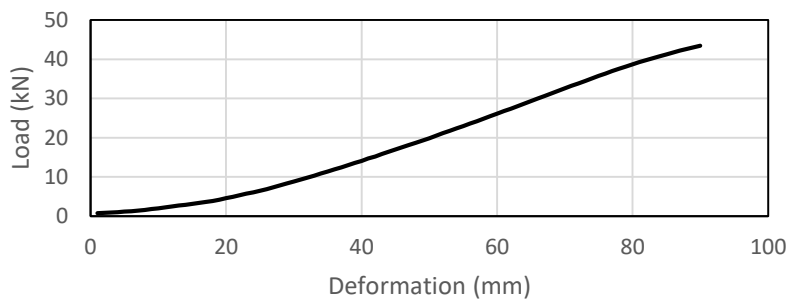


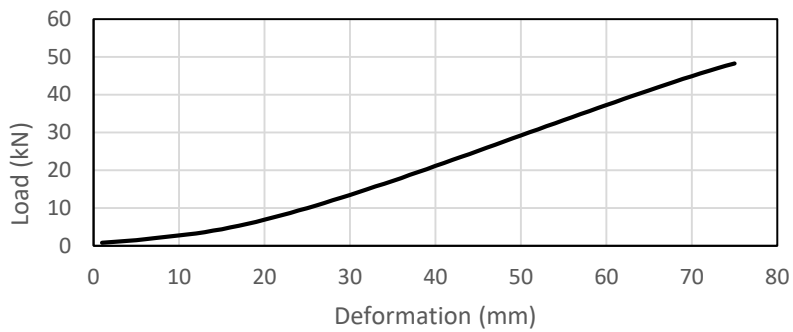
Figure A.4. Fracture plots of samples tested with IDT at -10°C

Symbols used: Aggregate: L=limestone. B=basalt; Gradation: C=Coarse. F=Fine; Aging: A=aged. U=unaged; Hydrated lime content: H=2% hydrated lime. Z=0% hydrated lime

BCUZ (II)



BFAZ (I)



BFAZ (II)

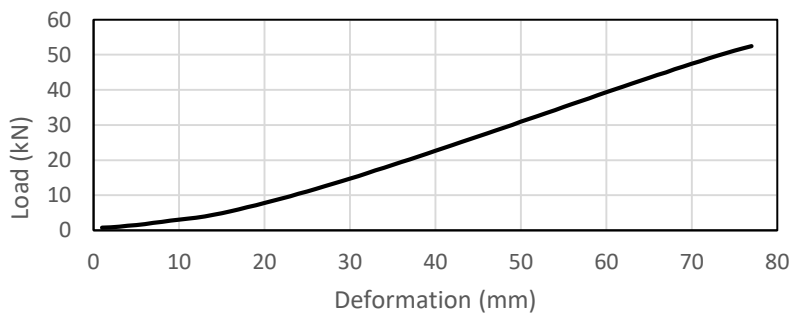


Figure A4 (continued)

Symbols used:

Aggregate: L=limestone. B=basalt; Gradation: C=Coarse. F=Fine; Aging: A=aged. U=unaged; Hydrated lime content: H=2% hydrated lime. Z=0% hydrated lime

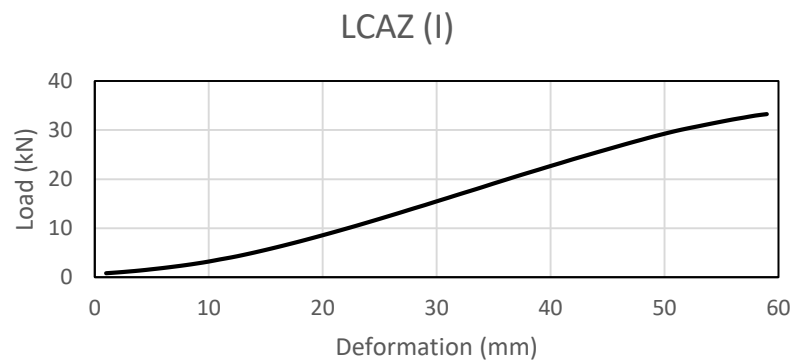
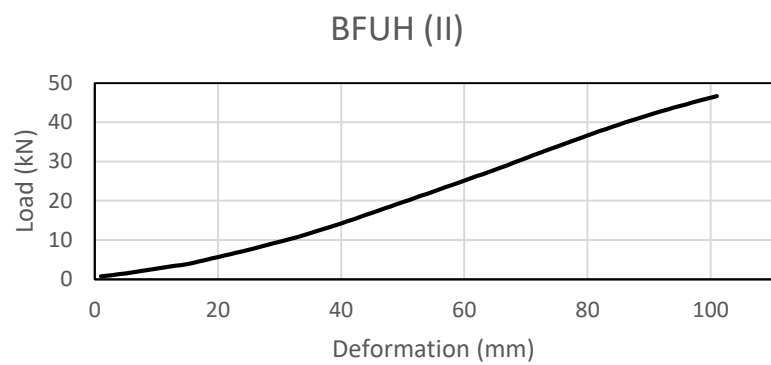
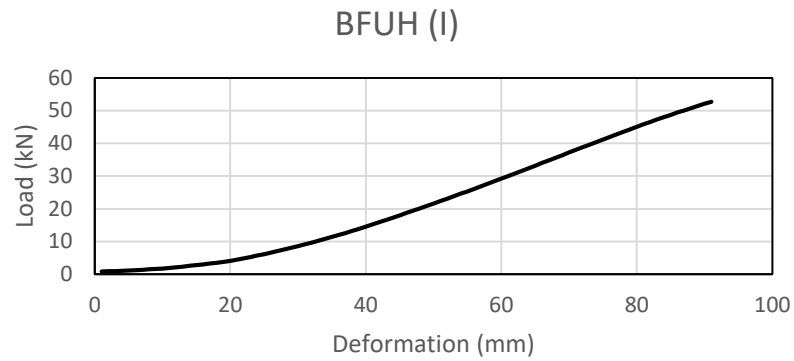
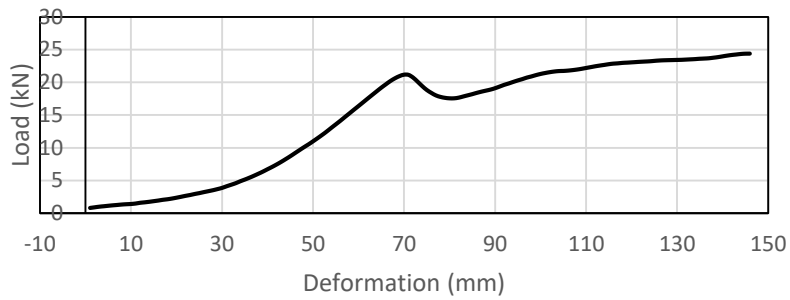


Figure A4 (continued)

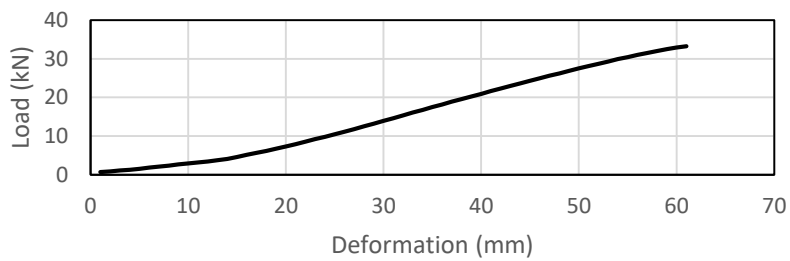
Symbols used:

Aggregate: L=limestone. B=basalt; Gradation: C=Coarse. F=Fine; Aging: A=aged. U=unaged; Hydrated lime content: H=2% hydrated lime. Z=0% hydrated lime

LCAZ (II)



LCUH (I)



LCUH (II)

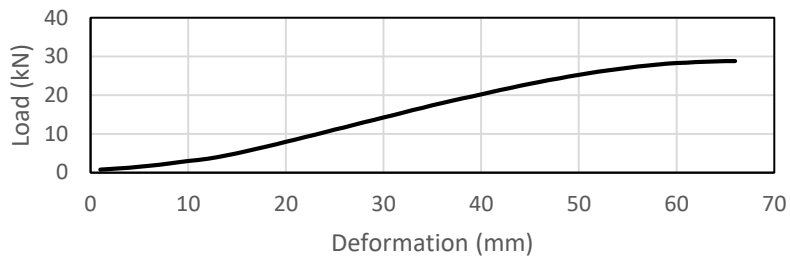


Figure A4 (continued)

Symbols used:

Aggregate: L=limestone. B=basalt; Gradation: C=Coarse. F=Fine; Aging: A=aged. U=unaged; Hydrated lime content: H=2% hydrated lime. Z=0% hydrated lime

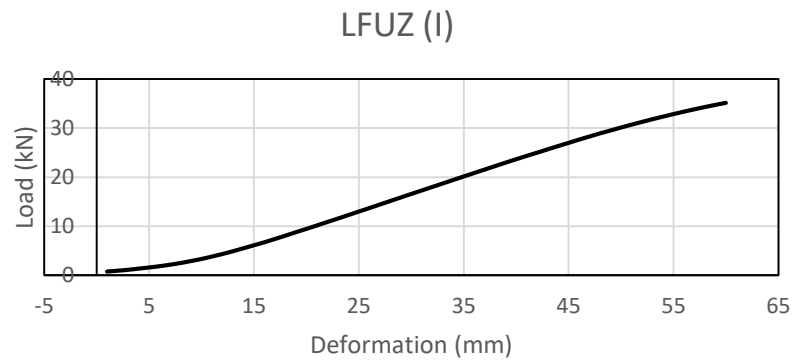
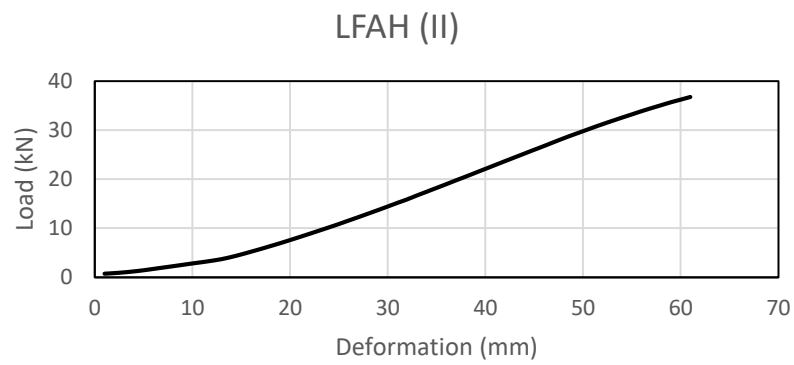
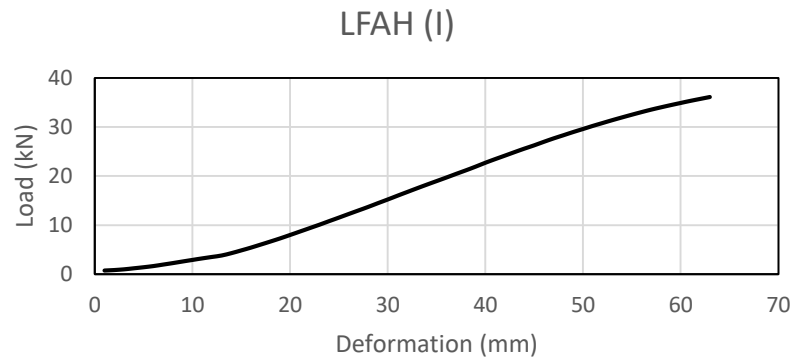
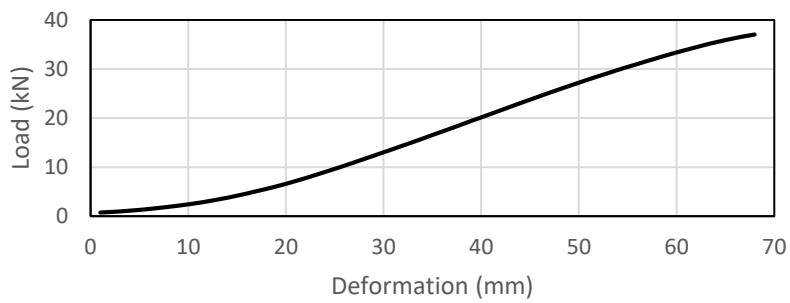


Figure A4 (continued)

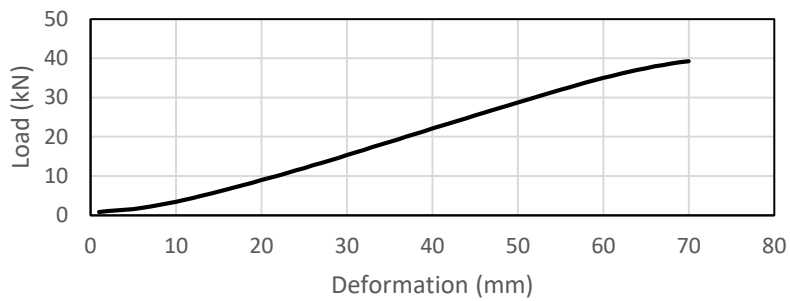
Symbols used:

Aggregate: L=limestone. B=basalt; Gradation: C=Coarse. F=Fine; Aging: A=aged. U=unaged; Hydrated lime content: H=2% hydrated lime. Z=0% hydrated lime

LFUZ (II)



BCAZ (I)



BCAZ (II)

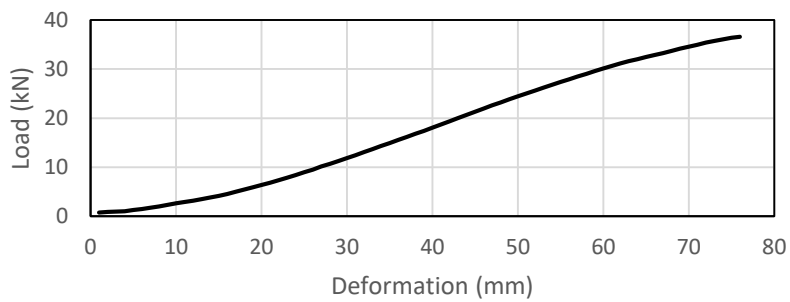


Figure A4 (continued)

Symbols used:

Aggregate: L=limestone. B=basalt; Gradation: C=Coarse. F=Fine; Aging: A=aged. U=unaged; Hydrated lime content: H=2% hydrated lime. Z=0% hydrated lime

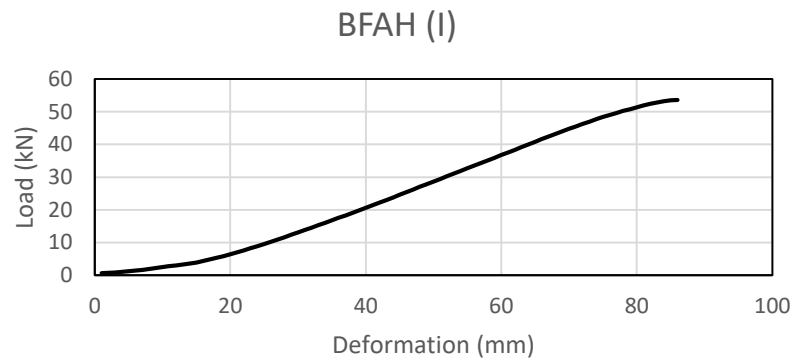
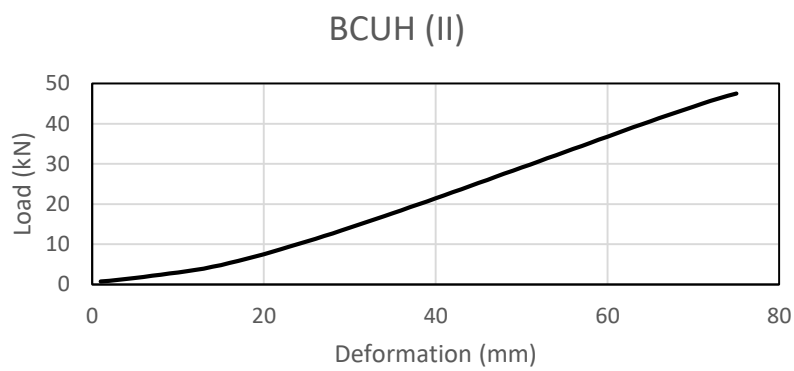
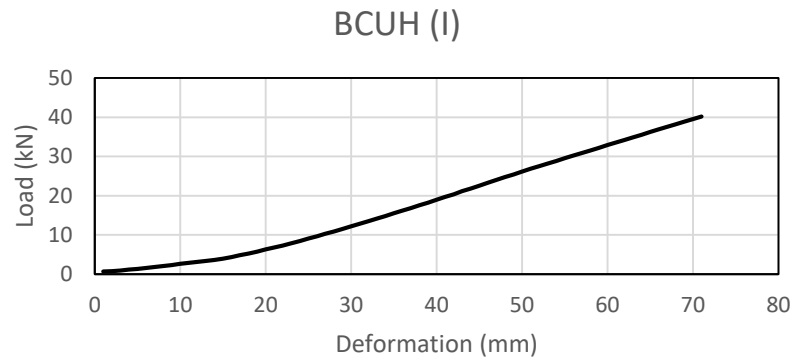
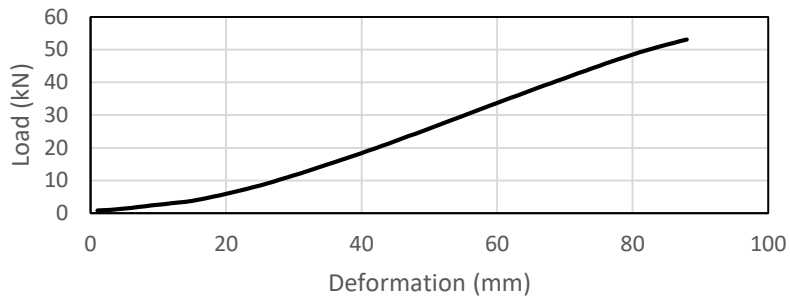


Figure A4 (continued)

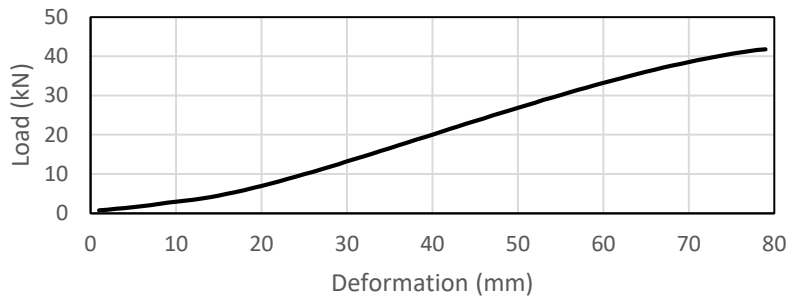
Symbols used:

Aggregate: L=limestone. B=basalt; Gradation: C=Coarse. F=Fine; Aging: A=aged. U=unaged; Hydrated lime content: H=2% hydrated lime. Z=0% hydrated lime

BFAH (II)



BFUZ (I)



BFUZ (II)

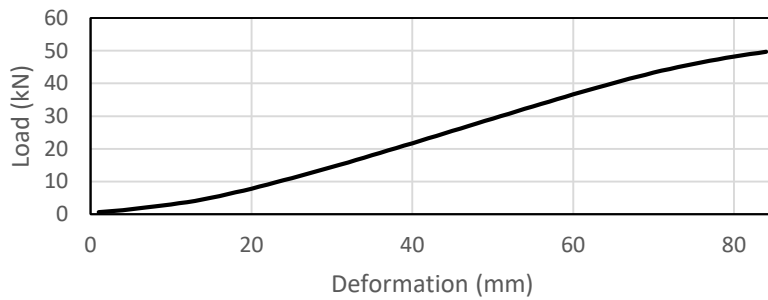


Figure A4 (continued)

Symbols used:

Aggregate: L=limestone. B=basalt; Gradation: C=Coarse. F=Fine; Aging: A=aged. U=unaged; Hydrated lime content: H=2% hydrated lime. Z=0% hydrated lime

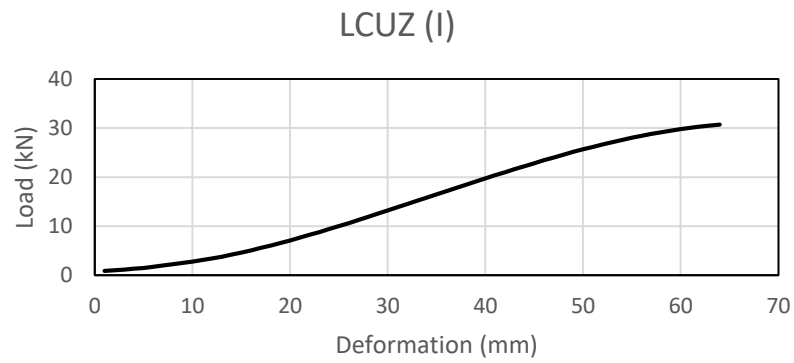
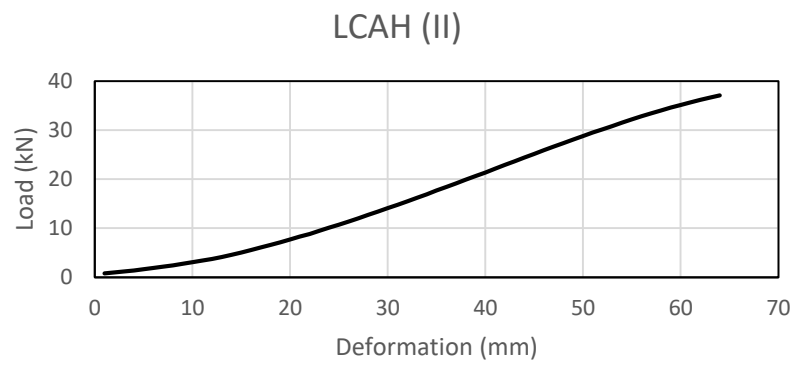
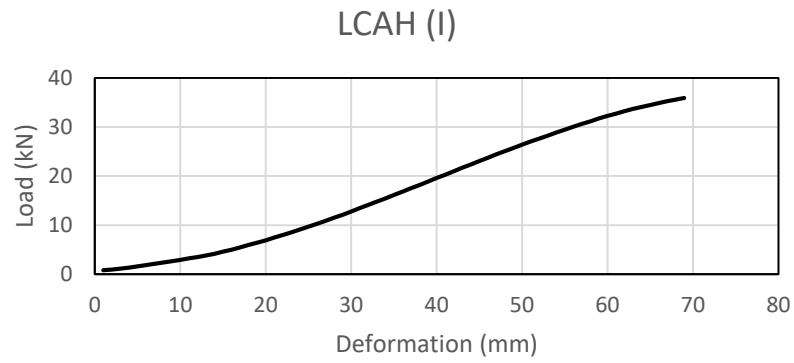
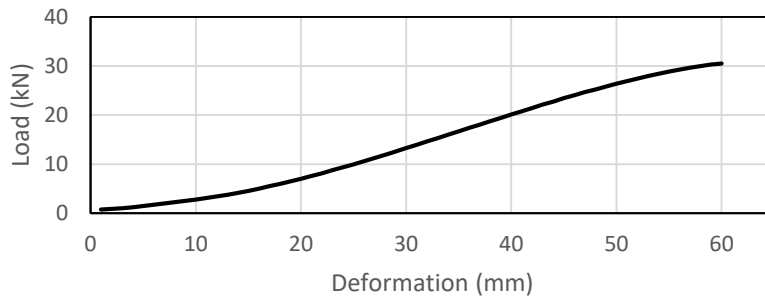


Figure A4 (continued)

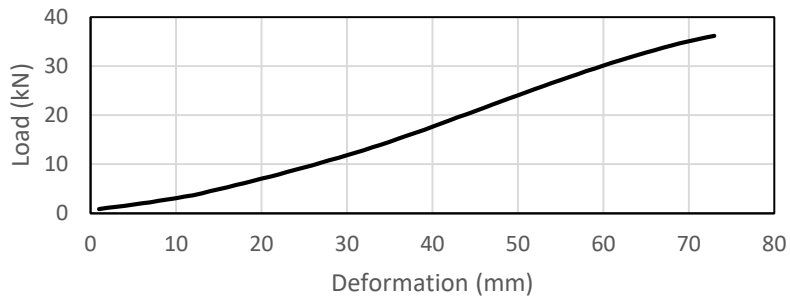
Symbols used:

Aggregate: L=limestone. B=basalt; Gradation: C=Coarse. F=Fine; Aging: A=aged. U=unaged; Hydrated lime content: H=2% hydrated lime. Z=0% hydrated lime

LCUZ (II)



LFAZ (I)



LFUH (I)

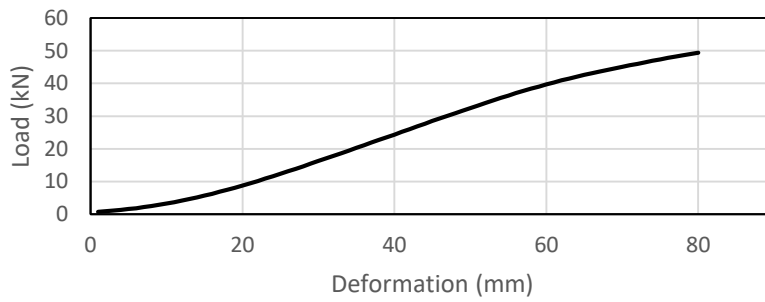


Figure A4 (continued)

Symbols used:

Aggregate: L=limestone. B=basalt; Gradation: C=Coarse. F=Fine; Aging: A=aged. U=unaged; Hydrated lime content: H=2% hydrated lime. Z=0% hydrated lime

LFUH (II)

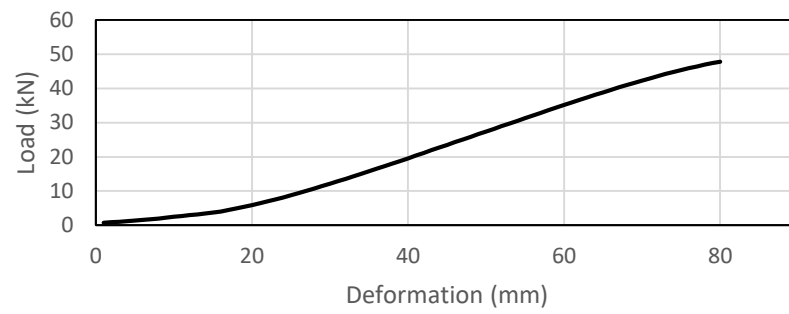


Figure A4 (continued)

Symbols used:

Aggregate: L=limestone. B=basalt; Gradation: C=Coarse. F=Fine; Aging: A=aged. U=unaged; Hydrated lime content: H=2% hydrated lime. Z=0% hydrated lime

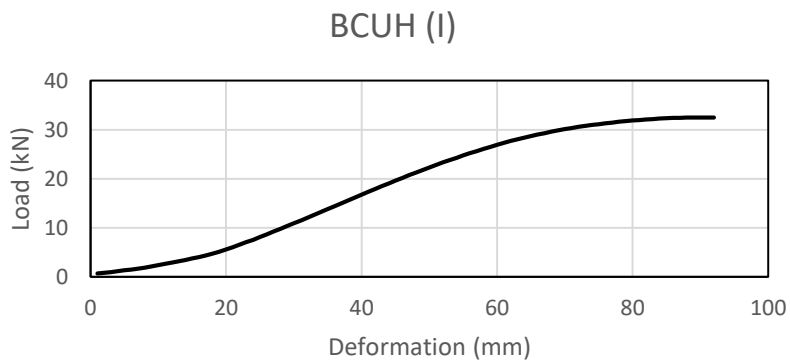
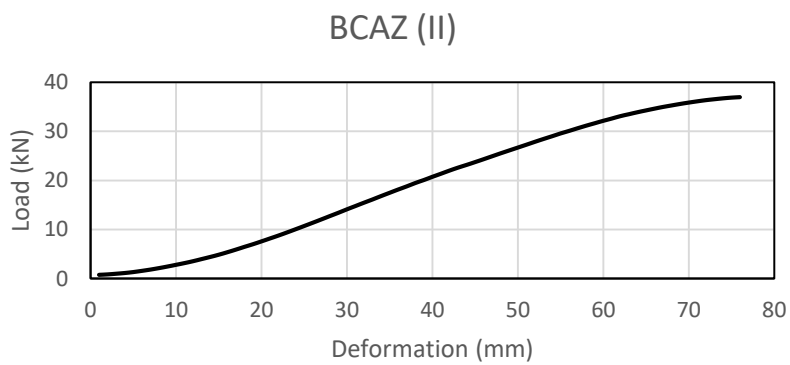
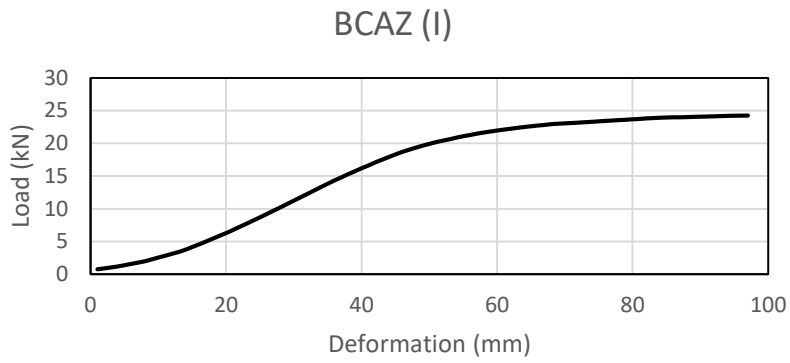


Figure A.5. Fracture plots of samples tested with IDT at 0°C

Symbols used:

Aggregate: L=limestone. B=basalt; Gradation: C=Coarse. F=Fine; Aging: A=aged. U=unaged; Hydrated lime content: H=2% hydrated lime. Z=0% hydrated lime

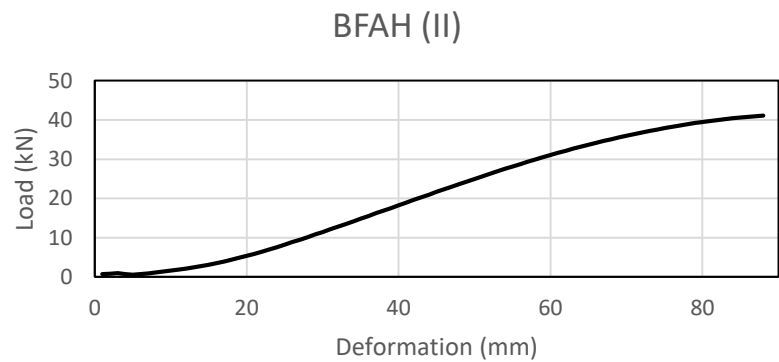
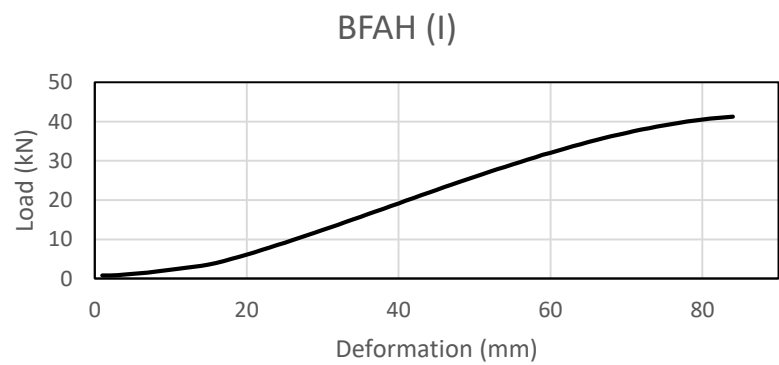
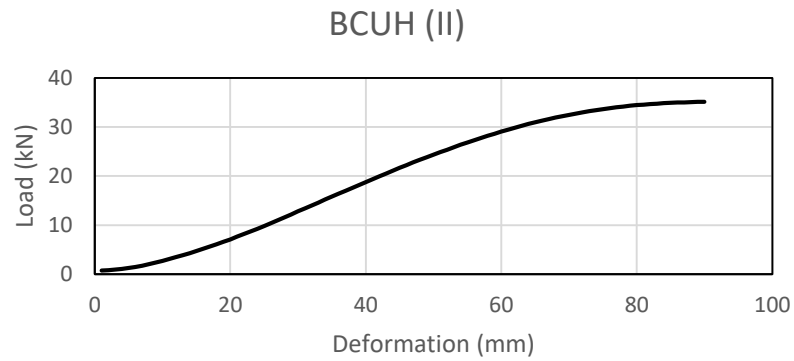


Figure A5 (continued)

Symbols used:

Aggregate: L=limestone. B=basalt; Gradation: C=Coarse. F=Fine; Aging: A=aged.
 U=unaged; Hydrated lime content: H=2% hydrated lime. Z=0% hydrated lime

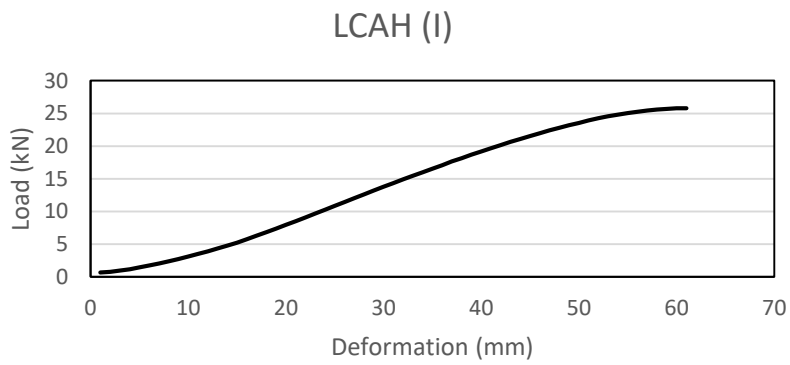
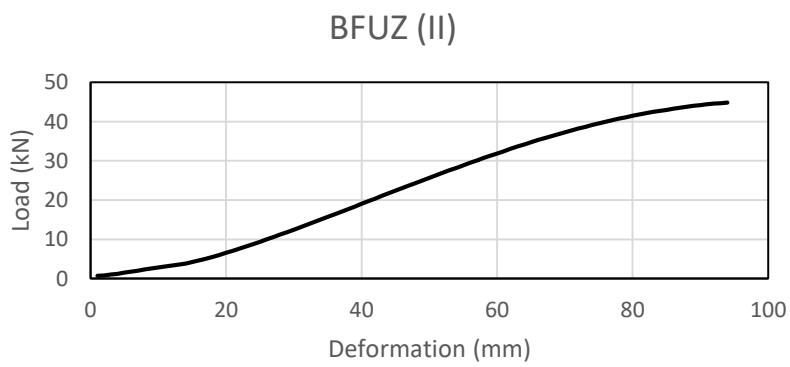
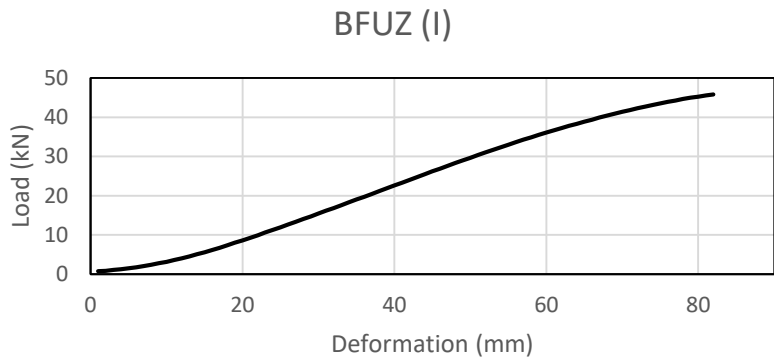
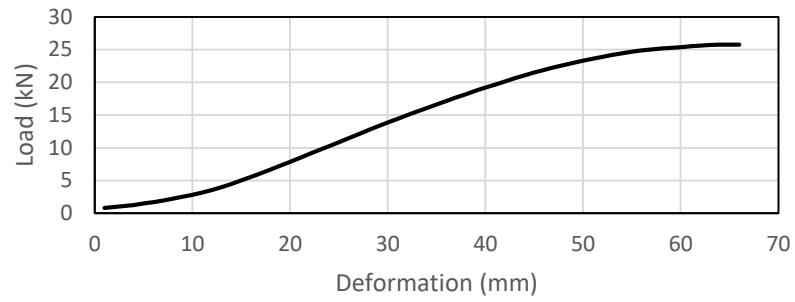


Figure A5 (continued)

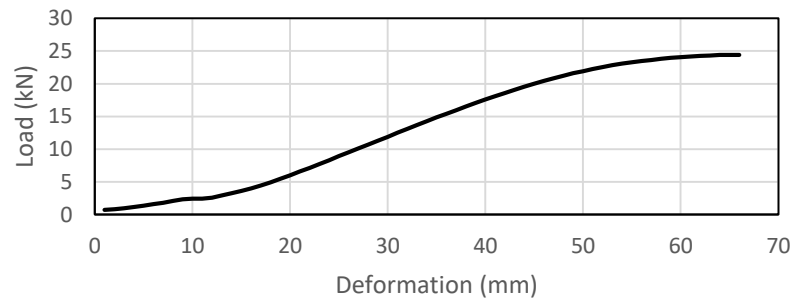
Symbols used:

Aggregate: L=limestone. B=basalt; Gradation: C=Coarse. F=Fine; Aging: A=aged.
 U=unaged; Hydrated lime content: H=2% hydrated lime. Z=0% hydrated lime

LCAH (II)



LCUZ (I)



LCUZ (II)

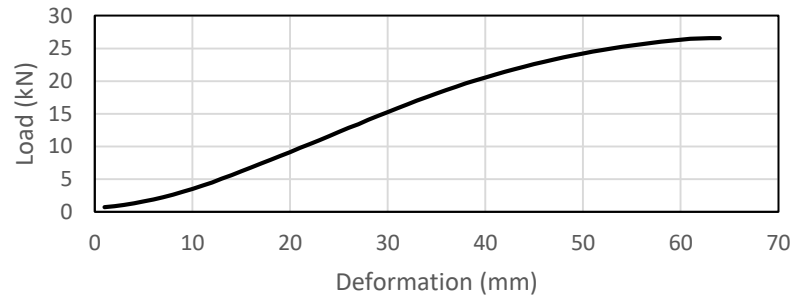


Figure A5 (continued)

Symbols used:

Aggregate: L=limestone. B=basalt; Gradation: C=Coarse. F=Fine; Aging: A=aged. U=unaged;
Hydrated lime content: H=2% hydrated lime. Z=0% hydrated lime

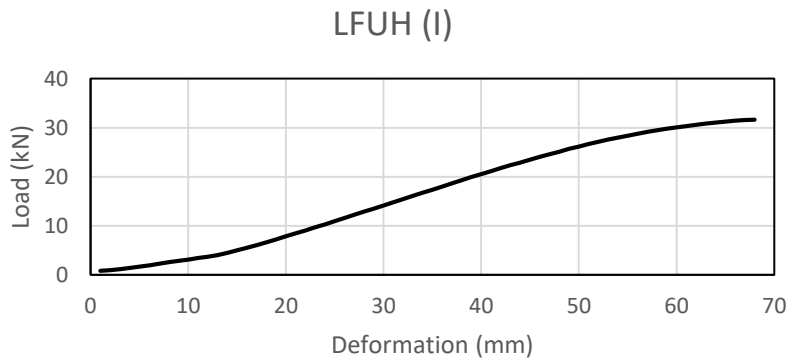
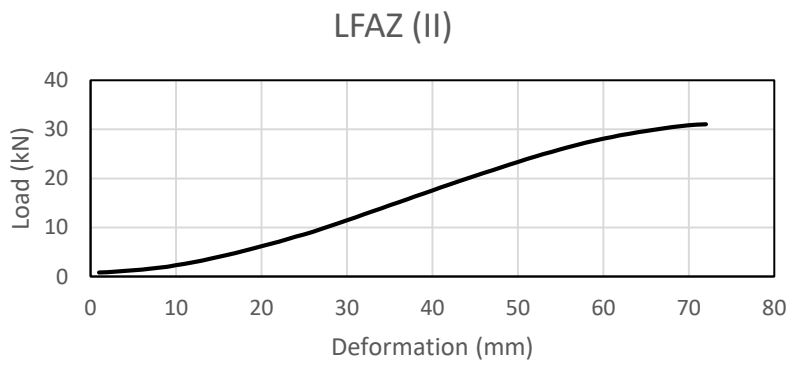
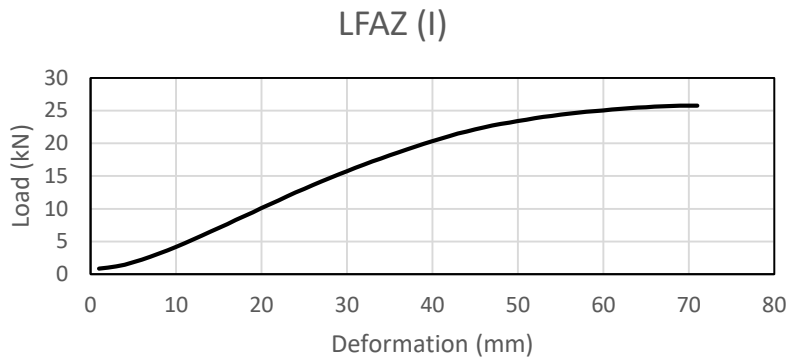


Figure A5 (continued)

Symbols used:

Aggregate: L=limestone. B=basalt; Gradation: C=Coarse. F=Fine; Aging: A=aged.
 U=unaged; Hydrated lime content: H=2% hydrated lime. Z=0% hydrated lime

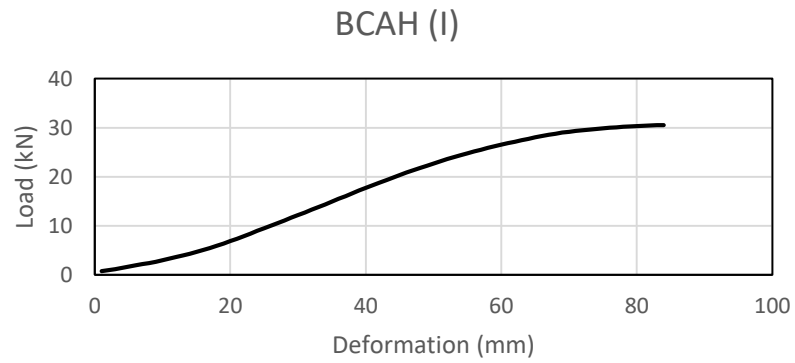
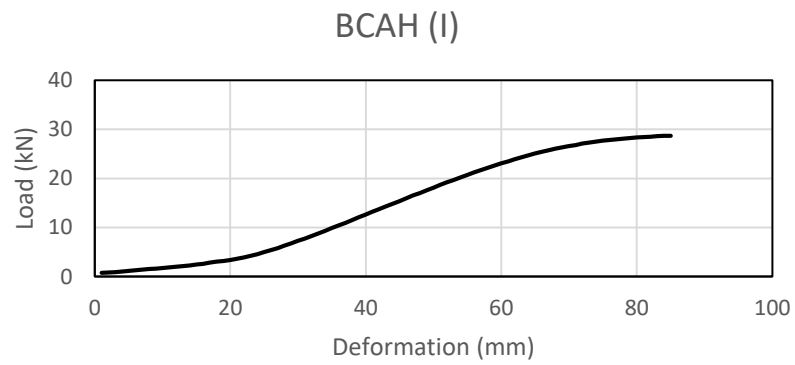
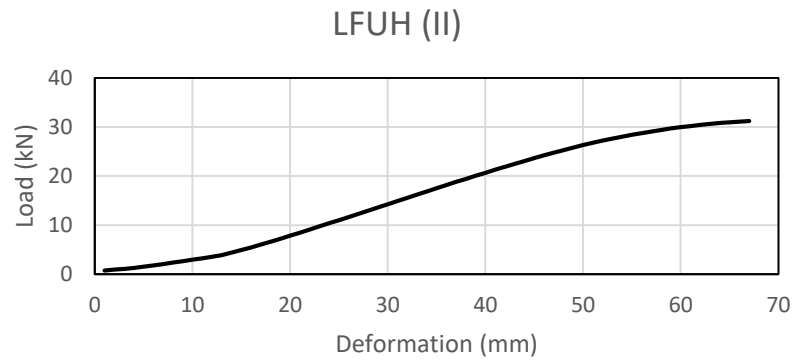


Figure A5 (continued)

Symbols used:

Aggregate: L=limestone. B=basalt; Gradation: C=Coarse. F=Fine; Aging: A=aged.
 U=unaged; Hydrated lime content: H=2% hydrated lime. Z=0% hydrated lime

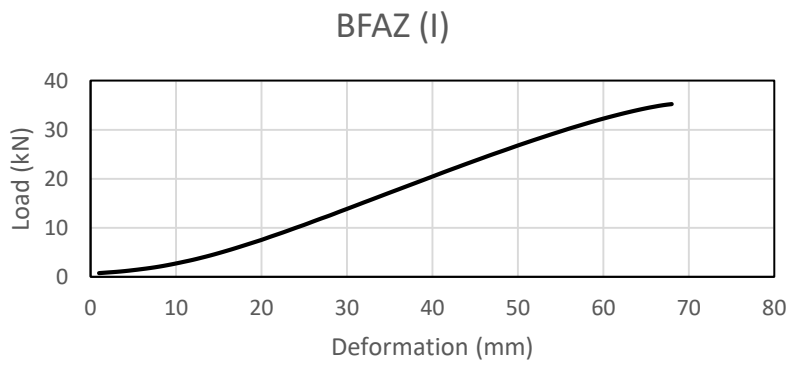
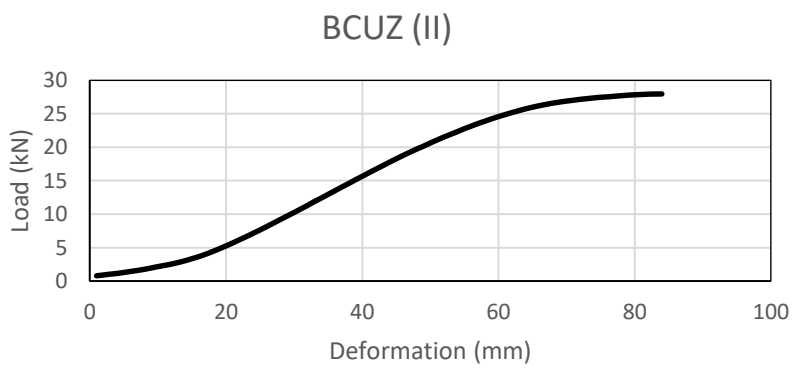
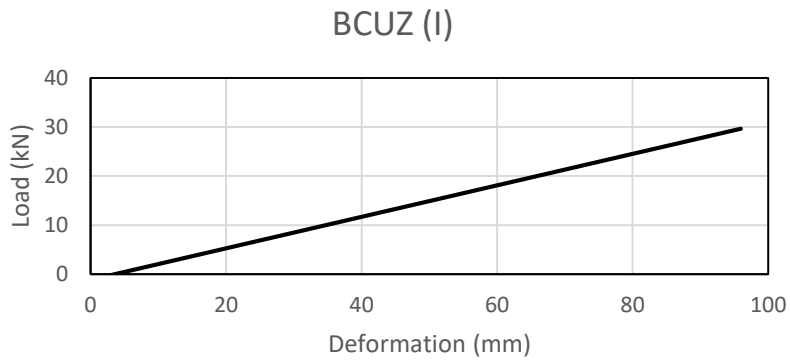


Figure A5 (continued)

Symbols used:

Aggregate: L=limestone. B=basalt; Gradation: C=Coarse. F=Fine; Aging: A=aged.
 U=unaged; Hydrated lime content: H=2% hydrated lime. Z=0% hydrated lime

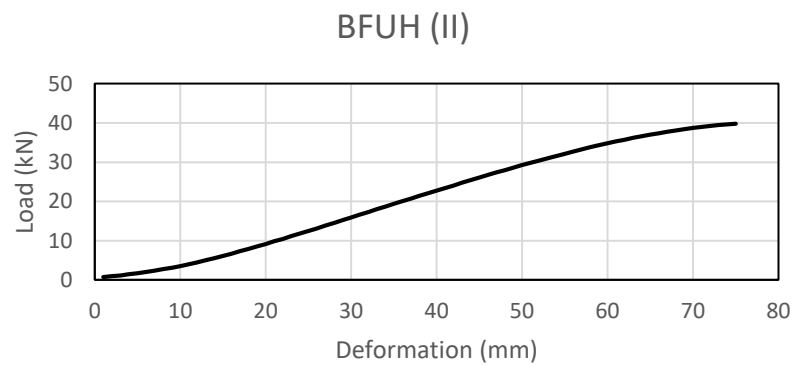
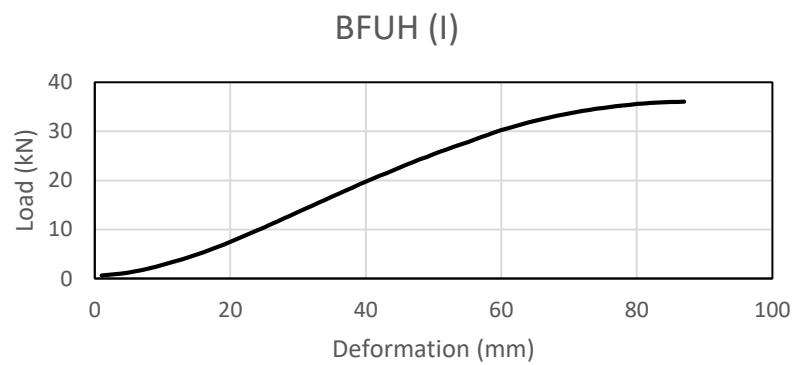
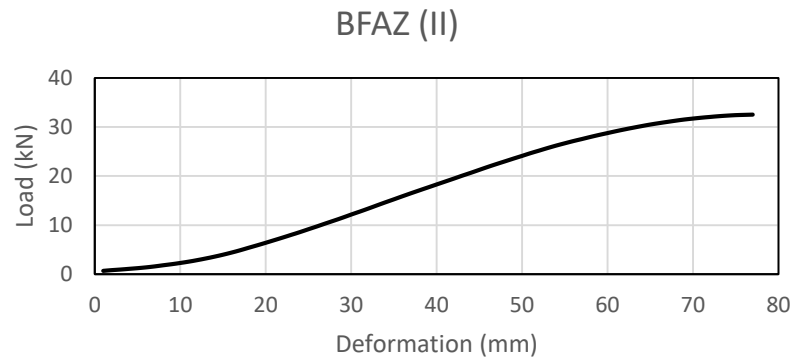


Figure A5 (continued)

Symbols used:

Aggregate: L=limestone. B=basalt; Gradation: C=Coarse. F=Fine; Aging: A=aged.
 U=unaged; Hydrated lime content: H=2% hydrated lime. Z=0% hydrated lime

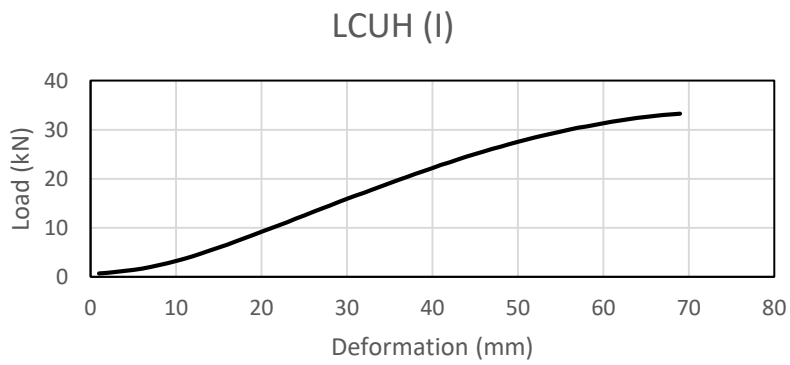
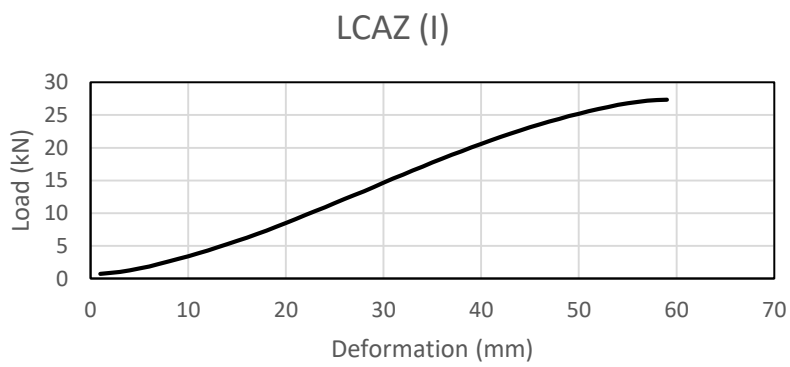
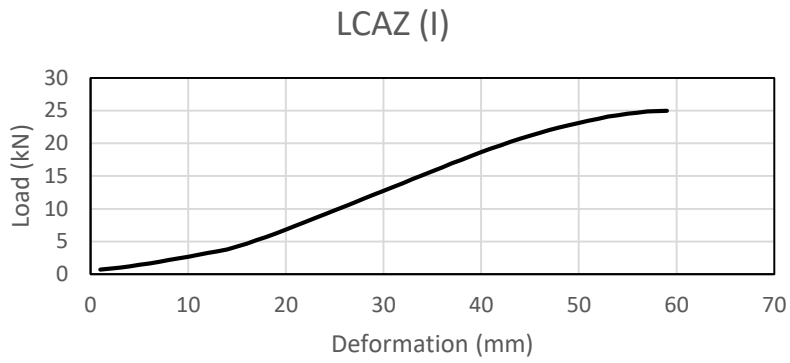


Figure A5 (continued)

Symbols used:

Aggregate: L=limestone. B=basalt; Gradation: C=Coarse. F=Fine; Aging: A=aged.
 U=unaged; Hydrated lime content: H=2% hydrated lime. Z=0% hydrated lime

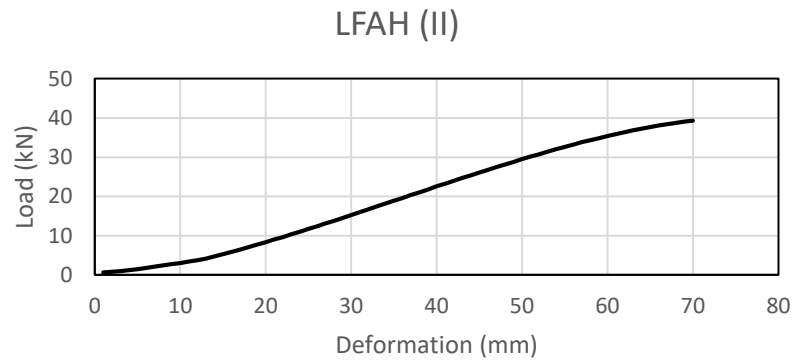
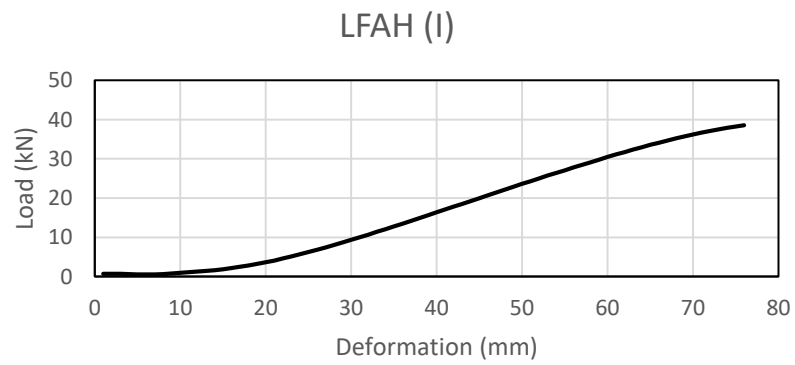
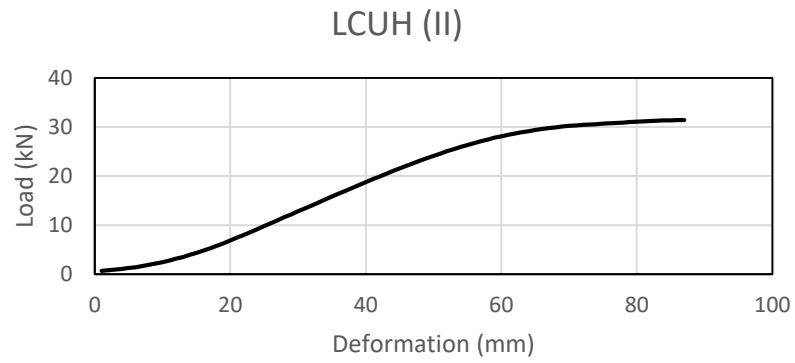


Figure A5 (continued)

Symbols used:

Aggregate: L=limestone. B=basalt; Gradation: C=Coarse. F=Fine; Aging: A=aged.
 U=unaged; Hydrated lime content: H=2% hydrated lime. Z=0% hydrated lime

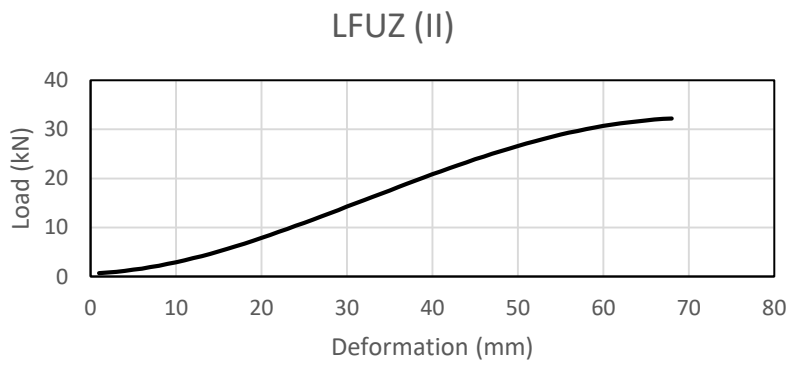
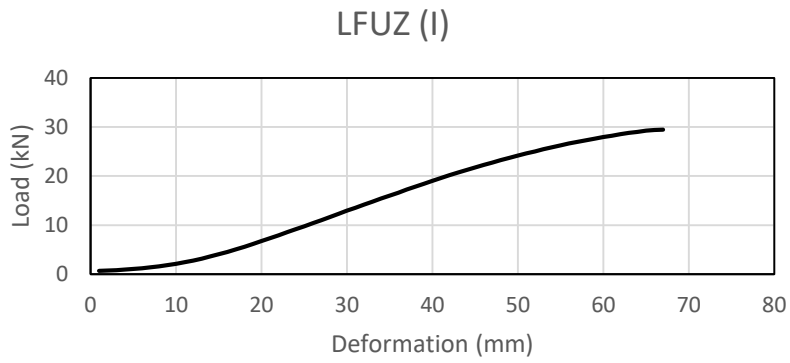


Figure A5 (continued)

Symbols used:

Aggregate: L=limestone. B=basalt; Gradation: C=Coarse. F=Fine; Aging: A=aged.
 U=unaged; Hydrated lime content: H=2% hydrated lime. Z=0% hydrated lime

B. Dynamic Mechanical Analysis Results

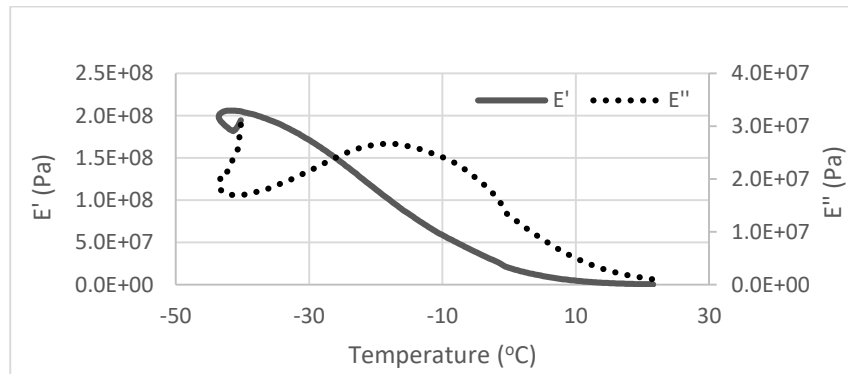


Figure B1 DMA curves and Tg of unaged bitumen

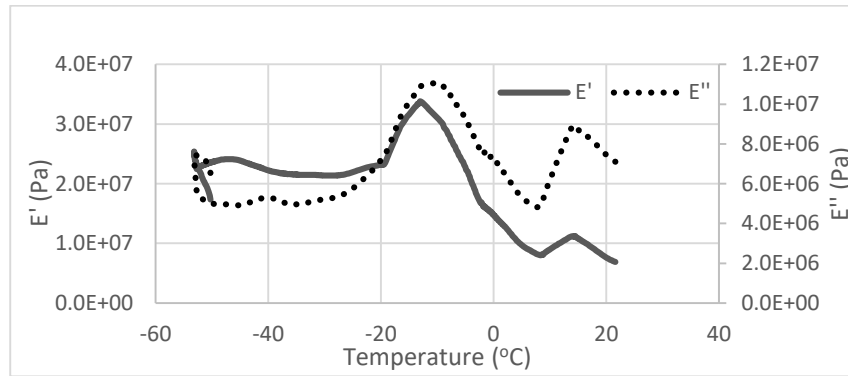


Figure B2 DMA curves and Tg of aged bitumen

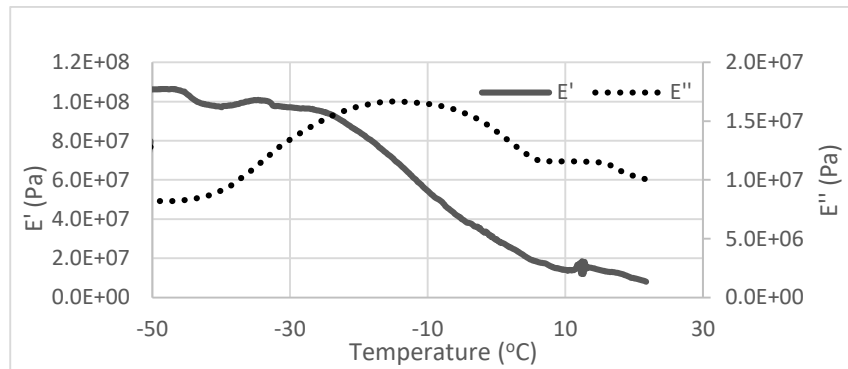


Figure B3 DMA curves and Tg of unaged bitumen mastic containing limestone

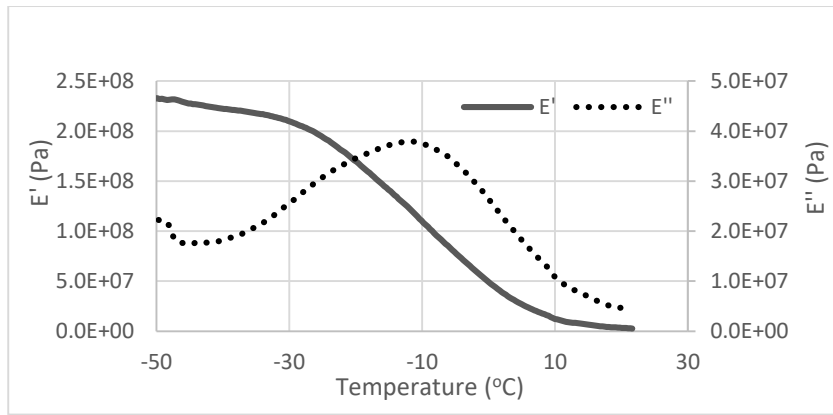


Figure B4 DMA curves and Tg of aged bitumen mastic containing limestone

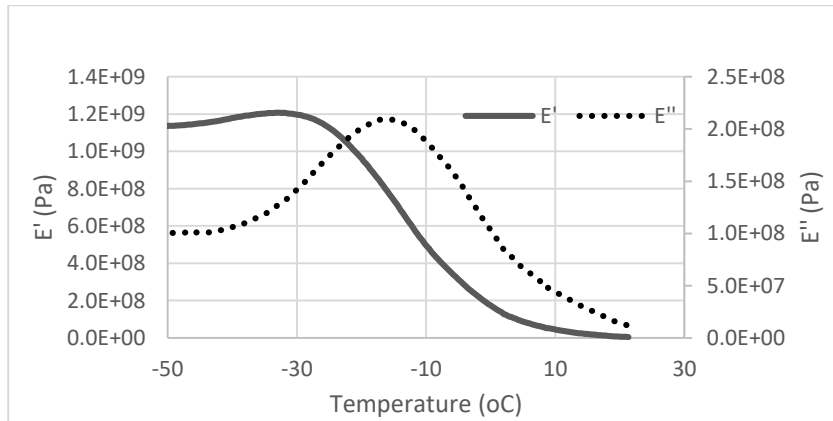


Figure B5 DMA curves and Tg of bitumen mastic containing basalt

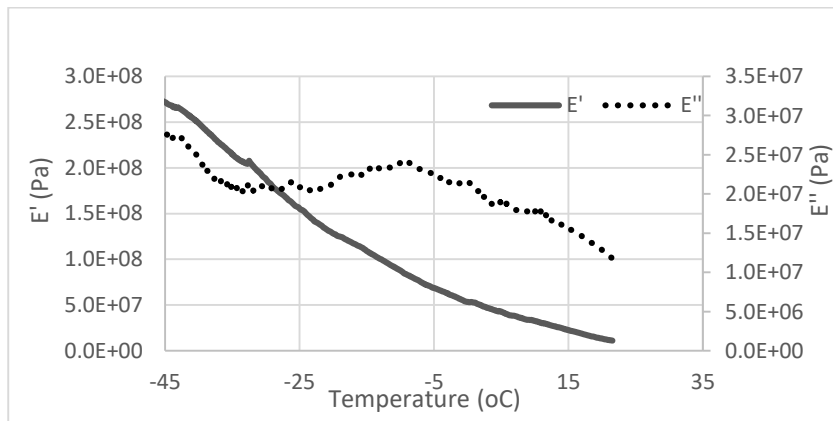


Figure B6 DMA curves and Tg of aged bitumen mastic containing basalt

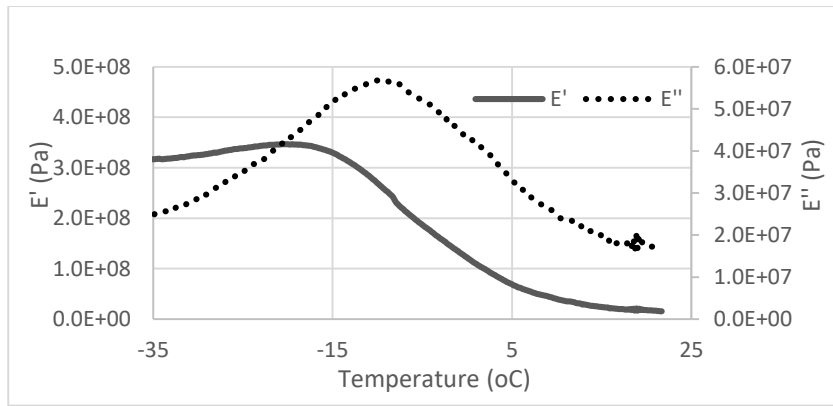


Figure B7 DMA curves and Tg of bitumen mastic containing basalt and hydrated lime

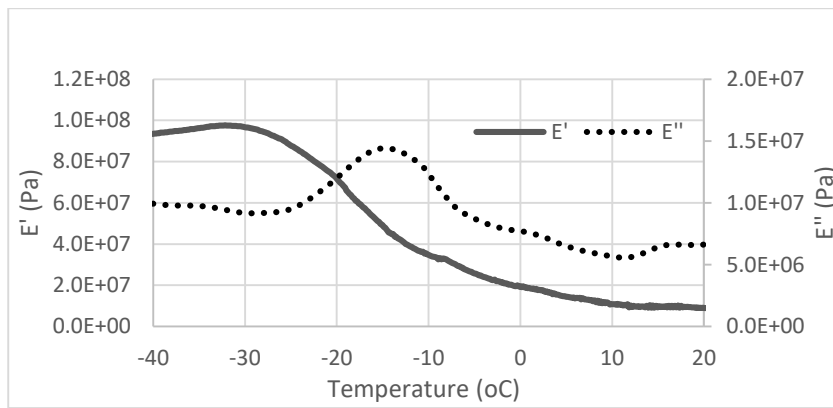


Figure B8 DMA curves and Tg of aged bitumen mastic containing basalt and hydrated lime

C. ANOVA Results

Table C.1 Response for DTT 0°C

Analysis of Variance					
Source	DF	Adj SS	Adj MS	F-Value	P-Value
Aggregate type	1	1,71403	1,71403	57,23	0,000
Gradation	1	0,25669	0,25669	8,57	0,008
Aging	1	0,06462	0,06462	2,16	0,157
Hydrated Lime Content	1	0,02040	0,02040	0,68	0,418
Aggregate type*Gradation	1	0,00289	0,00289	0,10	0,759
Aggregate type*Aging	1	0,01066	0,01066	0,36	0,557
Aggregate type*Hydrated Lime Content	1	0,00383	0,00383	0,13	0,724
Gradation*Aging	1	0,07296	0,07296	2,44	0,133
Gradation*Hydrated Lime Content	1	0,01088	0,01088	0,36	0,553
Aging*Hydrated Lime Content	1	0,02322	0,02322	0,78	0,389
Error	21	0,62890	0,02995		
Lack-of-Fit	5	0,53623	0,10725	18,52	0,000
Pure Error	16	0,09267	0,00579		
Total	31	2,80907			

Table C.2 Response for DTT -10°C

Analysis of Variance					
Source	DF	Adj SS	Adj MS	F-Value	P-Value
Aggregate type	1	1,56203	1,56203	23,73	0,000
Gradation	1	1,17428	1,17428	17,84	0,000
Aging	1	0,00475	0,00475	0,07	0,791
Hydrated Lime Content	1	1,12875	1,12875	17,15	0,000
Aggregate type*Gradation	1	0,01163	0,01163	0,18	0,679
Aggregate type*Aging	1	0,42550	0,42550	6,47	0,019
Aggregate type*Hydrated Lime Content	1	0,35490	0,35490	5,39	0,030
Gradation*Aging	1	0,08925	0,08925	1,36	0,257
Gradation*Hydrated Lime Content	1	0,52275	0,52275	7,94	0,010
Aging*Hydrated Lime Content	1	0,00008	0,00008	0,00	0,973
Error	21	1,38212	0,06582		
Lack-of-Fit	5	1,19127	0,23825	19,97	0,000
Pure Error	16	0,19085	0,01193		
Total	31	6,65605			

Table C.3 Response for TSRST Fracture Stress

Analysis of Variance					
Source	DF	Adj SS	Adj MS	F-Value	P-Value
Aggregate type	1	0,46561	0,46561	4,57	0,044
Gradation	1	0,90451	0,90451	8,88	0,007
Aging	1	0,05281	0,05281	0,52	0,479
Hydrated Lime Content	1	0,08611	0,08611	0,85	0,368
Aggregate type*Gradation	1	1,00111	1,00111	9,83	0,005
Aggregate type*Aging	1	0,20801	0,20801	2,04	0,168
Aggregate type*Hydrated Lime Content	1	0,00281	0,00281	0,03	0,870
Gradation*Aging	1	0,00781	0,00781	0,08	0,785
Gradation*Hydrated Lime Content	1	0,00101	0,00101	0,01	0,922
Aging*Hydrated Lime Content	1	0,41861	0,41861	4,11	0,056
Error	21	2,13946	0,10188		
Lack-of-Fit	5	1,74296	0,34859	14,07	0,000
Pure Error	16	0,39650	0,02478		
Total	31	5,28789			

Table C.4 Response for TSRST Fracture Temperature

Analysis of Variance					
Source	DF	Adj SS	Adj MS	F-Value	P-Value
Aggregate type	1	113,692	113,692	60,31	0,000
Gradation	1	76,005	76,005	40,32	0,000
Aging	1	5,668	5,668	3,01	0,098
Hydrated Lime Content	1	25,157	25,157	13,34	0,001
Aggregate type*Gradation	1	37,574	37,574	19,93	0,000
Aggregate type*Aging	1	7,983	7,983	4,23	0,052
Aggregate type*Hydrated Lime Content	1	0,526	0,526	0,28	0,603
Gradation*Aging	1	5,542	5,542	2,94	0,101
Gradation*Hydrated Lime Content	1	8,756	8,756	4,64	0,043
Aging*Hydrated Lime Content	1	0,166	0,166	0,09	0,770
Error	21	39,588	1,885		
Lack-of-Fit	5	19,942	3,988	3,25	0,033
Pure Error	16	19,647	1,228		
Total	31	320,656			

Table C.5 Response for IDT -10°C

Analysis of Variance					
Source	DF	Adj SS	Adj MS	F-Value	P-Value
Aggregate type	1	8,0842	8,08422	49,85	0,000
Gradation	1	2,9805	2,98046	18,38	0,000
Aging	1	0,3604	0,36040	2,22	0,151
Hydrated Lime Content	1	1,3317	1,33171	8,21	0,009
Aggregate type*Gradation	1	0,1463	0,14634	0,90	0,353
Aggregate type*Aging	1	0,5444	0,54445	3,36	0,081
Aggregate type*Hydrated Lime Content	1	0,0075	0,00750	0,05	0,832
Gradation*Aging	1	0,2805	0,28050	1,73	0,203
Gradation*Hydrated Lime Content	1	0,3011	0,30109	1,86	0,187
Aging*Hydrated Lime Content	1	0,0583	0,05831	0,36	0,555
Error	21	3,4056	0,16217		
Lack-of-Fit	5	3,3610	0,67220	241,20	0,000
Pure Error	16	0,0446	0,00279		
Total	31	17,5006			

Table C.6 Response for IDT 0°C

Analysis of Variance					
Source	DF	Adj SS	Adj MS	F-Value	P-Value
Aggregate type	1	2.9258	2.92578	10.95	0.003
Gradation	1	3.7142	3.71418	13.90	0.001
Aging	1	0.3285	0.32846	1.23	0.280
Hydrated Lime Content	1	1.0346	1.03464	3.87	0.062
Aggregate type*Gradation	1	0.6311	0.63113	2.36	0.139
Aggregate type*Aging	1	0.0245	0.02453	0.09	0.765
Aggregate type*Hydrated Lime Content	1	0.4301	0.43013	1.61	0.218
Gradation*Aging	1	0.0002	0.00020	0.00	0.978
Gradation*Hydrated Lime Content	1	0.0269	0.02691	0.10	0.754
Aging*Hydrated Lime Content	1	0.3256	0.32562	1.22	0.282
Error	21	5.6116	0.26722		
Lack-of-Fit	5	3.1799	0.63599	4.18	0.013
Pure Error	16	2.4316	0.15198		
Total	31	15.0532			

D. Software Manuals

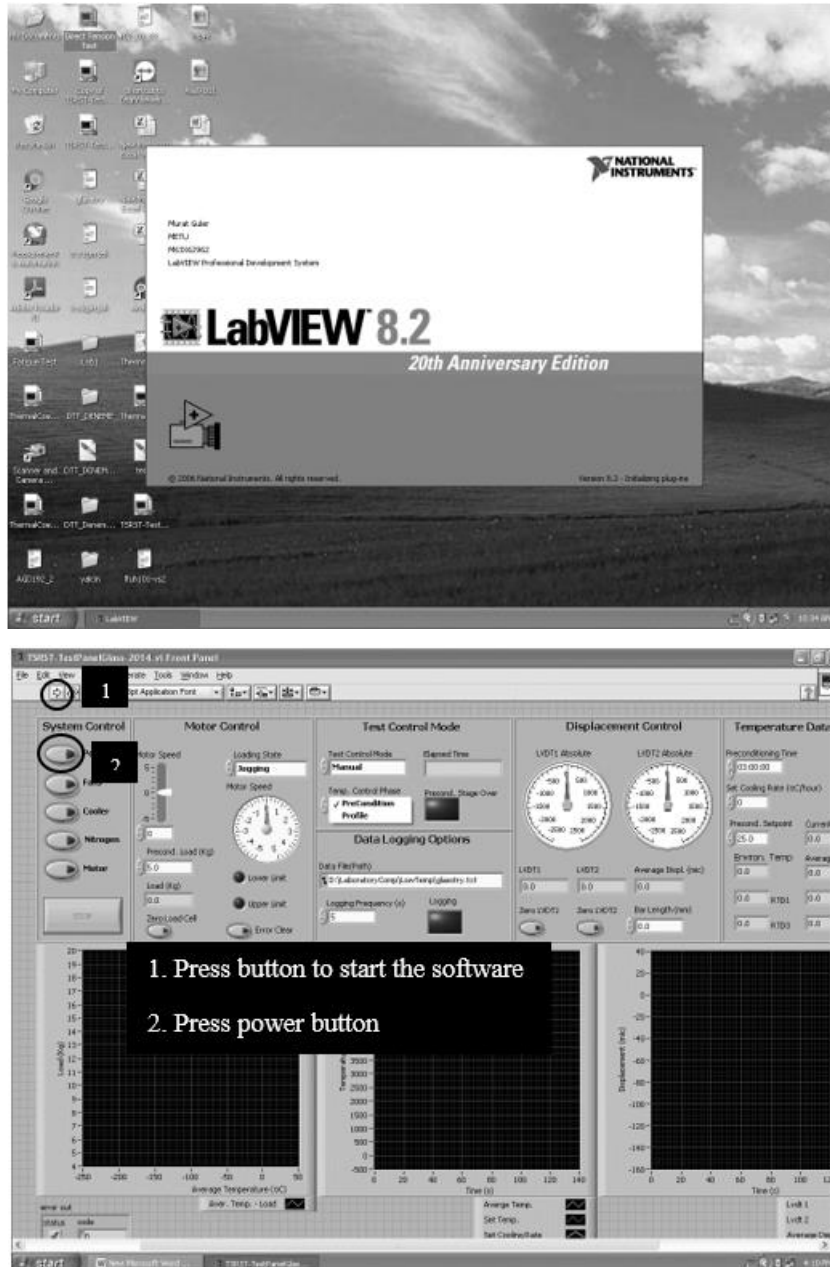


Figure D1 Software for TSRST

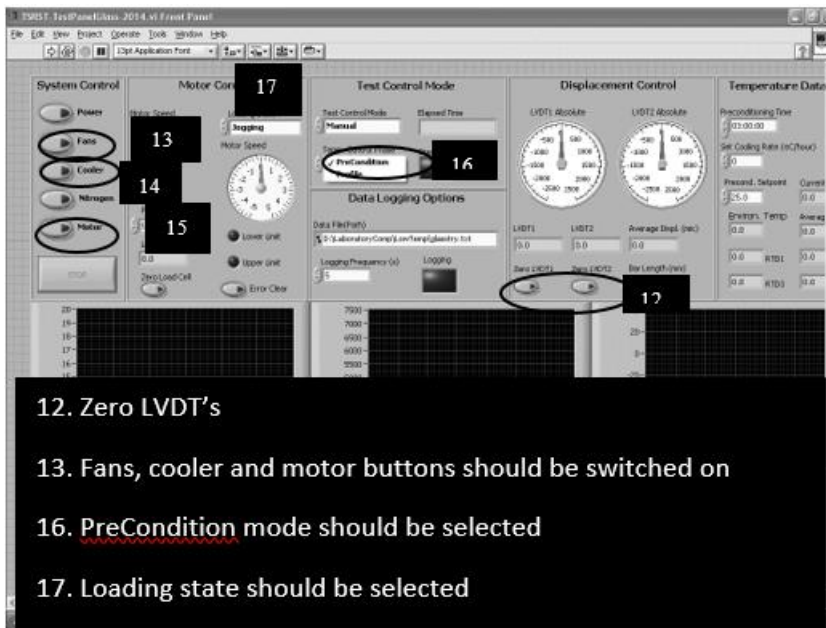
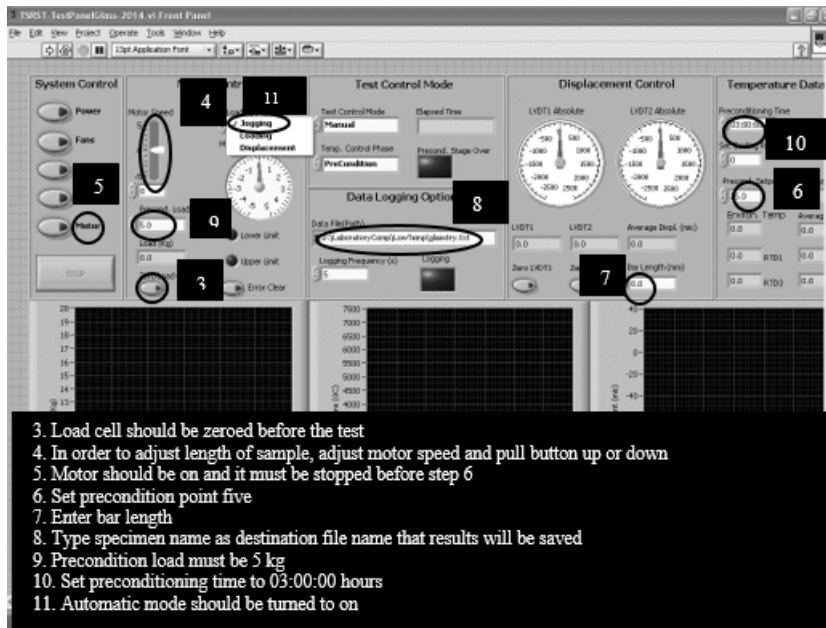


Figure D1 (continued)

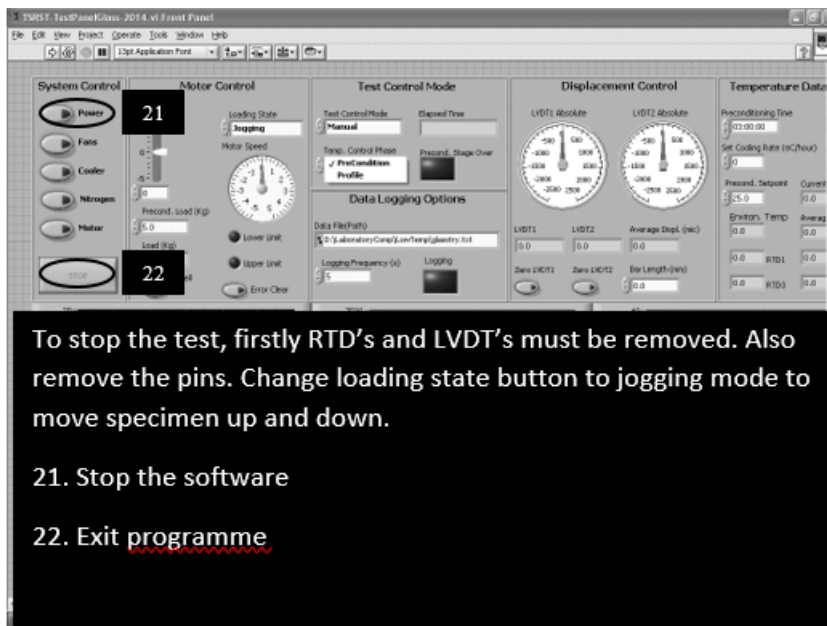
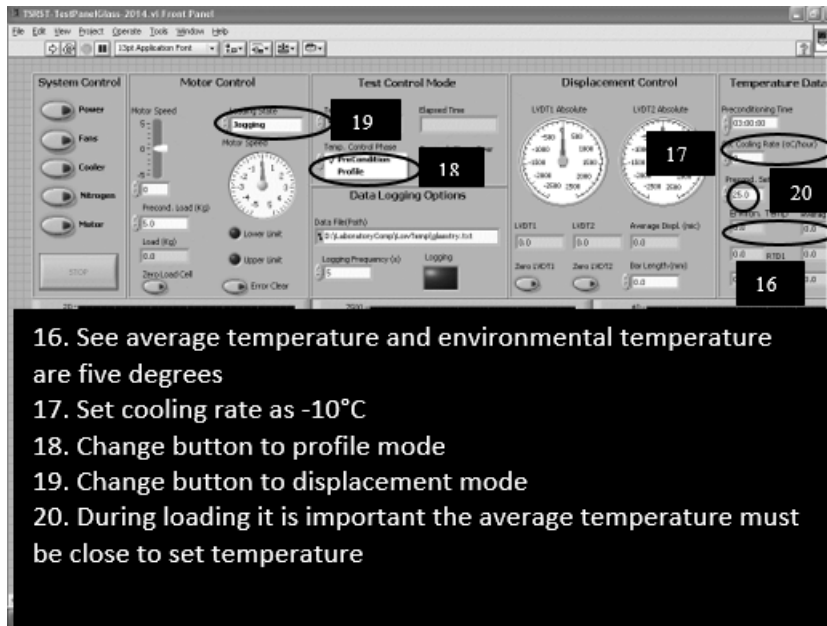


Figure D1 (continued)

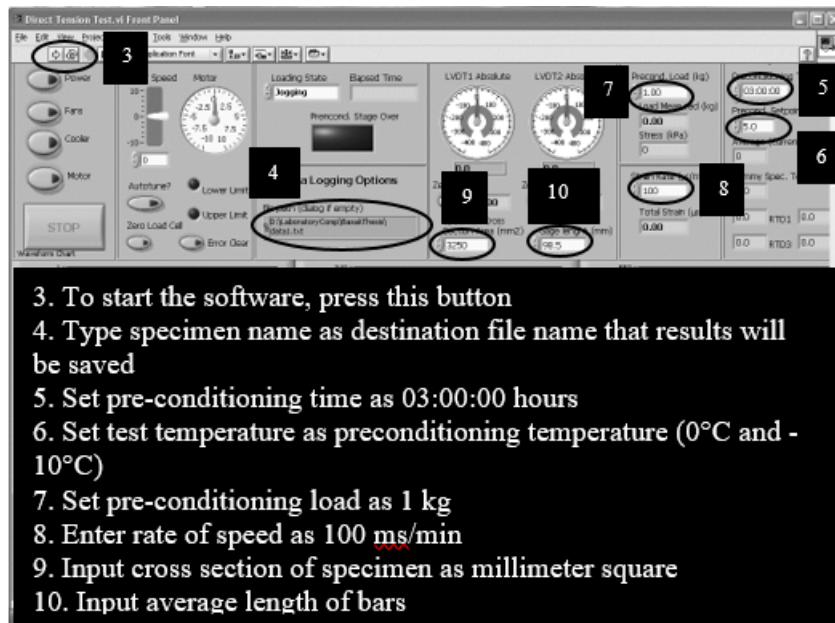
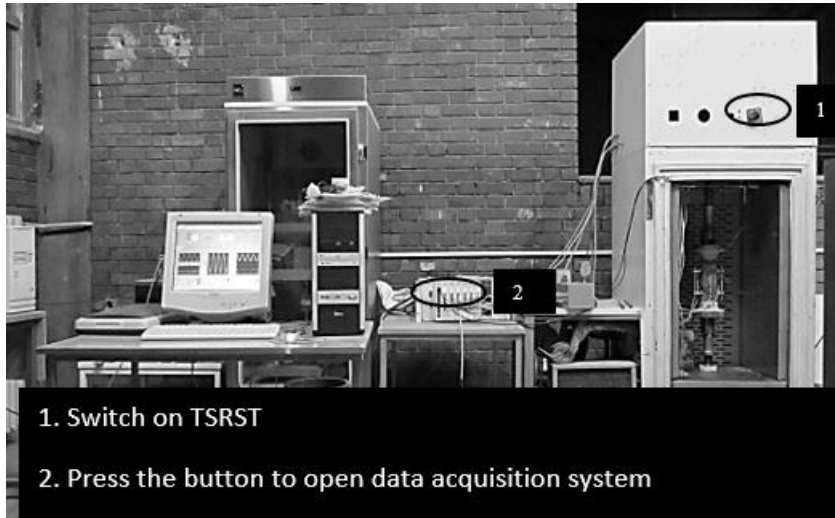
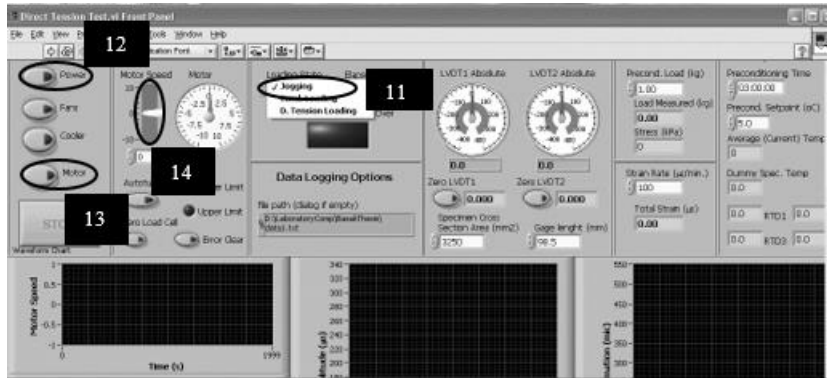
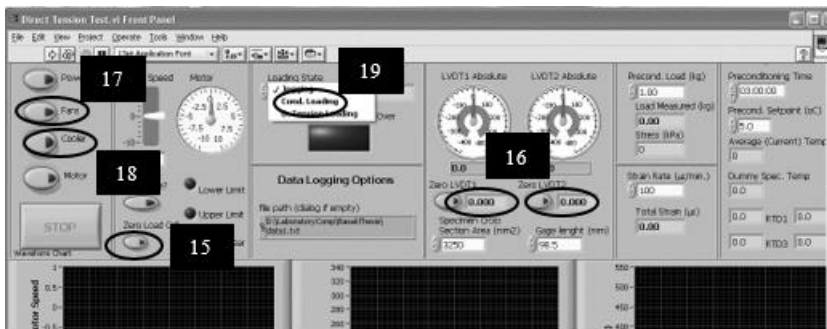


Figure D2 Software for DTT

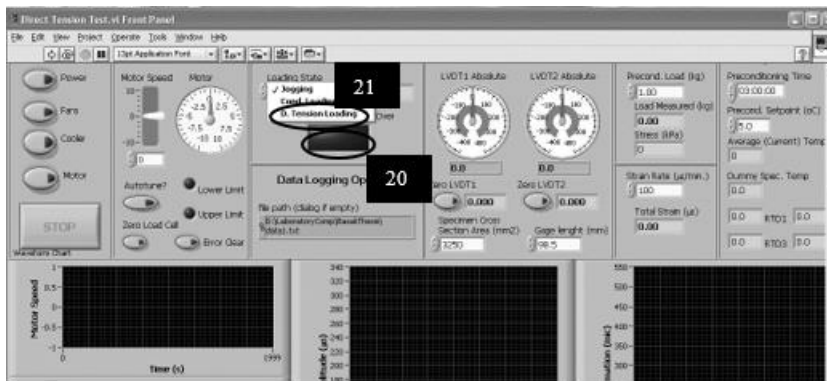


11. Select jogging mode
12. press power button
13. press motor button
14. Slide button to change the direction and speed of motor



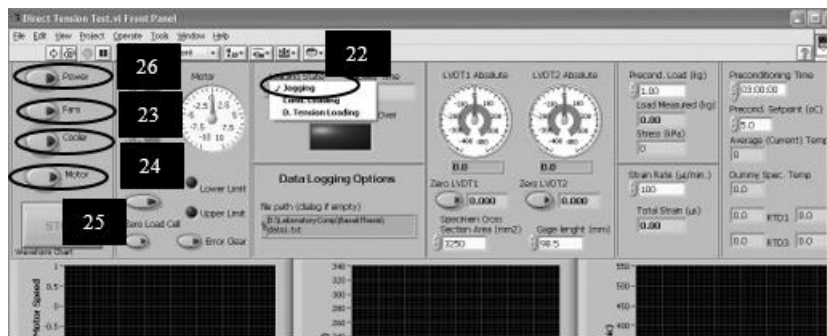
15. Zero load cell
16. Zero LVDT's
17. Turn on fans
18. Turn on cooler
19. Select loading state as conditioning loading

Figure D2 (continued)



20. This section turns green after pre-conditioning stage is over

21. Select direct tension loading mode to start the test



22. After test ends, turn motor into jogging mode

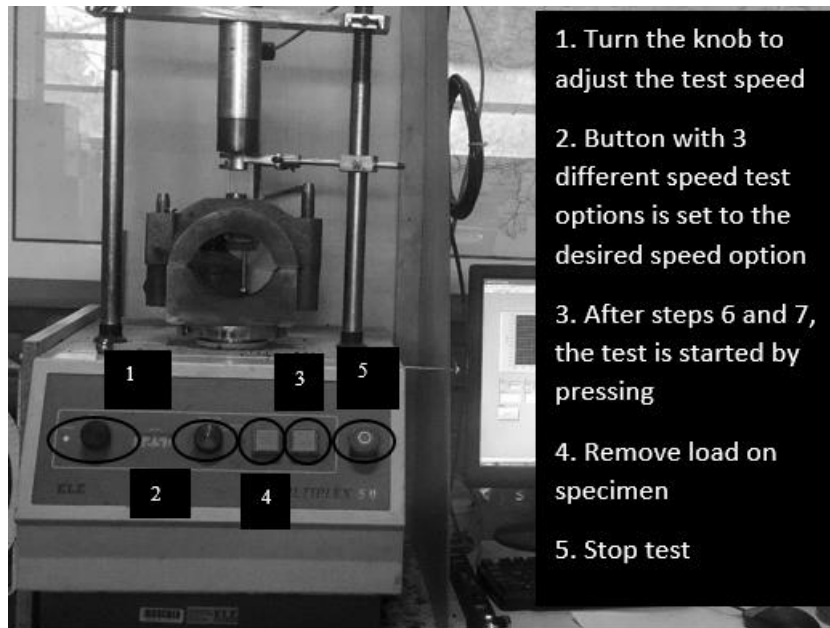
23. Turn off fans

24. Turn off cooler

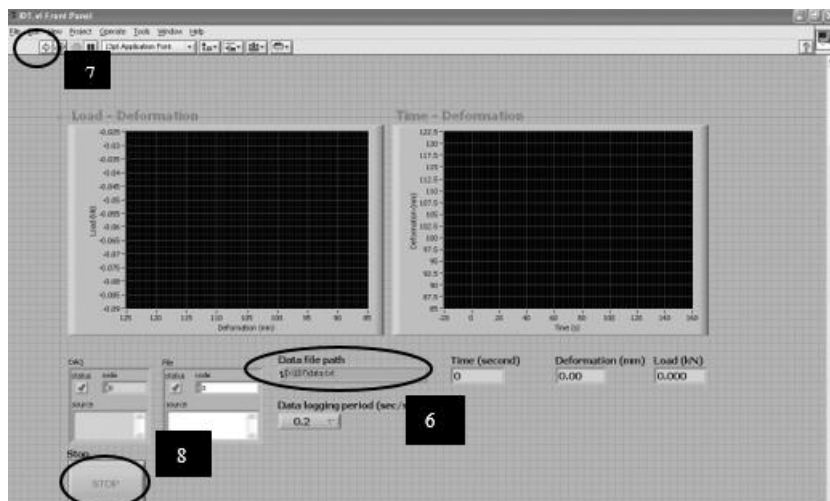
25. Turn off motor

26. Turn off power

Figure D2 (continued)



1. Turn the knob to adjust the test speed
2. Button with 3 different speed test options is set to the desired speed option
3. After steps 6 and 7, the test is started by pressing
4. Remove load on specimen
5. Stop test



6. Type specimen name as destination file name that results will be saved
7. Press to start test
8. Press to stop test

Figure D3 Software for IDT

CURRICULUM VITAE

PERSONAL INFORMATION

Surname. Name: Varli Bingöl. Başak
Nationality: Turkish (TC)
Date and Place of Birth: 12 September 1985. Ankara
Marital Status: Married
Phone: +90 312 210 74 74
Fax:
email: basakvarli@hotmail.com

EDUCATION

Degree	Institution	Year of Graduation
MS	MKU Civil Engineering	2008
BS	MKU Civil Engineering	2010
High School	Atatürk Anadolu High School. Ankara	2002

WORK EXPERIENCE

Year	Place	Enrollment
2018-Present	Hakkari University Civil Engineering	Research Assistant
2010-2018	Middle East Technical University Civil Engineering	Research Assistant
2009-2010	Mustafa Kemal University Civil Engineering	Research Asistant

FOREIGN LANGUAGES

Advanced English

PUBLICATIONS

1. Varli Bingol., B. and Güler M. (2018, 12-14 September). Effect of Hydrated Lime on Indirect Tensile Strength of Asphalt Concrete. 13th International Congress on Advances in Civil Engineering, İzmir, Turkey.
2. Varli Bingol., B. and Güler M. (2019, 17-20 April). Evaluation of Laboratory Performance of Zycotherm Additive for Extended Moisture Resistance of HMA Pavements. Interational Civil Engineering and Architecture Conference 2019, Trabzon, Turkey.
3. Demirci M., Kocaman S, Varli B. (2011). Hesaplamalı Akışkanlar Dinamiği ile Köprü Kenar Ayağı Etrafındaki Hız Dağılımlarının İncelenmesi. E-Journal of New World Sciences Academy.
4. Demirci M., Kocaman S, Varli B. (2012). Farklı Geometrilerdeki Köprü Kenar Ayakları Etrafındaki Hız Dağılımının Sayısal İncelenmesi. Erciyes Üniversitesi Fen Bilimleri Enstitüsü Dergisi.
5. Varli B., Demirci M, Kocaman S. (2010, 12-15 May) Hesaplamalı Akışkanlar Dinamiği ile Köprü Kenar Ayağı Etrafındaki Hız Dağılımlarının İncelenmesi. Bilimde Modern Yöntemler Sempozyumu 2010, Diyarbakır, Turkey.